University of Bielsko-Biała, Poland

Ternopil Ivan Puluj National Technical University, Ukraine

V.M. Glushkov Institute of Cybernetics of National Academy of Ukraine

Mykhaylo PETRYK

Tomasz GANCARCZYK

Oleksander KHIMICH

METHODS OF MATHEMATICAL MODELING AND IDENTIFICATION OF COMPLEX PROCESSES AND SYSTEMS ON THE BASIS OF HIGH-PERFORMANCE CALCULATIONS

(neuro- and nanoporous feedback cyber systems, models with sparse structure data, parallel computations)

Akademia
Techniczno-Humanistyczna
w Bielsku-Białej

Bielsko-Biała 2021

Redaktor Naczelny: dr hab. inż. Krzysztof Brzozowski, prof. ATH

Redaktor Działu: prof. dr hab. inż. Mikołaj Karpiński

Recenzenci: prof. dr hab. inż. Oleksandr Petrov
Katedra Informatyki Stosowanej
Akademia Górniczo-Hutnicza w Krakowie

prof. dr hab. inż. Jerzy Korostil
Zakład Informatyki
Instytut Techniczny
Państwowa Wyższa Szkoła Zawodowa
w Nowym Sączu

Sekretarz Redakcji: mgr Grzegorz Zamorowski

Wydawnictwo Naukowe
Akademii Techniczno-Humanistycznej w Bielsku-Białej
43-309 Bielsko-Biała, ul. Willowa 2
tel. 33 827 92 68
e-mail: wydawnictwa@ath.bielsko.pl

ISBN 978-83-66249-80-6

This monograph highlights new approaches to the development of high-performance supercomputer technologies for modeling and identification based on parallel computations of complex cyberphysical systems (neuro- and nanoporous systems) in the presence of a large amount of feedback and interactions controlled by a significant number of distributed and network computing elements. The design of the considered cyberphysical systems is based on new science-intensive technologies of object description, new computing solutions taking into account the architecture of computer systems and software (parallel algorithms of multiparameter identification). The monograph is intended for researchers, specialists in applied mathematics, mathematical modeling, high-performance parallel computing and software engineering, university professors, graduate students, engineers and students.

Content

PREFACE

This monograph highlights new approaches to the development of high-performance supercomputer technologies for modeling and identification based on parallel computations of complex cyberphysical systems (neuro-bio- and nanoporous systems) in the presence of a large amount of feedback and interactions that are controlled by the network of computing elements. Despite the different nature of the studied cyberphysical systems, their behaviors and the state are determined by many distributed feedback influences such as cognitive ones (influence of certain neural nodes of the cerebral cortex (CC) on the behavior of the behavior of a particular organ or part of the human body, such as the limbs of the right hand, eyelids, eyeballs etc.) and those of physical nature (concentration effects of adsorbed components of contaminants and nanosources in the conditions of dynamic equilibrium in a certain layer of the nanoporous system) and other interactions. The proposed methodology corresponds to a number of priority research areas of European programs (Horizon Europe), related to the modern computer technologies for cyberphysical systems (Computing technologies and engineering methods for cyberphysical systems of systems (CPSoS)). The design of the considered CPSoS is based on new science-intensive technologies of object description, new computing solutions taking into account the architecture of computer systems and software (parallel algorithms of multiparameter identification).

The key problem of the monograph is the developpment of the high-performance supercomputer technologies multiparameter identification of complex cyberphysical systems (neuro-bio-nanomedical and nanoporous physical systems) with feedback-connections and interactions on the basis of parallel computations. Such CPSoS may include also cognitive feedback (for neuro-biosystems) to determinate the parameters of the behavior and the state of individual executive elements of the systems and the optimal parameters of these influences to obtain the predicted systems behavior. In medical applications according to the specified European programs special attention is paid to new digital systems of diagnostics and treatment. In this context, the proposed methods of designing nanomedical neuro-bio-CPSoS are focused on determining the parameters of abnormal movements of

patients with tremor (T-objects) caused by the negative effects of a number of neural nodes of CC. The second type of considered feedback-systems (nanoporous CPSoS) are related to solving the problem of global warming and the implementation of safe energy strategies through the introduction of smart nanosystems to adsorption harmful emissions of carbon oxides and other greenhouse gases.

In Chapter 1, based on the results of cooperation with the French laboratories of the University of Pierre and Marie Curie Sorbonne Paris 6, the Institute of Brain and Spinal Cord, the Higher School of Industrial Physics and Chemistry of Paris, the authors proposed new hybrid models of wave signal propagation, describing the state and behavior - abnormal neurological movements (ANM) of certain parts of the body of a T-object due to the cognitive influence of a certain group of neural nodes (neuro-objects). This models are based on approaches to integrated transforms and spectral analysis for heterogeneous media. New science-intensive models of nanoporous CPSoS are also proposed, which take into account a set of limiting physical factors and mechanisms of feedback influences and nano-sources in the competent nanosorption processes occurring in such systems. Direct and inverse identification problems of multicomponent transfer systems in heterogeneous nanoporous media are implemented (by Petryk M. And Khimich A.). This methodology is based on parallelization and component-by-component evaluation of interactions when explicit expressions of gradients of incoherent functionals for implementation of gradient methods for identification of internal parameters and external feedback are obtained. The proposed hybrid model of the neuro-biosystems describes the state and behavior of T-objects on the basis of wave signal propagation, namely segmental description of 3D-elements of trajectories of abnormal neurological movements of the studied part (limb) of the T-object body of neuro objects. The high-speed analytical solution of the model describing 3D- trajectories on each ANM segment in the vector form is obtained using hybrid integral Fourier transforms. A new method for calculating the hybrid spectral function of ANM, the system of orthogonal basic functions and spectral values, which form the basis of the proposed hybrid transformation, provide an integrated vector solution to the model.

The authors solved new nonclassical problems of multiparameter identification of feedback-systems (neuro-bio- and nanoporous CPSoS) by

developing high-performance gradient algorithms based on the theory of optimal control of complex multicomponent systems to minimize the target residual functionalities. On the basis of hybrid integral transformations, new high-speed analytical solutions of models (direct and inverse problems) describing 3D elements of ANP trajectories and concentration distributions of absorbed components depending on feedback at macro and micro levels are implemented. High-performance regularization algorithms for identifying system parameters and inverse interactions at the macro and micro levels are built. Thes aigprithmes are based on the expressions of gradients of residual functionals and allow parallelization of calculations taking into account the supercomputer architecture of computer systems. The construction of high-velocity analytical solutions of both types of feedback models is based on the development of computational parallelization approaches using efficient decomposition and linearization schemes and methods of hybrid Fourier integral transforms and the Heaviside operating method.

Chapters 2 and 3 implement a similar approach to the use of new science-intensive models of nanopores CPSoS considering a set of physical factors and feedback in nanopores network of nanosources. The choice of the model is based on a number of important feedback effects in micro and macro levels, intrakinetic effects and physical postulates (dispersion and electrostatic forces (John-Leonard, Van der Waal), molecules adsorption interactions on the surface phases (Gibbs and Langmuir postulates) etc., determining a high degree of description of the adsorption kinetics in nanopores media. The mass transfer processes in such systems include two components: transport in interparticle space and transpost in intraparticle space. In our proposed model, the balance equations in interparticle space are supplemented by the influence of nanogradients of concentrations occurring along the radius of nanoporous particles and on their surfaces, which are determined by the equation of balance inside the particle. Feedback-models based on the development of computational parallelization approaches using efficient decomposition schemes, hybrid integral Fourier transforms, the Heaviside’s operationel method and Laplace integral transformation.

Some studies in Sections 1 and 3 and their descriptions are performed with the participation of graduate students of the Department of Software Engineering,

Ivan Puluj Ternopil National Technical University (Mudryk I.Ya. - Subsections 1.2, 1.3 and Petryk M.M. - Subsections 3.2, 3.3).

For the purpose of effective algorithmic-software implementation matrix procedures of parallelization of calculations and their performance on supercomputer platforms and clusters are offered. The advantage of the proposed vector approach to constructing solutions of models of the studied classes of CPSoS over the traditional one is the possibility to run in parallel any number of identification processes of different parameters, reducing by several orders of magnitude the identification procedures focused on supercomputer architecture. A comprehensive study of feedback systems (neuro-bio- and nanoporous CPSoS) is based on the creation of science-intensive hybrid models describing the states and behavior of the bio- and physical processes, taking into account the matrices of cognitive and physical feedback influences and development of high-performance supercomputer technologies to identify their parameters.

Chapter 4 highlights development of methods and algorithms for studying mathematical models with approximate data of sparse structure on the latest high-performance computers with parallel organization of calculations of different architecture. A new methodology for studying mathematical models with approximate data of sparse structure on the latest high-performance parallel and distributed computer systems using multilevel parallelism is developed. An approach is proposed to solving nonlinear problems on supercomputers, which arise in the mathematical modeling of the strength and stability of structures, in particular in the modeling of the life cycle of responsible welded structures of energy objects. Block and block-cyclic algorithms for parallel computations for solving linear algebra problems with sparse matrices on the basis of structural regularization and decomposition of sparse structure data is developed and investigated. Problems of linear algebra (systems of linear equations and matrix problems on eigenvalues) are a significant part of mathematical modeling. Improving the quality of mathematical modeling is directly related to increasing the productivity and efficiency of modern parallel computing systems. The key point in solving these problems is the choice, development and application of methods for automating the design of parallel programs for mathematical modeling, as well as software tools for configuring the

developed programs on various high-performance computing platforms, which include multi-core and cluster architectures - graphics processors, "cloud platforms", etc.

Chapter 5 outlines the basics of the theory of methods for hybrid integral transformations of multicomponent domains and algorithmic schemes of their applications in modeling and analysis of ANM-motions.

INTRODUCTION

This monograph highlights new approaches to the development of highly productive supercomputer modeling and identification technologies based on parallel computations of complex cyber-physical systems (neuro-, bio- and nanoporous systems) in the presence of a large amount of feedback and interactions, controlled by a large number of distributed and networked computing elements. Despite the different nature of the studied cyberphysical systems, their behaviors and the state of individual elements are determined by a multitude of distributed feedback influences of a cognitive nature (the influence of certain areas of neural nodes of the cerebral cortex on the behavior of a particular organ of the human body) and physical nature (concentration effects of adsorbed components of contaminants and nano-sources, conditions of dynamic equilibrium in a certain layer of nanoporous systems) and other interactions. The proposed methodology corresponds to a number of priority scientific areas of European programs ("Horizon 2020", PHC "DNIPRO") related to the latest computing technologies and engineering methods for cyber-physical systems of systems ("Computing technologies and engineering methods for cyber-physical systems (CPS) The design of the CPS under consideration is based on new science-intensive technologies for describing objects, new computing solutions taking into account the architecture of computer systems and software (parallel algorithms for multidimensional identification).

The main problem to be solved in the monograph is the creation, based on parallel computing of high-performance supercomputer technologies, of multidimensional identification of complex CPSoS (neuro-bio-nanomedical and nanoporous physical systems) with feedback-connections and interactions, including cognitive ones, for neuro-biosystems determination of behavior and state parameters of individual executive elements of systems and the optimal parameters of these influences and internal characteristics of the system to obtain the predictable behavior of its executive elements. In medical applications, according to these European programs, special attention is paid to new digital diagnostic and treatment systems and nanomedicine. In this context, the proposed design techniques for nanomedical neuro-bio-CPSoS are focused on determining the parameters of

abnormal movements of patients with tremor signs (T-objects) caused by the negative effects of a certain set of CC neural nodes. The identification of the parameters of these influences determines the ways of solving the problem. The second type of information systems being developed - nanoporous CPSoS - are related to solving another world problem - global warming and the implementation of a safe energy strategy by introducing reasonable systems for absorbing harmful emissions of carbon oxides and other greenhouse gases from energy and industrial facilities, etc.

In the first Section, based on the results of cooperation with the French laboratories of the University of Pierre and Marie Curie, Sorbonne Paris 6, the Institute of the Brain and Spinal Cord, the Higher School of Industrial Physics and Chemistry of Paris ESPCI Paris, the authors proposed a new an approach to the construction of hybrid models of wave signal propagation, described the state and behavior of abnormal neurological movements (ANM) of certain parts of the body of a T-object due to the cognitive impact of a certain group of neural nodes (hereinafter neuro-objects) of the CC. The authors also proposed a technique for constructing an adaptive matrix (recall), which determines the parameters of states from the action of certain neuro-objects of the CC. Also, new high-tech models of nanoporous CPSoS have been proposed, taking into account a complex of limiting physical factors and mechanisms of feedback influences and nano-rings in competent nanosorption processes occurring in such systems. Petryk M.R., Khimich A.N. formulated direct and inverse problems of identification of multicomponent transport systems in heterogeneous nanosources based on parallelization and component-wise estimation of mutual influence and obtained explicit expressions for the gradients of residual functionals for the implementation of gradient methods for identifying internal parameters of the system, external feedback interactions and nanosources.

The proposed hybrid model of a neuro-biosystems describes the state and behavior of T-objects based on the propagation of a wave signal, namely, the segment-by-segment description of 3D elements of the trajectories of abnormal neurological movements of the investigated part (limb of the hand) of the body of the T-object, taking into account the matrix of cognitive influences of groups of neuro-objects of the CC. On the basis of hybrid integral transform (Fourier, Bessel, Hilbert), a high-speed analytical solution to the model is obtained in the form of a

vector function that describes 3D elements of trajectories on each ANM segment. A new method is proposed for calculating the hybrid spectral function of ANM, a system of orthogonal basic functions and spectral values that form the basis of the proposed hybrid transformation and provide an integral vector decoupling of the model.

The authors have solved new nonclassical problems of multiparameter identification of feedback systems (neuro-bio- and nanoporous CPSoS) by developing high-performance gradient algorithms based on the theory of optimal control of complex component systems for minimizing target residual functionals. On the basis of hybrid integral transformations, new high-speed analytical solutions to models (direct and inverse problems) in vector form are constructed, which describe 3D elements of AMN trajectories and concentration distributions of absorbed components depending on feedback effects at the macro and micro levels. On the basis of these approaches, direct and inverse problems of multi-parameter identification of the studied feedback systems are formulated by parallelizing and component-wise estimation of mutual influence with obtaining explicit expressions for the gradients of residual functionals for the implementation of gradient methods for identifying system parameters and inverse interactions at the macro- and microlevels. The constructed high-performance regularization algorithms for identifying the parameters of systems and inverse interactions at the macro- and microlevels, based on the expressions for the gradients of the residual functionals, and allow parallelization of computations taking into account the supercomputer architecture of computing systems. The construction of high-speed analytical solutions to both types of feedback-models is based on the development of approaches to parallelizing computations using efficient decomposition and linearization schemes and methods of hybrid integral Fourier transforms and the Heaviside operational method.

In the second and third Sections, a similar approach is implemented to using nanoporous CPSoS for the construction of new high-tech models, taking into account a set of limiting physical factors and mechanisms of feedback effects and nano-rings in an extensive network of nanopores. The model is chosen taking into account the amount of important feedback influences at the micro- and macrolevels, intra-kinetic

effects and physical postulates (dispersion and electrostatic forces (John Lenard, Van der Waals), adsorption interaction between adsorptive molecules and active adsorption centres on the interface phases (the postulates of Gibbs, Langmuir), etc., determine a high degree of description of the kinetics of adsorption and desorption into nanopores of catalytic media. Transport processes in such systems include two components: transfer of interparticle space into macropores and microtransfer of spherical particles into nanopores (interparticle space) - intraparticle space. In the developed model, the balance equations in the interparticle space are supplemented by the influence of gradients of concentrations arising along the radii of nanoporous particles and on their surfaces, are determined by the balance equation inside the particle of both types of feedback models, based on the development of approaches to parallelizing computations using efficient decomposition and linearization schemes, methods of hybrid integral Fourier transforms and the operational Heaviside method and Laplace transform.

Part of the research in Sections 1 and 3, as well as its description, was carried out with the participation of graduate students of the Department of Software Engineering of the Ternopil Ivan Puluj National Technical University - Mudryk I. Ya. (Subsections 1.2, 1.3) and Petryk M.M. (Subsections 3.2, 3.3).

With the aim of efficient algorithmic-software implementation, matrix procedures for parallelizing computations and their execution on supercomputer platforms and clusters are proposed. The advantage of the proposed vector approach to constructing solutions to models of the studied classes of CPSoS over the traditional one is the ability to run in parallel an arbitrary number of identification processes with a different amount of parameters, reducing by several orders of magnitude the duration of identification procedures focused on supercomputer architecture. The developed software for high-performance supercomputer identification technologies and modeling tools is based on parallel computations of complex feedback systems (neuro-bio- and nanoporous systems), which is a significant step in the development and implementation of digital neurodiagnostics in Ukraine and the effective implementation of a safe energy strategy based on modern cyber-physical systems, high technologies and artificial intelligence. A comprehensive study of feedback systems (neuro-bio- and nanoporous CPSoS) was

carried out on the basis of science-intensive hybrid models describing the states and behavior of the bio- and physical processes, taking into account the matrices of cognitive and physical feedback influences and the development of high-performance supercomputer technologies on this basis for identifying their parameters.

In the fourth Section, methods and algorithms for studying mathematical models with approximate data of a sparse structure on the latest high-performance computers by organizing calculations of various architectures are developed. A new methodology for studying mathematical models with approximate data of a sparse structure on the latest high-performance parallel and distributed computer systems using multilevel parallelism is created.

An approach is developed to solve nonlinear problems on supercomputers that arise in mathematical modeling of the strength and stability of structures, in particular, when modeling the life cycle of critical welded structures of power engineering facilities. Block and block-cyclic algorithms for parallel computations when solving linear algebra problems with sparse matrices on the basis of structural regularization and decomposition of sparse structure data are developed and investigated. Linear algebra problems (systems of linear equations and matrix eigenvalue problems) make up a significant part of mathematical modeling.

Improving the quality of mathematical modeling is directly related to an increase in the productivity and efficiency of using modern parallel computing systems. The key point in solving these problems is the issue of the choice, development and application of design automation methods for parallel programs of mathematical modeling, as well as software tools for customizing the developed programs for various high-performance computing platforms, which include multicore and cluster architectures, Grid, video graphics processors, "Cloud platforms", etc.

In the fifth Section, the foundations of the theory of methods for hybrid integral transformations of multicomponent domains and algorithmic schemes for their applications in modeling and analysis of ANM are presented.

Chapter1. High-performance methods of diagnostics and identification of abnormal neurological state parameters caused by cognitive feedback influences of the cerebral cortex

1.1 Problems of human neurological conditions

Tremor is a series of unwanted, small fluctuating movements affecting an organ or part of the body (fingers, eyelids, eyeballs, speech organs, etc.), resulting from involuntary contraction of skeletal muscles responsible for the movement of these organs [1]. An increase in the amplitude and a change in the frequency and shape of oscillations relative to the norm (frequency and amplitude of physiological tremor) are signs of a violation of the central and peripheral neuronal mechanisms for regulating movements. The analysis of these parameters is important both for understanding the role of dysfunction of individual zones in neural nodes of the cerebral cortex (CC) in the processes of motion control, and for clinical studies of early detection, refined diagnosis of motor disorders, selection and correction of optimal methods of effective drug therapy.

The problem of the complexity of identification and assessment of limb tremor exists due to imperfection of methods of neurological diagnosis, in particular from [2]:

- low accuracy in assessing the degree of tremor;
- lack of unambiguity in the assessment results (subjective assessment);
- the impossibility of analyzing the information received in the context of many characteristics, a "narrow" view of the information received;
- lack of methods that take into account feedback-connections and the influence of CC neural nodes on the dynamics of tremor;
- the complexity and high cost of implementing the latest high-tech diagnostic methods in specialized clinics.

All this determines the need to improve the methods and approaches to the diagnosis of tremor in real conditions.

The most modern diagnostic technologies include 3D-motion test [1], or recording of human movements in space using high-sensitivity high-speed cameras. Its essence lies in the complete reading of the movements of most elements and parts of the human body using infrared tags and 3d cameras. In modern conditions, for the registration of tremors, systems and methods are widely used to determine the high-amplitude tremor characteristic of Parkinson's disease and essential tremor [2]. Thus, there is a known method for identifying a tremor on a plane by recognizing an Archimedes spiral pattern, which can be performed on a pen graphic tablet [3]. Separate studies related to the analysis of tremor and partially cognitive feedback-effects of CC neuronodules on the state of T-objects were carried out by a number of researchers, such as A. Legrand. M. Vedaet, Aparttiz E., Wang J., Louis E. et al. [2-5].

The main attention in them is focused on the study of parameters with respect to normal states and behavior (normal wave movements of certain parts of the body), for the analysis of which classical methods of digital processing based on the integral Fourier transform were used. In [1-3], cognitive feedback-connections were approximately estimated using the methods and software technologies of neural networks.

This approach does not make it possible to analyze abnormal neurological movements and to quantify the states and behavior inherent in patients whose individual body parts have pronounced signs with a high degree of tremor (T-objects). Another problem is that one-dimensional models and devices are mainly used for analysis, which record motion indicators only along one coordinate [4, 5]. Due to this, there is a loss of information from 40% to 80% that de facto determines the low level of indicators of such an analysis. On the other hand, due to the use of classical digital processing models, in turn, the quality of these studies for T-objects with abnormal states decreases by another 60 - 80%, since these methods reject, again, from 60% to 80% of important data into noise, which can answer the question about the real cognitive mechanisms of influence on individual segments of the ANM-curves [1-3]. In [5], a comparative analysis of information loss in the diagnosis of tremor using the

Archimedes spiral test for patients with varying degrees of tremor is presented. Table.1.1.):

Table.1.1

№ of the test	Duration of the execution, *c*	Pen Accelerometer Readout, %	Degree of tremor	Scale score due to Fahn-Tolossa-Marin
1	37	5	low	1.8
2	44	9	low	2.5
3	65	24	essential	6.8
4	57	37	essential	6.9
5	47	49	middle	4.5

The identification of the parameters that determine the above feedback-connections and influence on the nature of the ANM and the development of models and tools that increase the accuracy of the analysis of the neurological state of the T-objects is the subject of this section.

1.2 Comprehensive methodology and analysis tools for the diagnosis of neurological conditions of T-objects based on the hybrid ANM model. Problems of human neurological conditions

Analysis technique for diagnosing neurological states of T-objects proposed by us is focused primarily on determining the parameters of abnormal movements in patients with tremor signs caused by the negative effects of a certain set of CC neural nodes.

The technique is based on a hybrid model of the neuro-system (CC nodes and tremor-object) developed using the theory of wave signal propagation, which describes the states and behavior of T-objects. The model determines the segment-by-segment description of 3D elements of the ANM trajectories of the studied T-object (limbs of the hand), taking into account the matrix of cognitive influences of CC neuro-node groups on motion segments, the elements of which will include the

components of the hybrid spectral function of the system for all ANM segments [11, 12]. In order to decompose complex ANM movements into simpler elements, the number of partitions can be chosen arbitrarily depending on the complexity of the ANM image. The mathematical model assumes obtaining quantitative characteristics of tremor. In this method of analyzing the data of ANM motions of a T-object, an extremely important result is the ability to obtain a frequency response using a hybrid integral Fourier transform and digital signal processing methods on hybrid spectral functions and spectral values [12, 13].

1.2.1. ANM analysis hardware

The implementation of the hardware solution is based on the method of constant continuous determination of the electronic pen position in relation to any control coordinate [13]. To carry out empirical studies, a touch-sensitive Pen tablet (digitizer Wacom Cintiq 12WX) with a sampling rate of 133 Hz and an accuracy of ± 0.25 mm was used. The template has the form of the Archimedean spiral with several turns clockwise or counterclockwise, with an inter-loop of 9 mm. This template is located on the screen of an interactive tablet that allows a patient to draw with an electronic pen (Fig. 1.1.).

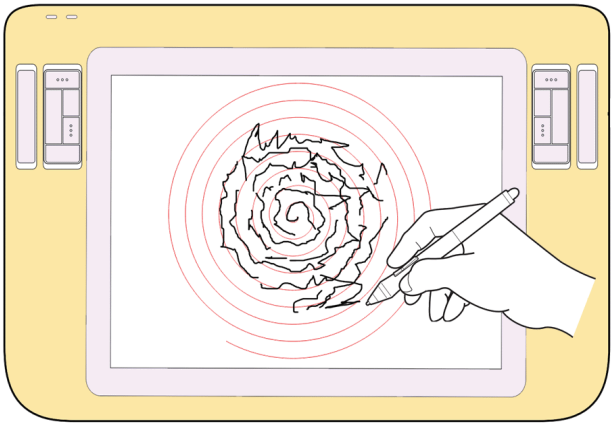

Figure 1.1. Example of using software to reproduce the Archimedean spiral pattern on a Wacom Cintiq pen tablet

An electronic pen is used to identify handwritten information (numbers, text information, template drawings) or when recording and digitizing arbitrary movements of the limb of the hand. We have proposed a graphic digital pen device with a built-in 3D microaccelerometer for carrying out a diagnostic test. The microcontroller reads and processes information from a three-axis acceleration sensor (microaccelerometer). According to the proposed formulas, the readings of the instantaneous coordinates of the position of the accelerometer in space are determined [11, 12]. In a parallel stream, information is received about the movement of the electronic pen on the plane of the graphics tablet.

When a zero value of the pen pressure is detected on the sensitive surface of the tablet (which indicates the separation of the pen from the surface), the necessary information about the movement of the pen is obtained from the displays of the microaccelerometer - the instantaneous coordinates of the position of the MEMS [13] accelerometer in space are determined, ensures the completeness of data collection about the trajectory of the ANM for T - object and their reliability.

The digitized value of the pen position is transmitted via WIFI transmitter to the PC. Thus, the complex increases the reliability of the system for identifying the ANM movements of the T-object (by interacting the sensitive element of the tablet with an electronic pen and the built-in MEMS accelerometer).

The data on the movement of the pen in the form of a 3D model of the ANM of the T-object is formed in the graphics window (Fig.1.2) with the possibility of providing the decomposition of complex 3D movements into 3 posible projections and the subsequent analysis of each of them and the choice of the most defining parameters of the ANM for identification and comprehensive assessment [12].

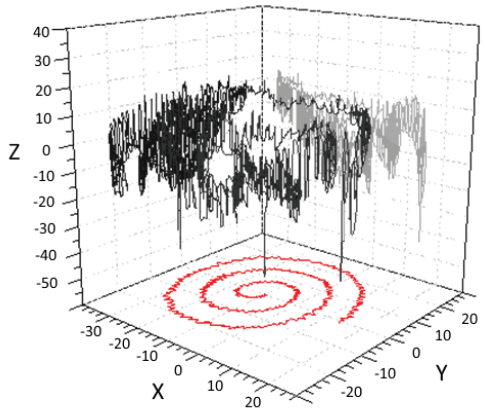

Figure 1.2. 3D-model of ANM of T-object based on data read from microaccelerometer

1.3 Hybrid mathematical model for the analysis of the ANM of the T-object based on feedback-connections and the effects of the neural nodes of the CC

1.3.1 Formulation and method of direct heterogeneous boundary value problem solving for ANM analysis based on cognitive feedback influences

Basic physical assumptions. According to the program of experimental studies of the ANM of T-objects, to obtain a qualitative statement of the problem and to construct a mathematical model of the ANM, the data of one of the defining projections of motion in the form of a spiral (according to the data in Fig. 1.2.) is used, which is easily transformed into a Cartesian graph (relative to the coordinate axis z, Fig. 1.3). This trajectory of movement is connected by cognitive feedback-connections with a certain set of neural nodes of the CC, which send signals to control these oscillatory neurological movements and determine, in general, the dynamics of the ANM of the studied T-object (Fig. 1.3). To measure signals during the entire duration of movement, a system of sensors in the form of a special helmet is used, in contact with the corresponding neural nodes of the patient's CC, during the entire duration of the movement of the electronic pen, recording the behavior of the T-object (limb of the hand) (Fig. 1.3).

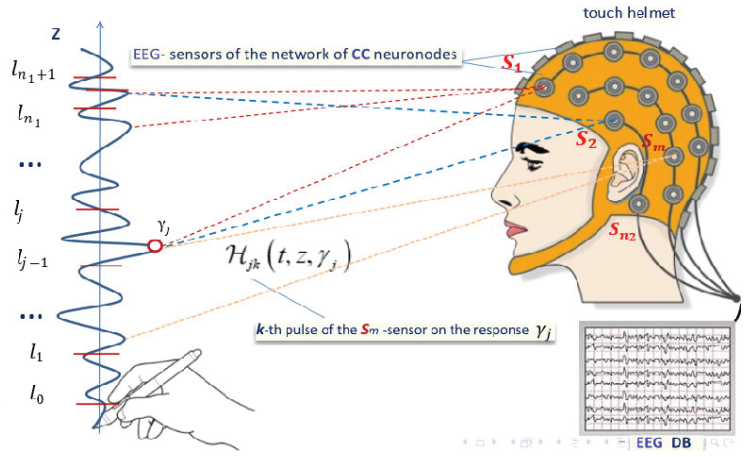

Figure 1.3. The system of interaction "neuro-nodes CC T-object". Component decomposition of a complex ANM track into an arbitrary finite number (n_l) of simple motion elements

Electroencephalogram (EEG) trends of signals recorded by the helmet's sensors are stored in the corresponding database [12]. In order to decompose a complex ANM-trace for the further formulation of the mathematical model, a scheme of its multicomponent decomposition of segments of the motion trajectory is used (Fig. 1.3). Due to this fact, the distributions of trends in the EEG signals of the neural nodes that control the oscillatory neurological movement are correlated and, in general, determine the dynamics of the ANM for each j-th segment of the track, where n1 is the number of splitting points of the ANM track (Fig. 1.4). The splitting can be set automatically in an arbitrary way, with any finite number of segments, the lengths of which can also be different depending on the level of detail of the traffic areas and the choice of acceptable basis functions and building on their basis acceptable dependences of their approximation [11, 12]. One of the criteria for determining the lengths of the partitioning elements can be the amplitude characteristics of individual trends in the trace of oscillating ANM motions, etc. [12].

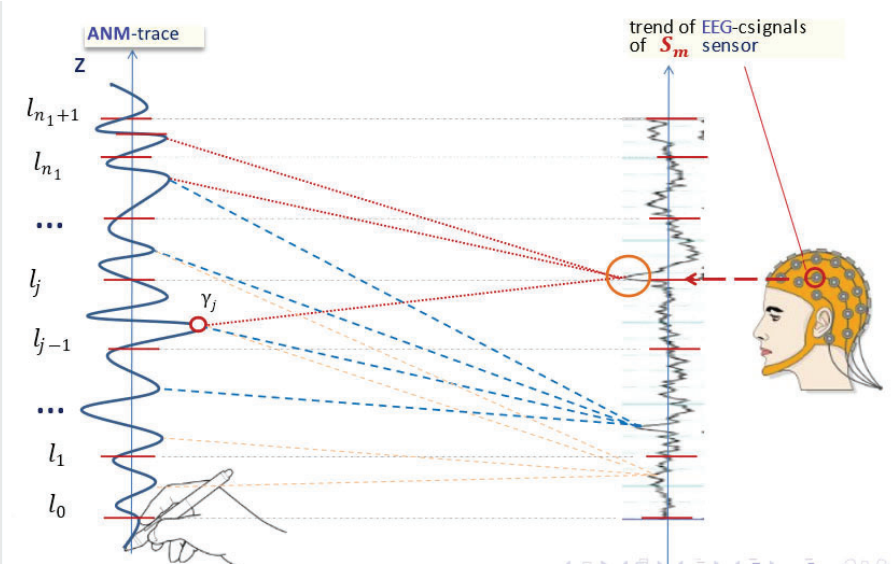

Figure 1.4. Schematization of the connections of cognitive feedback-effects of EEG-signals of a separately defined neurologic node on separate elements of the ANM-trace of the T-object

1.3.2. Mathematical statement of the problem.

Based on the stated physical assumptions of this subject area of neurological analysis, the direct heterogeneous initial-boundary value problem of determining the parameters for the ANM of a T-object can be described in the form of the system of equations [11, 12]

$$\frac{\partial^2 u_j(t,z)}{\partial t^2} = b_j^2 \frac{\partial^2 u_j}{\partial z^2} + S_j^*(t,z), \quad z \in (l_{j-1}, l_j), j = \overline{1, n_1+1} \qquad (1.1)$$

with homogeneous initial conditions:

$$u_j(t,z)\big|_{t=0} = 0, \qquad \frac{\partial u_j}{\partial t}\bigg|_{t=0} = 0 \qquad , j = \overline{1, n_1+1}, \qquad (1.2)$$

as well as homogeneous boundary conditions and a system of interface conditions:

$$\frac{\partial}{\partial z} u_1(t,z)_{z=0} = 0, \quad \frac{\partial}{\partial z} u_n(t,z)_{z=l} = 0, \qquad (1.3)$$

$$\left[u_j(t,z)-u_j(t,z)\right]\Big|_{z=l_j}=0,\quad \left(b_j^2\frac{\partial}{\partial z}u_k(t,z)-b_{j+1}^2\frac{\partial}{\partial z}u_{j+1}(t,z)\right)\Big|_{z=l_j}=0,\ j=\overline{1,n_1} \quad (1.4)$$

in the multicomponent region:

$$D_{n_1}^{+}=\left\{(t,z):t\in(0;T),z\in I_{n_1}=\bigcup_{j=1}^{n_1+1}(l_{j-1},l_j);\ l_0=0,\ l_{n_1+1}\equiv l<\infty\right\}.$$

Here (1.1) is a system of wave equations describing the ANM trajectories of tremor on each j-th segment of the trajectory $j=\overline{1,n_1+1}$ depending on the resulting action of the set of signals $S_j^*(t,z)$, received from EEG-sensors for a certain set of CC neural nodes that control the behavior of the studied T-object, b_j, $j=\overline{1,n_1+1}$ - components of the phase velocity of propagation of the ANM waves, which are the amplitude characteristics of the wave tremor motion; $S_j^*(\tau,\xi)=\sum_{i=1}^{n_2}\alpha_{ji}S_i(\tau,\xi)$, $\left[\alpha_{ji}\right]$, $j=\overline{1,n_1}$, $i=\overline{1,n_2}$ - an adaptive matrix that determines the connections and feedback-effects of specific CC neuronodules on individual small segments of the ANM-track. The matrix element α_{ji} is a weighting coefficient (from 0 to 1), which determines the integral influence of the i-th neuronode S_i on the j-th segment of motion (determined by machine learning methods based on data mining [13]. The interface conditions (1.3), (1.4) ensure the continuity and integrity of the solution of the problem for the entire multicomponent domain of its definition.

1.3.3. Construction of an analytical solution to the ANM boundary value problem

To construct an analytical solution to the direct heterogeneous problem (1.1) - (1.4), we apply the hybrid integral Fourier transform (HIFT), which we defined in [11]. The transformation is based on hybrid integral operators written in matrix form:

- of direct action:

$$F_{n_1}\left[...\right]=\left[\int_{l_0}^{l_1}...V_1(z,\beta_m)\sigma_1 dz\int_{l_1}^{l_2}...V_2(z,\beta_m)\sigma_2 dz...\int_{l_{n_1-1}}^{l_{n_1}}...V_{n_1}(z,\beta_m)\sigma_{n_1}dz\int_{l_{n_1}}^{l_{n_1+1}}...V_{n_1+1}(z,\beta_m)\sigma_{n_1+1}dz\right], \quad (1.5)$$

- of inverse action:

$$F_{n_1}^{-1}[\ldots]=\begin{bmatrix}\sum\limits_{m=1}^{\infty}\ldots V_1(z,\beta_m)\left(\left\|V(z,\beta_m)\right\|^2\right)^{-1}\\ \sum\limits_{m=1}^{\infty}\ldots V_2(z,\beta_m)\left(\left\|V(z,\beta_m)\right\|^2\right)^{-1}\\ \ldots\ldots\ldots\ldots\ldots\ldots\ldots\ldots\ldots\ldots\\ \sum\limits_{m=1}^{\infty}\ldots V_{n_1+1}(z,\beta_m)\left(\left\|V(z,\beta_m)\right\|^2\right)^{-1}\end{bmatrix}. \qquad (1.6)$$

Here $\left[V_k(z,\beta_m)\right]_{k=\overline{1,n_1+1}}$ - is the vector of the hybrid spectral function defined as follows:

$$\begin{bmatrix}V_1(z,\beta_m)\\ \ldots\\ V_k(z,\beta_m)\\ \ldots\\ V_{n_1+1}(z,\beta_m)\end{bmatrix}=\begin{bmatrix}\prod\limits_{i=1}^{n_1}\xi_{i+1}\dfrac{\beta_m}{b_{i+1}}\left(\omega_0^2(\beta_m)\vartheta_1^{11}\left(\dfrac{\beta_m}{b_1}z\right)-\omega_0^1(\beta_m)\vartheta_1^{21}\left(\dfrac{\beta_m}{b_1}z\right)\right)\\ \ldots\\ \prod\limits_{i=k}^{n_1}\xi_{i+1}\dfrac{\beta_m}{b_{i+1}}\left(\omega_{k-1}^2(\beta_m)\vartheta_k^{11}\left(\dfrac{\beta_m}{b_k}z\right)-\omega_{k-1}^1(\beta_m)\vartheta_k^{21}\left(\dfrac{\beta_m}{b_k}z\right),\ _{k=\overline{2,n_1}}\right)\\ \ldots\\ \omega_{n_1}^2(\beta_m)\vartheta_{n_1+1}^{11}\left(\dfrac{\beta_m}{b_{n_1+1}}z\right)-\omega_{n_1}^1(\beta_m)\vartheta_{n_1+1}^{21}\left(\dfrac{\beta_m}{b_{n_1+1}}z\right)\end{bmatrix}. \qquad (1.7)$$

$\{\beta_m\}_{m=0}^{\infty}$ - the set of spectral values of the GIPF, which are the roots of the transcendental equation:

$$\omega_{n_1}^2(\beta)\vartheta_{n+1}^{11}\left(\frac{\beta}{b_{n_1+1}}l_{n_1+1}\right)-\omega_{n_1}^1(\beta)\vartheta_{n_1+1}^{21}\left(\frac{\beta}{b_{n_1+1}}l_{n_1+1}\right)=0. \qquad (1.8)$$

In the paper [11] it was established that the set of spectral values is a monotonically increasing sequence and coincides with the point + ∞.

On the basis of this, a recurrent technique for calculating the components of the hybrid spectral function of the ANM based on the choice of a system of orthogonal basic functions is proposed; it forms the basis of the proposed hybrid transformation and provides an integral vector solution of the model:

$$\omega_k^j(\beta)=\omega_{k-1}^2(\beta)\psi_{1j}^k\left(\frac{\beta}{b_k}l_k,\frac{\beta}{b_{k+1}}l_k\right)-\omega_{k-1}^1(\beta)\psi_{2j}^k\left(\frac{\beta}{b_k}l_k,\frac{\beta}{b_{k+1}}l_k\right)$$

$$\psi_{ij}^{k}\left(\frac{\beta}{b_k}l_k,\frac{\beta}{b_{k+1}}l_k\right)=\vartheta_k^{i1}\left(\frac{\beta}{b_k}l_k\right)\vartheta_k^{j2}\left(\frac{\beta}{b_{k+1}}l_k\right)-\vartheta_k^{i2}\left(\frac{\beta}{b_k}l_k\right)\vartheta_k^{j1}\left(\frac{\beta}{b_{k+1}}l_k\right),\quad i,j=\overline{1,2},\ k=\overline{1,n_1}$$

$$\vartheta_k^{11}\left(\frac{\beta}{b_s}l_k\right)=\cos\left(\frac{\beta}{b_s}l_k\right),\ \vartheta_k^{21}\left(\frac{\beta}{b_s}l_k\right)=\sin\left(\frac{\beta}{b_s}l_k\right)$$

$$\vartheta_k^{12}\left(\frac{\beta}{b_s}l_k\right)=-\xi_s\frac{\beta}{b_s}\sin\left(\frac{\beta}{b_s}l_k\right),\quad \vartheta_k^{22}\left(\frac{\beta}{b_s}l_k\right)=\xi_s\frac{\beta}{b_s}\cos\left(\frac{\beta}{b_s}l_k\right),\ s\in\{k,k+1\}$$

$$\omega_0^1(\beta)=-\vartheta_0^{11}\left(\frac{\beta}{b_1}l_0\right),\qquad \omega_0^2(\beta)=-\vartheta_0^{21}\left(\frac{\beta}{b_1}l_0\right).$$

$$\sigma_j=\frac{1}{b_j^2},\ j=\overline{1,n_1}.$$

Next, we write the system of equations (1.1) and conditions (1.2) of the boundary value problem (1.1) - (1.4) in the matrix form:

$$\begin{bmatrix}\left(\frac{\partial^2}{\partial t^2}-b_1^2\frac{\partial^2}{\partial z^2}\right)u_1(t,z)\\ \left(\frac{\partial^2}{\partial t^2}-b_2^2\frac{\partial^2}{\partial z^2}\right)u_2(t,z)\\ \ldots\ldots\ldots\ldots\ldots\ldots\ldots\ldots\\ \left(\frac{\partial^2}{\partial t^2}-b_{n_1+1}^2\frac{\partial^2}{\partial z^2}\right)u_{n_1+1}(t,z)\end{bmatrix}=\begin{bmatrix}S_1(t,z)\\ S_2(t,z)\\ \ldots\ldots\\ S_{n_1+1}(t,z)\end{bmatrix},\quad \begin{bmatrix}u_1(t,z)\\ u_2(t,z)\\ \ldots\ldots\\ u_{n_1+1}(t,z)\end{bmatrix}\Bigg|_{t=0}=0,\quad \frac{\partial}{\partial t}\begin{bmatrix}u_1(t,z)\\ u_2(t,z)\\ \ldots\ldots\\ u_{n_1+1}(t,z)\end{bmatrix}\Bigg|_{t=0}=0 \tag{1.9}$$

Applying to problem (1.9) the direct-action HIFT integral operator F_{n_1} (1.5), where $F_{n_1}\left[L_{n_1}[(z)]\right]=-\beta_m^2u_m$ $L_{n_1}[...]=\sum_{j=1}^{n_1+1}b_j^2\theta\left(z-l_{j-1}\right)\theta\left(l_j-z\right)\frac{d^2}{dz^2}$ - hybrid Fourier differential operator, θ - is the Heaviside step unit function, we obtain the Cauchy problem:

$$\left(\frac{d^2}{dt^2}+\beta_m^2\right)u_m(t)=S_m^*(t);\qquad u_m(t)\big|_{t=0}=0,\qquad \frac{d}{dt}u_m(t)\big|_{t=0}=0,$$

whose solution is the function [11, 12]

$$u_m(t)=\int_0^t\frac{\sin\beta_m(t-\tau)}{\beta_m}S_m^*(\tau)\,d\tau \tag{1.10}$$

Applying to (1.10) the inverse integral HIFT operator $F_{n_1}^{-1}$ (1.6), after transformations, we obtain a unique solution to the homogeneous boundary value problem of ANM (1.1) - (1.4)

$$u_j(t,z)=\sum_{k=1}^{n_1+1}\int_0^t\int_{l_{k-1}}^{l_k} \mathrm{H}_{jk}(t-\tau,z,\xi)S_k^*(\tau,\xi)\sigma_k d\xi d\tau, \qquad j=\overline{1,n_1+1}. \tag{1.11}$$

Here, the impact matrix is the response of the ANM system to the influence of the *k*-th segment of the resulting action of signals, S_k^* - a certain set of CC neural nodes on the j-segment of the ANM track:

$$\mathrm{H}_{jk}(t,z,\xi)=\sum_{m=1}^{\infty}\frac{\sin\beta_m t}{\beta_m}\frac{V_j(z,\beta_m)V_k(\xi,\beta_m)}{\left\|V(z,\beta_m)\right\|^2}; j,k=1,\overline{n+1} \tag{1.12}$$

1.4 Identification of ANM amplitude components. Inverse heterogeneous boundary value problem taking into account the cognitive feedback influences of the neuro-nodes of the CC

1.4.1. Choice of residual functional

It is assumed that the amplitude components of the phase velocity of propagation of the ANM wave b_k, $k=\overline{1,n_1+1}$ boundary value problem (1.1) - (1.4) are unknown functions of time. However, on the surfaces of the regions $\gamma_k\subset\Omega_k$, $k=\overline{1,n_1+1}$ of anheterogeneous media, traces of solutions (trajectories of the ANM) are as follows:

$$u_k(t,z)\big|_{\gamma_k}=U_{l_k}(t,z)\big|_{\gamma_k} \tag{1.13}$$

Thus, we have obtained problem (1.1) - (1.4), (1.13), which consists in finding the functions b_k, $k=\overline{1,n_1+1}\in D$,

where $D=\left\{\nu(t,z):\ \nu\big|_{\Omega_{k_T}}\in C\left(\Omega_{k_T}\right),\ \nu>0,\ k=\overline{1,n_1+1}\right\}$.

The residual functional, which determines the deviation of the desired decoupling from the traces of the decoupling, obtained empirically on surfaces γ_k, can be written as follows:

$$J(b_k)=\frac{1}{2}\int_0^T\sum_{k=1}^{n+1}\left\|u_{s_k}(\tau,z,b_k)-U_k^*\right\|^2_{L_2(\gamma_k)}\sigma_k\,d\tau \quad , \tag{1.14}$$

where $\|\varphi\|^2_{L_2(\gamma_k)}=\int_{\gamma_k}\varphi^2 d\gamma_k$ – squared norm. In this case $\|\varphi\|_{L_2(\gamma_k)}=\left|\varphi(t,z)\right|_{z=\gamma_k}$.

1.4.2. The problem of the ANM amplitude parameters functional identification

Problem (1.1) - (1.4) due to the need to present it for its solution in the form of the implementation of the procedure for functional identification of the amplitude components of the phase velocity of propagation of the ANM b_k^2, $k = \overline{1, n_1 + 1}$ as a function of time and conditions, known decoupling traces for each sufficiently thin *k*-th segment, $k = \overline{1, n_1 + 1}$, is transformed into a direct boundary value problem (1.15) - (1.17) as a system of homogeneous initial boundary value problems for successive thin segments of the ANM:

$$\frac{\partial^2}{\partial t^2} u_k(t,z) = b_k^2 \frac{\partial^2}{\partial z^2} u_k + S_k^*(t,z) \tag{1.15}$$

with initial conditions:

$$u_k(t,z)\big|_{t=0} = 0, \qquad \frac{\partial u_k}{\partial t}\bigg|_{t=0} = 0, \ k = \overline{1, n_1 + 1} \tag{1.16}$$

Boundary conditions on each of the thin segments of the ANM on *Z* coordinate*:*

$$u_{k-1}(t,z)\big|_{z=l_{k-1}} = U_{L_{l_{k-1}}}, \qquad u_k(t,z)\big|_{z=l_k} = U_{l_k}, \ k = \overline{1, n_1 + 1} \tag{1.17}$$

Choice of residual functional. It is assumed that the components of the phase velocity of propagation of the ANM wave b, $k = \overline{1, n_1 + 1}$ of the boundary value problem (1.15) - (1.17) are unknown functions of time. With known values of the pen position $u_k(t,z)$ at observation points on segments of the ANM $\gamma_k \subset \Omega_k$, $k = \overline{1, n_1 + 1}$

$$u_k(t,z)\big|_{\gamma_k} = U_{l_k}(t,z)\big|_{\gamma_k} \tag{1.18}$$

the initial-boundary value problem (1.15) - (1.17) can be considered for each point *z* for each thin k_1-th segment of the ANM trace and will consist in finding the functions $b_k \in D$, where $D = \left\{ \nu(t,z) : \ \nu\big|_{\Omega_{k_1 T}} \in C\left(\Omega_{k_1 T}\right), \ \nu > 0, \ k = \overline{1, n_1 + 1} \right\}$.

The residual functional of the deviation of the solution from its traces on $\gamma_{k_1} \in \Omega_{k_1}$, due to [13, 20] can be obtained as follows:

$$J_k\left(b_{kk}\right)=\frac{1}{2}\int_0^T\left(\left\|u_k\left(t,z,b_{\mathrm{k}}\right)-U_k^*\right\|^2\right)dt \tag{1.19}$$

1.4.3. Method for solving direct boundary of identification value problem

The construction and mathematical substantiation of the solution to the problem is carried out by using the finite integral Fourier transform [11, 12]. Applying the integral operators [12] to problem (1.15) - (1.17):

$$F\left[u_k\left(t,z\right)\right]=\int_{k-1}^{l_k}u_k\left(t,z\right)V_m\left(\beta_m,z\right)dz\equiv U_{km}(t)\ ,$$

$$F^{-1}\left[U_{km}\left(t\right)\right]=\sum_{m=0}^{\infty}U_{\mathrm{km}}\left(t\right)\frac{V_m\left(\beta_m,z\right)}{\left\|V_m\left(\beta_m,z\right)\right\|^2}\equiv u_k\left(t,z\right)\ , \tag{1.20}$$

$$F\left[\frac{\partial^2}{\partial^2 z}u_k\left(t,z\right)\right]=-\beta_m^2U_{km}(t)+\beta_mU_{l_{k-1}}\left[1-\left(-1\right)^m\frac{U_{l_k}}{U_{l_{k-1}}}\right]=-\beta_m^2U_{km}(t)+\beta_mU_{l_{k-1}}-\beta_m\left(-1\right)^mU_{l_k}$$

,

$$V_m\left(\beta_m,z\right)=\sin\beta_m\left(z-l_{k-1}\right)\ ,\ \beta_m=\frac{m\pi}{\Delta h}\ ,\qquad \left\|V_m\right\|^2=\int_{l_{k-1}}^{l_k}\left[V_m\left(\beta_m,z\right)\right]^2dz=\frac{\Delta l}{2}\ ,$$

the Cauchy problem is obtained:

$$\frac{d^2}{dt^2}U_{km}\left(t,z\right)=-b_k^2\beta_m^2U_{km}(t)+b_k^2\beta_mU_{l_{k-1}}\left[1-\left(-1\right)^m\frac{U_{l_k}}{U_{l_{k-1}}}\right]+S_{km}^*\left(t\right) \tag{1.21}$$

$$u_{km}\left(t,z\right)\Big|_{t=0}=0,\ \frac{\partial u_{km}}{\partial t}\Big|_{t=0}=0,k=\overline{1,n_1+1}\ . \tag{1.22}$$

The unique solution to the Cauchy problem (1.21), (1.22) has the form:

$$U_{km}\left(t\right)=\int_0^t\frac{\sin b_k\beta_m\left(t-\tau\right)}{b_k\beta_m}\left[S_{km}^*\left(\tau\right)+b_k^2\beta_m\left(U_{l_{k-1}}-\left(-1\right)^mU_{l_k}\right)\right]d\tau \tag{1.23}$$

Passing to the originals in (1.23), we obtain a unique solution to the original boundary value problem (1.15) - (1.17) in the classical form [12].

$$u_k\left(t,z\right)=\int_0^t\int_{l_{k-1}}^{l_k}\mathrm{H}_k^1\left(t-\tau,z,\xi\right)S_k^*\left(\tau,\xi\right)d\xi d\tau+\int_0^t\left(\mathrm{H}_k^{21}\left(t-\tau,z,l_{k-1}\right)U_{l_{k-1}}-\mathrm{H}_k^{22}\left(t-\tau,z,l_k\right)U_{l_k}\right)d\tau\ . \tag{1.24}$$

Here, the components of the influence vectors have the form:

$$\mathrm{H}_k^1\left(t-\tau,z,\xi\right)=\frac{2}{\Delta h}\sum_{m=0}^{\infty}\frac{\sin b_k\beta_m\left(t-\tau\right)}{b_k\beta_m}\sin\beta_m\left(\xi-l_{k-1}\right)\sin\beta_m\left(z-l_{k-1}\right)$$

$$\mathrm{H}_k^{21}\left(t,z,l_{k-1}\right)=\frac{2b_k}{\Delta h}\sum_{m=0}^{\infty}\sin b_k\beta_m t\sin\beta_m\left(z-l_{k-1}\right) \tag{1.25}$$

$$\mathrm{H}_k^{22}\left(t,z,l_k\right)=\frac{2b_k}{\Delta h}\sum_{m=0}^{\infty}\sin\left(b_k\beta_m t\right)\left(-1\right)^m\sin\beta_m\left(z-l_{k-1}\right).$$

Solution (1.24) to the problem (1.15) - (1.17) after a series of transformations is converted into a form convenient and efficient for numerical iterative calculations and for use in the procedures for identifying parameters. After integrating and substituting specific expressions for the influence functions and a number of transformations, formulas (1.25) are reduced to ordinary algebraic expressions convenient for the identification procedure, the need to use iterations at this stage of the regularization of identification process is eliminated, significantly intensifying it as a whole. So, after integration we obtain:

$$S_k^*\int_0^t\int_{l_{k-1}}^{l_k}\mathrm{H}_k^{11}\left(t-\tau,z,\xi\right)d\xi d\tau=\frac{2}{\Delta h}S_k^*\sum_{m=\dot{a}}^{\infty}\frac{1-\cos\left(b_k\beta_m t\right)}{\left(b_k\beta_m\right)^2}\frac{1}{\beta_m}\left(\left(-1\right)^m-1\right)\sin\beta_m\left(z-l_{k-1}\right)$$

$$U_{l_{k-1}}\int_0^t\mathrm{H}_k^{21}\left(t,z,l_{k-1}\right)d\tau=U_{l_{k-1}}\frac{2}{\Delta h}\sum_{m=0}^{\infty}\frac{1-\cos\left(b_k\beta_m t\right)}{\beta_m}\sin\beta_m\left(z-l_{k-1}\right) \tag{1.26}$$

$$U_{l_k}\int_0^t\mathrm{H}_k^{22}\left(t,z,l_{k-1}\right)d\tau=U_{l_k}\frac{2}{\Delta h}\sum_{m=0}^{\infty}\left(-1\right)^m\frac{1-\cos\left(b_k\beta_m t\right)}{\beta_m}\sin\beta_m\left(z-l_{k-1}\right).$$

After substituting expressions (1.26) into (1.24), we finally obtain:

$$u_k\left(t,z\right)=\frac{2}{\Delta h}\sum_{m=0}^{\infty}\frac{1-\cos\left(b_k\beta_m t\right)}{\beta_m}\sin\beta_m\left(z-l_{k-1}\right)\left(S_k^*\frac{1}{\left(b_k\beta_m\right)^2}\left(\left(-1\right)^m-1\right)+U_{l_{k-1}}\left(1-\left(-1\right)^m\frac{U_{l_k}}{U_{l_{k-1}}}\right)\right) \tag{1.27}$$

1.5 Initial-boundary value problems accompanying algorithms for identifying parameters in the ANM

1.5.1. Initial-boundary value problems for increments

Taking into account the increments in the identification parameters of the ANM $b_k^{2n}+\Delta b_k^n$ based on problem (1.1) - (1.4), we obtain the corresponding increments v_{s_k} for motion components on path segments u_k+v_k. Neglecting the terms of the second order of smallness, for the increments we obtain the following initial-boundary value problem [12]:

$$\frac{\partial^2}{\partial t^2} v_k(t,z) = \frac{\partial}{\partial z}\left(b_{\mathrm{k}}^n \frac{\partial}{\partial z} v_k \right) + \Delta b_{\mathrm{k}}^n \frac{\partial^2}{\partial z^2} u_k, \ z \in \Omega_{k_T}, k = \overline{1, N_1 + 1} \qquad (1.28)$$

with initial conditions:

$$v_k(t,z)_{t=0} = 0, \qquad \frac{\partial}{\partial t} v_k(t,z)_{t=0} = 0, \ z \in \Omega_k, \quad k = \overline{1, N_1 + 1}, \qquad (1.29)$$

boundary and interface conditions between the ANM segments by *z* coordinate:

$$\frac{\partial}{\partial z} v_1(t,z)_{z=0} = 0 \ , \qquad \frac{\partial}{\partial z} v_{N_1+1}(t,z)_{z=l} = 0, \ t \in (0,T) \ ,$$

$$\left[v_k(t,z) - v_{k+1}(t,z) \right]\Big|_{z=l_k} = 0, \qquad (1.30)$$

$$\left(b_{\mathrm{k}}^{2n} \frac{\partial}{\partial z} v_k(t,z) + \Delta b^n_{\ \mathrm{k}} \frac{\partial}{\partial z} u_k(t,z) - b_{\mathrm{k+1}}^{2n} \frac{\partial}{\partial z} v_{k+1}(t,z) - \Delta b^n_{\ \mathrm{k+1}} \frac{\partial}{\partial z} u_{k+1}(t,z) \right)\Big|_{z=l_k} = 0, \ k = \overline{1, n_1}$$

$$\left(\left(b_{\mathrm{k}}^{2n} + \Delta b^n_{\ \mathrm{k}} \right) \frac{\partial}{\partial z} \left(u_k(t,z) + v_k(t,z) \right) - \left(b_{\mathrm{k+1}}^{2n} + \Delta b^n_{\ \mathrm{k+1}} \right) \frac{\partial}{\partial z} \left(u_{k+1}(t,z) + v_{k+1}(t,z) \right) \right)\Big|_{z=l_k} -$$

$$- \left(b_{\mathrm{k}}^{2n} \frac{\partial}{\partial z} u_k(t,z) - b_{\mathrm{k+1}}^{2n} \frac{\partial}{\partial z} u_{k+1}(t,z) \right)\Big|_{z=l_k} = 0, \ k = \overline{1, \mathrm{n}_1}$$

1.6 Statement and methodology for the conjugate boundary value problem solving

1.6.1. Problem statement in general

Taking into account the above considerations, in accordance with the original direct initial-boundary value problem (1.1) - (1.4), according to [12, 21] for each approximation $\tilde{b}_k^n = b_k^{2n}$ of the solution $\tilde{b}_k = b_k^2$ the conjugate time-boundary value problem is considered:

$$\frac{\partial^2}{\partial t^2} \phi_k(t,z) + b_k^2 \frac{\partial^2}{\partial z^2} \phi_k(t,z) = \left(u_{k_k}^n - U_k^* \right)\Big|_{z=\gamma_k} \delta(z - \gamma_k), \quad k = \overline{1, n_1 + 1} \ . \qquad (1.31)$$

Initial conditions at $t = T$

$$\phi_{\ k}(t,z)_{|t=T} = 0 \ ; \qquad (1.32)$$

boundary and interface conditions between thin ANM segments along the coordinate z*:*

$$\frac{\partial}{\partial z}\phi_1(t,z)_{|z=0}=0;\ \frac{\partial}{\partial z}\phi_{n_1+1}(t,z)_{|z=l}=0,\ t\in(0,T)\ ;$$

$$\left[\phi_k(t,z)-\phi_{k+1}(t,z)\right]_{z=l_m}=0\ , \tag{1.33}$$

$$\left(b_k^2\frac{\partial}{\partial z}\phi_k(t,z)-b_{k+1}^2\frac{\partial}{\partial z}\phi_{k+1}(t,z)\right)\Big|_{z=l_k}=0,\ k=\overline{1,n_1}\ .$$

Construction of an analytical solution to the conjugate time-boundary value problem. To construct analytical solutions to the conjugate heterogeneous time-boundary value problem of parametric identification (1.31) - (1.33), we used the approach described above to the direct problem using the introduced integral transform [12]. As a result, we obtain

$$\phi_{1_k}(t,z)=\int_t^T\sum_{k_1=1}^{n+1}\int_{l_{k_1-1}}^{l_{k_1}}\bar{\mathrm{H}}_{k,k_1}(t-\tau,z,\xi)\left(u_{k_1}^n-U_{k_1}^*\right)(\tau)\Big|_{z=\gamma_{k_1}}d\xi d\tau\ , \tag{1.34}$$

where $\bar{\mathrm{H}}_{jk}(t,z,\xi)=\sum_{m=1}^{\infty}\frac{\mathrm{sh}\,\beta_m t}{\beta_m}\frac{V_j(z,\beta_m)V_k(\xi,\beta_m)}{\left\|V(z,\beta_m)\right\|_1^2};\ j,k=\overline{1,n_1+1}$ – ANM conjugate influence matrix.

1.7 Statement and methodology for solving conjugate initial-boundary value problems of functional identification of the ANM

Taking into account the above considerations, in accordance with the original boundary value problem of functional identification (1.15) - (1.17), based on [12, 21] and provided that the traces of the decoupling are known for each sufficiently thin k-th segment of the trajectory, $k=\overline{1,n_1+1}$, can be transformed into the adjoint boundary value problem (1.31) - (1.33) into a system of conjugate homogeneous time-boundary value problems of functional identification for successive thin segments of the ANM:

$$\frac{\partial^2}{\partial t^2}\phi_k(t,z)+b_k\frac{\partial^2}{\partial z^2}\phi_k(t,z)=\left(u_{k_k}^n-U_k^*\right)\Big|_{z=\gamma_k}\delta(z-\gamma_k),\quad k=\overline{1,n_1+1} \tag{1.35}$$

with initial conditions at $t=T$:

$$\phi_k(t,z)_{|t=T}=0 \tag{1.36}$$

and boundary conditions of the first kind for each approximation b_k^n, in the solution:

$$\phi_k(t,z)\big|_{z=l_{k-1}} = 0; \quad \phi_k(t,z)\big|_{z=l_k} = 0 \ . \tag{1.37}$$

Analytical solution to the conjugate time-boundary value problem of functional identification.

Applying the finite integral Fourier transform defined by integral operators (1.38) [12] to problem (1.35) - (1.37), we obtain the Cauchy problem:

$$\frac{d^2}{dt^2}\phi_{km}(t,z) - b_k^2\beta_m^2\phi_{km}(t) = \mathrm{F}_{km}(t) \tag{1.38}$$

with initial conditions:

$$\phi_k(t,z)\big|_{t=T} = 0, \ \frac{\partial\phi_k}{\partial t}\bigg|_{t=T} = 0, \ k = \overline{1, n_1+1}. \tag{1.39}$$

We obtain a unique solution to the Cauchy problem (1.38), (1.39):

$$\phi_{km}(t) = \int_t^T \frac{\mathrm{sh}\, b_k\beta_m(t-\tau)}{b_k\beta_m}\mathrm{F}_{km}(\tau)\,d\tau, \tag{1.40}$$

where $\mathrm{F}_{km}(t) = \left(u_{k_k}^n - U_k^*\right)\big|_{z=\gamma_k}\delta(z-\gamma_k)$, which results in

$$\phi_{km}(t) = \int_\tau^T \frac{\mathrm{sh}\, b_k\beta_m(t-\tau)}{b_k\beta_m}\left(u_{k_k}^n - U_k^*\right)\big|_{z=\gamma_k}(\tau)\delta(z-\gamma_k)_m\,d\tau, \ k = \overline{1, n_1+1}\ .$$

Passing to the originals in (1.40), we obtain a unique solution to the conjugate boundary value problem (1.35) - (1.37) in the classical form [12]:

$$\phi_k(t,z) = \int_t^T\int_{l_{k-1}}^{l_k} \bar{\mathrm{H}}_k(t-\tau,z,\xi)\left(u_{k_k}^n - U_k^*\right)\big|_{z=\gamma_k}(\tau)\delta(\xi-\gamma_k)\,d\xi\,d\tau, \ k = \overline{1, n_1+1}\ . \tag{1.41}$$

Here the components of the influence matrix $\left[\bar{\mathrm{H}}_k(t,z,\xi)\right]$, $k = \overline{1, n_1+1}$ are as follows:

$$\bar{\mathrm{H}}_k(t-\tau,z,\xi) = \frac{2}{\Delta h}\sum_{m=0}^{\infty}\frac{\mathrm{sh}\, b_k\beta_m(t-\tau)}{b_k\beta_m}\sin\beta_m(\xi-l_{k-1})\sin\beta_m(z-l_{k-1})\ . \tag{1.42}$$

Solution (1.41) to problem (1.35) - (1.37) after a series of transformations is converted in a form convenient and efficient for numerical iterative calculations for use in the procedures for identifying parameters. Substituting (1.42)

$$\phi_k(t,z)=\int_t^T\int_{l_{k-1}}^{l_k}\frac{2}{\Delta h}\sum_{m=0}^{\infty}\frac{\mathrm{sh}\,b_k\beta_m(t-\tau)}{b_k\beta_m}\sin\beta_m(\xi-l_{k-1})\sin\beta_m(z-l_{k-1})\left(u_{k_k}^n-U_k^*\right)\Big|_{z=\gamma_k}(\tau)\delta(z-\gamma_k)\,d\xi d\tau, k=\overline{1,n_1+1}$$

after integration we finally obtain:

$$\phi_k(t,z)=\frac{2}{\Delta h}\sum_{m=0}^{\infty}\frac{1-\mathrm{ch}\left(b_k\beta_m(T-t)\right)}{\left(b_k\beta_m\right)^2}\sin\beta_m\gamma_k\sin\beta_m(z-l_{k-1})\left(U_k^*-u_{k_k}^n\right),\ k=\overline{1,n_1+1}\,. \qquad (1.43)$$

1.8 Expressions for gradient components and regularization expressions

Expressions for gradient components. According to [12, 21], we obtain analytical expressions for the components of the gradients of the residual functional:

$$\nabla J_{\tilde{b}_k}=\int_0^T\int_{l_{k-1}}^{l_k}\phi_k(t,z)\frac{\partial^2}{\partial z^2}u_k(t,z)dzdt\ . \qquad (1.44)$$

For the functional identification problem, according to [11, 21], we obtain the following formulas for the components of the gradients of the residual functional:

$$\nabla J_{\tilde{b}_k}(t)=\int_{l_{k-1}}^{l_k}\phi_k(t,z)\frac{\partial^2}{\partial z^2}u_k(t,z)dz\ , \qquad (1.45)$$

$$\phi_k(t,z)=\frac{2}{\Delta h}\sum_{m=0}^{\infty}\frac{1-\mathrm{ch}\left(b_k\beta_m(T-t)\right)}{\left(b_k\beta_m\right)^2}\sin\beta_m\gamma_k\sin\beta_m(z-l_{k-1})\left(U_k^*-u_{k_k}^n\right),\ k=\overline{1,n_1+1}$$

$$u_k(t,z)=\frac{2}{\Delta h}\sum_{m=0}^{\infty}\frac{1-\cos\left(b_k\beta_m t\right)}{\beta_m}\sin\beta_m(z-l_{k-1})\left(S_k^*\frac{1}{\left(b_k\beta_m\right)^2}\left((-1)^m-1\right)+U_{l_{k-1}}\left(1-(-1)^m\frac{U_{l_k}}{U_{l_{k-1}}}\right)\right)$$

$$\frac{\partial^2}{\partial z^2}u_k(t,z)=-\frac{2}{\Delta h}\sum_{m=0}^{\infty}\beta_m\left(1-\cos\left(b_k\beta_m t\right)\right)\sin\beta_m(z-l_{k-1})\left(S_k^*\frac{1}{\left(b_k\beta_m\right)^2}\left((-1)^m-1\right)+U_{l_{k-1}}\left(1-(-1)^m\frac{U_{l_k}}{U_{l_{k-1}}}\right)\right)$$

Regularization expressions for the n+1 th step of defining the identifying functional dependency. According to [20, 21], using the method of minimum errors to determine the dependence of the identification of the amplitude components of the phase velocity of propagation of the ANM wave $\tilde{b}_k^{n+1}$ on time for each k-th element of the ANM $k=\overline{1,n_1+1}$, we obtain:

$$\tilde{b}_k^{n+1}(t)=\tilde{b}_k^n(t)-\nabla J_{b_k}^n(t)\frac{\left\|u_k^n\left(t,\gamma_k,\tilde{b}_k^n\right)-U_k^*\right\|^2}{\left\|\nabla J_{b_k}^n(t)\right\|_{\gamma_k}^2},\ t\in(0,T),\ k=\overline{1,n_1}\ .\quad(1.46)$$

Spatial visualization of the results of digital analysis of the ANM trajectory of the T-object. In Fig 1.5 the results of a digital analysis of abnormal neurological violent movements performed by the tip of an electronic pen on an electronic tablet along the circumference of the testing template (Archimedean spiral) by the hand of a patient with severe signs of tremor (T-object) are shown.

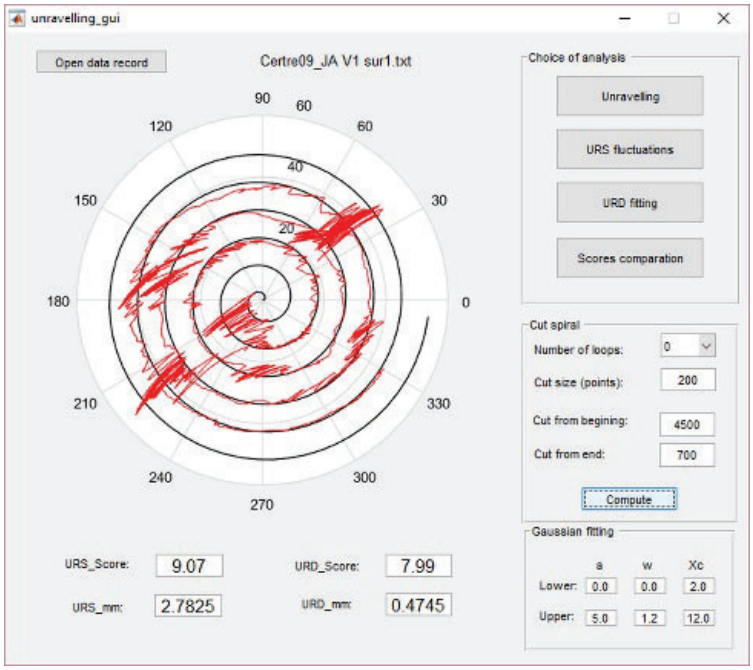

Figure 1.5. Results of digital analysis of highly fluctuating ANM movements performed by the tip of an electronic pen on an electronic tablet along the circumference of the Archimedean spiral by the hand of a patient with strong signs of tremor

As can be seen in Fig. 1.6., such movements are highly heterogeneous; moreover, they contain many areas with abnormal movements with high amplitude and frequency characteristics. For better visualization of the graph describing the trajectory of the ANM of the T-object, a temporal-spatial format is shown in Fig. 1.5, where

sections of the trajectories of abnormal oscillating movements are clearly visible, depending on time, and highly variable in small intervals of time (Fig. 1.6).

Such sections of ANM movements can be studied in more detail by dividing them into separate segments according to the studied time interval, by establishing the dependence of their real amplitude and frequency characteristics on the integral time distributions of cognitive signals of the CC nodes.

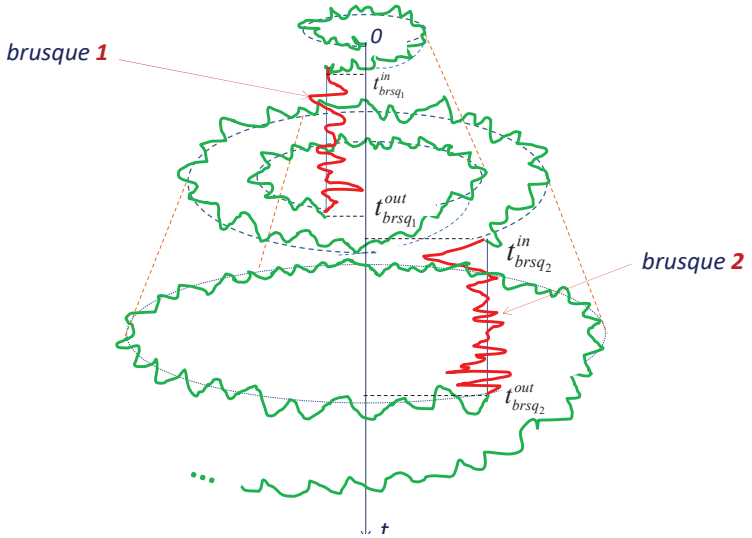

Figure 1.6. Temporal-spatial visualization of the ANM of the T-object, with the inclusion of segments of highly vibrational abnormal movements dependent on time in small time intervals

A useful and effective way to analyze the obtained results is the ability to perform cyclic calculations based on a proportional reduction in the analyzed data sets. In other words, the estimates are obtained and compared for each iteration of the analyzed data constraint. The results, presented in the form of frequency and amplitude characteristics of the curve, form the basis for assessing the patient's condition by the method of computerized diagnostics. Important elements of development are algorithms for obtaining the values of the parameters of the simulated system, the ability to visually represent the results obtained, the need for dynamic setting of the system parameters. All this makes it possible to present the

results with greater visibility and contributes to the targeted use of technology. An effective solution and a positive element of this development is its implementation as a separate module, a library with the ability to constantly update methods and maintain the relevance of research. The implementation of software in this way contributes to an increase in adaptability, ease of use in various systems during research. Mathematical methods, namely their calculation algorithms, are implemented as a set of classes with methods that simulate behavior. Software modules, classes, and their interaction are implemented as a single library module, which will allow flexible use of the input data analysis method in various applied tasks and programs.

By using the built-in 3D microaccelerometer module in the digital pen of a graphics tablet, the condition for maintaining the existing satisfactory measurement accuracy with the additional ability to control the separation of the pen from the surface (Z axis) is provided.

1.9 Modeling and identification of parameters of complex multicomponent non-bio-feedback systems on multicore computers

Within the framework of the set task of identifying cognitive feedback EEG on the ANM-trajectory was developed using the developed hybrid ANM model taking into account the feedback effects of EEG signals. To set up the identification model, a fragment of the ANM trace of the investigated T-object was used according to Fig.1.7.

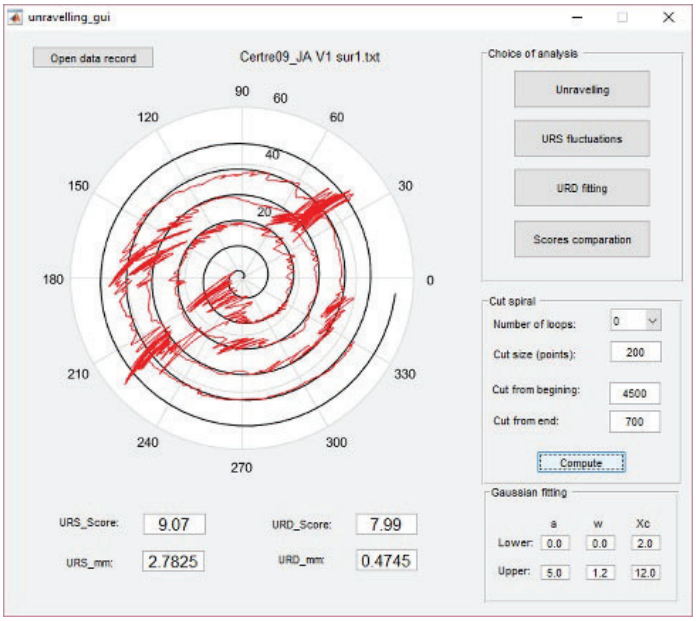

Figure 1.7. ANM-trace of the spiral type, made by the patient on the tablet

The corrected fragment of this spiral example in the number of discretized 4000 points-trace positions is shown in Fig.1.8. Here the abscissa is the position numbers of the deflection of the feather from equilibrium during the passage of the spiral pattern.

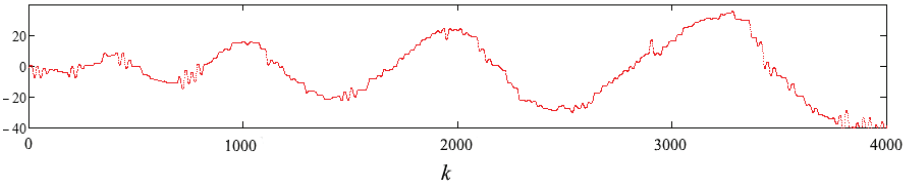

Figure 1.8. Expanded spiral type ANM track

To test the model and adjust the model trace, a test sample of EEG (signals of a hypothetical neuro node of CC (cerebral cortex)) was used according to Fig.1.9.

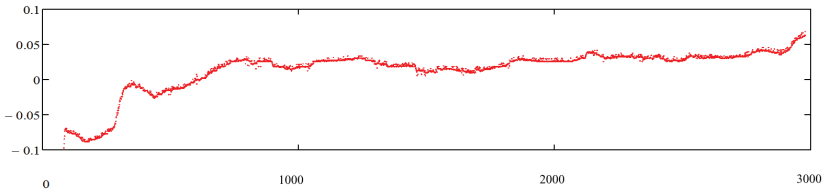

Figure 1.9. Test distribution of EEG signals that cognitively affect the movement of the pen during the entire time of movement of the pen when drawing a fragment of the ANM.

Here the times are proportionally compared and given in accordance with the length of the ANM fragment of the T-object. Setting up the ANM model track and its step-by-step and segment-by-segment identification (amplitude and frequency parameters for each segment, taking into account the integrity of the system) to a specific sample of the path performed by the patient (observation curve or experimental curve) was carried out according to the feedback scheme and analytical solutions to the hybrid model of the ANM-trace (Fig. 1.7, Fig. 1.10).

$$\begin{bmatrix} u_1(t,z) \\ \dots \\ u_j(t,z) \\ \dots \\ u_{n+1}(t,z) \end{bmatrix} = \int_0^t \begin{bmatrix} \int_{l_0}^{l_k} \mathrm{Hh}_{11}(t-\tau,z,\xi) & \dots & \int_{l_n}^{l_{n+1}} \mathrm{Hh}_{1,n_1+1}(t-\tau,z,\xi) \\ \dots & \dots & \dots \\ \int_{l_0}^{l_k} \mathrm{Hh}_{j1}(t-\tau,z,\xi) & \dots & \int_{l_n}^{l_{n+1}} \mathrm{Hh}_{j,n+1}(t-\tau,z,\xi) \\ \dots & \dots & \dots \\ \int_{l_0}^{l_k} \mathrm{Hh}_{n+1,1}(t-\tau,z,\xi) & \dots & \int_{l_n}^{l_{n+1}} \mathrm{Hh}_{n_1+11,n_1+1}(t-\tau,z,\xi) \end{bmatrix} \cdot \begin{bmatrix} S_1(\tau,\xi) \\ \dots \\ S_i(\tau,\xi) \\ \dots \\ S_n(\tau,\xi) \end{bmatrix} d\xi d\tau$$

ETG

EEG

feedback

Figure 1.10. ANM trace model with feedback

The results of testing the model are presented in the graphs, which are given below. At first, we took a relatively small number of points in an attempt to recreate the profile of the observation curve (profile of the ANM trace made by the patient taking into account the picture of the feedback-effects curve of the test EEG (Fig.1.9).

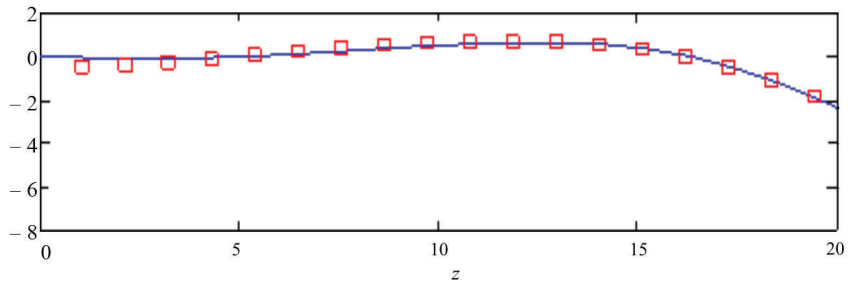

Figure 1.11. Comparative analysis of the model ANM trace (blue solid line) and the real patient trace (red squares) for the first 20 points of the trace.

As can be seen in Fig. 1.11, the accuracy of the coincidence of the model path and the real path of the patient is very high (up to 1.5-2%) for 20 observation points. Amplitude and frequency characteristics due to the hybrid spectral function built by us, systemically for all division segments (taking into account their connectivity, and not each separately), made it possible to obtain almost complete coincidence of the model track with the real track of the patient. Then we gradually increased the number of track points. For the number of points 50, the results turned out to be practically the same (Fig. 1.11).

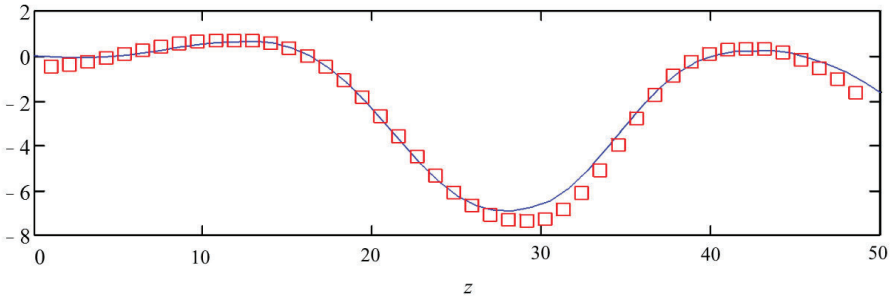

Figure 1.12. Analysis of the model track ANM (blue solid line) and the real patient path (red squares) for the first 50 points of the path

Then the number of points gradually increased to 50, 100, 500, 1000, 2000 and 4000 and the behavior of the model curve was studied, evaluating its possible deviations from the experimental ANM of the patient's trace (Fig. 1.11-1.17).

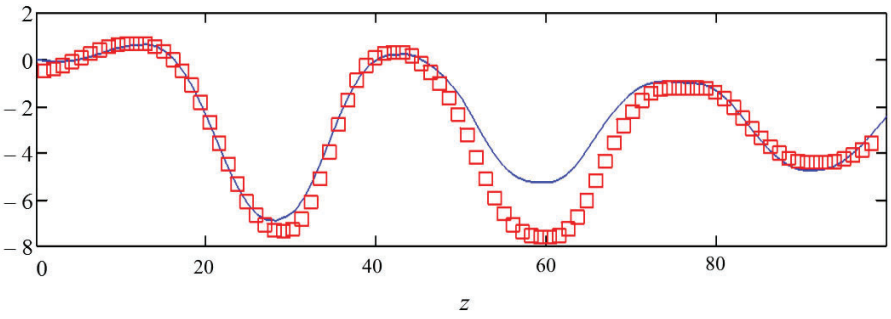

Figure 1.13. Analysis of the model ANM trace (blue solid line) - and the real patient trace (red squares) for the first 100 points of the trace

In Fig. 1.13, for a segment of 100 points, we observe a slight deviation in the saddle zone in circle 60 of that point of the track at 5-7%. However, this problem can be solved technically by making the route segmentation in this zone smaller. By the way, the model itself allows for arbitrary partitioning with arbitrary sizes of each segment and making them as small as necessary. Here, all the graphs on the abscissa axes for the sake of compactness show the relative values of the number of track points (for example, Number 1 corresponds to the 100th track point, 5 to the 500th, 0.2 to the twentieth position, etc.).

A positive point is that for all other graphs with an increasing number of points up to 500, 1000, 2000 and 4000 (Fig. 1.14 -1.17), we also have a high degree of accuracy of coincidence of the model and experimental curves, which provides a high-level reproduction of the amplitude-frequency characteristics of the AMR trace (the frequency of the model curves almost completely corresponds to the frequency of the curves made by the patient). With an increase in the number of points under study in individual saddle or ridge points, the deviations of the amplitude characteristics slightly increase. But, as noted, these deflections can always be reduced by choosing a finer partition in these zones.

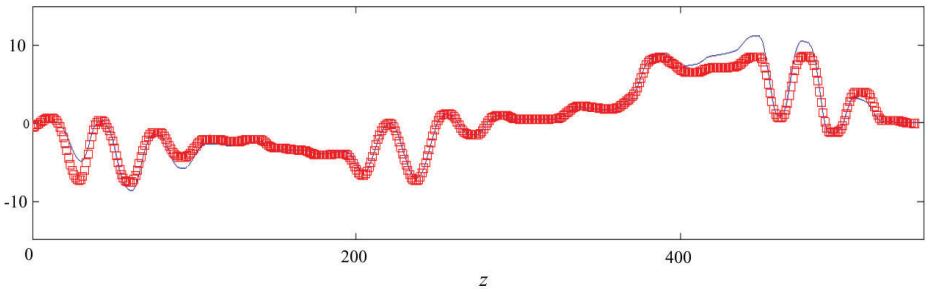

Figure 1.14. Analysis of the simulated ANM trace (blue solid line) and the real patient trace (red lines / squares) for the first 500 trace points

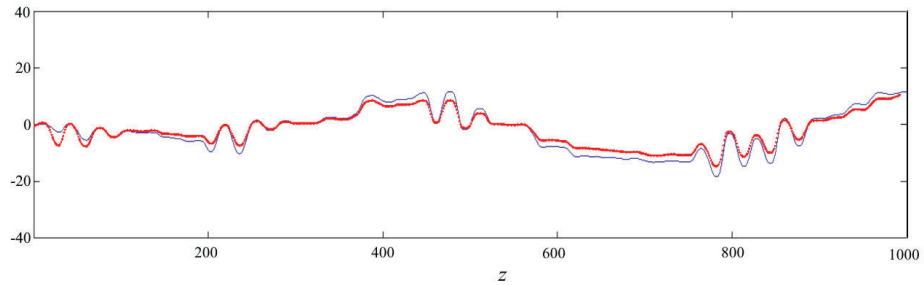

Figure 1.15. Analysis of the simulated ANM trace (blue solid line) and the real patient trace (red lines / squares) for the first 1000 trace points

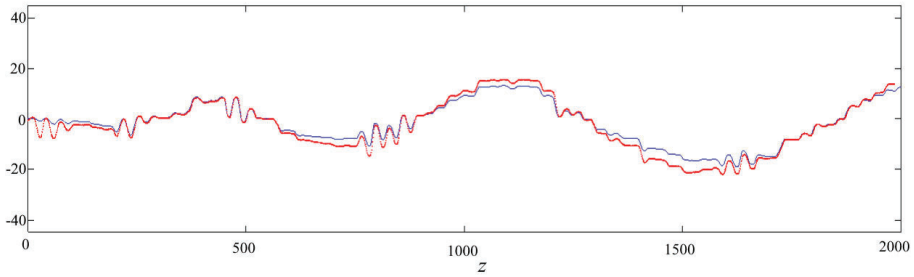

Figure 1.16. Analysis of the simulated ANM trace (blue solid line) and the real patient trace (red lines / squares) for the first 2000 trace points

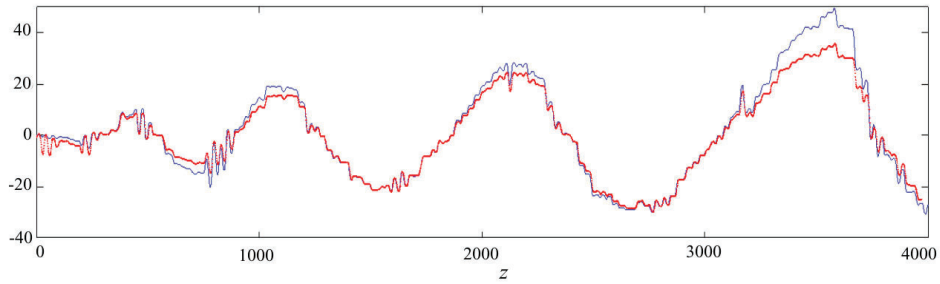

a)

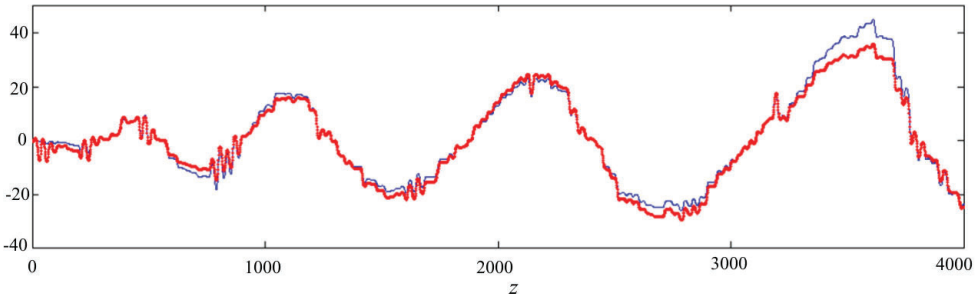

b)

Figure 1.17. Analysis of the model ANM trace (blue solid line) and the real patient trace (red lines / squares) for the first 4000 points of the trace (5690 points were actually taken).

Here (Fig. 1.17) the same curves (a, b) are presented for different numbers of iterative cycles of parameter identification and different graphic images in order to identify more acceptable options. A positive point is that on all the graphs we see a complete reproduction of the frequency characteristics of the trace (the frequency of the model curves almost completely corresponds to the frequency of the curves made by the patient). With an increase in the number of points studied in individual saddle or ridge points, it decreases. But this can always be washed by choosing a finer partition in these zones.

As can be seen in the presented graphs, the developed model reproduces the patient's behavior at a high level, reflecting the ANM trace, which practically coincides with the one plotted on the tablet. The most important thing is that the model includes the possibility of displaying the mechanisms of its feedback effects by the BCC-neural nodes in the form of a matrix of EEG signals that determine the

behavior of these movements. Further research may include a change in this behavior, apparently for the better, depending on the change in the magnitudes of these EEG feedback effects after certain therapeutic procedures, and expansion of the scope of application.

Conclusions for Chapter 1

A hybrid model of a neuro-bio-system has been developed, which describes the state and behavior of 3D elements of trajectories of T-objects of ANM taking into account the matrix of cognitive influences of neuro-node groups of the CC. Using the methods of hybrid integral Fourier transforms, an analytical solution to the model is constructed in the form of vector functions, defining trajectory elements on each ANM segment. On the basis of this, high-performance algorithms for identifying the parameters of the studied feedback systems are proposed for component-wise estimation of mutual influence by obtaining explicit expressions for the gradients of the residual functional, allowing parallelization of computations on multicore computers. In contrast to the generally accepted classical approach, the proposed hybrid model, focused on deep decomposition of the system without violating its integrity and all-important connections makes it possible to describe more qualitatively the complex of hidden mechanisms process with a large number of internal connections and feedback influences of a cognitive nature, provide more data completeness, previously disappeared during classical statistical processing.

Chapter 2. High-performance methods of modeling and identification of feedback influences of competitive adsorption of gaseous air pollutants at micro- and macro-levels in nanoporous systems

The experimental and theoretical study of the competitive adsorption and competitive diffusion of several gases through a microporous solid and the instantaneous (out of equilibrium) distribution of the adsorbed phases is particularly important in many fields, such as gas separation, heterogeneous catalysis, purification of confined atmospheres, reduction of exhaust emissions contributing to global warming, etc. The original NMR imaging technique used gives a signal characteristic of each adsorbed gas at each instant and at each level of the solid, and therefore the distribution of several gases in competitive diffusion and adsorption. But it does not allow one to separately determine inter and intra-crystallite quantities.

A new fast and accurate analytical method for calculation of the coefficients of co-diffusing gases in intra and inter-crystallite spaces of microporous solid (here ZSM 5 zeolite) is developed, using high-performance methods (iterative gradient methods of residual functional minimization and analytical methods of influence functions) and mathematical competitive adsorption models, as well as the NMR spectra of each adsorbed gas in the bed. These diffusion coefficients and the gas concentrations in inter and intra crystallite spaces are obtained for each position in the bed and for different adsorption times.

2.1. Analysis of research state

Knowledge of the competitive diffusion and competitive adsorption coefficients of reactants and products is essential when a heterogeneous catalytic reaction is performed by gas flow through a microporous catalyst bed. But generally, the distribution of the various reactants adsorbed on the catalyst is very

heterogeneous and, moreover, very variable from one reactant to another. It is therefore necessary to determine at every moment the diffusion coefficient of each reactant in the presence of the others and its instantaneous distribution along the length of the catalyst bed.

Classical H-MRI should be a good technique for monitoring the competitive diffusion and competitive adsorption of several gases flowing through a microporous bed. However, since the signal obtained is not specific for each gas, this requires that each experiment be performed several times under identical conditions, and each time with only one not deuterated gas. To remedy the drawbacks of classical imaging, we have used the NMR imaging technique, named slice selection procedure, to follow the diffusion and adsorption of a gas in a microporous bed [6,7]. The sample is displaced vertically, step-by-step, relative to a very thin coil detector during the adsorption of the gas. The bed is assumed to consist of N very thin layers of solid, and the region probed is limited to each layer, so that the variation of the concentration of gas absorbed at the level of each layer is obtained as a function of time. An interesting feature of this technique is its ability to visualize directly the competitive diffusion of several gases. Indeed, the NMR signals are quantitatively characteristic of the adsorbed gases. They can, therefore, provide directly the distribution of several gases competing in diffusion and adsorption at every moment and at every level of the bed. We presented the experimental results of the competitive diffusion of benzene and hexane through a silicalite bed in a previous paper [15]. In [16-18] we developed a mathematical methodology for efficient linearization of similar models. Using Heaviside's operational method and Laplace's integral transformation method, we made solutions allowing fast calculations for two-component competitive adsorption in a heterogeneous zeolite bed and for the dehydration of natural gas [19]. In this chapter we have improved the methods previously used to compute the diffusion coefficients against time, increasing the accuracy and speed of calculations by significantly reducing the iterations number. This made it possible to use them for the competitive adsorption of several gases diffusing along such a column.

2.2 Experimental setup

The NMR imaging technique, the sample-holder bulb containing the liquid phase in equilibrium with the gas phase, and the narrow zone monitored by the detector were described in [15, 16] respectively.

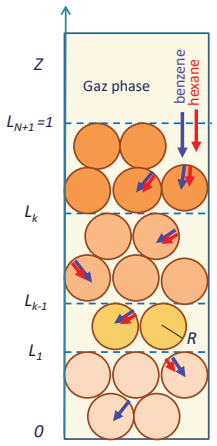

Diffusion in macropores; length of the bed, *l*
Characteristic position of the layer: l_k
Thickness of the k-th layer: $\Delta l_k = l_k - l_{k-1}$
Intercrystallite diffusion coefficient in the *k*-th layer: $D_{inter,k}$
In the theoretical part, *l* is the top of the bed and 0 is the bottom.

Diffusion in micropores;
Intracrystallite diffusion coefficient in the *k*-th layer: $D_{intra,k}$
In the theoretical part, zeolite crystallites are assumed to be spherical (radius R); x = 0 corresponds to the center of the sphere and x = R to its surface.

$$l >> R \; ; \; D_{inter,k} >> D_{intra,k}$$

Figure 2.1. Distribution of the layers (left) and corresponding parameters (right)

The upper face of the cylindrical bed of zeolite crystallites is exposed to a constant pressure of each gas (Figure 2.1). The diffusion of the two gases is axial in the macropores of the intercrystallite space (z direction along the height, *l*, of the bed) and radial in the micropores of the zeolite. According to the experimental conditions, the zeolite bed consists of a large number, N, of very thin layers of solid, of thickness $\Delta l_k = l_k - l_{k-1}$, perpendicular to the propagation of the gas in the z direction. The corresponding coefficients of inter and intra-crystallite space are $D_{inter,k}$ and $D_{intra,k}$, respectively.

2.3 Experimental results: Gaseous benzene and hexane competitive adsorption curves

The experimental results were summarized in [15-17]: the spectrum of each gas at every instant and every level of the solid, and the benzene and hexane concentrations along the sample, for each diffusion time. Here we shall only use the

evolution, as a function of time, of the benzene and hexane concentrations at different levels of the sample, on which are based the calculations of the diffusion coefficients and the instantaneous inter- and intracrystallite concentrations [16]. Figure 2.2 clearly shows that under the chosen experimental conditions, benzene hinders the diffusion of hexane at every moment. Moreover, it can be noticed that at equilibrium the amount of benzene within zeolite is twice that of hexane, indicating quantitatively the relative affinity to the two adsorbates.

These curves display modulations as a function of time, which must be averaged for all subsequent mathematical representations. These modulations are weak at the lower layers of the tube and can be due to errors in the measurement of small amounts. Those closer to the arrival of the gas are greater and are similar for the two gases. We suggested that these fluctuations may be due to the fact that intercrystallite adsorption at levels close to the gas phase is fast compared to the liquid-gas equilibrium, which is not as instantaneous for a mixture as for a single component [16]. To each slight decrease of the gas pressure could correspond a slight fast desorption.

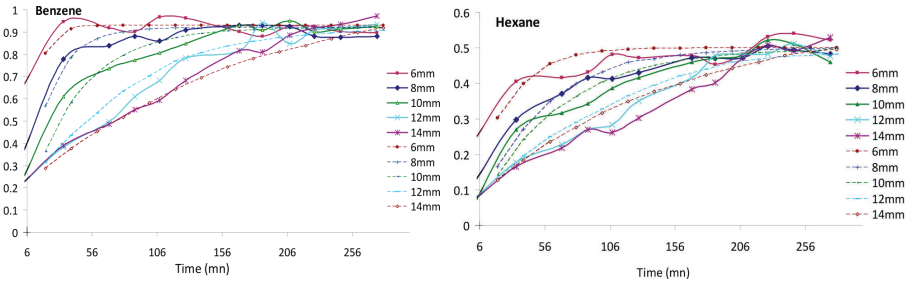

Figure 2.2. Evolution *versus* time of the benzene and hexane concentrations (arbitrary units) at different levels of the sample (*continuous* – experimental curves; *dotted* – their approximations used for simulation) [from reference 16, reprinted with permission from ACS]

2.4 A mathematical model of competitive adsorption and competitive diffusion in microporous solids

2.4.1. Competitive adsorption model in general formulation

The model presented is similar to the bipolar model [7-9]. By developing the approach described by Ruthven & Kärger [10] and Petryk et al. [15] concerning the elaboration of a complex process of competitive adsorption and competitive diffusion, it is necessary to specify the most important hypotheses limiting the process.

The general hypothesis adopted to develop the model presented in the most general formulation is that the interaction between the co-adsorbed molecules of several gases and the adsorption centers on the surface in the nanoporous crystallites is determined by the nonlinear competitive equilibrium function of the Langmuir type, taking into account physical assumptions [10, 16]:

1. Competitive adsorption is caused by the dispersion forces whose interaction is established by Lennard-Jones and the electrostatic forces of gravity and repulsion described by Van der Waals [10].

2. The competitive diffusion process involves two types of mass transfer: diffusion in the macropores (intercrystallite space) and diffusion in the micropores of crystallites (intracrystallite space).

3. During the evolution of the system towards equilibrium there is a concentration gradient in the macropores and/or in the micropores;

4. Competitive adsorption occurs on active centres distributed over the entire inner surface of the nanopores (intracrystallite space) [10]. All crystallites are spherical and have the same radius R; the crystallite bed is uniformly packed.

5. Active adsorption centres adsorb molecules of the *i*-th adsorbate, forming molecular layers of adsorbate on their surfaces.

6. Adsorbed molecules are held by active centers for a certain time, depending on the temperature of the process.

Taking into account these hypotheses, we have developed a nonlinear competitive adsorption model. The meaning of the symbols is given in the nomenclature.

$$\frac{\partial C_s\left(t,Z\right)}{\partial t}=\frac{D_{inter_s}}{l^2}\frac{\partial^2 C_s}{\partial Z^2}-e_{\text{inter}}\tilde{K}_s\frac{D_{intra_s}}{R^2}\left(\frac{\partial Q_s}{\partial X}\right)_{X=1}, \tag{2.1}$$

$$-H\frac{\partial T(t,Z)}{\partial t}-uh_g\frac{\partial T}{\partial Z}-\sum_{s=1}^{m}\Delta\bar{H}_s\frac{\partial\bar{Q}_s}{\partial t}-2\frac{\alpha_h}{R_{column}}T+\Lambda\frac{\partial^2 T}{\partial Z^2}=0, \tag{2.2}$$

$$\frac{\partial Q_s\left(t,X,Z\right)}{\partial t}=\frac{D_{intra_s}}{R^2}\left(\frac{\partial^2 Q_s}{\partial X^2}+\frac{2}{X}\frac{\partial Q_s}{\partial X}\right) \tag{2.3}$$

with initial conditions:

$$C_s\left(t=0,Z\right)=0;\quad Q_s\left(t=0,X,Z\right)=0;\ Z\in\left(0,1\right),\ X\in\left(0,1\right),\ s=\overline{1,\mathrm{m}}, \tag{2.4}$$

boundary conditions for coordinate X of the crystallite:

$$\frac{\partial}{\partial X}Q_s\left(t,X=0,Z\right)=0 \qquad \text{(symmetry conditions)} \tag{2.5}$$

$$Q_s\left(t,X=1,Z\right)=\frac{K_s\left(T\right)C_s\left(t,Z\right)}{1+\sum\limits_{s_1=1}^{m}K_{s_1}\left(T\right)C_{s_1}\left(t,Z\right)},\ s=\overline{1,m}\text{(Langmuir competitive equilibrium)}, \tag{2.6}$$

boundary and interface conditions for coordinate Z:

$$C_s\left(t,1\right)=1,\ \frac{\partial C_s}{\partial Z}\left(t,Z=0\right)=0,\qquad t>0 \tag{2.7}$$

$$T(t,\mathrm{Z})\,|_{Z=1}=T_{initial}\ ,\frac{\partial}{\partial z}T(t,\mathrm{Z})\,|_{Z=0}=0, \tag{2.8}$$

where $K_s\left(T\right)=k_{0s}\exp\left(-\frac{\Delta H_s}{R_gT}\right)$.

Here the activation energy is the heat of adsorption defined as: $\Delta H_s=\bar{\phi}-(U_{g_s}-U_{ads_s})-R_gT$, where $U_{g_s}-U_{ads_s}$ - the difference between the kinetic energies of the molecule of the i-th component of the adsorbate in the gaseous and adsorbed states is the magnitude of the Lennard-Jones potential, averaged over the pore volume of the adsorbent [10].

The non-isothermal model (2.1) - (2.8) can easily be transformed into isothermal model, removing the temperature equations (2.2) and conditions (8) and replacing the functions $K_s\left(T\right)$ with the corresponding equilibrium constants K_s. The competitive diffusion coefficients D_{intra_s} and D_{inter_s} can be considered as functions of the time and the position of the particle in the zeolite bed.

2.4.1. The inverse model of competitive diffusion coefficients identification. Application to the benzene-hexane mixture

On the basis of a developed nonlinear co- adsorption model (2.1) - (2.8), we construct an inverse model for the identification of the competitive diffusion coefficients D_{intra_s} and D_{inter_s} as a function of time and coordinate in the zeolite bed.

The mathematical model of gas diffusion kinetics in the zeolite bed is defined in domains:

$\Omega_{k_t} = (0, t^{total}) \times \Omega_k$, $\left(\Omega_k = \left(L_{k-1}, L_k\right), k = \overline{1, N+1}, L_0 = 0 < L_1 < ... < L_{N+1} = 1\right)$ by the solutions to the system of differential equations:

$$\frac{\partial C_{s_k}\left(t,Z\right)}{\partial t} = \frac{D_{inter_{s_k}}}{l^2}\frac{\partial^2 C_{s_k}}{\partial Z^2} - e_{\text{inter}_k}\tilde{K}_{s_k}\frac{D_{intra_{s_k}}}{R^2}\left(\frac{\partial Q_{s_k}}{\partial X}\right)_{X=1}, \tag{2.9}$$

$$\frac{\partial Q_{s_k}\left(t,X,Z\right)}{\partial t} = \frac{D_{intra_{s_k}}}{R^2}\left(\frac{\partial^2 Q_{s_k}}{\partial X^2} + \frac{2}{X}\frac{\partial Q_{s_k}}{\partial X}\right) \tag{2.10}$$

with initial conditions:

$$C_{s_k}\left(t=0,Z\right)=0;\ Q_{s_k}\left(t=0,X,Z\right)=0;\ X\in(0,1), Z\in\Omega_k,\ k=\overline{1,N+1}, \tag{2.11}$$

boundary and interface conditions for coordinate Z:

$$C_{s_1}(t,L_1)=1,\ \frac{\partial C_{s_1}}{\partial Z}(t,Z=0)=0,\quad t\in\left(0,t^{total}\right); \tag{2.12}$$

$$\left[C_{s_k}(t,Z)-C_{s_k}(t,Z)\right]_{Z=L_k}=0\ ,$$

$$\frac{\partial}{\partial Z}\left[D_{inter_{s_{k-1}}}C_{s_{k-1}}(t,Z)-D_{inter_{s_k}}C_{s_k}(t,Z)\right]_{Z=L_k}=0, \tag{2.13}$$

$$k=\overline{1,N},\ t\in\left(0,t^{total}\right);$$

boundary conditions for coordinate X in the particle:

$$\frac{\partial}{\partial X}Q_{s_k}(t,X=0,Z)=0\ ,$$

$$Q_{s_k}(t,X=1,Z)=K_sC_{s_k}(t,Z) \qquad \text{(equilibrium conditions)}, \tag{2.14}$$

$Z\in\Omega_k,\ k=\overline{1,N+1}$;

Additional condition (NMR-*experimental data*):

$$\left[C_{s_k}(t,Z)+\bar{Q}_{s_k}(t,Z)\right]\Big|_{h_k}=M_{s_k}(t,Z)\Big|_{h_k},\quad s=\overline{1,2};\ h_k\in\Omega_k. \tag{2.15}$$

The problem of the calculation (2.9) - (2.15) is to find unknown functions $D_{\text{intra}_s}\in\Omega_1,\ D_{\text{inter}_s}\in\Omega_1$ $(D_{\text{intra}_s}>0,\ D_{\text{inter}_s}>0, s=\overline{1,2})$, when absorbed masses $C_{s_k}(t,Z)+\bar{Q}_{s_k}(t,Z)$ satisfy the condition (2.15) for every point $h_k\subset\Omega_k$ of the *k*-th layer [16, 21].

Here:

$$\mathrm{e}_{\text{inter}_k}=\frac{\varepsilon_{\text{inter}_k}c_{sk}}{\varepsilon_{\text{inter}_k}c_{sk}+(1-\varepsilon_{\text{inter}_k})q_{sk}}\approx\frac{\varepsilon_{\text{inter}_k}}{(1-\varepsilon_{\text{inter}_k})\tilde{\mathrm{K}}_{sk}},\qquad \tilde{\mathrm{K}}_{s_k}=\frac{\mathrm{q}_{s_k\infty}}{\mathrm{c}_{s_k\infty}},$$

$\bar{Q}_s(t,Z)=\int_0^1 Q_s(t,X,Z)XdX$ - average concentration of adsorbed component *s* in micropores; $M_s(t,Z)\big|_{h_k}$ - experimental distribution of the mass of the s-th

component absorbed in macro- and micropores at $h_k \subset \Omega_k$ (results of NMR data, Figure 2.2).

2.4.2. Iterative Gradient method of competitive diffusion coefficients identification

The calculation of $D_{\text{intra}_{s_k}}$ and $D_{\text{inter}_{s_k}}$ is a complex mathematical problem. In general, it is not possible to obtain a correct formulation of the problem (2.9) - (2.15) and to construct a unique analytical solution, because of the complexity of taking into account all the physical parameters (variation of temperature and pressure, crystallite structures, non-linearity of Langmuir isotherms, etc.), as well as the insufficient number of reliable experimental data, measurement errors and other factors.

Therefore, according to the principle of Tikhonov and Arsenin [22], later developed by Lions [23] and Sergienko et al [24], the calculation of diffusion coefficients requires the use of the model for each iteration, by minimizing the difference between the calculated values and the experimental data.

The calculation of the diffusion coefficients (2.9) - (2.15) is reduced to the problem of minimizing the functional of error (16) between the model solution and the experimental data, the solution being refined incrementally by means of a special calculation procedure which uses fast high-performance gradient methods [15, 16, 20, 24].

According to [16, 20], and using the error minimization gradient method for the calculation of $D_{\text{intra}_{s_k}}$ and $D_{\text{inter}_{s_k}}$ of the s-th diffusing component, we obtain the iteration expression for the $n+1$-th calculation step:

$$D^{n+1}_{\text{intra}_{s_k}}(t) = D^{n}_{\text{intra}_{s_k}}(t) - \nabla J^{n}_{D_{\text{intra}_{s_k}}}(t) \frac{\left[C_{s_k}\left(D^{n}_{\text{inter}_{s_k}}, D^{n}_{\text{intra}_{s_k}}; t, h_k \right) + \bar{Q}_{s_k}\left(D^{n}_{\text{inter}_{s_k}}, D^{n}_{\text{intra}_{s_k}}; t, h_k \right) - M_{s_k}(t) \right]^2}{\left\| \nabla J^{n}_{D_{\text{intra}_{s_k}}}(t) \right\|^2 + \left\| \nabla J^{n}_{D_{\text{inter}_{s_k}}}(t) \right\|^2},$$

$$D^{n+1}_{\text{inter}_{s_k}}(t) = D^{n}_{\text{inter}_{s_m}}(t) - \nabla J^{n}_{D_{\text{inter}_{s_k}}}(t) \frac{\left[C_{s_k}\left(D^{n}_{\text{inter}_{s_k}}, D^{n}_{\text{intra}_{s_k}}; t, h_k \right) + \bar{Q}_{s_k}\left(D^{n}_{\text{inter}_{s_k}}, D^{n}_{\text{intra}_{s_k}}; t, h_k \right) - M_{s_k}(t) \right]^2}{\left\| \nabla J^{n}_{D_{\text{intra}_{s_k}}}(t) \right\|^2 + \left\| \nabla J^{n}_{D_{\text{inter}_{sk}}}(t) \right\|^2}, \qquad (2.16)$$

$$t \in \left(0, t^{total}\right)$$

where $J\left(D_{\text{inter}_{s_k}}, D_{\text{intra}_{s_k}}\right)$ - the error functional, which describes the deviation of the model solution from the experimental data on $h_k \in \Omega_k$, is written as:

$$J\left(D_{\text{inter}_{s_k}}, D_{\text{intra}_{s_k}}\right)=\frac{1}{2}\int_0^T\left[C_s\left(\tau, Z, D_{\text{inter}_{s_k}}, D_{\text{intra}_{s_k}}\right)+\bar{Q}_s\left(t, Z, D_{\text{inter}_{s_k}}, D_{\text{intra}_{s_k}}\right)-M_{s_k}(t)\right]_{h_k}^2 d\tau,$$

$$h_k \in \Omega_k,\ k=\overline{1, N+1}, \tag{2.17}$$

$\nabla J^n_{D_{\text{intter}_{s_k}}}(t), \nabla J^n_{D_{\text{intra}_{s_k}}}(t)$ - the gradients of the error functional, $J\left(D_{\text{inter}_{s_k}}, D_{\text{intra}_{s_k}}\right)$.

$$\left\|\nabla J^n_{D_{\text{inter}_{sk}}}(t)\right\|^2=\int_0^T\left[\nabla J^n_{D_{\text{inter}_{sk}}}(t)\right]^2 dt,\ \left\|\nabla J^n_{D_{\text{intra}_{sk}}}(t)\right\|^2=\int_0^T\left[\nabla J^n_{D_{\text{intra}_{sk}}}(t)\right]^2 dt.$$

2.4.3. Analytical method of competitive diffusion coefficients identification

With the help of iterative gradient methods on the basis of the minimization of the residual functional, very precise and fast analytical methods have been developed making it possible to express the diffusion coefficients in the form of time dependent analytic functions (2.16). For their efficient use, it is necessary to have an extensive experimental database, with at least two experimental observation conditions for the simultaneous calculation of $D_{\text{intra}_{s_k}}$ and $D_{\text{inter}_{s_k}}$ coefficients. Our experimental studies were carried out for 5 Z positions of the swept zeolite layer for each of the adsorbed components. The data were not sufficient to fully apply this simultaneous identification method to these 5 positions. We, therefore, used a combination of the analytical method and the iterative gradient method for determining the competitive diffusion coefficients.

Using equations (2.9) - (2.15), it is possible to calculate $D_{\text{intra}_{s_k}}$, $D_{\text{inter}_{sk}}$ as a function of time using the experimental data obtained by NMR scanning. In particular, in the equations (2.9) and (2.10), the competitive diffusion coefficients can be set directly as functions of the time *t*: $D_{\text{intra}_{s_k}}(t)$, $D_{\text{inter}_{sk}}(t)$. In this case, the boundary condition (2.11) can be given in a more general form - also as a function of time

$$C_{s_1}(t,1) = C_s^{initial}(t)\ . \tag{2.18}$$

Experimental NMR scanning conditions are defined simultaneously for all P observation surfaces:

$$\left[C_{sk}(t,Z) + \int_0^1 Q_{sk}(t,X,Z)dX\right]_{Z=h_i} = M_{sk_i}(t,Z)\Big|_{h_i},\ i=\overline{1,P},\ s=\overline{1,2};\ h_i \in \bigcup_{k=1}^{N+1}\Omega_k\ , \tag{2.19}$$

For simplicity we design: $u(t,Z)=C_{sk}(t,Z),\ v(t,X,Z)=Q_{sk}(t,X,Z)$,

$$b(t) = D_{intra_{sk}}(t)/R^2,\ \ \chi_i(t) = M_{sk_i}(t),\ \ i=\overline{1,P}$$

and considering equation (2.10) in flat form its solution can be written as [26]:

$$v(t,\mathrm{X},\mathrm{Z}) = -\int_0^t \mathrm{H}_{4\xi}^{(2)}(t,\tau,\mathrm{X},1))b(\tau)u(\tau,\mathrm{Z})\,d\tau\ , \tag{2.20}$$

where $\mathrm{H}_{4\xi}^{(2)}(t,\tau,\mathrm{X},\xi) = -2\sum_{m=0}^{\infty} e^{-\eta_m^2(\theta_2(\mathrm{t})-\theta_2(\tau))}\eta_m \cos\eta_m X(-1)^m$.

Here the Green influence function of the particle $\mathrm{H}_k^{(2)}$, $\overline{k=1,4}$ is used; it has the form [12]:

$$\mathrm{H}_4^{(2)}(t,\tau,\mathrm{X},\xi) = 2\sum_{m=0}^{\infty} e^{-\eta_m^2(\theta_2(\mathrm{t})-\theta_2(\tau))}\cos\eta_m X\cos\eta_m\xi,\ \ \eta_m = \frac{2m+1}{2}\pi,$$

$$\mathrm{H}_3^{(2)}(t,\tau,\mathrm{X},\xi) = 2\sum_{m=0}^{\infty} e^{-\eta_m^2(\theta_2(\mathrm{t})-\theta_2(\tau))}\sin\eta_m X\sin\eta_m\xi\ ,\qquad \eta_m = \frac{2m+1}{2}\pi,$$

$$\mathrm{H}_2^{(2)}(t,\tau,\mathrm{X},\xi) = 1 + 2\sum_{m=1}^{\infty} e^{-\eta_m^2(\theta_2(\mathrm{t})-\theta_2(\tau))}\cos\eta_m X\cdot\cos\eta_m\xi\ ,\qquad \eta_m = m\pi,$$

where $\theta_2(t) = \int_0^t b(s)\,ds$.

The notation $\mathrm{H}_{4\tau\xi}^{(2)}$, $\mathrm{H}_{4\xi\xi}^{(2)}$ means partial derivatives of the influence function $\mathrm{H}_4^{(2)}$ relative to the definite variables τ and ξ respectively.

Based on formula (2.20), we calculate

$$v_X(t,\mathrm{X},\mathrm{Z}) = -\int_0^t \mathrm{H}_{4\xi X}^{(2)}(t,\tau,\mathrm{X},1))b(\tau)u(\tau,\mathrm{Z})\,d\tau\ . \tag{2.21}$$

Integrating parts (2.21), taking into account the relations:

$$\mathrm{H}_{4X}^{(2)}(t,\tau,\mathrm{X},\xi) = -\mathrm{H}_{3\xi}^{(2)}(t,\tau,X,\xi),\ \mathrm{H}_{3\tau}^{(2)}(t,\tau,X,\xi) = -b(\tau)\mathrm{H}_{3\xi\xi}^{(2)}(t,\tau,X,\xi),$$

and the initial condition $u_{|t=0} = 0$, we find

$$v_X(t,\mathrm{X},\mathrm{Z}) = \int_0^t \mathrm{H}_3^{(2)}(t,\tau,\mathrm{X},1))u_\tau(\tau,\mathrm{Z})d\tau\,. \qquad (2.22)$$

We substitute the expression $v(t,\mathrm{X},\mathrm{Z})$ (2.20) in the observation conditions (2.19):

$$u(t,h_i) - \int_0^1 XdX \int_0^t \mathrm{H}_{4\xi}^{(2)}(t,\tau,\mathrm{X},1))b(\tau)u(\tau,h_i)d\tau = \chi_i(\mathrm{t}),\ i=\overline{1,\mathrm{P}}\,. \qquad (2.23)$$

Integrating parts (2.23) and taking into account equality

$$\mathrm{H}_{4\xi}^{(2)}(t,\tau,X,1) = -\mathrm{H}_{3X}^{(2)}(t,\tau,X,1)\,,$$

we obtain [26]:

$$\begin{aligned} u(t,h_i) &= \chi_i(\mathrm{t}) - \int_0^t \mathrm{H}_3^{(2)}(t,\tau,1,1))b(\tau)u(\tau,h_i)d\tau + \\ &+ \int_0^t\int_0^1 \mathrm{H}_3^{(2)}(t,\tau,\mathrm{X},1))b(\tau)u(\tau,h_i)dXd\tau,\ i=\overline{1,\mathrm{P}} \end{aligned}\,. \qquad (2.24)$$

Let's first put $u(t,h_P) = \mu_{sP}(t) = C_s^{initial}(t)$, where $Z = h_P$ - the observation surface, approaching the point of entry into the work area Z = 1.

Then equation (2.24) for $i = P$ will be :

$$\int_0^t \mathrm{H}_3^{(2)}(t,\tau,1,1))b(\tau)\mu_{sP}(t)d\tau = \chi_{sP}(t) - \mu_{sP}(t) + \int_0^t\int_0^1 \mathrm{H}_3^{(2)}(t,\tau,\mathrm{x},1))b(\tau)\mu_{sP}(t)dxd\tau\,. \qquad (2.25)$$

Applying the formula $\int_\tau^t b(\sigma)\mathrm{H}_2^{(2)}(t,\sigma,0,0))\mathrm{H}_4^{(2)}(t,\sigma,0,0))d\sigma = 1$,

obtained by Ivanchov [26], to (2.25) and taking into account $\mathrm{H}_3^{(2)}(t,\sigma;1,1) = \mathrm{H}_4^{(2)}(t,\sigma;0,0)$, we obtain:

$$\begin{aligned} \int_0^t b(\tau)\mu_{sP}(\tau)d\tau &= \int_0^t \mathrm{H}_2^{(2)}(t,\sigma,0,0))b(\sigma)(\chi_{sP}(\sigma) - \mu_{sP}(\sigma))d\sigma + \\ &+ \int_0^t \mathrm{H}_2^{(2)}(t,\sigma,0,0))b(\sigma)d\sigma \int_0^\sigma\int_0^1 \mathrm{H}_3^{(2)}(\sigma,\tau,\mathrm{x},1))b(\tau)\mu_{sP}(t)dXd\tau,\ t\in[0,t^{total}] \end{aligned}\,. \qquad (2.26)$$

Differentiating (26) by *t*, after the transformations series we obtain

$$\mu_{sP}(t) = \int_0^t \mathrm{H}_2^{(2)}(t,\sigma,0,0))(b(\sigma)\mu_{sP}(\sigma) + \chi_{sP}(\sigma) - \mu_{sP}(\sigma))d\sigma\,. \qquad (2.27)$$

After multiplying eq. (2.27) on the expression $\mathrm{H}_4^{(2)}\left(t,\sigma,0,0\right))b(\sigma)$, the integration by τ and the differentiation by t:

$$b(t)\mu_{sP}(t)+\chi_{sP}(\sigma)-\mu_{sP}(\sigma)=b(t)\int_0^t \mathrm{H}_2^{(2)}\left(t,\tau,0,0\right))\mu'_{sP}(\tau))d\tau\,.$$

So, we obtain the expression for calculating the competitive diffusion coefficient in the intracrystallite space:

$$D_{\mathrm{int}\,ra_{sP}}(t)\equiv R^2 b(t)=R^2\frac{\chi'_{sP}(t)-\mu'_{sP}(t)}{\int_0^t \mathrm{H}_2^{(2)}\left(t,\tau,0,0\right))\mu'_{sP}(\tau)d\tau-\mu_{sP}(t)},\ t\in[0,\ t^{total}]\,. \qquad (2.28)$$

Using calculated $D_{\mathrm{intra}_{sP}}(t)$ with the formula (2.28) on the observation limit h_P, we define the gradient method $D_{\mathrm{inter}_{sP}}(t)$ in the same way. With $D_{\mathrm{intra}_{sP}}(t)$ and $D_{\mathrm{inter}_{sP}}(t)$ in h_P, we calculate $C_{sk}(t,h_P)$, substituting it in $\mu_{sP-1}\left(t\right)=C_{sk}(t,h_P)$ for next coefficients $D_{\mathrm{inter}_{si}}(t),\ i=\overline{P-1,1}$ calculations. All subsequent coefficients $D_{\mathrm{int}\,ra_{si}}(t)$ will be calculated by the formula

$$D_{\mathrm{int}\,ra_{si}}(t)\equiv R^2 b_{si}(t)=R^2\frac{\chi'_{si}(t)-\mu'_{si}(t)}{\int_0^t \mathrm{H}_2^{(2)}\left(t,\tau,0,0\right))\mu'_{si}(\tau)d\tau-\mu_{si}(t)},\ i=\overline{P-1,1} \qquad (2.29)$$

with parallel computing $D_{\mathrm{inter}_{si}}(t),\ i=\overline{P-1,1}$.

2.5 Numerical simulation and analysis: Competitive diffusion coefficients. Concentration profiles in inter- and intracrystallite spaces

The variation against time of the benzene and hexane intracrystallite diffusion coefficients, $D_{\mathrm{intra}_{1,\mathrm{k}}}$ and $D_{\mathrm{intra}_{2,\mathrm{k}}}$ respectively, are presented in Figure 2.3 for the five coordinate positions: 6, 8, 10, 12 and 14 mm, defined now from the top of the bed. The curves for benzene $D_{\mathrm{intra}_{1,\mathrm{k}}}$ are pseudo exponentials. $D_{\mathrm{intra}_{1,\mathrm{k}}}$ decreases from 9.0 E-13 to about 1.0 E-14 a.u. (equilibrium) depending on the position of the crystallite and the time, as well as on the amount of adsorbed gas. The shapes of the variations of $D_{\mathrm{intra}_{2,\mathrm{k}}}$ for hexane are roughly the same, but the diffusion coefficients are higher, from about 9.0 E-12 to 3.0 E-13 a.u.

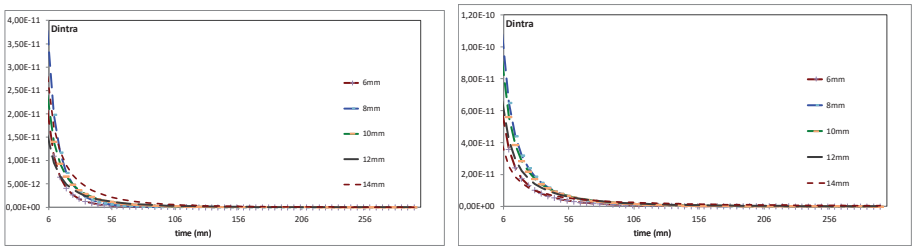

Figure 2.3. Variation of intracrystallite diffusion coefficients (arbitrary units) for benzene $D_{\text{intra}_{1,k}}$ (left) and hexane $D_{\text{intra}_{2,k}}$ (right) against time, at different positions in the bed. (Top) time range 6-240 mn, (bottom) time range 100-240 mn

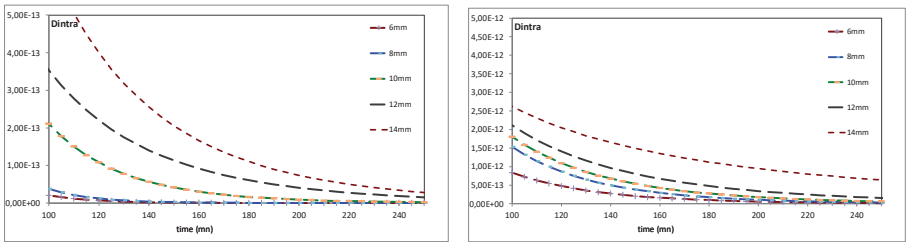

Figure 2.4 presents the variation against time of the benzene and hexane diffusion coefficients in intercrystallite space, $D_{\text{inter}_{1,k}}$ and $D_{\text{inter}_{2,k}}$, for the same positions

These coefficients decrease with time from 2.0 E-6 to 1.0 E-7 a.u. (equilibrium) for benzene and from 3 E-5 to 1.0 E-6 a.u. for hexane, depending on bed position and increase adsorbed concentrations.

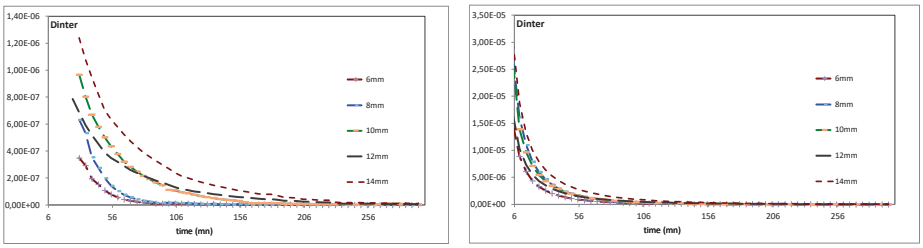

Figure 2.4. Variation of intercrystallite diffusion coefficients (2.u.) for benzene (left), and hexane (right) against time at different positions of the bed

Figure 2.5 shows the variation against time of the calculated concentrations C for benzene and hexane in the intercrystallite space. As can be seen, these

concentrations approach the equilibrium values for a diffusion time around 250 min. But the variations of the concentrations with time are rather different for the two gases.

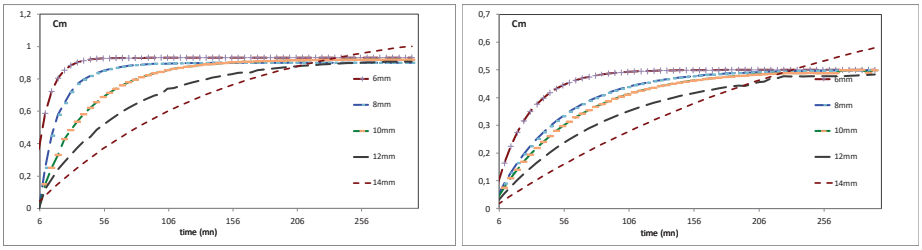

Figure 2.5. Variation of the intercrystallite concentration (2.u.) calculated for benzene (left) and hexane (right) against time and at different positions in the bed

Figure 6 shows the variation of the concentrations $Q(t,X,z)$ of adsorbed benzene (left) and hexane (right) in the micropores of the intracrystallite space from the surface (abscissa -1) to the center (abscissa -0) of the crystallites located between 6 to 14 mm from the top of the bed, and after 25 to 200 min. of diffusion (a, b, c, and d, respectively). The gradients increase and the mean concentrations decrease with the increasing distance of the particles from the arrival of the gases. The particles at 6 and 8 mm are saturated with benzene after 100 min., but not yet with hexane.

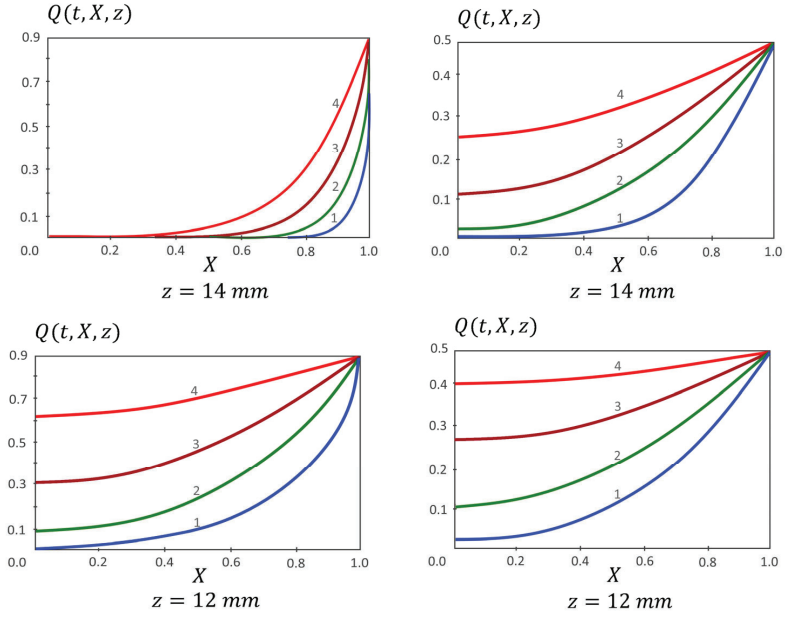

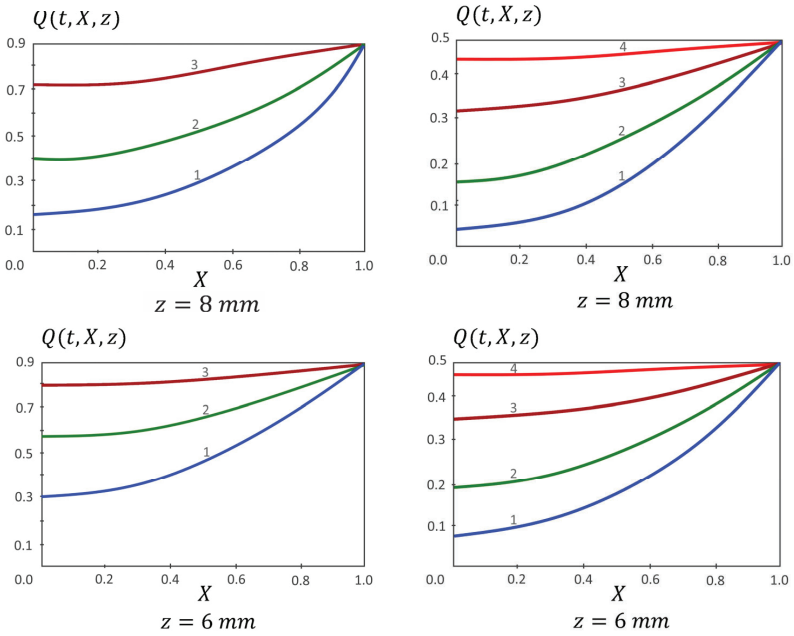

Figure 2.6. Distribution of the benzene (left) and hexane (right) concentrations in the intracrystallite space from the surface (abscissa 1) to the center (abscissa 0) of the crystallites, at different times *1- dark blue: t = 25 min.; 2 -green: t 50 min; 3 - brown: t =100 min.; 4 - red: t =200 min*

2.6 Iterative gradient method of the identification of competitive diffusion coefficients

The methodology for solving the direct boundary problem (2.9) - (2.15), which describes the diffusion process in a heterogeneous nanoporous bed was developed in [16, 20]. According to [20] the procedure for determining the diffusion coefficients (2.16) requires a special technique for calculating the gradients $\nabla J^n_{D_{\text{intra}_{sk}}}(t)$, $\nabla J^n_{D_{\text{inter}_{sk}}}(t)$ of the residual functional (2.17). This leads to the problem of optimizing the extended Lagrange functional [21].

$$\Phi\left(D_{\text{inter}_{\text{sk}}}, D_{\text{intra}_{\text{sk}}}\right) = J_s + I_{s_{macro}} + I_{s_{micro}}, \tag{2.31}$$

where $I_{s_{macro}}, I_{s_{micro}}$ are the components given by equations (2.32) and (2.33), corresponding to the macro- and micro- porosity, respectively:

$$I_{s_{macro}} = \int_0^T \int_{L_{k-1}}^{L_k} \phi_{s_k}(t,Z)\left(\frac{\partial C_{s_k}}{\partial t} - \frac{D_{\text{inter}_{sk}}}{l^2}\frac{\partial^2 C_{s_k}}{\partial Z^2} + e_{\text{inter}_k} K_{s_k} \frac{D_{\text{intra}_{sk}}}{R^2}\left(\frac{\partial Q(t,X,Z)_{s_k}}{\partial X}\right)_{X=1}\right) dZdt\,, \quad (2.32)$$

$$I_{s_{micro}} = \int_0^T \int_0^1 \int_{L_{k-1}}^{L_k} \psi_{s_k}(t,X,Z)\left(\frac{\partial Q_{s_k}(t,X,Z)}{\partial t} - \frac{D_{\text{int}\,ra_{sk}}}{R^2}\left(\frac{\partial^2 Q_{s_k}}{\partial X^2} + \frac{2}{X}\frac{\partial Q_{s_k}}{\partial X}\right)\right) XdXdZdt\,, \quad (2.33)$$

J_s is the residual functional (2.17), ϕ_{s_k}, ψ_{s_k}, $s,=\overline{1,2}$ – unknown factors of Lagrange to be determined from the stationary condition of the functional $\Phi\left(D_{\text{inter}_{sk}}, D_{\text{intra}_{sk}}\right)$ [16, 21]:

$$\Delta\Phi\left(D_{\text{inter}_{sk}}, D_{\text{intra}_{sk}}\right) \equiv \Delta J_s + \Delta I_{s_{macro}} + \Delta I_{s_{micro}} = 0\,. \quad (2.34)$$

The calculation of the components in eq. (2.34) is carried out by assuming that the values $D_{\text{inter}_{sk}}, D_{\text{intra}_{sk}}$ are incremented by $\Delta D_{\text{inter}_{sk}}$, $\Delta D_{\text{intra}_{sk}}$. As a result, concentration $C_{s_k}(t,Z)$ changes by increment $\Delta C_{sk}(t,Z)$ and concentration $Q_{s_k}(t,X,Z)$ by increment $\Delta Q_{s_k}(t,X,Z)$, $s=\overline{1,2}$.

Conjugate problem. The calculation of the increments $\Delta J_s, \Delta J_{s_{macro}}$, $\Delta J_{s_{micro}}$ in (2.34) (using integration by parts and the initial and boundary conditions of the direct problem (2.9)-(2.15)), leads to solving the additional conjugate problem to determine the Lagrange factors ϕ_{s_k}, ψ_{s_k} of the functional (2.31) [20] :

$$\frac{\partial \phi_{s_k}(t,Z)}{\partial t} + \frac{D_{\text{inter}_{sk}}}{l^2}\frac{\partial^2 \phi_{s_k}}{\partial Z^2} + e_{\text{inter}_k} K_{s_k} \frac{D_{\text{intra}_{sk}}}{R^2}\frac{\partial \psi_{s_k}(t,X,Z)}{\partial X}\bigg|_{X=1} = E^n_{s_k}(t)\delta(Z-h_k), \quad (2.35)$$

where $E^n_{s_k}(t) = C_{s_k}\left(D^n_{\text{int}\,ra_{sk}}, D^n_{\text{int}\,er_{sk}}; t, h_k\right) + \bar{Q}_{s_k}\left(D^n_{\text{int}\,ra_{sk}}, D^n_{\text{int}\,er_{sk}}; t, h_k\right) - M_{sk}(t)$,

$\delta(Z-h_k)$ - function of Dirac [22].

$$\frac{\partial \psi_{s_k}(t,X,Z)}{\partial t} + \frac{D_{\text{int}\,ra_{sk}}}{R^2}\left(\frac{\partial^2 \psi_{s_k}}{\partial X^2} + \frac{2}{X}\frac{\partial \psi_{s_k}}{\partial X}\right) = E^n_{s_k}(t)\delta(Z-h_k). \quad (2.36)$$

$$\phi_{s_k}(t,Z)\big|_{t=t^{total}} = 0;\ \psi_{s_k}(t,X,Z)\big|_{t=t^{total}} = 0 \text{ (conditions at } t = t^{total}); \quad (2.37)$$

$$\frac{\partial}{\partial X}\psi_{s_k}(t,X,Z)\big|_{X=0} = 0;\ \psi_{s_k}(t,X,Z)\big|_{X=1} = \varphi_{s_k}(t,Z); \quad (2.38)$$

$$\phi_{s_k}\left(t, Z = L_k\right) = 0,\ \ \phi_{s_{k-1}}\left(t, Z = L_{k-1}\right) = 0;\ \ s = \overline{1,2},\ \ k = \overline{N,2}, \tag{2.39}$$

$$\phi_{s_1}\left(t, L_1\right) = 0\,,\ \ \frac{\partial \phi_{s_1}}{\partial Z}\left(t, Z = 0\right) = 0\,. \tag{2.40}$$

We have obtained the solution ϕ_{sk}, ψ_{sk} to problem (2.35) - (2.40) using Heaviside operational method in [29].

Substituting in the direct problem (2.9) - (2.15) $D_{\text{inter}_{\text{sk}}}, D_{\text{intra}_{\text{sk}}}$, $C_{s_k}\left(t, Z\right)$ and $Q_{s_k}\left(t, X, Z\right)$ by the corresponding values with increments $D_{\text{inter}_{\text{sk}}} + \Delta D_{\text{inter}_{\text{sk}}}$, $D_{\text{intra}_{\text{sk}}} + \Delta D_{\text{intra}_{\text{sk}}}$, $C_{s_k}\left(t, Z\right) + \Delta C_{s_k}\left(t, z\right)$ and $Q_{s_k}\left(t, X, Z\right) + \Delta Q_{s_k}\left(t, X, Z\right)$, subtracting the first equations from the transformed ones and neglecting second-order terms of smallness, we obtain the basic equations of the problem (2.9) - (2.15) in terms of increments $\Delta C_{s_k}\left(t, Z\right)$ and $\Delta Q_{s_k}\left(t, X, Z\right)$, $s = \overline{1,2}$ in the operator form:

$$\mathrm{L} w_{s_k}(t, X, Z) = \mathrm{X}_{s_k},\ \ w_{s_k} \in (0,1) \bigcup \Omega_{kt},\ \ k = \overline{1, N+1}\,. \tag{2.41}$$

Similarly, we write the system of the basic equations of conjugate boundary problem (2.35) -(2.40) in the operator:

$$\mathrm{L}^{*} \Psi_{s_k}(t, X, Z) = E_{s_k}(t)\delta\left(Z - h_k\right),\ \ \Psi_{s_k} \in (0,1) \bigcup \Omega_{kt},\ \ k = \overline{1, N+1}, \tag{2.42}$$

$$\text{where} = \mathrm{L} = \begin{bmatrix} \dfrac{\partial}{\partial t} - \dfrac{\partial}{\partial Z}\left(D_{\text{inter}_{\text{sk}}} \dfrac{\partial}{\partial Z}\right) & e_{\text{inter}_k} \dfrac{D_{\text{intra}_{\text{sk}}}}{R} \dfrac{\partial}{\partial X}\Big|_{X=1} \\ 0 & \dfrac{\partial}{\partial t} - \dfrac{D_{\text{intra}_{\text{sk}}}}{R^2}\left(\dfrac{\partial^2}{\partial X^2} + \dfrac{2}{X}\dfrac{\partial}{\partial X}\right) \end{bmatrix},$$

$$= \mathrm{L}^{*} = \begin{bmatrix} \dfrac{\partial}{\partial t} + \dfrac{\partial}{\partial Z}\left(D_{\text{inter}_{\text{sk}}} \dfrac{\partial}{\partial Z}\right) & e_{\text{inter}_k} \dfrac{D_{\text{intra}_{\text{sk}}}}{R^2} \dfrac{\partial}{\partial X}\Big|_{X=1} \\ 0 & \dfrac{\partial}{\partial t} + \dfrac{D_{\text{intra}_{\text{sk}}}}{R^2}\left(\dfrac{\partial^2}{\partial X^2} + \dfrac{2}{X}\dfrac{\partial}{\partial X}\right) \end{bmatrix},$$

$$w_{s_k}\left(t, X, Z\right) = \begin{bmatrix} \Delta C_{s_k}\left(t, Z\right) \\ \Delta Q_{s_k}\left(t, X, Z\right) \end{bmatrix},\ \ \Psi_{s_k}\left(t, X, Z\right) = \begin{bmatrix} \phi_{s_k}\left(t, Z\right) \\ \psi_{s_k}\left(t, X, Z\right) \end{bmatrix}.$$

$$\mathrm{X}_{s_k}(t,X,Z)=\begin{bmatrix} \dfrac{\partial}{\partial Z}\left(\Delta D_{\text{inter}_{sk}}\dfrac{\partial}{\partial Z}C_{s_k}\right)-e_{\text{inter}_k}\dfrac{\Delta D_{\text{intra}_{sk}}}{R^2}\dfrac{\partial}{\partial X}Q_{s_k}(t,X,Z)_{X=1} \\ \dfrac{\Delta D_{\text{intra}_{sk}}}{R^2}\left(\dfrac{\partial^2}{\partial X^2}+\dfrac{2}{X}\dfrac{\partial}{\partial X}\right)Q_{s_k}(t,X,Z) \end{bmatrix}, \qquad (2.43)$$

where L^* is the conjugate Lagrange operator of operator L.

The calculated increment of the residual functional (2.17), neglecting second-order terms, has the form:

$$\Delta J_s\left(D_{\text{intra}_{sk}},D_{\text{inter}_{sk}}\right)=\int_0^T\int_{L_{k-1}}^{L_k}\mathrm{L}^{-1}\mathrm{X}_{s_k,1}(t,Z)\cdot E_{s_k}(t)\delta\left(Z-h_k\right)dZdt+ \\ +\int_0^T\int_{L_{k-1}}^{L_k}\int_0^1\mathrm{L}^{-1}\mathrm{X}_{s_k2}(t,X,Z)\cdot E_{s_k}(t)\delta\left(Z-h_k\right)XdXdZdt \qquad (2.44)$$

where $w_{s_k}=\mathrm{L}^{-1}\mathrm{X}_{s_k}$, L^{-1} is the inverse operator of operator L.

Defining the scalar product:

$$\left(\mathrm{L}w_{s_k}(t,X,Z),\Psi_{s_k}(t,X,Z)\right)=\begin{bmatrix} \iint\limits_{\Omega_{kT}}\mathrm{L}\Delta C_{s_k}(t,Z)\phi_{s_k}(t,Z)\,dZdt \\ \iiint\limits_{(0,R)\cup\Omega_{kT}}\mathrm{L}\Delta Q_{s_k}(t,X,Z)\psi_{s_k}(t,X,Z)\,XdXdZdt \end{bmatrix}, \qquad (2.45)$$

and taking into account (2.19) Lagrange's identity [16, 21]:

$$\left(\mathrm{L}w_{s_k}(t,X,Z),\Psi_{s_k}(t,X,Z)\right)=\left(w_{s_k}(t,X,Z),\mathrm{L}^*\Psi_{s_k}(t,X,Z)\right), \qquad (2.46)$$

and the equality: $\mathrm{L}^{-1*}\left[E_{s_k}(t)\delta\left(Z-h_k\right)\right]=\Psi_{s_k}$, we obtain the increment of the residual functional expressed by the solution of conjugate problem (2.35) – (2.40) and the vector of the right-hand parts of equations (2.43):

$$\Delta J_s\left(D_{\text{inter}_{sk}},D_{\text{intra}_{sk}}\right)=\left(\Psi_{s_k}(t,X,Z),\ \mathrm{X}_{s_k}(t,X,Z)\right), \qquad (2.47)$$

where $\phi_{s_k}(t,Z)$ and $\psi_{s_k}(t,X,Z)$ belong to $\bar{\Omega}_{kt}$ and $[0,1]\cup\bar{\Omega}_{kt}$, respectively; L^{-1*} - conjugate operator to inverse operator L^{-1}, Ψ_{s_k} - solution to conjugate problem (2.35) - (2.40).

Reporting in equation (2.47) the components $\mathrm{X}_{s_k}(t,X,Z)$ taking into account the equality (2.48), we obtain the formula which establishes the relationship between the direct problem (2.9) - (2.15) and the conjugate problem (2.36) - (2.40) and which

makes it possible to obtain the analytical expressions of components of the residual functional gradient:

$$\Delta J_s\left(D_{\text{intra}_{sk}}, D_{\text{inter}_{sk}}\right) = \begin{array}{l} \left(\phi_{s_k}(t,Z),\ \dfrac{\partial}{\partial Z}\left(\Delta D_{\text{inter}_{sk}}\dfrac{\partial}{\partial Z}C_{s_k}\right) - e_{\text{inter}_k}\dfrac{\Delta D_{\text{intra}_{sk}}}{R^2}\dfrac{\partial}{\partial X}Q_{s_k}\left(t,X,Z\right)_{X=1}\right) + \\ + \left(\psi_{s_k}(t,X,Z),\ \dfrac{\Delta D_{\text{intra}_{sk}}}{R^2}\left(\dfrac{\partial^2}{\partial X^2}+\dfrac{2}{X}\dfrac{\partial}{\partial X}\right)Q_{s_k}\left(t,X,Z\right)\right) \end{array} \tag{2.48}$$

Differentiating expression (2.18), by $\Delta D_{\text{intra}_{sk}}$ and $\Delta D_{\text{inter}_{sk}}$, respectively, and calculating the scalar products according to (2.45), we obtain the required analytical expressions for the gradient of the residual functional in the intra- and intercrystallite spaces, respectively:

$$\begin{array}{l} \nabla J_{D_{\text{intra}_{sk}}}\left(t\right) = -\dfrac{e_{\text{inter}_k}}{R^2}\int\limits_{L_{k-1}}^{L_k}\dfrac{\partial}{\partial X}Q_{s_k}\left(t,1,Z\right)\phi_{s_k}(t,Z)dZ + \\ + \dfrac{1}{R^2}\int\limits_{L_{k-1}}^{L_k}\int\limits_0^1\left(\dfrac{\partial^2}{\partial X^2}+\dfrac{2}{X}\dfrac{\partial}{\partial X}\right)Q_{s_k}\left(t,X,Z\right)\psi_{s_k}(t,X,Z)XdXdZ \end{array}, \tag{2.49}$$

$$\nabla J_{D_{\text{inter}_{sk}}}\left(t\right) = \int\limits_{L_{k-1}}^{L_k}\frac{\partial^2 C_{s_k}(t,Z)}{\partial Z^2}\phi_{s_k}(t,Z)dZ\ . \tag{2.50}$$

The formulas of gradients $\nabla J^n_{D_{\text{intra}_{sk}}}\left(t\right)$, $\nabla J^n_{D_{\text{inter}_{sk}}}\left(t\right)$ include analytical expressions of the solutions to the direct problem (2.9) - (2.14) and inverse problem (2.35) - (2.40). They provide high performance of computing process, avoiding a large number of inner loop iterations by using exact analytical methods [20].

2.7 The linearization schema of the nonlinear competitive adsorption model. System of linearized problems and construction of solutions

The linearization schema of nonlinear competitive adsorption (2.1) - (2.8) is shown in order to demonstrate the simplicity of implementation for the case of two diffusing components ($m = 2$) and isothermal adsorption. The simplified model (2.1) - (2.8) for the case $m = 2$ is converted into the form:

$$\frac{\partial C_s\left(t,Z\right)}{\partial t} = \frac{D_{inter_s}}{l^2}\frac{\partial^2 C_s}{\partial Z^2} - e_{\text{inter}}\tilde{K}_s\frac{D_{intra_s}}{R^2}\left(\frac{\partial Q_s}{\partial X}\right)_{X=l}, \tag{2.51}$$

$$\frac{\partial Q_s\left(t,X,Z\right)}{\partial t}=\frac{D_{intra_s}}{R^2}\left(\frac{\partial^2 Q_s}{\partial X^2}+\frac{2}{X}\frac{\partial Q_s}{\partial X}\right),\quad s=\overline{1,2} \tag{2.52}$$

with initial conditions:

$$C_s\left(t=0,Z\right)=0;\quad Q_s\left(t=0,X,Z\right)=0;\ X\in\left(0,1\right),\ s=\overline{1,2}\ , \tag{2.53}$$

boundary conditions for coordinate X of the crystallite:

$$\frac{\partial}{\partial X}Q_s\left(t,X=0,Z\right)=0\ , \tag{2.54}$$

$$Q_1\left(t,X=1,Z\right)=\frac{K_1C_2\left(t,Z\right)}{1+K_1C_1\left(t,Z\right)+K_2C_2\left(t,Z\right)},\ \text{(Langmuir equilibrium)}$$

$$Q_2\left(t,X=1,Z\right)=\frac{K_2C_2\left(t,Z\right)}{1+K_1C_1\left(t,Z\right)+K_2C_2\left(t,Z\right)}, \tag{2.55}$$

boundary and interface conditions for coordinate Z:

$$C_s\left(t,1\right)=1,\ \frac{\partial C_s}{\partial Z}\left(t,Z=0\right)=0\ ,\quad t\in\left(0,t^{total}\right); \tag{2.56}$$

$K_1=\dfrac{\bar{\theta}_1}{p_1\left(1-\bar{\theta}_1-\bar{\theta}_2\right)}$, $K_2=\dfrac{\bar{\theta}_2}{p_2\left(1-\bar{\theta}_1-\bar{\theta}_2\right)}$, p_1, p_2 - competitive adsorption equilibrium constants and partial pressure of the gas phase for 1-th and 2-th component, $\bar{\theta}_1$, $\bar{\theta}_2$ - the intracrystallite space occupied by the corresponding adsorbed molecules. The expression $\varphi_s\left(C_1,C_2\right)=\dfrac{C_s\left(t,Z\right)}{1+K_1C_1\left(t,Z\right)+K_2C_2\left(t,Z\right)}$ is represented by the series of Tailor [17, 26]:

$$\varphi_s\left(C_1,C_2\right)=\varphi_s\left(0,0\right)+\left(\left.\frac{\partial\varphi_s}{\partial C_1}\right|_{(0,0)}C_1+\left.\frac{\partial\varphi_s}{\partial C_2}\right|_{(0,0)}C_2\right)+\frac{1}{2!}\left(\begin{array}{l}\left.\dfrac{\partial^2\varphi_s}{\partial C_1^2}\right|_{(0,0)}C_1^2+2\left.\dfrac{\partial^2\varphi_s}{\partial C_1C_2}\right|_{(0,0)}C_1C_1+\\ \qquad\qquad+\left.\dfrac{\partial^2\varphi_s}{\partial C_2^2}\right|_{(0,0)}C_2^2\end{array}\right)+\ldots \tag{2.57}$$

As a result of transformations limited to the series not higher than the second order, we obtain:

$$\frac{K_1 C_1(t,Z)}{1+K_1 C_1(t,Z)+K_2 C_2(t,Z)} = K_1 C_1(t,Z) - \left(K_1^2 C_1^2(t,Z) + \frac{1}{2} K_1 K_2 C_1(t,Z) C_2(t,Z) \right),$$

$$\frac{K_2 C_2(t,Z)}{1+K_1 C_1(t,Z)+K_2 C_2(t,Z)} = K_2 C_2(t,Z) - \left(\frac{1}{2} K_1 K_2 C_1^2(t,Z) C_2^1(t,Z) + K_2^2 C_2^2(t,Z) \right). \quad (2.58)$$

Substituting the expanded expression (2.58) in the equations (2.55) of nonlinear system (2.50)-(2.56), we obtain:

$$Q_1(t,\mathrm{X},Z)_{X=1} = K_1 C_1(t,Z) - \varepsilon \left(C_1^2(t,Z) + \frac{1}{2} \frac{K_2}{K_1} C_1(t,Z) C_2(t,Z) \right),$$

$$Q_2(t,\mathrm{X},Z)_{X=1} = K_2 C_2(t,Z) - \varepsilon \left(\frac{1}{2} \frac{K_2}{K_1} C_1(t,Z) C_2(t,Z) + \left(\frac{K_2}{K_1} \right)^2 C_2^2(t,Z) \right), \quad (2.59)$$

where $\varepsilon = K_1^2 << 1$ - small parameter .

Taking into account the approximate equations of the competitive adsorption kinetic (2.59) containing the small parameter ε, we search for the solution to the problem (2.51)-(2.56) by using asymptotic series with a parameter ε in the form [20, 26]:

$$C_s(t,\mathrm{Z}) = C_{s_0}(t,\mathrm{Z}) + \varepsilon C_{s_1}(t,\mathrm{Z}) + \varepsilon^2 C_{s_2}(t,\mathrm{Z}) + \ldots , \quad (2.60)$$

$$Q_s(t,X,Z) = Q_{s_0}(t,X,Z) + \varepsilon Q_{s_1}(t,X,Z) + \varepsilon^2 Q_{s_2}(t,X,Z) + \ldots , \; s = \overline{1,2} . \quad (2.61)$$

As the result of substituting the asymptotic series (2.30)-(2.31) into equations of the nonlinear boundary problem (2.51)-(2.56) considering eq. (2.58), the problem (2.51)-(2.56) will be parallelized into two types of linearized boundary problems [26]:

The problem A_{s_0}, $s = \overline{1,2}$ (*zero approximation with initial and boundary conditions of the initial problem*): to find a solution in the domain

$D = \{(t, \mathrm{X}, \mathrm{Z}):\ t > 0,\ X \in (0,1), Z \in (0,1)\}$ of a system of partial differential equations :

$$\frac{\partial C_{s_0}(t,Z)}{\partial t} = \frac{D_{inter_s}}{l^2}\frac{\partial^2 C_{s_0}}{\partial Z^2} - e_{\text{inter}}\tilde{K}_s \frac{D_{intra_s}}{R^2}\left(\frac{\partial Q_{s_0}}{\partial X}\right)_{X=1}, \tag{2.62}$$

$$\frac{\partial Q_{s_0}(t,X,Z)}{\partial t} = \frac{D_{intra_s}}{R^2}\left(\frac{\partial^2 Q_{s_0}}{\partial X^2} + \frac{2}{X}\frac{\partial Q_{s_0}}{\partial X}\right), \tag{2.63}$$

with initial conditions:

$$C_{s_0}(t=0,Z)=0; \quad Q_{s_0}(t=0,X,Z)=0;\ X \in (0,1),\ s=\overline{1,2}, \tag{2.64}$$

boundary conditions for coordinate X of the crystallite:

$$\frac{\partial}{\partial X} Q_{s_0}(t, X=0, Z) = 0 \tag{2.65}$$

$$Q_{s_0}(t, X=1, Z) = K_s C_{s_0}(t,Z),\ s=\overline{1,2} \tag{2.66}$$

boundary and interface conditions for coordinate Z:

$$C_{s_0}(t,1)=1,\ \frac{\partial C_{s_0}}{\partial Z}(t, Z=0)=0,\quad t \in (0,T); \tag{2.67}$$

The problem $A_n; n=\overline{1,\infty}$ (*n*-th *approximation with zero initial and boundary conditions*): to construct in the domain D a solution to a system of equations:

$$\frac{\partial C_{s_n}(t,Z)}{\partial t} = \frac{D_{inter_s}}{l^2}\frac{\partial^2 C_{s_n}}{\partial Z^2} - e_{\text{inter}}\tilde{K}_s \frac{D_{intra_s}}{R^2}\left(\frac{\partial Q_{s_n}}{\partial X}\right)_{X=1}, \tag{2.68}$$

$$\frac{\partial Q_{s_n}(t,X,Z)}{\partial t} = \frac{D_{intra_s}}{R^2}\left(\frac{\partial^2 Q_{s_n}}{\partial X^2} + \frac{2}{X}\frac{\partial Q_{s_n}}{\partial X}\right), \tag{2.69}$$

with initial conditions:

$$C_{s_n}\left(t=0,Z\right)=0;\quad Q_{s_n}\left(t=0,X,Z\right)=0;\ s=\overline{1,2}\ , \tag{2.70}$$

boundary conditions for coordinate X of the crystallite:

$$\frac{\partial}{\partial X}Q_{s_n}\left(t,X=0,Z\right)=0 \tag{2.71}$$

$$Q_{l_n}\left(t,X,Z\right)_{X=1}=K_1C_{l_n}\left(t,Z\right)-\sum_{\nu=0}^{n-1}C_{l_\nu}\left(t,Z\right)\left(C_{1,n-1-\nu}\left(t,Z\right)+\frac{1}{2}\frac{K_2}{K_1}C_{2,n-1-\nu}\left(t,Z\right)\right),$$

$$Q_{2_n}\left(t,X,Z\right)_{X=1}=K_2C_{2_n}\left(t,Z\right)-\sum_{\nu=0}^{n-1}C_{2_s}\left(t,Z\right)\left(\frac{1}{2}\frac{K_2}{K_1}C_{1,n-1-\nu}(t,Z)+\left(\frac{K_2}{K_1}\right)^2C_{2,n-1-\nu}\left(t,Z\right)\right), \tag{2.72}$$

boundary and interface conditions for coordinate Z:

$$C_{s_n}\left(t,1\right)=0\ ,\ \frac{\partial C_{s_0}}{\partial Z}\left(t,Z=0\right)=0\ ,\quad t\in\left(0,t^{total}\right); \tag{2.73}$$

The problems A_{s_0}, $s=\overline{1,2}$ are linear with respect to zero approximation C_{s_0}, Q_{s_0}. The problems $A_{s_n};\mathrm{n}=\overline{1,\infty}$ are linear with respect to the *n*-th approximation C_{s_n}, Q_{s_n} and nonlinear with respect to all previous *n-1* approximations $C_{s_0},...,C_{s_{n-1}}$.

As demonstrated for the 2 component adsorption model (2.21) - (2.26), our proposed methodology can easily be developed and applied to the competitive adsorption of any number of gases.

The main result of this work is the possibility, from a single experiment, of simultaneously distributing several co-diffusing gases in a porous solid and using the methods of mathematical modeling to analyze for each of them the distribution of their concentrations in the intra and inter-crystallite spaces. Using experimental NMR data and proposed competitive adsorption models, the identification procedures for calculating the competitive diffusion coefficients for two or more components in intra- and inter-crystallite spaces are developed. These procedures use the iterative gradual identification methods on minimizing of the Lagrange error function and rapid analytic methods based on the influence function. The competitive

diffusion coefficients were obtained as a function of time for different positions along the catalyst bed. In particular, those in the intracrystallite space were computed by the analytical method which allowed a calculation with a relatively high degree of discretization over time and to reduce practically twice the volume of iterative calculations. Using these results, the concentrations of co-diffusing benzene and hexane in the inter- and intra-crystallite spaces were calculated for each time and each position in the bed.

Nomenclature for Chapter 2

$k = \overline{1, N+1}$ - layer number, subscript k will be added to all the following symbols to specify that they are characteristic of the k-th layer,

c - adsorbate concentration in macropores,

c_∞ - equilibrium adsorbate concentration in macropores,

$C = c/c_\infty$: dimensionless adsorbate concentration in macropores,

D_{inter} - diffusion coefficient in macropores, m^2/s,

D_{intra} - diffusion coefficient in micropores, m^2/s,

$\tilde{K}$ - adsorption equilibrium constant,

l - bed length, m,

$\Delta l = l_k - l_{k-1}; k = \overline{1, N+1}$: layer thickness (all layers have the same thickness),

L - dimensionless bed length (L = 1),

q - adsorbate concentration in micropores,

q_∞ - equilibrium adsorbate concentration in micropores,

$Q = q/q_\infty$ - dimensionless concentration of adsorbate in micropores,

T - temperature of gas phase flow, °K and time total, s,

M – mass total,

u - velocity of gas phase flow, m/s^2,

Λ - coefficient of thermal diffusion along the columns;

h_g - gas heat capacity, kJ/(kg.K),

μ – molecular mass of adsorbat, kg/mole,

H - total heat capacity of the adsorbent and gas, kJ/(kg.K),

α_h - heat transfer coefficient;

R_{column} - column radius, m

R_g - gas constant, kJ.mol/(m^3·K),

ΔH_i - activation energy ($\Delta H_i = \Delta \bar{H}_i / \mu$), kJ/mol;

$\Delta \bar{H}_i$ - adsorption heat, kJ/kg;

k_{0i} – empirical equilibrium coefficient for the i adsorbat, depends on the adsorbent properties and the diffusing adsorbate component (k_{0i} equal to the ratio of the desorption and adsorption rate constants) ;

x – distance from crystallite center, m,

R – mean crystallite radius, m (we assume that the crystallites are spherical),

X = x/R: dimensionless distance from crystallite center,

z – distance from the bottom of the bed for mathematical simulation, m ,

$Z = z/l$ – dimensionless distance from the bottom of the bed,

t – time,

τ, ξ - variables of integration,

t^{total} - total duration of competitive adsorption, mn,

L_k - dimensionless position of the k-th layer,

$h_k = (L_k - L_{k-1})/2$,

ε_{inter} – intercrystallite bed porosity,

e_{inter} - value utilized in eq. (9),

n - iteration number of identification,

m - number of adsorbed components,

P - number of NMR-observation surfaces,

s - index of adsorbat component,

i - index of NMR-observation surface,

initial – index of initial value (concentations, temperature),

macro – index of extended Lagrange functional component for intercrystallite space,

micro – index of extended Lagrange functional component for intracrystallite space,

Chapter 3. High computational methods and simulation technology nanoporous systems with feedback adsorption for gas purification

The experimental and theoretical study of the adsorption and diffusion of several gases through a microporous solid and the instantaneous (out of equilibrium) distribution of the adsorbed phases is particularly important in many fields, such as gas separation, heterogeneous catalysis, purification of confined atmospheres, reduction of exhaust emissions contributing to global warming, etc. [6] Taking into account the influence of physical factors that limit the adsorption kinetics on the surface of nanopores, the quality of the mathematical models for the adsorption of exhaust gases (hydrocarbon components, CO_2) in a microporous bed determines the effectiveness of technological solutions to the neutralization of gas emissions [6-8].

However, most of these models do not fully reflect the complex spatial-temporal representations of the variations of the heat and mass transfers in inter- and intra-crystalline spaces, including the internal kinetics of the adsorption and desorption. In particular, the equations of adsorption equilibrium are mainly determined by simplified quasi-stationary and isothermal dependences without taking into account changes in gas flow, ambient temperature and activation energy of adsorption which is determined by the Lennard-Jones energy potential and is the main thermal characteristic of adsorption. Therefore, it is necessary to develop rigorous mathematical models of adsorption processes in the form of systems of differential equations in partial derivatives, taking into account the completeness of all the physical factors mentioned above, including efficient methods of constructing their solutions and implementing software. The development of such models should summarize the available results of experimental research and optimize programs for their implementation in the future. In this publication, which is the development of references [15-20], we propose a solution to this problem.

For modelling, we use the high-performance methods of the Heaviside operational calculus and the Landau approach to linearization and expansion into a

series of non-isothermal Langmuir adsorption equilibrium at the temperature of desorption equilibrium [10, 17, 27].

3.1 Nonlinear mathematical model of nonisothermal adsorption and desorption based on the generalized Langmuir adsorption equilibrium equation

The inlet gas diffuses into the macropores (inter-crystalline space) and micropores of the crystallites. The model we have implemented in a generalized formulation takes into account the dependence of the Langmuir adsorption equilibrium on the gas flow temperature and the activation energy ΔH of adsorption, which determines the degree of adsorption exothermicity. These two important limiting kinetics factors are interrelated and included in the exponential dependence into the nonlinear equilibrium equation, taking into account the physical assumptions described in [7, 10, 11]. In this case, the residence time of the adsorbed molecules on the adsorption sites in crystallites decreases exponentially as its temperature grows. This approach should make it possible to deepen the nanoprocess rather than treating it as a "black box".

Therefore, taking into account the previous remarks, the kinetics of nonisothermal adsorption for capture of gas (for example greenhouse) in nanoporous materials is described by the following system of nonlinear differential equations [10, 11]:

$$\frac{\partial c(t,z)}{\partial t}+\frac{\partial a(t,z)}{\partial t}+u\frac{\partial c}{\partial z}=D_{\text{int}er}\frac{\partial^2 c}{\partial z^2}, \tag{3.1}$$

$$-H\frac{\partial T(t,z)}{\partial t}-uh_g\frac{\partial T}{\partial z}-Q_{ads}\frac{\partial a}{\partial t}-\frac{2\alpha_h}{R_{column}}T+\Lambda\frac{\partial^2 T}{\partial z^2}=0, \tag{3.2}$$

$$\frac{\partial a}{\partial t}=\beta\left(c-\frac{1}{b_0\exp\left(-\frac{\Delta H}{RT}\right)}\frac{a}{a_{full}-a})\right). \tag{3.3}$$

Differential equations (3.1) - (3.3) satisfy the following initial conditions:

a) adsorption: b) desorption:

$$c(t,z)\big|_{t=0} = 0, \qquad c(t,z)\big|_{t=0} = c_0^{(0)},$$

$$T(t,z)\big|_{t=0} = T_0^{(0)}, \qquad T(t,z)\big|_{t=0} = T_0^{(0)}, \quad (3.4)$$

and boundary conditions:

a) adsorption: b) desorption:

$$c(t,z)|_{z=o} = c_{in}, \qquad c(t,z)|_{z=0} = c_{in}(t),$$

$$\frac{\partial}{\partial z}c(t,z)|_{z=\infty} = 0, \qquad \frac{\partial}{\partial z}c(t,z)|_{z=\infty} = 0$$

$$T(t,z)|_{z=0} = T_{in} \quad \frac{\partial}{\partial z}T(t,z)|_{z=\infty} = 0 \quad T(t,z)|_{z=0} = T_{in}(t) \quad T(t,z)|_{z=0} = T_{in}(t) \quad (3.5)$$

The different symbols are defined at the end of the nomenclature. Model (3.1) - (3.5) is presented mathematically in a more generalized form.

The length of the column is considered infinite for the construction of a general solution based on the Heaviside method. In the specific calculations, a finite value l is used.

Parallelizing a nonlinear model to the system of linearized boundary problems.

We develop some elements of differential equation (3). By expanding the expression $\exp\left(\frac{\Delta H}{RT}\right)$ in $\frac{1}{\exp\left(-\frac{\Delta H}{RT}\right)}\frac{a}{a_{full}-a}$, according to the Landau approach, in a Taylor series in the vicinity of the desorption equilibrium temperature T_{eq} we obtain [17, 27, 28]:

$$\exp\left(\frac{\Delta H}{RT}\right) = \exp\left(\frac{\Delta H}{RT_{eq}}\right) - \frac{\Delta H}{R}\exp\left(\frac{\Delta H}{RT_{eq}}\right)\frac{1}{T_{eq}^2}\left(T - T_{eq}\right) + \frac{1}{2!}\left(\frac{\Delta H}{R}\right)^2 \exp\left(\frac{\Delta H}{RT_{eq}}\right)\left(\frac{1}{T_{eq}^4} + \frac{R}{2\Delta H}\frac{1}{T_{4eq}^3}\right)\left(T - T_{eq}\right)^2 + \ldots \quad (3.6)$$

Taking into account that $a / a_{full} < 1$, the expression $\left(a / a_{full}\right) / \left(1 - \frac{a}{a_{full}}\right)$ is laid out in a series of Maclaurin as:

$$\frac{a / a_{full}}{1 - \frac{a}{a_{full}}} = \frac{1}{1 - \frac{a}{a_{full}}} - 1 = \frac{a}{a_{full}} + \left(\frac{a}{a_{full}}\right)^2 + \ldots + \left(\frac{a}{a_{full}}\right)^n + \ldots \,. \tag{3.7}$$

Neglecting terms of at least second order in (6) and (7), the expression $\frac{1}{\exp\left(-\frac{\Delta H}{RT}\right)} \frac{a}{a_{full} - a}$ takes the form [17]:

$$\frac{1}{b_0 \exp\left(-\frac{\Delta H}{RT_{eq}}\right)} \frac{a / a_{full}}{1 - a / a_{full}} \approx \gamma a(t,z) + \varepsilon a^2(t,z) - \varepsilon\theta\varepsilon a(t,z) T(t,z) \,. \tag{3.8}$$

Substituting (3.8) in eq. (3.3) we obtain:

$$\frac{\partial a}{\partial t} = \beta(c - \gamma a(z,t) - \varepsilon a(z,t)\left(a(t,z) - \theta T(t,z)\right)) \,, \tag{3.9}$$

where $\gamma = \frac{1 + \frac{\Delta H}{R}}{a_{full} b_0} \exp\left(\frac{\Delta H}{RT_{eq}}\right)$ - the coefficient of the linear component of the transformed function of adsorption equilibrium (8); $\varepsilon = \frac{1 + \frac{\Delta H}{R}}{b_0 (a_{full})^2} \exp\left(\frac{\Delta H}{RT_{eq}}\right) = \gamma / a_{full}$ small parameter taking into account the nonlinear component of the adsorption isotherm, $\theta = \frac{a_{full}}{1 + \frac{\Delta H}{R}} \frac{\Delta H}{R} \frac{1}{T_{eq}^2}$.

Taking into account (3.9), the solution to the problem (3.1)-(3.5) will be in the form of the series [21]:

$$\begin{aligned} c(t,\mathrm{z}) &= c_0(t,\mathrm{z}) + \varepsilon c_1(t,\mathrm{z}) + \varepsilon^2 c_2(t,\mathrm{z}) + \ldots \,, \\ T(t,\mathrm{z}) &= T_0(t,\mathrm{z}) + \varepsilon T_1(t,\mathrm{z}) + \varepsilon^2 T_2(t,\mathrm{z}) + \ldots \,, \\ a(t,\mathrm{z}) &= a_0(t,\mathrm{z}) + \varepsilon a_1(t,\mathrm{z}) + \varepsilon^2 a_2(t,\mathrm{z}) + \ldots \end{aligned} \tag{3.10}$$

As a result of substituting the asymptotic sums (10) into equation (3.1) - (3.5), the output nonlinear problem (3.1) - (3.5) is parallelized into two types of quasi-linear boundary -value problems [18]:

Problem A_0 **(**zero approximation with initial and boundary conditions of the original nonlinear problem): find a solution in the field $D = \{(t,z): t > 0,\ z \in (0,\infty)\}$ of a system of partial differential equations:

$$\frac{\partial c_0(t,z)}{\partial t} + \frac{\partial a_0(t,z)}{\partial t} + u\frac{\partial c_0}{\partial x} = D_{inter}\frac{\partial^2 c_0}{\partial z^2}, \tag{3.11}$$

$$-H\frac{\partial T_0(t,z)}{\partial t} - uh_g\frac{\partial T_0}{\partial z} - Q_{ads}\frac{\partial a_0}{\partial t} - \frac{2\alpha_h}{R_{column}}T_0 + \Lambda\frac{\partial^2 T_0}{\partial z^2} = 0, \tag{3.12}$$

$$\frac{\partial a_0}{\partial t} = \beta(c_0 - \gamma a_0). \tag{3.13}$$

Initial conditions:

a) adsorption:	b) desorption:
$c_0(t,z)\big\|_{t=0} = 0,$	$c_0(t,z)\big\|_{t=0} = c_0^{(0)},$
$T_0(t,z)\big\|_{t=0} = T_0^{(0)},$	$T_0(t,z)\big\|_{t=0} = T_0^{(0)},$

(3.14)

and boundary conditions:

a) adsorption:	b) desorption:
$c_0(t,z)\big\|_{z=o} = c_{in},$	$c_0(t,z)\big\|_{z=0} = c_{in}(t),$

(3.15)

$$\frac{\partial}{\partial z}c_0(t,z)|_{z=\infty}=0\,,\qquad \frac{\partial}{\partial z}c_0(t,z)|_{z=\infty}=0\,,$$

$$T_0(t,z)|_{z=0}=T_{in}\,,\ \frac{\partial}{\partial z}T_0(t,z)|_{z=\infty}=0\,,\qquad T_0(t,z)|_{z=0}=T_{in}(t)\,,\ \frac{\partial}{\partial z}T_0(t,z)|_{z=\infty}=0\,.$$

Problem $A_n;\ n=\overline{1,\infty}\,3.$

$$\frac{\partial c_n(t,\mathrm{z})}{\partial t}+\frac{\partial a_n(t,\mathrm{z})}{\partial t}+u\frac{\partial c_n}{\partial z}=D_{\text{inter}}\frac{\partial^2 c_n}{\partial z^2}\,, \tag{3.16}$$

$$-H\frac{\partial T_n(t,z)}{\partial t}-uh_g\frac{\partial T_n}{\partial z}-Q_{ads}\frac{\partial a_n}{\partial t}-\frac{2\alpha_h}{R_{column}}T_n+\Lambda\frac{\partial^2 T_n}{\partial z^2}=0\,, \tag{3.17}$$

$$\frac{\partial a_n}{\partial t}=\beta\left(c_n-\gamma a_n-\sum_{i=0}^{n-1}\left(a_i(t,\mathrm{z})\left(a_{n-1-i}(t,\mathrm{z})-\frac{R}{\Delta H}T_{n-1-i}(t,\mathrm{z})\right)\right)\right). \tag{3.18}$$

The problem A_0 is linear respectively to the zero approximation $c_0,\ a_0,\ T_0$**;** the problem $A_n;\ n=\overline{1,\infty}$ is linear in the *n*-th approximation and nonlinear in all previous approximations, $i=\overline{0,n-1}$.

3.2 The methodology for constructing analytical solution systems to heterogeneous adsorption / desorption problems

We construct analytical solutions to problems A_0 and $A_n;\ n=\overline{1,\infty}$, using the Heaviside operational method [29, 30]. Applying the integral operator of the direct Laplace transform to the time variable t in problems (3.11) - (3.15) and (3.16) - (3.18), we obtain the corresponding system of problems in Laplace images [29]:

Problem A_0^*: to find in the domain $D^*=\{z\in(0,\infty)\}$ a solution to the system of equations:

$$\frac{d^2c_0^*(p,\mathrm{z})}{dz^2}-u_1\frac{dc_0^*}{dz}-q_1^2(p)c_0^*=-\mathrm{F}_{c_0}^{\ *}(p)\,, \tag{3.19}$$

$$\frac{d^2}{dz^2}T_0^* - u_2\frac{d}{dz}T_0^* - q_2^2(p)T_0^* = -\mathrm{F}_{T_0}{}^*(p), \tag{3.20}$$

$$a_0^*(p,\mathrm{z}) = \beta\frac{1}{p+\beta\gamma}c_0^*(p,\mathrm{z}). \tag{3.21}$$

Boundary conditions are as follows:

a) adsorption: b) desorption:

$$\begin{aligned} &c_0^*(p,z)|_{z=o} = c_{in}^*(p), && ,\frac{d}{dz}c_0^*(p,z)|_{z=\infty} = 0, \\ &\frac{\partial}{\partial z}c_0^*(p,z)|_{z=\infty} = 0, && c_0^*(p,z)|_{z=o} = \frac{1}{p}c_{in}, \end{aligned} \tag{3.22}$$

$$T_0^*(p,z)|_{z=0} = \frac{1}{p}T_{in},\ \frac{\partial}{\partial z}T_0^*(p,z)|_{z=\infty} = 0, \qquad \frac{\partial}{\partial z}T_0^*(p,z)|_{z=\infty} = 0,\ T_0^*(p,z)|_{z=0} = T_{in}^*(p).$$

Problem $A_n^*;\ n=\overline{1,\infty}$: to find in the domain $D^* = \{z \in (0,\infty)\}$ a solution to the system of equations:

$$\frac{d^2c_n^*}{dz^2} - u_1\frac{dc_n^*}{dz} - q_1^2(p)c_n^* = -\mathrm{F}_{c_n}{}^*(p,\mathrm{z}), \tag{3.23}$$

$$\frac{d^2}{dz^2}T_n^* - u_2\frac{d}{dz}T_n^* - q_2^2(p)T_n^* = -\mathrm{F}_{T_n}{}^*(p,z), \tag{3.24}$$

$$a_n^*(p,z) = \beta\frac{1}{p+\beta\gamma}\left(c_n^* - \left(\sum_{i=0}^{n-1}a_i a_{n-1-i}\right)^*(p,z)\right), \tag{3.25}$$

where

$$\begin{aligned} &u_1 = \frac{u}{D_{\text{inter}}},\ q_1^2(p) = \frac{p(p+\beta(\gamma+1))}{D_{\text{inter}}(p+\beta\gamma)}, \quad q^2(p) = \frac{1}{\Lambda}\left(Hp + \frac{2\alpha_h}{R_{column}}\right), \\ &\mathrm{F}_{c_0}^* = \frac{c_0^0}{D_{\text{inter}}},\ \mathrm{F}_{T_0}{}^*(p,z) = \frac{1}{\Lambda}\left(HT_0 - \beta Q_{ads}\left(1 - \frac{\beta\gamma}{p+\beta\gamma}\right)c_0^*(p,z)\right), \end{aligned} \tag{3.26}$$

$$\mathrm{F}_{c_n}{}^{*}(p,z)=\frac{\beta}{D_{\text{inter}}}\left(1-\frac{\beta\gamma}{p+\beta\gamma}\right)\left(\sum_{i=0}^{n-1}a_i\left(a_{n-1-i}-\frac{R}{\Delta H}T_{n-1-i}\right)\right)^{*}(p,z),$$

$$\mathrm{F}_{T_n}{}^{*}(p,z)=-\frac{\beta Q_{ads}}{\Lambda}\left(1-\frac{\beta\gamma}{p+\beta\gamma}\right)\left(c_n^{*}(p,z)-\left(\sum_{i=0}^{n}a_i\left(a_{n-1-i}-\frac{R}{\Delta H}T_{n-1-i}\right)\right)^{*}(p,z)\right),$$

$$c^{*}(p,z)=\int_0^{\infty}c(t,z)\mathrm{e}^{-pt}dt\equiv L[c],\ a^{*}(p,Z)=\int_0^{\infty}a(t,z)\mathrm{e}^{-pt}dt\equiv L[a],\ T^{*}(p,z)=\int_0^{\infty}T(t,z)\mathrm{e}^{-pt}dt\equiv L[T].$$

Solution to problem A_0. We construct a solution to the heterogeneous problem A_0^{*} (using the Cauchy method) [29, 30]:

$$c_0^{*}(p,z)=(pc_{in}^{*}(p))e^{\frac{u_1}{2}z}\frac{e^{-\omega_1(p)z}}{p}+c_0^0\frac{\gamma}{\gamma+1}\left(\frac{1}{p}+\frac{1}{p+\beta(\gamma+1)}-\frac{\gamma+1}{\gamma}e^{\frac{u_1}{2}z}\frac{e^{-\omega_1(p)z}}{p}\right)+$$
$$+c_0^0\frac{\beta}{(p+\beta(\gamma+1))}\frac{e^{-\omega_1(p)z}}{p}e^{\frac{u_1}{2}z} \qquad (3.27)$$

$$T_0^{*}(p,z)=pT_{in}^{*}(p)\frac{e^{\left(\frac{u_2}{2}-\omega_2(p)\right)z}}{p}+\int_0^{\infty}e^{\frac{u_2}{2}(z-\xi)}\left(\frac{e^{-\omega_2(p)|z-\xi|}}{2\omega_2(p)}-\frac{e^{-\omega_2(p)(z+\xi)}}{2\omega_2(p)}\right)\mathrm{F}_{T_0}{}^{*}(p,z,\xi)d\xi \quad ,(3.28)$$

where

$$\omega_1(p)=\left(\frac{u_1^2}{4}+q_1^2(p)\right)^{1/2},\ \omega_2(p)=\left(\frac{u_2^2}{4}+q_2^2(p)\right)^{1/2},\ \mathrm{Re}\omega_1>0,\ \mathrm{Re}\omega_2>0. \qquad (3.29)$$

Applying the integral operator of the inverse Laplace transform

$$L^{-1}\left[\ldots^{*}(p,\mathrm{z})\right]=\frac{1}{2\pi i}\int_{\sigma_0-i\infty}^{\sigma_0+i\infty}\ldots^{*}(p,\mathrm{z})e^{pt} \qquad (3.30)$$

to formulas (3.27) and (3.28), we obtain their originals on the basis of [29] and form an analytical solution to the zero-approximation problem: the dependence on the temperature and time of the adsorbate concentration in inter-particle space and in micropores along the coordinate z:

$$c_0(t,z)=c_{in}(0)e^{\frac{u}{2D_{\text{inter}}}z}\Phi_c^0(t,z)+e^{\frac{u}{2D_{\text{inter}}}z}\int_0^t\frac{d}{d\tau}c_{in}(\tau)\Phi_c^0(t-\tau,z)d\tau+$$
$$+c_0^0\frac{\gamma}{1+\gamma}\left(1+\frac{1}{\gamma}e^{-\beta(\gamma+1)t}-\frac{\gamma+1}{\gamma}e^{\frac{u}{2D_{\text{inter}}}z}\Phi_c^0(t,z)\right)+\beta c_0^0e^{\frac{u}{2D_{\text{inter}}}z}\int_0^t e^{-\beta(\gamma+1)(t-s)}\Phi_c^0(\tau,z)d\tau \quad ,(3.31)$$

$$T_0(t,z)=T_{in}(0)\Phi_T^0(t,z)+\int_0^t\Phi_T^0(t-\tau,z)\frac{d}{d\tau}T_{in}(\tau)d\tau+$$
$$+\frac{1}{\Lambda}\int_0^t\int_0^\infty\left(H\Pi_0^0\mathrm{H}_T(t-\tau,z,\xi)-\beta Q_{ads}\left(\mathrm{H}_T(t-\tau,z,\xi)-\beta\gamma\int_0^{t-\tau}\mathrm{H}_T(\tau-s,z,\xi)e^{-\beta\gamma(t-\tau-s)}ds\right)c_0(\tau,\xi)\right)d\xi d\tau \quad ,(3.32)$$

$$a_0(t,z)=\beta\int_0^t e^{-\gamma\beta(t-\tau)}c_0(\tau,z)d\tau \quad (3.33)$$

Solution to problem $A_n;\ n=\overline{1,\infty}$**.** The solutions to problem $A_n^*;\ n=\overline{1,\infty}$ are functions [29, 30]:

$$c_n^*(p,\mathrm{z})=\int_0^\infty e^{\frac{u_1}{2}(z-\xi)}\left(\frac{e^{-\omega_1(p)|z-\xi|}}{2\omega_1(p)}-\frac{e^{-\omega_1(p)(z+\xi)}}{2\omega_1(p)}\right)\mathrm{F}_{c_n}{}^*(p,\xi)d\xi \quad , \quad (3.34)$$

$$T_n^*(p,z)=\int_0^\infty e^{\frac{u_2}{2}(z-\xi)}\left(\frac{e^{-|z-\xi|\omega_2(p)}}{2\omega_2(p)}-\frac{e^{-(z+\xi)\omega_2(p)}}{2\omega_2(p)}\right)\mathrm{F}_{T_n}^*(p,\xi)d\xi \quad , \quad (3.35)$$

$$a_n^*(p,\mathrm{z})=\frac{\beta}{p+\gamma\beta}\left[c_n^*(p,\mathrm{z})-\left(\sum_{i=0}^{n-1}a_i\left(a_{n-1-i}-\frac{R}{\Delta H}T_{n-1-i}\right)\right)^*(p,\mathrm{z})\right]. \quad (3.36)$$

Substituting the $\mathrm{F}_{c_n}{}^*(p,\xi)$ and $\mathrm{F}_{T_n}{}^*(p,\xi)$, respectively, into equation (3.31), (3.32) and applying the operator of the inverse Laplace transform to formulas (3.34) - (3.36), we obtain on the basis of [29, 30, 31] their originals, which form the analytical solution to the problem $A_n;\ n=\overline{1,\infty}$**:**

$$c_n(t,\mathrm{z})=\frac{\beta}{D_{\text{int}er}}\int_0^\tau\int_0^\infty\left[\mathrm{H}_c(t-\tau;z,\xi)-\beta\gamma\int_0^{t-\tau}e^{-\beta\gamma(\tau-s)}\mathrm{H}_c(\mathrm{s};z,\xi)ds\right]\left(\sum_{i=0}^{n-1}a_i\left(a_{n-1-i}-\frac{R}{\Delta H}T_{n-1-i}\right)\right)(\tau,\xi)d\xi d\tau \quad , \quad (3.37)$$

$$T_n(t,z)=\frac{\beta Q_{ads}}{\Lambda}\int_0^t\int_0^\infty\left(\mathrm{H}_T(t-\tau,z,\xi)-\beta\gamma\int_0^{t-\tau}\mathrm{H}_T(\tau-s,z,\xi)e^{-\beta\gamma(t-\tau-s)}ds\left(\sum_{i=0}^{n-1}a_i\left(a_{n-1-i}-\frac{R}{\Delta H}T_{n-1-i}\right)\right)(\tau,\xi)-c_0(\tau,\xi)\right)d\xi d\tau, \quad (3.38)$$

$$a_n(t,\mathrm{z}) = \beta\int_0^t e^{-\beta\gamma(t-\tau)}\left(c_n(\tau,\mathrm{z}) - \sum_{i=0}^{n-1} a_i\left(a_{n-1-i} - \frac{R}{\Delta H}T_{n-1-i}\right)(\tau,\mathrm{z})\right)d\tau \quad (3.39)$$

Here $c_n(t,z), a_n(t,z)$ - the n-th approximation of the adsorbate concentration in inter-crystallites space and in nanopores of crystallites, $T_n(t,z)$ - the n-th approximation of temperature of gaze flow;

$$\Phi_c^0(t,z) = = \frac{1}{\pi}\int_0^\infty e^{-\varphi_1(\nu)z}\frac{\sin\left(\nu t - z\varphi_2(\nu)^2\right)}{\nu}d\nu + e^{-\frac{u}{2D_{\text{inter}}}z},$$

$$\Phi_c(t,\mathrm{z}) = \frac{1}{2\pi}\int_0^\infty \frac{\varphi_1(\nu)\cos\left(\nu t - \varphi_2(\nu)\mathrm{z}\right) + \phi_2(\nu)\sin\left(\nu t - \varphi_2(\nu)\mathrm{z}\right)}{\left(\Gamma_1^2(\nu) + \nu^2\Gamma_2^2(\nu)\right)^{1/2}}d\nu.$$

$$\Phi_T^0(t,z) = \frac{1}{\pi}\int_0^\infty e^{-\phi_1(\nu)z}\frac{\sin\left(\nu t - z\phi_2(\nu)^2\right)}{\nu}d\nu + e^{-\frac{u}{2D_{\text{inter}}}z},$$

$$\Phi_T(t,\mathrm{z}) = \frac{1}{2\pi}\int_0^\infty \frac{\phi_1(\nu)\cos\left(\nu t - \phi_2(\nu)\mathrm{z}\right) + \phi_2(\nu)\sin\left(\nu t - \phi_2(\nu)\mathrm{z}\right)}{\left(\Gamma_{T_1}^2(\nu) + \nu^2\Gamma_{T_2}^2(\nu)\right)^{1/2}}d\nu, \quad (3.40)$$

$$\mathrm{H}_T(\tau;z,\xi) = e^{-\frac{u_2}{2}(z-\xi)}\left(\Phi_T(\tau,|z-\xi|) - \Phi_T(\tau,z+\xi)\right)$$

$$\mathrm{H}_c(\tau;z,\xi) = e^{-\frac{u_1}{2}(z-\xi)}\left(\Phi_c(\tau,|z-\xi|) - \Phi_c(\tau,z+\xi)\right)$$

$$\varphi_{1,2}(\nu) = \left[\frac{\left(\Gamma_1^2(\nu) + \nu^2\Gamma_2^2(\nu)\right)^{1/2} \pm \Gamma_1^2(\nu)}{2}\right]^{1/2}, \quad \Gamma_1(\nu) = \frac{u^2}{4D_{\text{inter}}^2} + \frac{\nu^2\beta}{D_{\text{inter}}^2\left(\nu^2+\beta^2\gamma^2\right)}$$

$$\Gamma_2(\nu) = \frac{\nu^3 + \nu\beta^2(\gamma+1)\gamma}{D_{\text{inter}}\left(\nu^2+\beta^2\gamma^2\right)}, \quad \phi_{1,2}(\nu) = \left[\frac{\left(\Gamma_{T_1}^2(\nu) + \nu^2\Gamma_{T_2}^2(\nu)\right)^{1/2} \pm \Gamma_{T_1}^2(\nu)}{2}\right]^{1/2}$$

$$\Gamma_{T_1}(\nu) = \frac{u^2 + 4\Lambda\mathrm{X}^2}{4\Lambda^2}, \quad \Gamma_{T_2}(\nu) = \frac{H\nu}{\Lambda}.$$

3.3 Computer simulation. Analysis of the distributions of the adsorbent concentration in the gas phase and nanopores of zeolite and temperatures

The objective of this computer modelling is to study the capabilities of the proposed model for its use in gas separation technologies, in catalysis, for the purification of air, in particular for the elimination of carbon emissions into the atmosphere from industry and transport (propane, CO_2 and other combustion products). This is one of the main ways to solve the problem of global warming and to create a secure energy strategy [6].

Propane was chosen as the adsorbate because it corresponds to approximately 30% by volume of the total gas flow emitted by car engines [7]. Using the developed mathematical theory and technology oriented to parallel multicore computer calculations, the modeling and calculation of concentration dependences of non-isothermal adsorption and desorption curves in a zeolite ZSM 5 bed are carried out.

Computational calculations were performed with such experimental conditions [10, 17]**:**

- geometric dimensions of the column open at both ends: length: $l = 1.5 \cdot 10^{-2}$ m and radius $R_{collon} = 0,3$ m;

-thermal and mass transfer characteristics: Q_{ads}=2800 kJ/kg; Λ= 0,5 kJ /(m^2·K·h), h_g = 1,2 kJ / m^3·K (for propane at 3 bar); ρ_a= 600-700 kg/m^3 (bulk density of zeolite); H = 0,96 kJ/kg·K; α_h = 20 kJ/(m^2·K·h);

- D_{inter}= 5,0.10^{-6} m^2/c ; β=0,95 c^{-1} [10, 17].

Initial gas flow temperature: for adsorption T = 20 °C, for desorption T = 300 - 350°C. In order to analyze the effect of changes in flow velocity, a range of 0.2 -2 m/s was considered (adsorption, desorption). The number of members in the series of approximation expressions (3.13) was taken from 15 to 20.

To desorb propane from the nanopores of the zeolite, the column with zeolite simple was heated to a temperature of 300-350 °C and an inert gas (argon) was passed through it at a pressure of 10-12 bar.

Using the equations (3.36) and (3.40), the adsorbate concentrations in inter- and intra-crystallites spaces were calculated. Figures 1a, 1b, c, d show the variation against time of the concentration, C, in such column and at the temperature of 30 °C, 60 °C, 100° C, 350°C of the bed.

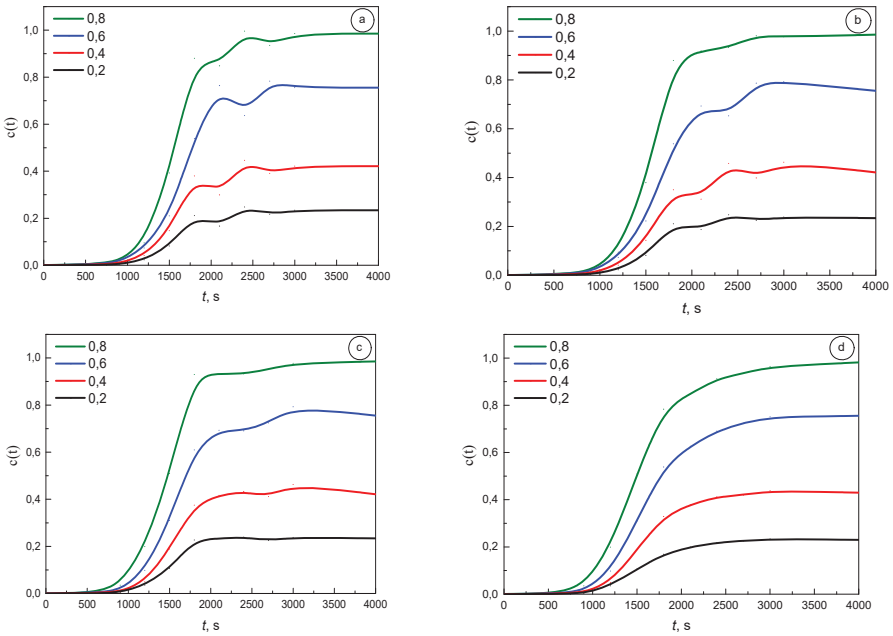

Figure 3.1. Variations against time of the adsorbate concentration in the inter-crystallites space $c = c(t, z)$ at different levels of the column z $(z / l = 0,2;\ 0,4;\ 0,6;\ 0,8)$ were calculated at the temperature of 30 ^{0}C (**a**), 60 ^{0}C (**b**), 100 ^{0}C (**c**), 350^{0}C (**d**) of the bed

As can be seen, their general character is qualitatively similar: for each of the values z / l, the adsorbate concentration $c(t)$ increases with time. Moreover, in Figure 3.1 a, b, a slight decrease in the concentration of the adsorbate can be observed, and then an increase again, reaching equilibrium. It should be noted that with increasing temperature the detected effect is becoming less and less pronounced. The appearance of this effect is due to the fact that at low temperatures the molecules repel each other, as shown by the Lennard-Jones relationship, and cause a slight decrease in the molecules adsorbed in the nanopores. With increasing temperature, the repulsive forces between the molecules weaken, and the aforementioned effect becomes weaker.

Figure 3.2 a, b, c, d show modelled variations against time of the adsorbate concentration, a(t,z), in the nanopores, at different position *z* and temperature of the bed.

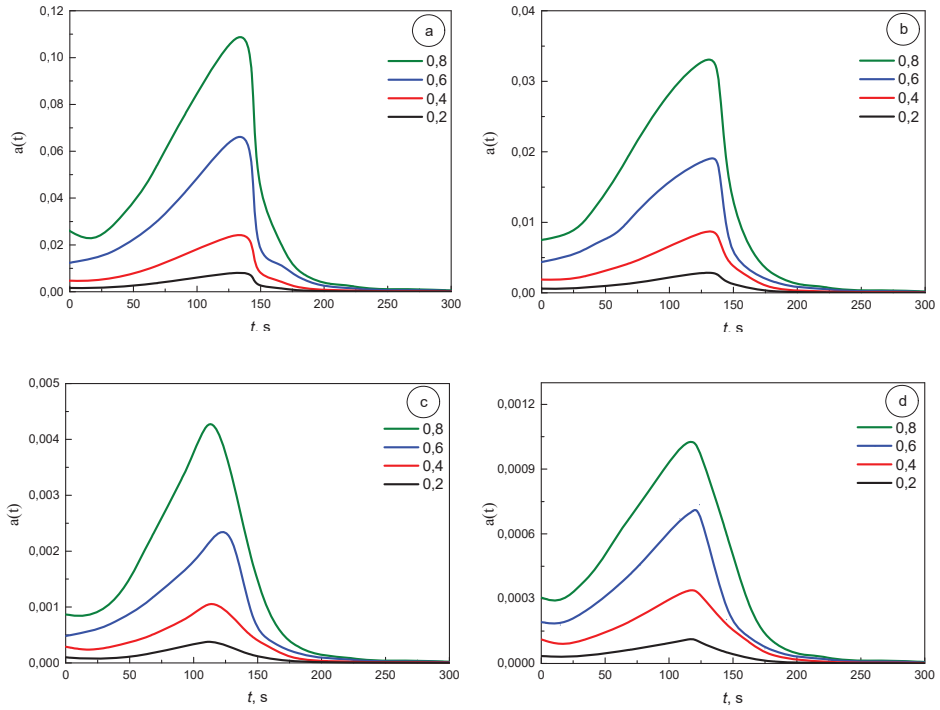

Figure 3.2. The dependence of the concentration $a = a(t,z)$ in the nanopores of the adsorbent at fixed values $z\ (z/l = 0,2;\ 0,4;\ 0,6;\ 0,8)$ calculated at the temperature of 30 ^{0}C (**a**), 60 ^{0}C (**b**), 100 ^{0}C (**c**), 350^{0}C (**d**)

These four Figures all have the same shape and the same relative position of the curves with Z position in the column. After a few minutes the adsorption in the pores increases rapidly with time and reaches a maximum in about 125 seconds regardless of the adsorption temperature T, whose value decreases with increasing T and decreasing *z/l*.

After reaching the maximum, a rapid desorption can be obtain which is practically complete after about 125 seconds.

Comparing the dependences of Figure 2 a, b, c, d and Figure 3.3, it can be seen that the process of absorption in nanopores occurs in the interval from 25 s to 250 s, while the temperature inside the test sample varies on average from 30 °C to 350 °C. This process is significantly affected by an increase in temperature inside the bed.

Figure 3.4. represents the variation of the adsorbate concentration in the interparticle space, C as a function of the flow rate at the inlet and the temperature at fixed values of the adsorption time t = 300 *s*.

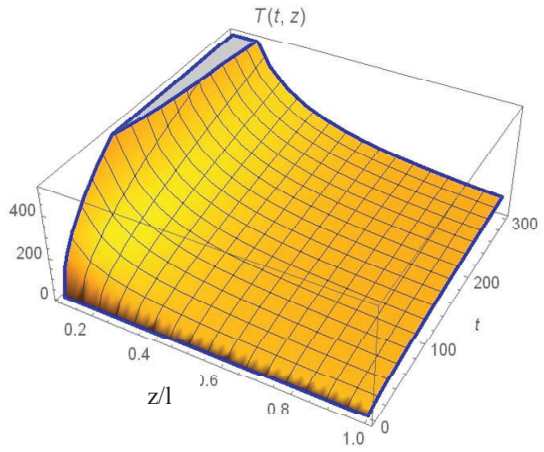

Figure 3.3. The time dependence on the temperature $T = T(t,z)$ inside the micropores for fixed values z $(z/l = 0,2;\ 0,4;\ 0,6;\ 0,8)$

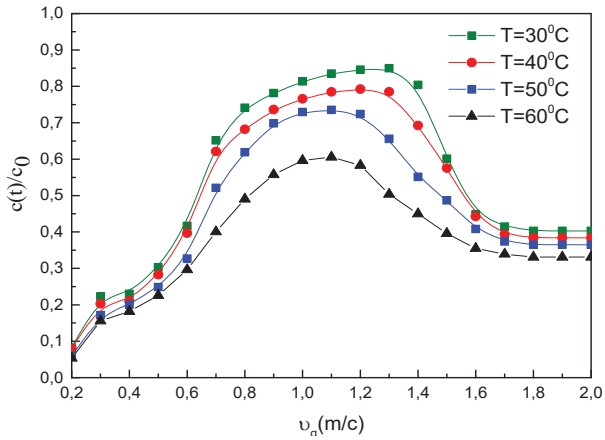

Figure 3.4. Adsorbate concentration C in the interparticle space as a function of the inlet flow rate ν and temperature of gas flow at fixed adsorption durations t=400 *s* and $z/l = 0.4$

Our computer-based research has confirmed the effectiveness of the proposed model and software for adsorption-desorption technology to absorb gases, in particular carbon oxydes that cause global warming. The spatial distribution of the adsorbate concentrations in inter-particle space and in micropores of solid are obtained with the achievement of equilibrium conditions, as well as the distributions of the gas flow temperature over time and the coordinates of the column length. It also allows to evaluate the behavior of concentration dependences, achieving their equilibrium from temperature and gas flow rate for different coordinate positions along the column length and other factors. But this was not only the main goal of this study. Analytical solutions to the proposed mathematical model of the gas adsorption on microporous bed is based on the original mathematical apparatus and an efficient high-performance algorithm using the Heaviside operational method and the Laplace transform using the generalized Langmuir equilibrium equation, which most fully describes the processes of phase transformations. The development of calculations is quite original. The result allows to instantly get the dynamics of the kinetics of the process in columns during non-isothermal adsorption and desorption - the current adsorbate concentrations in interparticle space and in micropores of the bed and the temperature of gas flow. This original mathematical treatment can serve as a model

for many applications related to this type of process, mainly to clean atmospheres, which will help reduce the impact of global warming

Nomenclature for Chapter 3

c – current adsorbate concentration in interparticle space,

c_0 – current adsorbate concentration in interparticle space at $z=0$,

T– current temperature of gas phase flow, ^0C

T_{eq} – the desorption equilibrium temperature, ^0C ($T_{eq}=350\ ^0C$)

a – current adsorbate concentration in micropores,

D_{inter} – effective longitudinal diffusion coefficient, m^2/s,

ΔH – adsorption activation energy, *kJ/mol,*

R – *gas* constant, $kJ/mol/(m^3)$,

$0 < b_0 < 1$, b_0 – empirical coefficients depending on the properties of nanoporous adsorbents and adsorbate components (b_0 equal to the rate constants of desorption and adsorption),

a_{full} – concentration of adsorbate in nanopores with full filling of adsorption centers, *mol/g,*

R_{column} – radius of adsorption column, *m,*

l - height of adsorption column, *m* ($l >> R_{column}$);

Q_{ads} – heat of adsorption on micropores *kJ/kg;* ($\Delta H = M_{ads} Q_{ads}$),

M_{ads} – molecular weight of the adsorbent,

u – gas flow rate, *m/c;*

Λ – coefficient of thermal diffusion of the adsorption along the column, $kJ/(m^2 \cdot K \cdot c)$,

H – total heat capacity of gas and adsorbent *kJ /(kg·K),*

h_g – heat capacity of gas,

$2\alpha_h / R_{collon}$ – coefficient of heat loss through the wall of the column,

α_h – coefficient of heat transfer,

D_{inter} – diffusion coefficient in interparticle space, m^2/c,

β – total mass transfer coefficient, c^{-1},

z – distance coordinate from the top of the bed, m,

Z – dimensionless coordinate = abscissa *z/height* of the column,

ρ – specific masse of the adsorbent kg/m^3.

Chapter 4. High-performance algorithms for solving systems of nonlinear equations on supercomputers with parallel organization of computations

In the numerical modeling of natural phenomena, the behavior of objects under the influence of the environment, the design of buildings and mechanisms, etc. often arise, for example, when using three-dimensional models, computational (discrete) problems to an extremely large number (which can exceed 10^7) equations, including nonlinear ones. Moreover, the data (Jacobi matrices) of such nonlinear systems (SNQ) have a sparse structure, for example, block-tridiagonal or block-five-diagonal. That is, the number of nonzero elements is much less (approximately equal to k_n, where n is the order of the matrix, and $k << n$) - the total number of matrix elements.

The growth o f the parameters for the problems being solved, the calculation on computers of more complete models of objects, processes, phenomena requires a corresponding increase in the productivity of computers. Currently, the increase in computing performance is achieved through parallelization, based on the use of computers with many processor devices, in particular with multi-core processors. In these computers, as a rule, the MIMD architecture (architecture with multiple instructions and data flow) is implemented. In recent years, hybrid computing systems have also become widespread, in which coprocessors are used, for example, graphics processing units (GPUs) to speed up computations when performing large volumes of homogeneous arithmetic operations. On such coprocessor accelerators, as a rule, the SIMD parallel computing architecture is implemented. Such computers of hybrid architecture have already taken leading positions in the world ranking of the most computers TOP500 [32].

Let us consider the solutions to systems of nonlinear equations on computers of hybrid architecture and computers with multi-core Intel Xeon Phi x200 series processors, in particular, using a multilevel model of parallel computing.

4.1 Layered parallel computing model

The architecture of modern high-performance computers allows the use of a multilevel parallel computing model - multilevel parallelism:

– upper level (MIMD model) - process level parallelism (PLP) - processes in parallel perform macro-operations (subtasks), for example, multiplication of matrix blocks, using both distributed between them and shared memory and synchronizing calculations and data exchanges;

– the second level (SIMD model) - thread level parallelism (TLP) - parallelization of the execution of each of the macro-operations using several threads and shared memory;

– the third level (vectorization) parallelism of data processing by vector processing units (data level parallelism, DLP) - operations with vectors are performed in parallel, for example, addition of vectors.

At the top level, MPI tools are used (as a rule), at the second level, OpenMP (Open Multi-Processing) tools (directives) or program modules of the Intel MKL multithreaded library are used. The third level is to automatically enable parallelism when compiling a program.

Problem statement. In the region $D = \{a_i \le x_i \le b_i,\ i = 1, 2, \ldots, n\}$ find n-dimensional vector $x = (x_1, x_2, \ldots, x_n)^T \in D$, which satisfies a system of n linear equations

$$F(x) = 0, \tag{4.1}$$

where $F(x) = (F_1(x), F_2(x), \ldots, F_n(x))^T$ – n-dimensional vector function, and $F(x)$ is an approximation to the exact vector function $\Phi(x)$ and these functions satisfy the inequality $\| F(x) - \Phi(x) \| \le \delta$ for any $x \in D$. To solve problem (4.1), an initial approximation is given $x^{(0)} \in D$ and the required accuracy ε of obtaining an approximation to the solution of the system.

In applied sciences, in particular, in calculating the stress-strain state of structures of complex energy systems and objects [33], the following formulation of a nonlinear problem is used. The mathematically static nonlinear problem of calculating the strength of structures of these objects, using the principle of possible displacements, can be posed in the infinite-dimensional functional space of possible displacements U_0 in the form of a variational problem: find the vector function $u \in U_0$, which for any vector function $v \in U_0$ satisfies the corresponding integral identity

$$a(u,v) = l(f,v), \tag{4.2}$$

where the functional $a(u,v)$ nonlinear on u and linear on v is proportional to the potential energy of deformation, and the functional $l(f,v)$ linear on v is proportional to the work of the applied forces f under load.

Solutions to nonlinear problems (4.2) are found by one of the projection-variational methods, mainly by the finite element method (FDM). Approximate ITU solutions are sought in the finite-dimensional (n-dimensional) subspace $U_0^h \subset U_0$. Vector functions from a subspace U_0^h are piecewise polynomial and can be represented as a linear combination of basis vector functions $u_h(\chi) = \sum_{j=1}^{n} x_j \varphi_j(\chi)$,

where $\varphi_j (j = 1, 2, \ldots, n)$ – the mentioned above piecewise polynomial basis U_0^h. Substituting vector functions from the subspace U_0^h into (4.2), we obtain the system of nonlinear (with respect to x_j) equations

$$a(u_h, \varphi_k) = l(f, \varphi_k), \quad k = 1,2,\ldots,n. \tag{4.3}$$

The solution of SNE (4.3) is based, as a rule, on the linearization of nonlinear equations - the search for solutions is realized through the solution of a sequence of linear systems with approximate Jacobi matrices. In many applications, this is done using the derivative of the functional $a(u,v)$

$$a'(u,v,w) = \frac{d}{d\tau} a(u + \tau w, v)\Big|_{\tau=0}, \quad w \in U_0 \tag{4.4}$$

for calculating approximations of the Jacobian matrix of system (4.3). Then the matrix of the linearized system

$$Ax = b \tag{4.5}$$

can be calculated by the formula

$$\left\{a_{ij}\right\}_{i.j=1}^{n} = \left\{a'(u_h, \varphi_i, \varphi_j)\right\}_{i.j=1}^{n}, \tag{4.6}$$

where u_h is the approximate solution obtained in the previous step (iteration step). The matrix $\left\{a_{ij}\right\}_{i.j=1}^{n}$ can be obtained by differentiating (according to (4.4)) $a(u_h, \varphi_k)$ on x_i from (4.3).

In many applied applications, iterative methods for solving the SNS (4.1) or (4.3) are implemented, based (see papers [34, 35]) on the classical Newton's method to one degree or another, have a quadratic convergence rate. In this case, at each iteration, a SLAE is solved with the Jacobian matrix of the system or some matrix close to it, and the elements of the matrices and the components of the vectors of the right-hand sides of these SLAE's are calculated using the solutions obtained at the previous iteration.

We denote $H(x) = \left\{\frac{\partial F_i}{\partial x_j}\right\}_{i,j=1}^{n}$ – the Jacobi matrix of the system (4.1) or (4.3), $B(x)$ – some approximation to $H(x)$. If the derivative of the functional is often used to calculate the approximate Jacobian matrix of system (4.3) $a(u,v)$ (4.4), then $a'(u_h, v_h, w_h) = H(x)y$ (if $y = (y_1, y_2, \ldots, y_n)^T$, $u_h = \sum_{j=1}^{n} x_j \varphi_j$, $w_h = \sum_{j=1}^{n} y_j \varphi_j$, $v_h = \sum_{j=1}^{n} \varphi_j$).

The iterative process is the same if an estimate is performed $\| x^{(k)} - x \| \le c \| x^{(k-1)} - x \|^{\alpha}$, where c – some quantity bounded from above; α – method convergence order. If $\alpha = 2$, then the quadratic rate of convergence of the iterative process is achieved, if $1 < \alpha < 2$, then the iterative process coincides nonlinearly.

The iterative process of Newton's method for a given initial approximation is written as (k = 1, 2, ... – is the iteration number, $F^{(k)} \equiv F(x^{(k)})$ and $B^{(k)} \equiv H^{(k)} \equiv H(x^{(k)}))$

$$B^{(k-1)} w^{(k)} = -F^{(k-1)}, \tag{4.7}$$

$$x^{(k)} = x^{(k-1)} + w^{(k)}. \tag{4.8}$$

In many cases, to solve the SNE, modifications of the Newton method are used, which, with some approximations to the Jacobi matrix (these methods often have an overline convergence rate), include:

– Broyden's and Powell's methods (for symmetric Jacobi matrices), in which in the course of the iterative process (4.7), (4.8) are calculated based on the initial approximation $B^{(0)} \equiv H^{(0)}$ matrices are refined using matrix-vector operations according to the formulas: in Powell's method – $B^{(k)} = B^{(k-1)} + \frac{y^{(k)}(w^{(k)})^T + w^{(k)}(y^{(k)})^T}{(w^{(k)})^T w^{(k)}} - \frac{((y^{(k)})^T w^{(k)}) w^{(k)}(w^{(k)})^T}{((w^{(k)})^T w^{(k)})^2}$, in Broyden's method – $B^{(k)} = B^{(k-1)} + \frac{y^{(k)}(w^{(k)})^T}{(w^{(k)})^T w^{(k)}}$; here $y^{(k)} = F^{(k)} - F^{(k-1)} - B^{(k-1)} w^{(k)}$;

– Burdakov's method, which, with a special choice of the iterative parameter, ensures global convergence to one of the solutions of the system based on a given initial approximation; the iterative process is realized by formulas (4.7) and $x^{(k)} = x^{(k-1)} + \alpha_k w^{(k)}$, where $B^{(k)}$ – finite-difference approximation of the Jacobi matrix $H^{(k)}$, and the iterative parameter α_k is calculated by special way.

So, the solution to a SNE with a sparse data structure, as a rule, is based on the linearization of nonlinear equations - the search for solutions is realized through the solution to a sequence of systems of linear equations. These SLAEs (4.4) have several features that affect the choice of methods and means for solving them on computers by organizing computations, namely:

– high order - from 100,000 to tens of millions;

– sparse structure of SLAE matrices - strip, profile, block-sparse, etc.;

– symmetry or asymmetry of SLAE matrices;
– positive definiteness or semi-definiteness of the matrices of the SLAE.

When choosing an iterative method for solving the SNE, an important condition is the preservation of the sparse structure of the SLAE matrices, which is solved at each iteration. Therefore, the decisive algorithm for the choice of computation distribution schemes, decomposition and data storage on parallel computers is the corresponding SLAE solution algorithm. This algorithm, in turn, is chosen based on the type and sparse structure of the SLAE matrix.

4.2 Parallel algorithms for solving SNE with a sparse data structure

In the general case, the iterative processes of the above methods for solving an SNQ with a sparse data structure can be written in the following form $B^{(k-1)}w^{(k)} = -F^{(k-1)}$, $x^{(k)} = x^{(k-1)} + \alpha_k w^{(k)}$ ($k = 1, 2, ...$).

For the case of block-diagonal matrices with framing, block (non-cyclic) algorithms are used. Accordingly, in this case, block schemes for the distribution and storage of matrix elements and the right side of the SLAE are used. At the upper level of parallelism, nonzero data blocks distributed to a given process (stream) are calculated, maximally using (if possible) the lower levels of parallelism to perform matrix-vector and matrix-matrix operations [36, 37].

To solve SLAEs with sparse matrices other than block-diagonal structures with framing, block-cyclic algorithms are used. In accordance with the requirements of the parallel algorithms used, the elements of the matrices and the right-hand sides of such SLAEs are distributed. That is, block-cyclic schemes are used. In this case, also (but according to a block-cyclic scheme), at the upper level of parallelism, non-zero data blocks are distributed to a given process (stream), the maximum using (if possible) the lower levels of parallelism to perform matrix-vector and matrix-matrix operations.

SNE solution methodology. So, the main operation at each iteration is the solution of SLAE (4.4) with a sparse matrix $B^{(k-1)}$. The following sequence of actions is proposed for solving the SNE with sparse data on modern high-performance computers, including hybrid architecture:

– using one of the structural regularization algorithms, the formation of a block-sparse structure of matrices of SLAE (4.6) based on the original structure of its nonzero elements;

– decomposition of sparse matrices and distribution of the resulting rows or columns of nonzero blocks between processor devices;

– iterative process for solving SNE – on *k*-th iteration (k = 1, 2, …) algorithm of Newton's or quasi-Newtonian method, the following macro-operations are performed:

1) computation of components of a vector function distributed between MPI processes $F^{(k-1)}$ and elements of nonzero blocks of the matrix $B^{(k-1)}$;

2) solution to the obtained SLAE (4.4) using the corresponding (in the structure of the matrix $B^{(k-1)}$) parallel algorithm [37, 39], and calculation of the components of the next approximation to the solution distributed between MPI processes NSE $x^{(k)}$;

3) checking the conditions for the end of the iterative process by formulas [34]: first – $\| F^{(k)} \| \le \varepsilon$, next – $\| (H^{(k)})^{-1} \| \| F^{(k)} \| \le \varepsilon$.

These macro-operations are performed at the upper level of parallelism, using the lower levels to perform large amounts of homogeneous computations, including matrix-vector and matrix-matrix operations.

It should be noted that the number of arithmetic operations in the development of matrices of SLAEs is significant (for example, for strip matrices - about m times, m is the half-width of the tape) more than the number of other arithmetic operations. Therefore, the decomposition of sparse matrices of SLAE plays a decisive role in assessing the efficiency of the algorithm for solving the SNS. The efficiency of the algorithm can be increased if the solution to the SLAE with a lower triangular matrix (direct move) is performed simultaneously with the developed matrices of the system.

Structural regularization of sparse matrices. So, the main operation at each iteration is the solution to SLAE (4.4) with a sparse matrix $B^{(k-1)}$. The structure of sparse matrices is determined by the numbering of the unknowns and can be regular (e.g., Band) or irregular.

In order to reduce the number of arithmetic operations for solving SLAE (4.5) with a sparse matrix by structural regularization - permutations of rows and columns (i.e., renumbering unknowns), such a matrix leads to one of the standard looks: strip, profile, block-diagonal with framing, "skyscraper" and others. There are several algorithms [39] for optimizing the structure of a sparse matrix (factor trees, Cathill-McKee, parallel sections, minimum degree, etc.).

Multilevel parallelism assumes the use of block and block-loop algorithms based on the block representation of matrices. Therefore, it is advisable to structurally regularize the sparse matrix - to optimize the block-sparse structure of the matrix by defining zero blocks in the block partition and filling nonzero blocks as much as possible and using one of the above algorithms (moreover, the algorithms use blocks instead of matrix elements) [49].

4.3 Parallel algorithms for solving systems of linear equations with a sparse matrix

As was noted above, most of the methods for solving computational problems that go into the mathematical modeling of various processes, phenomena and objects are based on the solution to systems of linear algebraic equations (SLAE) with sparse matrices.

The SLAE can be solved by direct and iterative methods. Most direct methods are based on the idea of successive equivalent transformations of a given system in order to eliminate unknowns from a part of the equations. Various modifications of the elimination methods are, in fact, methods of factorizing the matrix of the system, that is, decomposing the matrix into a product, for example, of triangular matrices or orthogonal and triangular matrices. Matrix factorization can also be used in iterative methods.

In this case, in the problems of solving the SLAE, as a rule, three subproblems can be distinguished: (i) decomposition of the matrix of the system $A = LR$, (ii) solutions to a SLAE with a left matrix (direct substitution or direct move) $Ly = b$, (iii) solutions to a SLAE with a right matrix (backward substitution or backward move) $Rx = y$.

When factorizing a matrix, much more arithmetic operations are performed than when solving a SLAE with decomposition matrices. For example, the decomposition of a strip symmetric matrix requires $O(nm^2)$ arithmetic operations with floating point, and the solution of two SLAEs with decomposition matrices requires $O(nm)$. Therefore, the efficiency of factorization of sparse matrices plays a key role in the development of efficient methods and parallel algorithms for solving computational problems arising in mathematical modeling. Next, we will consider methods and parallel algorithms for factorizing sparse matrices.

4.3.1 Block algorithms for the decomposition of non-degenerate matrices

As noted above, the highest performance of modern computers can be achieved using matrix-matrix operations and the corresponding program modules of program libraries from hardware developers, for example, Intel MKL [40] (on multi-core processors) or CUBLAS [41] (in coprocessor-accelerators - GPU). Therefore, the classical methods and algorithms (Gauss, Cholesky [42]) should be modified by presenting them in block form.

Block algorithm of the Gauss method *LU*-decomposition of square matrices. Consider the *LU*-decompositions of a square matrix A of order n. Let's break it down into blocks of size $s \times s$. Without losing the generality of reasoning, we can assume that n/s – integer. After K-1 (K = 1, 2, …, n/s–1) steps blocks of the modified matrix $A^{(k-1)}$ can be schematically represented in the form shown in Fig. 4.1 on the left. Here blocks, for which *LU*-decompositions are obtained, are indicated: $A_f^{(k-1)} = L_1^{(k-1)} U_1^{(k-1)}$ – square diagonal block of order $ks–s$, $A_l^{(k-1)} = L_2^{(k-1)} U_1^{(k-1)}$ – subdiagonal rectangular block of size $(r+s)\times(ks–s)$, where $r=n–ks$, $A_u^{(k-1)} = L_1^{(k-1)} U_2^{(k-1)}$ – superdiagonal rectangular block of size $(ks–s)\times(r+s)$, and a square diagonal block whose expansion is still in progress, $A_R^{(k-1)} = P^{(k-1)} A_R^{(0)} - L_2^{(k-1)} U_2^{(k-1)}$ of order $r+s$. In the $A_R^{(k-1)}$ in turn, 4 blocks are allocated: A_{11} – square diagonal block of order s (k-th step leading block), A_{12} – rectangular block of size $s \times r$, A_{21} – rectangular block of size $r \times s$, A_{22} – square diagonal block of order r.

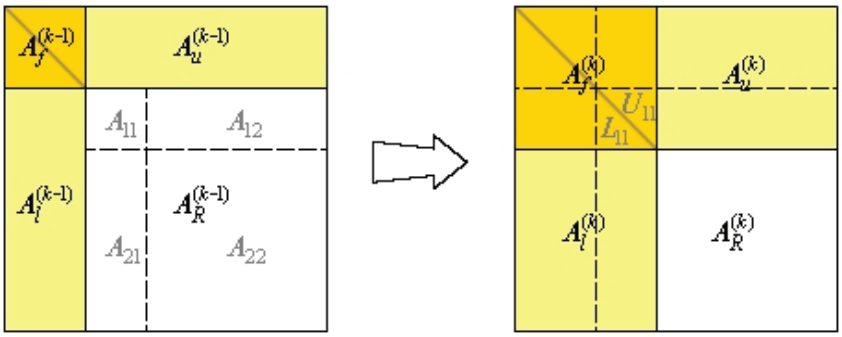

Figure 4.1 – Scheme of one step of the block version of the *LU*-decomposition

At the *k*-th step, decomposition (modification) of the block is performed $A_R^{(k-1)}$ due to the formulas:

$$\begin{pmatrix} A_{11} & A_{12} \\ A_{21} & A_{22} \end{pmatrix} = P_k \begin{pmatrix} L_{11} & 0 \\ L_{21} & I_r \end{pmatrix} \begin{pmatrix} U_{11} & U_{12} \\ 0 & A_R^{(k)} \end{pmatrix} = P_k \begin{pmatrix} L_{11}U_{11} & L_{11}U_{12} \\ L_{21}U_{11} & L_{21}U_{12} + A_R^{(k)} \end{pmatrix}, \qquad (4.9)$$

where P_k – *k*-th step permutation matrix.

First, according to (4.9), the *LU* decomposition of the block is performed by the Gaussian method A_{11}, and blocks L_{21} and U_{12} it is possible to obtain solutions to matrix SLAEs $U_{11}^T L_{21}^T = \widetilde{A}_{21}^T$ and $L_{11}U_{12} = \widetilde{A}_{12}$, where $\widetilde{A}_{IJ}$ - the corresponding matrix blocks after permutations have been denoted. The black $A_R^{(k)}$ is calculated due to the expression:

$$A_R^{(k)} = \widetilde{A}_{22} - L_{21}U_{12}. \qquad (4.10)$$

This operation is also called *s*-rank modification.

It should be noted that the efficiency of block algorithms is greatly influenced by the strategy of choosing the main element. For example, the selection of the main element only within the diagonal block A_{11} allows all other calculations to be reduced to matrix-matrix operations. But if the search for the main element is performed, for example, in a column, then blocks A_{11} and A_{21} must be decomposed simultaneously (in this case, using transformations of columns, that is, vectors). The pivot selection strategy affects the number and volume of data exchanges between parallel processes. In the case of a sparse matrix, a good choice of strategy can reduce the total amount of arithmetic operations.

We note that it is not necessary to perform block row permutations $L_1^{(k-1)}$, $L_2^{(k-1)}$ or/and columns of blocks $U_1^{(k-1)}$, $U_2^{(k-1)}$, but these permutations must be taken into account when using the matrices of the *LU*-decomposition of the original matrix.

In the case of a sparse matrix of system *A*, the decomposition matrices *L* and *U* also remain sparse, although in the general case the number of nonzero elements increases (and only within the matrix profile). Therefore, when the expansion (4.9) of the block $A_R^{(k-1)}$, it is advisable to carry out calculations only with nonzero elements of the corresponding blocks of the matrix. So, the element with indices *i* and *j* of the matrix (block) $A_R^{(k)}$ is modified only if the scalar product of the *i*-th row of the matrix L_{21} and *j*-th columns of the matrix U_{12} is not identically zero. The same is true for the blocks into which the matrix is divided. Therefore, the *s*-range modification (4.10) is performed only from the submatrix of the matrix $L_{21}U_{12}$, which consists of its nonzero elements or nonzero blocks.

Block algorithms of the Cholesky method of decomposition of symmetric matrices. LL^T- decomposition of a symmetric matrix is carried out in a similar way, taking into account that in this case $U_{12} = (L_{21})^T$. This allows us to reduce the number of arithmetic operations by almost 2 times.

In the case of the LDL^T decomposition in formulas (4.9) and (4.10), it is necessary to set $U_{11} = D_1(L_{11})^T$, $U_{12} = D_1(L_{21})^T$, where D_1 is the diagonal matrix for LDL^T- decomposition of the block A_{11}. We note that in this case the product $L_{21}U_{12} \equiv L_{21}D_1(L_{21})^T$ – is the symmetric matrix. Therefore, in this case, the number of arithmetic operations decreases by almost 2 times, if the calculations are carried out in such a sequence: (i) LDL^T- decomposition of the block A_{11}, (ii) - calculation of the block U_{12}, (iii) - calculation of the block $L_{21} = (U_{12})^T(D_1)^{-1}$, (iv) *s*- range modification (4.10).

4.3.2 Block-cyclic algorithms for LU-decomposition of sparse asymmetric matrices

For the case of a multilevel model of parallel computations in [43-57], a number of variants of parallel block-cyclic algorithms for solving SLAEs with sparse, in particular, strip matrices, are proposed and investigated. These algorithms use cyclic distribution schemes of nonzero matrix blocks - row and column. Moreover, the distribution is carried out so that each process (thread) has at least one row or column of blocks, it is modified according to (4.10) at this stage. If it is necessary to select the principal elements in the columns of the matrix, the cyclic distribution scheme of the columns of the matrix blocks turns out to be the more effective.

Block cyclic algorithm for *LU*-decomposition of a banded non-symmetric matrix. We consider on the matrix A of order n with m subdiagonal and m overdiagonal. When LU is developed due to permutations choosing a principal element, in the general case, the number of superdiagonals in the upper triangular matrix U can increase to $m_u + m_l$. In most cases, the lower triangular matrix L is not explicitly formed, and permutations are taken into account when solving the SLAE $Ly = Pb$ [48, 54].

The proposed algorithm is based on the above-mentioned block algorithm of the Gauss method – LU decomposition of square matrices.

Decomposition and distribution of matrix elements between processing units. The matrix A is divided into square blocks of order s (to simplify the presentation, we will assume that $n = Ns$, $m_l = M_{LS}$, $m_l + m_u = M_{US}$):

$$A = \begin{pmatrix} A_{1,1} & A_{1,2} & \cdots & A_{1,M_U+1} & 0 & 0 & \cdots & 0 \\ A_{2,1} & A_{2,2} & \cdots & A_{2,M_U+1} & A_{2,M_U+2} & 0 & \cdots & 0 \\ \vdots & \vdots & \ddots & & & & & \\ A_{M_L+1,1} & A_{M_L+1,2} & & & & & & \\ 0 & A_{M_L+2,2} & & & & & & \\ 0 & 0 & & & & \ddots & \vdots & \vdots \\ \vdots & \vdots & & & & \cdots & A_{N-1,N-1} & A_{N-1,N} \\ 0 & 0 & & & & \cdots & A_{N,N-1} & A_{N,N} \end{pmatrix}.$$

Taking into account the following division of one step of the algorithm into macro-operations, it is advisable between threads of the highest level of parallelism

cyclically distribute columns of matrix blocks (they are also called "tiles" - tiles) so that each process must have at least one column of blocks, modified according to (4.10) at this stage. For example, the blocks that are in the t column are allocated by the stream with the logical number (t-1) mod p. In the algorithms presented here and below, it is advisable to combine square blocks of the corresponding column of blocks into rectangular blocks, the size of which should be optimal from the point of view of data caching (to optimize data exchange between memories of different performance) or the use of GPU computers of hybrid architecture. From the same considerations, the storage scheme (column or row) of the elements of these blocks is also selected.

MPI- process (thread) that contains the K-th column of blocks at the K-th step of the algorithm (the block's $A_{11}^{(K)}$ and $A_{21}^{(K)}$), hereinafter referred to as the master CPU (like the associated GPU in the case of the hybrid algorithm). In the GPU memory, at each step of the hybrid algorithm, it is sufficient to store only (also cyclically distributed) nonzero submatrix blocks that are processed.

Algorithm. In Fig. 4.2 the form of fragments of an asymmetric banded matrix is shown before the K-th step of the algorithm - on the right, if $m_l + m_u > s$, and on the left, if the width of the tape $m_l + m_u \le s$. As we can see in Fig. 4.2, the ability to parallelize computations between threads of the highest level of parallelism is only in the case $m_l + m_u \ge ps$, $p > 1$, and the larger p is, the higher the efficiency of this parallelization. On the other hand, as shown by numerical experiments, the highest efficiency of using both modern GPUs and multi-core Intel Xeon Phi x200 series processors is achieved for sufficiently large values s – from 64 to 192. Therefore, the algorithm proposed below should be applied precisely in the case $m_l + m_u \ge ps$, $p > 1$.

In the case of selecting the main element in the columns of the diagonal block for $K = 1, ..., N$ the following macrooperations are performed (below the tilde marks the blocks of the matrix after the permutations, see Fig. 4.2)

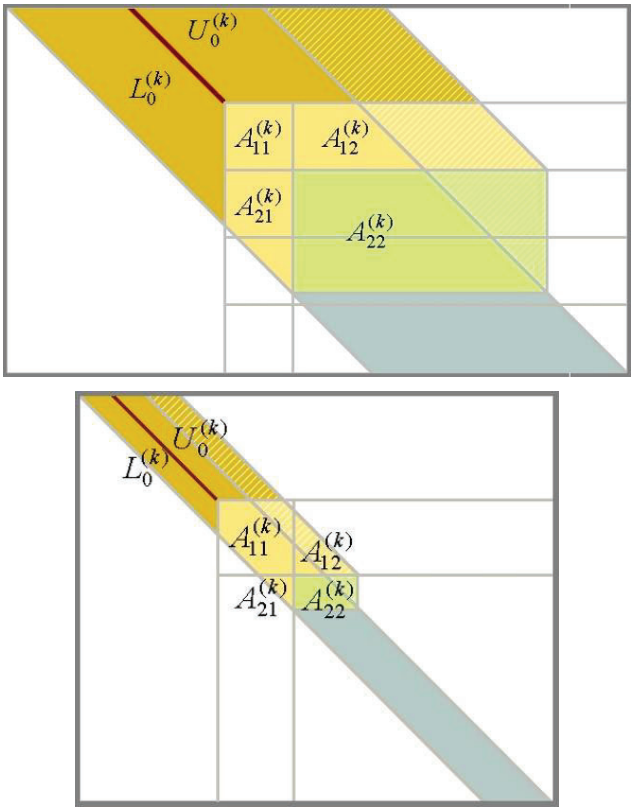

Figure 4.2 – Schemes of one step of the block *LU* decomposition of banded matrices

1) For $K > 1$, using the *s*-rage modification (4.10) for calculating diagonal block $A_{11}^{(K)} = \widetilde{A}_{K,K} - L_{K,K-1} U_{K-1,K}$.

2) For $K > 1$ sending the computed block to the master CPU of the K-th step $A_{11}^{(K)}$ (on a hybrid computer or when using distributed memory).

3) *LU*-decompositions with partial choice of the principal element of the diagonal block

$$A_{11}^{(K)} = L_{11}^{(K)} U_{11}^{(K)}. \qquad (4.11)$$

It is advisable to perform decompositions (4.11) on the master CPU using high-performance program modules of the multithreaded Intel MKL library [40], with a partial choice of principal elements in the columns of the submatrix $A_{11}^{(K)}$.

4) For $K < N$-1 *s*-range modification (4.10) for nonzero block's $\widetilde{A}_{I,J}$ ($K \le I \le N$, $K \le J \le N$, including the nondiagonal block $\widetilde{A}_{K,K}$) of the submatrix $\widetilde{A}_{22}^{(K)}$:

$$A_{I,J} \leftarrow \widetilde{A}_{I,J} - L_{I,K-1} U_{K-1,J}. \tag{4.12}$$

Macro-operations (4.12) are executed at the lower levels of parallelism under the conditions $L_{I,K}, U_{K,J} \neq 0$ according to block allocation $A_{I,J}$ between processor devices.

5) For $K < N$-1 distribution of calculated blocks $L_{11}^{(K)}, U_{11}^{(K)}$ and information about permutations to all processor devices that are used.

6) For $K < N$-1 computation of nonzero blocks $L_{I,K}$ $(K+1 \le I \le N)$ submatrix $L_{21}^{(K)}$ – solutions of matrix SLAEs with lower triangular matrix:

7)

$$(U_{11}^{(K)})^T (L_{I,K})^T = (\widetilde{A}_{I,K})^T. \tag{4.13}$$

The macrooperations (4.13) are executed on the master processor units of the K-th step at the lower levels of parallelism.

8) For $K < N$-1 broadcasting non-zero computed blocks to all processor devices that are in use $L_{I,K}$ $(K+1 \le I \le N)$ submatrix $L_{21}^{(K)}$.

9) For $K < N$-1 computation of nonzero blocks $U_{K,J}$ ($K+1 \le J \le N$) of the submatrix $U_{12}^{(K)}$ – solutions of matrix SLAEs with lower triangular matrix:

10)

$$L_{11}^{(K)} U_{K,J} = \widetilde{A}_{K,J}. \tag{4.14}$$

Macro-operations (4.14) are performed (taking into account row permutations) at the lower levels of parallelism in accordance with the block allocation $\widetilde{A}_{K,J}$.

An analysis of formulas (4.11) - (4.14) showed that most calculations can be implemented at lower levels of parallelism, using software modules for matrix-matrix (or matrix-vector) operations from hardware developers, for example, the Intel MKL multithreaded library (on multicore processors) or the CUBLAS library (on coprocessor-accelerators - GPU).

The efficiency of the algorithm can be increased by performing decompositions (4.11) (item 3) and sending the decomposition blocks (item 5) simultaneously (in parallel, asynchronously) with the end of the macrooperations (4.12) (item 4) of the previous step, using different streams of the upper level of parallelism or CPU and GPU on hybrid computers. It is also possible to increase the efficiency of the algorithm due to the simultaneous execution of computations and data exchanges between different processor devices, for example, data exchanges (items 2, 7) are performed against the background of computations.

If the GPU memory is not enough to store all the data that is distributed by a given processor device, then Section 5 is supplemented with the operations of sending the previously calculated nonzero submatrix blocks to the CPU and sending the blocks of the original matrix necessary for the K-th step to the GPU in accordance with their distribution. Copying to the CPU memory is also performed to save the *LU*-decomposition matrices for their reuse.

If you need to select the main elements in the columns of submatrices $A_{11}^{(K)}$ and $A_{21}^{(K)}$, then instead of (4.11) and (4.13) the expansions

$$\begin{pmatrix} A_{I,I} \\ \vdots \\ A_{K,I} \end{pmatrix} = P_I \begin{pmatrix} L_{I,I} \\ \vdots \\ L_{K,I} \end{pmatrix} U_{I,I}, \tag{4.15}$$

and the following changes must be made to the algorithm laid out: 1-3 replace the diagonal block $A_{11}^{(K)}$ of a rectangular submatrix, consisting of a diagonal block $A_{11}^{(K)}$ and a subdiagonal rectangular block $A_{21}^{(K)}$, item 6 - exclude.

We note that at the I-th step of this algorithm, operations are performed only with blocks of the submatrix of size $(J+1)s \times (K+1)s$, the upper left block of which is $A_{I,I}$. The number of arithmetic operations can be reduced by excluding operations with the last zero columns of a rectangular block in (4.12) and (4.13) U_{12} from (4.9)

(block lines $U_{I,I+1}$, $U_{I,I+2}$, …, $U_{I,J}$). In this case, at the I-th step of the algorithm, operations will be performed from a submatrix of size $(j_I - Is+s) \times (K+1)s$, where j_I – maximum value of the second index of nonzero elements of the block U_{12}.

As it was noted above, the efficiency of algorithms that implement the block version of the *LU*-decomposition is greatly influenced by the strategy of choosing the pivot element. This strategy affects the number and volume of data exchanges between computing devices that are used. For example, with a partial selection of the main element among the elements of the matrix column, the most effective option is when the main element is selected only among the elements of the column of the leading diagonal block; number of operations, exchanges and synchronizations) is a choice among all non-zero elements of the column.

The proposed algorithm can be implemented both on single-node computers with several GPUs (using POSIX Threads, OpenMP) and on multi-node computers (using MPI).

The efficiency of the algorithm. The efficiency of parallelizing the solution of a SLAE is determined by the efficiency of the decomposition algorithms for the matrix of the system, since the number of arithmetic operations performed during the development of (4.11) is many times greater than the number of operations performed when solving systems $PLy = b$ or $Ux = y$.

Let us investigate the efficiency of the hybrid version of the block cyclic *LU*-decomposition algorithm (with the choice of the principal element within the diagonal block) of a banded asymmetric matrix of order n with m_l subdiagonals and m_u superdiagonals (architecture used with p CPU and p GPU).

Let O_k denote the number of arithmetic operations performed in the implementation of the k-th macro-operation of the algorithm. The following estimates are valid: $O_{4a} \approx 2s^3/3$, $O_{4b} \approx m_l s^2$, $O_6 \approx 2m_l m_u s/p$, $O_8 \approx m_u s^2/p$ (operations of item 1 of the leading GPU are taken into account in O_6). We denote: t_C, t_G – average execution times of one arithmetic operation on the CPU and on the GPU, respectively, n_o - the number of arithmetic operations the GPU can perform simultaneously. Since the GPU implements the SIMD architecture, the average time spent by one GPU on performing O homogeneous arithmetic operations is estimated as $t_G O/n_O$.

Macro operations items 2, 3, 5, 7, 8 are associated with data exchange within or between processor devices. In most cases, the time of exchange between the CPU and the GPU, as well as row permutations, can be neglected. If the "tree" algorithm [41] is used to send data from one GPU to all others, then the total time of a multi-force (with one GPU p CPU or with one CPU p GPU, including synchronization) of an array of q double words can be estimated on average by the value $q(t_{CG} + t_{CC} \log_2 p)$. Here t_{CC} – average time to transfer one double word between two CPUs; t_{CG} – double word exchange time between CPU and GPU.

For the variant of the hybrid algorithm under consideration, the following estimates are valid (T_k - execution time of one step of the algorithm for k CPU and k GPU, $S_p = T_1 / T_p$ – is the acceleration factor, $E_p = S_p / p$ – efficiency ratio [52]).

If $2ps \le m_u$, $t_{CG} \le \frac{2}{3}\frac{ps^2}{m_u} t_C$, $t_{CG} + \frac{s}{3} t_C \le \frac{m_l m_u - ps^2}{ps}\frac{t_G}{n_o}$,

then, for the hybrid block-cyclic algorithm for the LU-decomposition of a nonsymmetrical banded matrix, the following estimates are valid:

$$T_1 \approx \left((2m_u + s)m_l + sm_u\right) s \frac{t_G}{n_o},\ T_p \approx \left((2m_u + ps)m_l + \tau\right)\frac{s}{p}\frac{t_G}{n_o},$$

$$S_p \approx p\left(1 - \frac{(p-1)sm_l - sm_u + \tau}{(2m_u + ps)m_l) + \tau}\right),\ E_p \approx 1 - \frac{(p-1)sm_l - sm_u + \tau}{(2m_u + ps)m_l) + \tau}, \qquad (4.16)$$

where $\tau = \begin{cases} sm_u, & \text{if } \frac{n_o(t_{CG} + t_{CC}\log_2 p)}{t_G} \le \frac{s}{p}\frac{m_u}{m_l} \\ pm_l \frac{n_o(t_{CG} + t_{CC}\log_2 p)}{t_G}, & \text{if } \frac{n_o(t_{CG} + t_{CC}\log_2 p)}{t_G} \le m_l \end{cases}$.

We note that the conditions can be met by choosing the number of processing units p and the block size s.

Estimates (4.16) show that the efficiency of the algorithm does not depend on the order of the matrix, and under certain conditions is determined by the number of nonzero blocks in a row of blocks and the sizes of these blocks. The efficiency of the algorithm can also be influenced by the ratio of the time of the multi-force of one double word and the value t_G/n_o. If the proposed algorithm is implemented on a computer with multi-core processors using the multilevel parallelism model, then the acceleration and efficiency of this version of the algorithm can be estimated by the

same formulas (4.16). In this case: p is the number of processes (threads) of the upper level of parallelism, $t_G = t_C$, n_o – the number of low-level parallelism threads associated with one high-level thread, $t_{CG} = 0$.

Block-cyclic algorithms for *LU*-decomposition of sparse matrices. The block-cyclic algorithm of *LU*-decomposition of a strip matrix without significant changes can be used for sparse asymmetric matrices with other structures (for example, profile, block-skyscraper), provided that either it is not necessary to perform a choice of the main element, or it is enough to make this choice within a diagonal block, or it is possible to provide for the structure of the upper triangular decomposition matrix U. The block algorithm for *LU*-decomposition of a block-diagonal matrix with a frame is considered below in Section 4.3.4.

4.3.3 Block cyclic algorithms for decomposition of sparse symmetric positive definite matrices

Similarly, to the block-cyclic implementation of the *LU*-decomposition of sparse matrices, the block-cyclic algorithms LL^T or LDL^T developed are implemented. It also uses a one-dimensional block-cyclic scheme for the distribution and processing of nonzero blocks of a symmetric matrix, but not all, and only the upper or lower triangle (and for symmetric matrices, these are the same blocks up to transposition). If operations are performed with the lower triangle, then columns of nonzero blocks or rows of nonzero blocks (including the lower or upper triangle of the diagonal block, respectively) are cyclically distributed if the upper triangle of the matrix is used.

Decomposition and distribution of elements of sparse matrices between processing units. We will consider the following sparse matrices: tape, profile and skyscraper structure. It should be noted that these are sparse structures of triangular developments of the original matrices, which are obtained by performing the corresponding symbolic development.

Divide the sparse symmetric matrix A into square blocks of order s (to simplify the presentation, we will assume that $n = Ns$). For example, the block representation of a strip matrix is ($M = \lceil m/s \rceil + 1$, m – half-width of the tape, $\lceil a \rceil$ – the integer part of number a):

$$A = \begin{pmatrix} A_{1,1} & A_{1,2} & \cdots & A_{1,M} & 0 & 0 & \cdots & 0 \\ A_{1,2}^T & A_{2,2} & \cdots & A_{2,M} & A_{2,M+1} & 0 & \cdots & 0 \\ \vdots & \vdots & \ddots & & & & & \\ A_{1,M}^T & A_{2,M}^T & & & & & & \\ 0 & A_{2,M+1}^T & & & & & & \\ 0 & 0 & & & & \ddots & \vdots & \vdots \\ \vdots & \vdots & & & & \cdots & A_{N-1,N-1} & A_{N-1,N} \\ 0 & 0 & & & & \cdots & A_{N-1,N}^T & A_{N,N} \end{pmatrix}. \quad (4.17)$$

Further, rows of matrix blocks are cyclically distributed between the threads (processes) of the higher level of parallelism so that each process must include at least one row of blocks, modified according to (4.10) at this stage. For example, the blocks that are in the line with the number t are allocated by the thread with the logical number (t–1) mod p.

It is advisable to combine nonzero blocks (or their nonzero parts) of the corresponding line of blocks located side by side into rectangular blocks, the size of which should be optimal from the point of view of data caching (to optimize data exchange between memories of different performance) or the use of GPU computers of hybrid architecture. From the same considerations, the storage scheme (column or row) of the elements of these blocks is also selected. In the case of a strip or profile matrix, with such a combination, each (K-th) row of blocks consists of a diagonal block (of order s) $A_{K,K}$ and rectangular block $A_{K,K+1}$ (which has s lines). Further, such a matrix can be considered (respectively) as a block-tape or block-profile. In the case of a matrix, a skyscraper structure with such a combination can be obtained in addition to the diagonal block $A_{K,\,K}$ several (M_K) nonzero rectangular blocks $A_{K,K+L}$ (L = 1, …, M_K), between which are rectangular zero blocks.

The MPI-process (stream), which contains the K-th line of blocks at the K-th step of the algorithm (the block's $A_{11}^{(K)}$ and $A_{12}^{(K)}$), hereinafter referred to as the master CPU (like the associated GPU in the case of the hybrid algorithm). In the GPU memory, at each step of the hybrid algorithm, it is sufficient to store only (also cyclically distributed) nonzero submatrix blocks that are processed.

Cyclic algorithm for LDL^{T}-decomposition of symmetric matrix of block-skyscraper structure. Consider the most general case of a block-sparse structure -

block-cloud. Indeed, block-tape or block-profile structures are in fact special cases of a block-skyscraper structure - with one over-diagonal block in a row of blocks. The choice of the LDL^{T} decomposition is due to the fact that the LDL^{T} decomposition can be used for a larger set of matrices than the LL^{T} decomposition, for example, for non-degenerate symmetric matrices. Moreover, the algorithms for these expansions do not differ significantly. Only for LDL^{T} decomposition, it is necessary to have an additional working array so that the number of arithmetic operations does not increase.

This algorithm is developed on the basis of parallel algorithms for LDL^{T} decomposition of symmetric matrices of strip, profile and cloud structures (see, e.g., [42, 44]) and is based on the block algorithms described in Section 4.3.1.

Consider a variant of the algorithm that uses a multilevel parallel computing model. At the highest level, p processes (threads) are used, which mainly provide communication between themselves and between processor devices that implement the vast majority of arithmetic operations at the lowest levels of parallelism.

We denote (hereinafter, the notation in Fig. 4.1, 4.2 is used) D_{K} is the diagonal matrix with the LDL^{T} decomposition of the diagonal block $A_{11}^{(K)}$, $U_{K,J}$ – square block of *s* submatrix order $U_{12}^{(K)}$, $G_{J,K} = U_{K,J}^{T} D_K$ ($K = 1, ..., N, J = K, ..., N$). Then for $K = 1, ..., N$ the following macro-operations are performed:

1) For $K > 1$ when condition $U_{K-1,K} \neq 0$ is fulfilled, using the s-range modification (4.10), computing the upper triangle of the diagonal block.

2)

$$A_{11}^{(K)} = A_{K,K} - G_{K,K-1} U_{K-1,K}. \tag{4.18}$$

3) For $K > 1$ sending the calculated block to the leading CPU of the *K*-th step $A_{11}^{(K)}$ (on a hybrid computer).

4) LDL^{T}- decomposition of the diagonal block.

5)

$$A_{11}^{(K)} = (U_{11}^{(K)})^{T} D_K U_{11}^{(K)}. \tag{4.19}$$

It is advisable to perform decompositions (4.19) on the master CPU using high-performance program modules of the multithreaded Intel MKL library.

6) For $K < N$-1 *s*- range modification (4.10) of nonzero blocks $A_{I,J}$ ($K \le I \le N$, $K \le J \le M_I$, excluding diagonal block $A_{K,K}$) of the submatrix $A_{22}^{(K)}$:

$$A_{I,J} \leftarrow A_{I,J} - G_{I,K-1} U_{K-1,J}. \tag{4.20}$$

Macro-operations (4.20) are performed at lower levels of parallelism under conditions $G_{I,K-1}, U_{K-1,J} \neq 0$ according to block allocation $A_{I,J}$ between processor devices.

7) For $K < N$-1 distribution of calculated blocks $D_K, U_{11}^{(K)}$ to all processor devices used.

8) For $K < N$-1 computation of nonzero blocks $G_{I,K}$ $(K+1 \le I \le N)$ – solutions of matrix SLAEs with lower triangular matrix:

$$(U_{11}^{(K)})^T (G_{I,K})^T = (A_{I,K})^T. \tag{4.21}$$

Macro-operations (4.21) are executed on the master processor units of the *K*-th step at the lower levels of parallelism.

9) For $K < N$-1 broadcasting non-zero computed blocks to all processor devices that are in use $G_{I,K}$ $(K+1 \le I \le N)$.

10) For $K < N$-1 computation of nonzero blocks $U_{K,J}$ ($K+1 \le J \le N$):

$$U_{K,J} = D_K^{-1} (G_{J,K})^T. \tag{4.22}$$

Macro operations (4.22) are performed at the lower levels of parallelism.

Analysis of formulas (4.18) - (4.22) showed that most calculations can be implemented at lower levels of parallelism, using software modules for matrix-matrix (or matrix-vector) operations from hardware developers, for example, the

Intel MKL multithreaded library (on multicore processors) or the CUBLAS library (on coprocessor-accelerators - GPU).

The efficiency of the algorithm can be increased by performing decompositions (4.19) (item 3) and sending the decomposition blocks (item 5) simultaneously (in parallel, asynchronously) with the end of the macrooperations (4.20) (item 4) of the previous step, using different streams of the upper level of parallelism or CPU and GPU on hybrid computers. It is also possible to increase the efficiency of the algorithm due to the simultaneous execution of computations and data exchanges between different processor devices, for example, data exchanges (items 2, 5, 7) are performed against the background of computations.

If the GPU memory on the hybrid computer is not enough to store all the data that is distributed by this processor device, then item 5 is supplemented with the operations of transferring the previously calculated nonzero submatrix blocks to the CPU and sending to the GPU the blocks of the original matrix necessary for the K-th step in accordance with their distribution. Copying the decomposition blocks to the CPU memory is also performed to save the LDL^{T} decomposition matrices for their reuse.

In this algorithm, the vast majority of arithmetic operations are performed at the lower levels of parallelism. Therefore, it is possible to use one top-level process (thread), but it is necessary to ensure efficient parallelization of computations at the lower levels (between the threads of the lower level or between GPUs).

***LL*^{T}- decomposition of a symmetric matrix of a block-cloud structure.** If LL^{T} decomposition is performed, then some changes must be made to the algorithm. In items 1, 4, 6, 7 to replace blocks $G_{J,K}$ with blocks $U^{T}_{K,J}$, in item 3 replace formula (4.19) with $A^{(K)}_{11} = (U^{(K)}_{11})^{T} U^{(K)}_{11}$ and delete item 8.

Everything else, including distribution of calculations between levels of parallelism and processor devices, remains without changes.

Decompositions of symmetric block-band and block-profile matrices. As was noted above, in the matrices of such structures, nonzero blocks of the decomposition matrix U are densely located above the diagonal. Therefore, in the algorithms for the decomposition of the symmetric matrix, the block-skyscraper structure N should be

replaced by $M_{K\text{-}1}$ or by M_K from condition (4.18) in the definitions of the set of index values J or I. That is, at the K-th step of these algorithms, operations are performed only with blocks of the submatrix of size $(M_K+1)s \times (M_K+1)s$, the upper left block of which $A_{K,K}$.

Efficiency of algorithms. Let us investigate the efficiency of the hybrid version of the block cyclic algorithm for LDL^{T} decomposition of a symmetric tape matrix of order n with tape half-width m (architecture with p CPU and p GPU is used).

Using here and below the notation of § 4.3.2, we have the following estimates: $O_3 \approx s^3/3$, $O_4 \approx m^2 s/p$, $O_6 \approx ms^2$, $O_6 \approx ms$ (operations of item 1 of the master GPU are taken into account in O_4).

Macro operations items 2, 5, 7 are associated with data exchanges within or between processor devices. In most cases, the transfer times between CPU and GPU can be neglected. If the "tree" algorithm [34] is used to send data from one GPU to all others, then the total time of a multi-force (with one GPU p CPU or with one CPU p GPU, including synchronization) of an array of q double words can be estimated on average by the value $q(t_{CG} + t_{CC}\log_2 p)$.

For the variant of the hybrid algorithm under consideration, the following estimates are valid.

If $2ps \le m$, $t_{CG} \le \frac{1}{3}\frac{ps^2}{m}t_C$, $t_{CG} + \frac{s}{3}t_C \le \frac{m^2 - ps^2}{ps}\frac{t_G}{n_o}$, then, for the hybrid block-cyclic algorithm for the LDL^{T} decomposition of a symmetric banded matrix, the following estimates are valid:

$$T_1 \approx (m+s)sm\frac{t_G}{n_o},\ T_p \approx ((m+ps)m+\tau)\frac{s}{p}\frac{t_G}{n_o},$$

$$S_p \approx p\left(1 - \frac{(p-1)sm+\tau}{(m+ps)m+\tau}\right),\ E_p \approx 1 - \frac{(p-1)sm+\tau}{(m+ps)m+\tau}, \qquad (4.23)$$

where $\tau = \begin{cases} sm, & \text{якщо } \dfrac{n_o(t_{CG}+t_{CC}\log_2 p)}{t_G} \le \dfrac{s}{p} \\ pm\dfrac{n_o(t_{CG}+t_{CC}\log_2 p)}{t_G}, & \text{якщо } \dfrac{n_o(t_{CG}+t_{CC}\log_2 p)}{t_G} \le m \end{cases}$.

Note that the conditions of the theorem can be fulfilled by choosing the number of processing units p and the size of blocks s.

Estimates (4.23) show that the efficiency of the algorithm does not depend on the order of the matrix, and under certain conditions is determined by the number of nonzero blocks in the row of blocks and the sizes of these blocks. The efficiency of the algorithm can also be influenced by the ratio of the time of the multi-force of one double word and the value t_G / n_o.

If the proposed algorithm is implemented on a computer with multicore processors using the multilevel parallelism model, then the acceleration and efficiency of this version of the algorithm can be estimated by the same formulas (4.23). In this case: p is the number of processes (threads) of the upper level of parallelism, $t_G = t_C$, n_o – the number of low-level parallelism threads associated with one high-level thread, $t_{CG} = 0$.

In the case of a block-profile matrix, estimates (4.23) are also valid if the half-width of the tape m is replaced by the average number of overdiagonal elements in one line of the profile of the upper triangular matrix U.

4.3.4 Parallel algorithms for decomposition of a block-diagonal matrix with a frame

Historically, the first parallel algorithms for triangular decomposition of a sparse matrix were developed for a block-diagonal with a framing s [39] (item 4.1 and Fig. 4.3.) for representation of this matrix. This algorithm is also used for the LU-decomposition of strip matrices with a narrow strip by virtual construction of the matrix in a block-diagonal form with a frame using the method of parallel sections. In [47], hybrid algorithms for LU-decomposition of a block-diagonal matrix with framing were proposed.

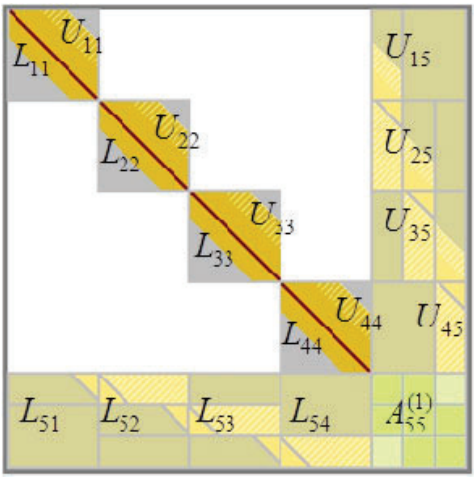

Figure 4.3 Scheme of *LU*-decomposition of a block-diagonal matrix with a frame

Parallel block algorithm for *LU*-decomposition of a block-diagonal matrix with framing. Consider a framed block-diagonal matrix consisting of p diagonal blocks $A_{k,k}$ and framing - diagonal block $A_{p+1,p+1}$, rows with p subdiagonal blocks $A_{p+1,k}$ and columns with p superdiagonal blocks $A_{k,p+1}$ ($k = 1, \ldots, p$). All diagonal blocks $A_{k,k}$ ($k = 1, \ldots, p$) have approximately the same order, significantly (by an order of magnitude or more) exceeds the block order $A_{p+1,p+1}$. We note that in the case of raising a banded matrix to a block-diagonal matrix with a frame, this frame has a block-two-diagonal structure.

The proposed algorithm is also based on the block algorithm of the Gauss method of *LU*-decomposition of square matrices, described above in Section 4.3.1, and the block-diagonal matrix structure with a frame allows performing LU-decompositions of large diagonal blocks $A_{k,k}$ ($k = 1, \ldots, p$) independently of each other, that is, in parallel.

Decomposition and distribution of matrix elements between processing units. It is advisable to distribute data between p parallel threads (processes) of the highest level of parallelism as follows: thread with ordinal number k ($k = 1, \ldots, p$) blocks are allocated $A_{k,k}$, $A_{p+1,k}$, $A_{k,p+1}$, in place of which the corresponding blocks of matrices can be placed in the future L and U, and memory is allocated for a square block $G_{k,k} = -L_{p+1,k}U_{k,p+1}$ and (if necessary) for blocks $L_{k,k}$, $L_{p+1,k}$, $U_{k,k}$, $U_{k,p+1}$. The

block $A_{p+1,p+1}$ is allocated to one of the streams, for example, with a sequence number p.

It should be noted that the capabilities of the algorithms of this group are limited due to a significant increase in density with the development of framing blocks. This, in turn, causes a significant increase in the number of arithmetic operations. So, the efficiency of the algorithm (for computers only with multi-core processors) for the case of a strip matrix is limited from above by 25% due to the fact that when raising such a matrix to a block-diagonal matrix with framing, the number of arithmetic operations increases by 4 times. Therefore, to implement operations with framing blocks, it is advisable to use parallelization at lower levels, for example, use a GPU on computers of hybrid architecture

The algorithm. Thus, the *LU*-decomposition of a block-diagonal matrix with a frame is performed in two stages according to (4.21). At the first stage, the following operations are performed independently ($k = 1, \ldots, p$):

1) *LU*- decomposition of the diagonal block $A_{k,k} = L_{k,k}U_{k,k}$ with partial selection of the main elements in the columns of the block $A_{k,k}$, for this decomposition, you can use the fine-tiled algorithm [55-56] and high-performance program modules of the multi-threaded Intel MKL library (on multi-core processors) or the CUBLAS library (on the GPU);

2) calculating the subdiagonal block $L_{p+1,k}$ – solutions to matrix SLAE $U_{k,k}^T L_{p+1,k}^T = A_{p+1,k}^T$ with lower triangular matrix;

3) superdiagonal block computation $U_{k,p+1}$ - solution to matrix SLAE $L_{k,k}U_{k,p+1} = A_{k,p+1}$ with lower triangular matrix;

4) calculating a square block $G_{k,k} = -L_{p+1,k}U_{k,p+1}$.

Calculations items 2-4 (subdiagonal blocks $L_{p+1,k}$, superdiagonal blocks $U_{k,p+1}$ and square blocks $G_{k,k}$) are performed at the lower levels of parallelism, taking into account the block structure using high-performance software modules of the multi-threaded Intel MKL library (on multi-core processors) or CUBLAS libraries (on the GPU).

At the second stage, the following macro-operations are performed:

5) diagonal block modification $A^{(1)}_{p+1,p+1} = A^{(0)}_{p+1,p+1} + \sum_{k=1}^{p} G_{k,k}$, executed by threads (processes) of the highest level of parallelism using multi-blocking operation $G_{k,k}$;

6) *LU*- diagonal block modification $A^{(1)}_{p+1,p+1} = L_{p+1,p+1}U_{p+1,p+1}$ with partial selection of the main elements in the columns of the block $A^{(1)}_{p+1,p+1}$, for this decomposition, the fine-tiled algorithm and high-performance program modules of the Intel MKL multithreaded library (on multi-core processors) or the CUBLAS library (on the GPU) can be used.

We note that it is possible to organize the parallel execution of the operations of items 1-4 at different levels of parallelism, using a small-tiled *LU*-decomposition algorithm for a block-diagonal matrix with a framing that implements this idea.

In the case of the original block-diagonal matrix with framing, the formation and further solution to the so-called summary system has a significant effect on the efficiency of the proposed algorithm (with matrix $A^{(1)}_{p+1,p+1}$). In order to reduce the number of computations required for this, it is advisable to optimize the sparse structure of both diagonal blocks and framing blocks.

Parallel block decomposition algorithm for symmetric positive definite block-diagonal matrices with framing. As noted above, matrices of this type can be obtained by applying the method of parallel sections to the original matrix. In particular, such a reordering is used for matrices with a narrow band (that is, if the condition $m_l + m_u \geq ps$, $p > 1$).

Decomposition and distribution of matrix elements between processing units. Taking into account the symmetry of the original matrix, only the elements of its upper triangle and the main diagonal are distributed and preserved. It is advisable to distribute data between p parallel threads (processes) of the highest level of parallelism as follows: thread with ordinal number k ($k = 1, \ldots, p$) nonzero block elements are allocated $A_{k,k}$, $A_{k,p+1}$, in the place of which the corresponding nonzero elements of the blocks of the matrix U and memory are allocated for the upper triangle (including the main diagonal)

of the square block $G_{kk} = -U^T_{k,p+1}U_{k,p+1}$ and (if necessary) for blocks $U_{k,k}$, $U_{k,p+1}$. The block $A_{p+1,p+1}$ is allocated to one of the streams, for example, with a sequence number p.

It should be noted that the capabilities of the algorithms of this group are also limited due to a significant increase in density with the development of framing blocks. Therefore, when implementing this algorithm, operations with framing blocks are advisable to use at lower levels of parallelism.

The algorithm. Thus, the LL^T decomposition of a symmetric block-diagonal matrix with a framing is performed as follows: ($i = 1, \ldots, p$):

1) LL^T- decomposition of diagonal blocks A_{ii}: $A_{i,i} = U^T_{i,i}U_{i,i}$;

2) computation of behind-angular blocks framing - solution to matrix SLAEs with triangular matrices $U^T_{i,i}U_{i,p+1} = A_{i,p+1}$;

3) calculating a square block $G_{i,i} = -U^T_{i,p+1}U_{i,p+1}$.

4) diagonal block change $A^{(1)}_{p+1,p+1} = A^{(0)}_{p+1,p+1} + \sum_{i1}^{p} G_{i,i}$, executed by threads (processes) of the highest level of parallelism. using multi-blocking operation $G_{i,i}$;

5) LL^T- decomposition of diagonal blocks $A^{(1)}_{p+1,p+1} = U^{(T)}_{p+1,p+1}U_{p+1,p+1}$, for this decomposition, the fine-tiled algorithm and high-performance program modules of the Intel MKL multithreaded library (on multi-core processors) or the CUBLAS library (on the GPU) can be used.

Each of the macro-operations of items 1-3 algorithms for one block does not depend on similar operations with other blocks and can be performed in parallel. For LL^T decompositions (items 1, 5), we can use a small-tiled algorithm and high-performance software modules of the multithreaded Intel MKL library (on multi-core processors) or the CUBLAS library (on the GPU). Calculations items 2, 3 (supra-diagonal blocks $U_{k,p+1}$, and square blocks $G_{k,k}$) are executed at the lower levels of parallelism, taking into account the block structure using high-performance software modules of the multithreaded Intel MKL library (on multi-core processors) or the CUBLAS library (on the GPU).

Thus, as a result, we obtain the upper triangular matrix

$$U = \begin{pmatrix} U_{11} & 0 & 0 & & 0 & U_{1,p} \\ & U_{22} & 0 & & 0 & U_{2,p} \\ & & U_{33} & & 0 & U_{13p} \\ \vdots & \vdots & & \ddots & & \\ & 0 & & & U_{p-1,p-1} & U_{p-1,p} \\ & & & & & U_{p,p} \end{pmatrix}.$$

The efficiency of the algorithm. As noted above, the efficiency of parallelization of the solution to SLAE is determined by the efficiency of the algorithms for decomposing the matrix of the system.

Let us investigate the efficiency of the hybrid version (architecture with p CPU and p GPU is used) of the block algorithm of LL^{T}-decomposition of a symmetric block-diagonal matrix with a framing of order n, obtained as a result of structural regularization of a banded symmetric matrix (whose tape half-width is equal to m).

We use the notation of Subsection 4.3.1. Then the following estimates are valid (if condition $n_i + m = (n+m)/p >> 2m$ is provided): $O_1 \approx n_i m^2$, $O_2 \approx 2n_i m^2$, $O_3 \approx n_i m^2$, $O_4 \approx 2m^2 \log_2 p$, $O_5 \approx m^3(7p-13)/3$. Macrooperations item 4 of the algorithm is associated with the operation of multi-rounding, that is, data exchange within and / or between processor devices. If the "tree" algorithm is used for this operation [35], then the total time of multi-rounding (with p GPUs to one GPU, including synchronization) of an array of q double words can be estimated on average by the value $q(2t_{CG} + t_{CC} \log_2 p)$ (in most cases, the time of exchange between CPU and GPU t_{CG} can be neglected).

We note that the efficiency of the algorithm under consideration can be estimated based on either the strip (original) structure of the matrix, or from the block-diagonal one with a frame. So, for the variant of the hybrid algorithm under consideration, the following estimates are valid: ($T_1^{(b)}$ – time of LL^{T}-decomposition of a strip matrix on 1 CPU and 1 GPU using a fine-tiled algorithm, $T_1^{(p)}$ – time of LL^{T}-development of a block-diagonal matrix with a frame with p large diagonal blocks on 1 CPU and 1 GPU, using a fine-tile algorithm).

If $n+m >> 2pm$, then, for the hybrid block LU decomposition algorithm for a banded symmetric matrix, which is rearranged into a block-diagonal matrix with a frame, the valid estimates

$$T_1^{(b)} \approx nm^2 \frac{t_G}{n_o}, \quad T_1^{(p)} \approx (4n-2m)m^2 \frac{t_G}{n_o}, \quad T_p \approx (4n+\alpha m+\tau)\frac{m^2}{p}\frac{t_G}{n_o},$$

$$S_p^{(b)} \approx \frac{p}{4}\left(1-\frac{\alpha m+\tau}{4n+\alpha m+\tau}\right), \quad E_p^{(b)} \approx \frac{1}{4}-\frac{\alpha m+\tau}{4(4n+\alpha m+\tau)}, \tag{4.24}$$

$$S_p^{(p)} \approx p\left(1-\frac{(\alpha+2)m+\tau}{4n+\alpha m+\tau}\right), \quad E_p^{(p)} \approx 1-\frac{(\alpha+2)m+\tau}{4n+\alpha m+\tau},$$

where $\alpha = \frac{7p^2-25p+12}{3}$, $\tau = 2p\log_2 p\frac{n_o t_{CC}}{t_G}$.

We note that the condition can be met by choosing the number of processor units p of the upper level of parallelism (respectively, and the number of the main diagonal blocks) Estimates (4.24) show that the reordering of a banded matrix into a block-diagonal matrix with a framing and this algorithm is expedient to use for $p > 4$. The efficiency of the algorithm can also be influenced by the ratio of the multi-hitting time of one double word and the value t_G/n_o.

If the proposed algorithm is implemented on a computer with multi-core processors using the multilevel parallelism model, then the acceleration and efficiency of this version of the algorithm can be estimated by the same formulas (4.24). In this case: p is the number of processes (threads) of the upper level of parallelism, $t_G = t_C$, n_o – the number of low-level parallelism threads associated with one high-level thread.

Similar estimates $S_p^{(p)}$ and $E_p^{(p)}$ can be obtained for other (other than strip) structures of the main diagonal blocks, as well as other structures of framing blocks.

4.3.5 Parallel algorithms for decomposition of block-diagonal matrices

In some iterative methods for solving linear algebra problems, a regularizer is used - a symmetric matrix of a block-diagonal structure. A matrix of such a structure, for example, can be obtained after rejecting the behind-angular blocks of a block-diagonal matrix with a frame or breaking the original (for example, strip) matrix into a relatively small number of square blocks (their order should significantly exceed

the average number of elements in one row of the matrix profile), we discard all out-of-diagonal blocks.

The block-diagonal regularizer makes it possible, when implementing the iterative process, to calculate corrections to the approximate solution by simultaneously and independently (in parallel) solving the SLAE with diagonal blocks of the pre-bummer, which are, in the general case, sparse symmetric positive definite matrices.

Thus, operations, including factorization of a block-diagonal matrix, are naturally parallelized between threads (processes) of the highest level of parallelism.

To parallelize the factorization of diagonal blocks at lower levels, you can use variants of the fine-tiled sparse matrix decomposition algorithm that uses one higher-level CPU and several lower-level threads (on multicore computers) or one GPU (on hybrid computers).

Fine-tiled sparse matrix decomposition algorithms. The variants of this algorithm, which were proposed to be used in the previous and in this Section, use one thread (process) of the highest level of parallelism on multicore computers or one CPU on computers of hybrid architecture.

Let us consider such a variant of the algorithm LL^{T}-decomposition of a sparse symmetric matrix. This algorithm essentially coincides with the block-cyclic decomposition algorithms for a sparse symmetric matrix described in Section 4.3.3. The difference is that there is no high-level parallelization. As in Section 4.3.3, the matrix is divided into square blocks of order *s*.

So, for $K = 1, ..., N$ the following macro-operations are performed.

1) For $K > 1$, using the s-rank modification (4.10), calculating the upper triangle of the diagonal block $A_{11}^{(K)} = A_{K,K} - U_{K-1,K}^{T} U_{K-1,K}$ taking into account $U_{K-1,K} \neq 0$; on a computer of hybrid architecture CPU forwards this calculated upper triangle.

2) LL^{T}- decomposition of the diagonal block $A_{11}^{(K)} = (U_{11}^{(K)})^{T} U_{11}^{(K)}$; on a computer of hybrid architecture, the resulting decomposition $U_{11}^{(K)}$ unit is sent to the GPU. It is advisable to perform these decompositions on a CPU using high-performance program modules of the Intel MKL multithreaded library.

3) For $K < N$-1 *s*- range modification (4.10) of nonzero blocks $A_{I,J}$ ($K \le I \le N$, $K \le J \le M_I$, excluding the diagonal submatrix $A_{K,K}$ block $A_{22}^{(K)}$: $A_{I,J} \leftarrow A_{I,J} - U_{K-1,I}^T U_{K-1,J}$. These macro-operations are performed under conditions $U_{K-1,I}, U_{K-1,J} \neq 0$ at the lower levels of parallelism.

4) For $K < N$-1 computation of nonzero blocks $U_{K,I}$ $(K+1 \le I \le N)$ – solutions to matrix SLAEs with lower triangular matrix: $(U_{11}^{(K)})^T U_{K,I} = A_{K,I}$. These macro-operations are also performed at the lower levels of parallelism.

Analysis of macro-operations items 1-4 of this algorithm shows, that most computations can be implemented at lower levels of parallelism using program modules for matrix-matrix (or matrix-vector) operations from hardware developers, for example, the Intel MKL multithreaded library (on multi-core processors) or the library CUBLAS (on coprocessor-accelerators - GPU).

The efficiency of the algorithm can be increased by performing LL^{T}-decomposition of the diagonal block (item 2) and sending of decomposition blocks (item 5) simultaneously (in parallel, asynchronously) with the end of the execution of s-rank modifications (4.10) of nonzero blocks (item 3) of the previous step, using different flows of the upper and lower levels of parallelism, or CPU and GPU on hybrid computers. It is also possible to increase the efficiency of the algorithm due to the simultaneous execution of computations and data exchanges between different processor devices, for example, data exchanges (items 1, 2) are performed against the background of computations.

A similar single-threaded drop-tile algorithm for the LU-decomposition of a sparse nonsymmetric matrix can be developed on the basis of the block-cyclic algorithm for the LU-decomposition of such a matrix (see Section 4.3.2).

The efficiency of such (single-threaded) drop-tile algorithms for decomposition of sparse matrices is determined by the efficiency of the implementation of matrix-matrix (or matrix-vector) operations in software from hardware developers - the Intel MKL multithreaded library (on multi-core processors) or the CUBLAS library (on the GPU).

4.4 Hybrid algorithms for solving linear systems with sparse matrices of irregular structure based on LLT-decomposition of block-diagonal matrices with framing

We consider on SLAE

$$Ax = b \tag{4.25}$$

$$\widetilde{A} = P^T AP = \begin{pmatrix} A_{11} & 0 & 0 & \cdots & 0 & A_{1p} \\ 0 & A_{22} & 0 & \cdots & 0 & A_{2p} \\ 0 & 0 & A_{33} & \cdots & 0 & A_{3p} \\ \vdots & \vdots & \vdots & \ddots & \vdots & \vdots \\ 0 & 0 & 0 & \cdots & A_{p-1,p-1} & A_{p-1,p} \\ A_{p1} & A_{p2} & A_{p3} & \cdots & A_{p,p-1} & A_{pp} \end{pmatrix},$$

where P – permutation matrix, and blocks A_{ii}, A_{ip}, A_{pi} preserve a sparse structure, p is the number of diagonal blocks in the matrix. Thus, solving the original problem (4.25) reduces to solving the equivalent problem $\tilde{A}\tilde{x} = \tilde{b}$, where $\tilde{x} = P^T x, \quad \tilde{b} = P^T b$, that is, to a system with a block-diagonal matrix with a frame. The most effective direct method for solving such a problem, as it is known, is the Cholesky method [53].

The solution to SLAE with a block-diagonal matrix framed by the Cholesky method is reduced to the steps i = 1, …, p-1 including such stages of calculations:

- factorization of diagonal blocks A_{ii} due to the formula

$$A_{ii} = L_{ii} L_{ii}^T ; \tag{4.26}$$

- modification of framing blocks - solution to SLAE with triangular matrices by the formula

$$L_{pi} = A_{pi} L_{ii}^{-T} ; \tag{4.27}$$

- calculating the product of matrices $L_{i,p}^T L_{i,p}$ and modifying the diagonal block A_{pp} by the formula

$$A_{pp}^{(m)} = A_{pp} - \sum_{i=1}^{p-1} (L_{pi} L_{pi}^T) ; \tag{4.28}$$

- block $A_{pp}^{(m)}$ factorization by formula

$$A_{pp}^{(m)} = L_{pp} L_{pp}^T \ . \qquad (4.29)$$

Since each of the first three operations for one block does not depend on similar operations with other blocks, they can be performed in parallel on a parallel computer.

As a result of the performed calculations, we obtain the lower triangular matrix

$$L = \begin{pmatrix} L_{11} & & & & & 0 \\ 0 & L_{22} & & & & \\ 0 & 0 & L_{33} & & & \\ \vdots & \vdots & & \ddots & & \\ 0 & 0 & 0 & & L_{p-1,p-1} & \\ L_{p1} & L_{p2} & L_{p3} & \cdots & L_{p,p-1} & L_{pp} \end{pmatrix}.$$

To solve the system $Ly = b$ it is necessary to perform for $i = 1, \ldots, p\text{-}1$ such matrix-vector operations:

- systems solutions $L_{ii} y_i = b_i$;
- modification $b_p^{(m)} = b_p - L_{pi} y_i$;
- system solutions $L_{pp} y_p = b_p^{(m)}$.

To solve the system $L^T x = y$ it is necessary to perform for $i = 1, \ldots, p\text{-}1$ such matrix-vector operations:

- system solutions $L_{pp}^T x_p = y_p$;
- modification $y_i^{(m)} = y_i - (L_{pi}^T x_p)$;
- systems solutions $L_{ii}^T x_i = y_i^{(m)}$.

Hybrid block algorithm for solving SLAE based on LL^T decomposition on architecture p CPU + p GPU includes the following steps:

1) Data decomposition:

- on GPUs corresponding to CPU processes with logical numbers $(i\text{-}1)$, $i = 1, \ldots, p$, sent out according to blocks A_{ii}, A_{pi} and parts of vectors x_i, y_i, b_i;
- on GPU, which corresponds to the CPU process with logical number 0, the block is saved $A_{p+1,p+1}$.

2) Implementing LL^T decomposition on architecture p CPU+p GPU:

- parallel to all p-processes, LL^{T}-opening of all diagonal blocks A_{ii} (i = 1, …, p) on formula (4.26) using GPU [45, 51]
- computation by all p GPUs of the corresponding framing blocks $L_{p+1,i}$, as solutions to matrix SLAEs, and products of blocks $L_{p+1,i}L_{p+1,i}^{T} \equiv G_i$ due to the formula (4.27);
- copying the corresponding CPU blocks to the memory G_i.
- multicollection of blocks G_i by the zero process, calculation of the modified diagonal block $A_{p+1,p+1}^{(m)} = A_{p+1\,p+1} - \sum_{i=1}^{p} G_i$, according to (4.28) and copying it into the memory of the corresponding GPU;
- LL^{T}- decomposition of the diagonal block $A_{p+1,p+1}^{(m)}$ on a zero process GPU by the formula (4.29).

3) Solution to the $Ly=b$ system on architecture p CPU+p GPU:

- parallel (simultaneous) solution by all p GPUs of the corresponding systems $L_{ii}y_i$;
- computation by all p GPUs of the corresponding products of blocks $L_{p+1,i}y_i \equiv g_i$
- copying the corresponding CPU blocks to the memory g_i;
- multicollection of blocks g_i by zero process, calculation of the modified block $b_{p+1}^{(m)} = b_{p+1} - \sum_{i=1}^{p} g_i$ and copying it to the memory of the corresponding GPU;
- GPU solutions to a zero-process system $L_{p+1,p+1}y_{p+1} = b_{p+1}^{(m)}$.

4) Solution to the $L^{T}x = y$ system on architecture p CPU+p GPU:

- Solution to the system $L_{p+1,p+1}^{T}x_{p+1} = y_{p+1}$ on a zero process GPU;
- copying to the memory of the zero process, multi-linking to other processes and copying to the memory of the corresponding GPU x_{p+1};
- modification on appropriate GPU $y_i^{(m)} = y_i - (L_{p+1,i}^{T}x_{p+1})$;
- development on alternate GPU systems $L_{ii}^{T}x_i = y_i^{(m)}$.

Depending on the structure of the diagonal blocks, hybrid algorithms for their decomposition are used on one CPU and on one GPU for dense or tape matrices.

It should be noted that the complexity of the hybrid factorization algorithm for one diagonal block is mainly determined by the component of the matrix processing on the GPU.

In case the blocks D_{ii} , $i = \overline{1, p-1}$ are band matrices of order q with half-width of the tape k, the block D_{pp} – the density matrix of order s satisfies the following estimates.

The number of operations performed per GPU to find the LL^{T}-decomposition of a sparse block-diagonal matrix with a frame A is estimated by the value

$$N_p \approx \frac{qs}{2}\left(4q + 4k + \frac{k^2}{s}\right).$$

Note. If $k << q$, $s \approx pk$, then $N_p \approx 2q^2 s$.

Hereinafter, $\tau_{opp} = \frac{n_o t_{opp}}{t_g}$, $\tau_{opg} = \frac{n_0 t_{opg}}{t_g}$.

Since the calculations are carried out for the most part on the GPU, it implements the SIMT (Single Instruction, Multiple Threads) architecture, then in further calculations it should be borne in mind that one instruction is executed on a group of data. That is, n_0 floating point operations occur simultaneously. The value of n_0 depends on the hardware characteristics of a particular graphics accelerator.

The acceleration of the hybrid algorithm LL^{T}-decomposition of a sparse block-diagonal matrix with framing A is

$$S_p \approx (p-1)\left(1 + \frac{s^2 p}{2N_p}\left(\tau_{opp} + 2\tau_{opg}\right)\right)^{-1}.$$

Note. If $k << q$, $s \approx pk$, then

$$S_p \approx (p-1)\left(1 + \frac{sp}{4q^2}\left(\tau_{opp} + 2\tau_{opg}\right)\right)^{-1}.$$

The proposed algorithm is most effective in cases when the diagonal blocks have a regular structure and can be represented as dense or strip matrices. In this case, efficiency is achieved through the use of optimized software libraries in calculations. One of the disadvantages of this algorithm is the large amount of memory for storing framing blocks and diagonal blocks.

Hybrid fine-tiled LL^T decomposition algorithm block-diagonal matrix with framing [55, 56]. We split the matrix A into blocks of size $c \times c$. To factorize a block-diagonal matrix, we apply the algorithm proposed in [58] for dense matrices.

To factorize the matrix at step k, we use the following relation

$$A^k = \begin{pmatrix} A_{11} & A_{12} \\ A_{21} & A_{22} \end{pmatrix} = \begin{pmatrix} L_{11} & 0 \\ L_{21} & L_{22} \end{pmatrix} \begin{pmatrix} L_{11}^T & L_{21}^T \\ 0 & L_{22}^T \end{pmatrix}, \tag{4.30}$$

where are the block sizes $A_{11} - c \times c$, $A_{21} - (n - kc)c$, $A_{22} - (n - kc)(n - kc)$, the block's A_{21} and A_{22} take into account the block structure D_{ii}, C_{pi}, D_{pp}.

From this we obtain an algorithm according to which the decomposition is carried out at the k step:

$$A_{11} = L_{11} \times L_{11}^T; \tag{4.31}$$

$$L_{21} = A_{21} \times \left(L_{11}^T\right)^{-1}; \tag{4.32}$$

$$\tilde{A}_{22} = A_{22} - L_{21} \times L_{21}^T. \tag{4.33}$$

We note that the implementation (4.31) - (4.33) at each step modifies only the blocks D_{ii}, C_{pi}, $i = \overline{1, p-1}$, D_{pp}.

To implement the algorithm, we will use the distribution proposed above. That is, in GPU$_i$, $i = \overline{1, p-1}$ contains blocks D_{ii}, C_{pi} and block $A_{pp}^{(i)}$ of the same size as D_{pp}; in GPU$_p$ the block D_{pp} is saved.

In Fig. 4.4 the block distribution of data at the k-th step of factorization of a block-diagonal matrix with a frame is shown, taking into account the above proposed decomposition.

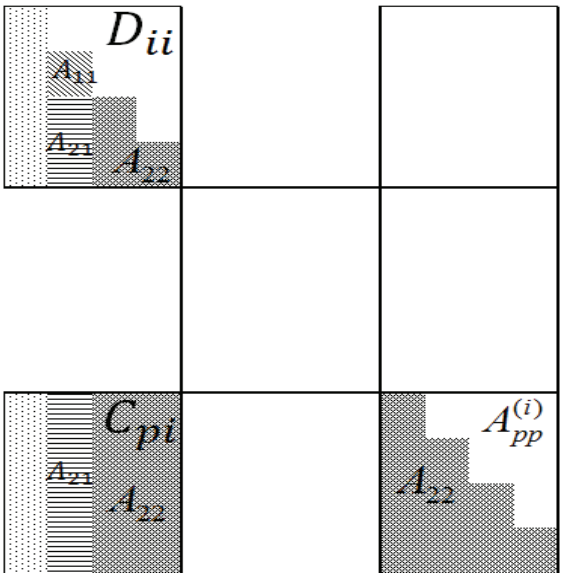

Figure 4.4 – data decomposition in GPU$_i$

Parallelization of triangular factorization calculations is that the decomposition of blocks A_{11} and A_{21} and A_{22} modification can be carried out independently in each CPU$_i$ and GPU$_i$, where $i = \overline{1, p-1}$.

At every step ($i = \overline{1, p-1}$) in all pairs of CPU$_i$ and GPU$_i$ we perform:

- in CPU$_i$, factorize A_{11} from D_{ii} $A_{11} = L_{11} \times L_{11}^T$;
- in GPU$_i$, the column of blocks is modified L_{21} $L_{21} = A_{21}\left(L_{11}^T\right)^{-1}$;
- in GPU$_i$, matrix blocks are modified A_{22} with $A_{pp}^{(i)}$ due to the

$\tilde{A}_{22} = A_{22} - L_{21}L_{21}^T$.

- In the CPU$_p$, using multicollection, we modify D_{pp}

$D_{pp}^* = D_{pp} - \sum_{i=1}^{p-1} A_{pp}^{(i)}$.

After that, we factorize the block D_{pp}^* , thereby completing the process of factorizing the matrix.

The number of operations performed on 1 GPU to find the factorization of a sparse block-diagonal matrix with framing is estimated by the value

$$N_p \approx \frac{q^3}{3} + sq^2 = \frac{q^2}{3}(q+3s).$$

The acceleration of the small-tiled hybrid algorithm LL^T-decomposition of a sparse block-diagonal matrix with framing A is as follows:

$$S_p \approx (p-1)\left(1+\frac{3(p-1)s^2}{2q^2(q+3s)}\left(\tau_{opp}+\left(\frac{2p}{(p-1)}+\frac{4qc}{s^2}+\frac{4c}{(p-1)s}\right)\tau_{opg}\right)\right)^{-1},$$

where c – is the plate dimension.

This algorithm has several advantages over the factorization algorithm proposed above. You can adjust the size of the block with which the calculations are carried out at each step of the algorithm. Due to this effect of caching, calculations can be achieved when the blocks are completely located in the fast memory of the GPU. Also, such a block structure allows us to work with continuous data arrays on the GPU, reduce the number of index operations and check, which are quite expensive on a graphics accelerator.

4.5 Experimental study of parallel algorithms

The developed parallel algorithms were tested on a MIMD-architecture computer with multicore processors, as well as on a hybrid computer. In particular, SNNs with strip Jacobi matrices, which arise in the mathematical modeling of nanoporous systems, were used as test ones [37].

The table shows the results of solving test SNS with banded Jacobi matrices, which arise in the mathematical modeling of the studied systems.

Table 4.1

№	Jacobi matrix parameters		solution time		
	rank	half-width of the tape	consistent algorithm	parallel algorithm	hybrid algorithm
1	55 650	1 052	≈ 84 h.	≈ 4 h.	≈ 2 h.
2	52 500	1 052	≈ 84 h.	5 h. 42 min.	1h. 12 min.

The testing results showed that the developed parallel algorithms are well scalable. It also provides higher performance for higher order SNNs with Jacobi matrices with larger tape widths due to increased use of computational resources.

Additionally, to test the algorithms proposed in the section for solving SLAEs with banded matrices, several SLAEs were used whose parameters are presented in Table 4.2.

Table 4.3 shows the solution times for the SLAE, the parameters of which are given in Table 4.2, on computers of different architectures, using different algorithms. Here, a computer with 1 Intel Core I7 4 core processor was mainly used as a personal computer (designated PC), the Inparkom cluster is equipped with multi-core Intel Xeon 5606 4 core processors, and on each of the four Inparkom_g nodes, 2 of the same processors and 2 Nvidia Tesla video cards are installed M2090. Clusters of the Inparkom family present a joint development of V.M. Glushkov Institute of Cybernetics of National Academy of Sciences of Ukraine and State Research and Production Enterprise "Electronmash".

Table 4.2.

№	Name	Rank n	Number of subdiagonals m_l	Number of superdiagonals m_u
1	A-126-20	126 000	2 001	2 001
2	A-126-09	126 000	902	902
3	A-055-10	55 650	1 052	1 052
4	A-052-10	52 500	1 052	1 052
5	A-137-44	137 826	4 448	4 448

Table 4.3.

The SLAU matrix	Solution time (sec.)		
	consistent algorithm	parallel algorithm	hybrid algorithm
	PC	Inparkom	Inparkom _g
A-126-20	≈ 2 240	62,32	
A-126-09	≈ 660	11,11	
A-055-10	≈ 170	7,08	3,96
A-052-10	≈ 210	14,28	2,93
A-137-44	≈ 7 080	202,70	

The results presented showed that the use of parallel computations can significantly reduce the time for solving problems - from 15 to 60 times. And the use of a computer of hybrid architecture reduces the time by another 2-5 times.

The study of the created hybrid algorithms for solving SLAEs with sparse matrices was carried out on a hybrid computer SKIT-4. The programs are written in the algorithmic language C using the parallelization systems MPI and CUDA [60]. The functions of the program libraries Intel MKL [40], cuBLAS [41], cuSPARSE [61] were also used.

In Table 4.4 test matrices are presented on which numerous experiments of the developed hybrid algorithms for solving SLAEs with sparse matrices were carried out.

Table 4.4 – Test matrices for the study of hybrid algorithms for solving SLAEs with sparse matrices

№	Name	Problem area	Matrix order	Quantity of non-zero elements
1.	ecology2	2D/3D problem	999999	49591
2.	apache2	structural problem	715176	4817870
3.	thermomech_dM	thermal problem	20416	1423116
4.	G2_circuit	circuit simulation problem	150102	726624
5.	Dubcova3	2D/3D problem	146689	3636643
6.	cvxbqp1	optimization problem	50000	349968
7.	minsurfo	optimization problem	40806	203622

In Fig. 4.5 the dependence of the solution time for SLAE with sparse matrices on the number of GPUs used are shown. To solve SLAEs with sparse matrices numbered 1, 2, 6, 7, we used a program that implements the hybrid block algorithm for LL^T - decomposition of block-diagonal matrices with framing, and for matrices numbered 3, 4, 5 the calculations were carried out by a program that implements fine -Tiled algorithm for LL^T-decomposition of block-diagonal matrices with framing.

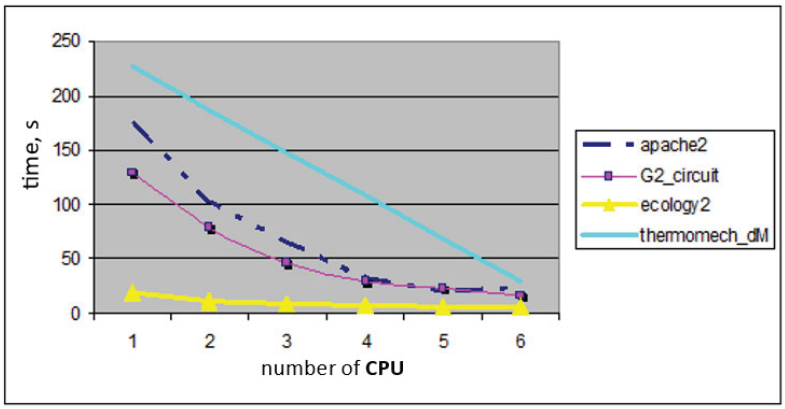

Figure 4.5– Solving times of SLAEs by hybrid algorithms of LL^T - decomposition of block-diagonal matrices with framing

In Fig. 4.6 the graphs of acceleration of hybrid algorithms for solving SLAEs with sparse matrices based on LL^T -decomposition of block-diagonal matrices with framing are shown.

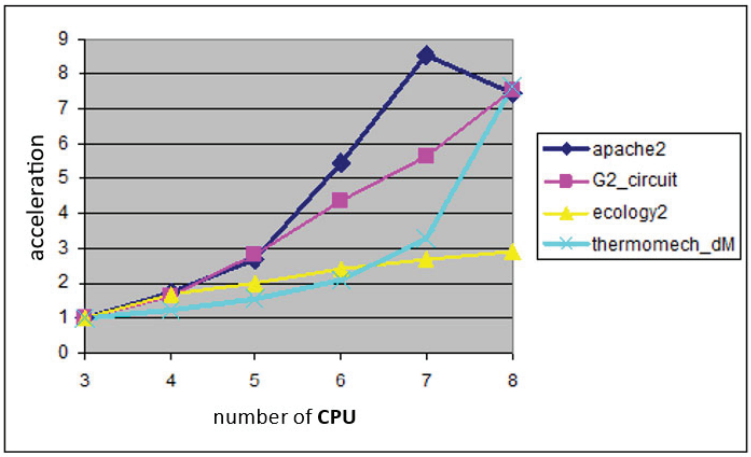

Figure 4.6 – Acceleration of hybrid algorithms for solving SLAE with sparse matrices based on LL^T decomposition

Conclusions for Chapter 4

Using a multilevel model of parallel computing, taking into account the peculiarities of the computer architecture, effective algorithms and programs for solving SNS and SLAE have been developed on parallel computers of hybrid architecture and with Intel Xeon Phi x200 series processors. Simultaneously, the time for solving problems is significantly reduced, which makes it possible to solve high-order problems in real time, which, nowadays, science is facing.

In this Section, new hybrid algorithms and programs of direct methods for sparse matrices of various structures are developed and investigated based on the methods of LU, LL^{T} -matrix linkage.

Experimental studies indicate high efficiency and scalability of the created algorithms. These algorithms and programs were included in the intellectual system of computer mathematics and were used in the mathematical modeling of a wide class of physical and technological processes in the creation of structures for energy facilities.

Chapter 5. The methods of integral transformations for creation of hybrid ANM-models

5.1. Finite integral Fourier transforms with spectral parameter for homogeneous domains

5.1.1. Finite integral Fourier transform for finite media

The finite integral Fourier transform on the set $I_1 = \{x : x \in [l_0, l_1]; l_0 \geq 0, l_1 < \infty\}$ was introduced and mathematically substantiated in [11]. The boundary conditions have the form: $B_{jk}[u] \equiv \left[\left(\alpha_{jk}\frac{d}{dx} + \beta_{jk}\right)u\Big|_{x=l_k}\right] = g_k, |\alpha_{jk}| + |\beta_{jk}| \neq 0; j,k = 1,2.$

This structure of boundary operators assumes that at the boundaries of the medium mass transfer occurs at constant gradients, i.e., stationary modes of motion are set.

Taking into account the rates of changing the gradients of the defining (basic) parameters of the ANM and their gradients in the formulation of boundary value problems, which are mathematical descriptions of the considered transfer in boundary conditions, the operator $\frac{\partial}{\partial t}$ or $\frac{\partial^2}{\partial t^2}$ (for dynamic problems) is presented. This leads to the appearance of a spectral parameter in the boundary conditions of the corresponding Sturm-Liouville spectral problem. We construct a finite integral Fourier transform using the Cauchy kernel, a fundamental solution to the Cauchy problem for an equation under a homogeneous boundary condition. We consider the boundary value problem of constructing a parabolic-type equation bounded in the solution domain $D = \{(t, x) : t \in (0, \infty), x \in (l_0, l_1); l_0 \geq 0, l_1 < \infty\}$ [11, 12]

$$\frac{\partial u}{\partial t} + \gamma^2 u - a^2 \frac{\partial^2 u}{\partial x^2} = 0, a > 0, \gamma^2 \geq 0 \qquad (5.1)$$

under the initial condition:

$$u(t,x)\big|_{t=0} = g(x) \tag{5.2}$$

and boundary conditions:

$$\begin{gathered}\left[\left(\alpha_{11}^0+\delta_{11}^0\frac{\partial}{\partial t}\right)\frac{\partial}{\partial x}+\beta_{11}^0+\gamma_{11}^0\frac{\partial}{\partial t}\right]u\Big|_{x=l_0}=0\\ \left[\left(\alpha_{11}^1+\delta_{11}^1\frac{\partial}{\partial t}\right)\frac{\partial}{\partial x}+\beta_{11}^1+\gamma_{11}^1\frac{\partial}{\partial t}\right]u\Big|_{x=l_1}=0.\end{gathered} \tag{5.3}$$

$$\beta_{11}^0\delta_{11}^0-\alpha_{11}^0\gamma_{11}^0\neq 0,\alpha_{11}^1\gamma_{11}^1-\beta_{11}^1\delta_{11}^1\neq 0,$$
$$\left(\left|\alpha_{11}^0\right|+\left|\beta_{11}^0\right|\neq 0,\left|\alpha_{11}^1\right|+\left|\beta_{11}^1\right|\neq 0,\delta_{11}^m\geq 0,\gamma_{11}^m\geq 0,m=0,1\right).$$

Assuming that the function $u(t,x)$ is a Laplace original with respect to the argument t [19]. In the image by Laplace

$$L[u]=\int_0^\infty u(t,x)e^{-pt}dt\equiv u^*(p,x) \tag{5.4}$$

we obtain the problem of constructing on the segment $[l_0,l_1]$ the solution to the heterogeneous modified Fourier differential equation

$$\frac{d^2u^*}{dx^2}-q^2u^*=-\bar{g}(x);\bar{g}=a^{-2}g,q^2=a^{-2}\left(p+\gamma^2\right),\gamma^2\geq 0 \tag{5.5}$$

under boundary conditions:

$$\left(\bar{\alpha}_{1l}^0\frac{d}{dx}+\bar{\beta}_{1l}^0\right)u^*\Big|_{x=l_0}=\varphi_l^0(l_0),\left(\bar{\alpha}_{1l}^l\frac{d}{dx}+\bar{\beta}_{1l}^l\right)u^*\Big|_{x=l_l}=\varphi_l^l(l_l). \tag{5.6}$$

Here: $\bar{\alpha}_{11}^m=\alpha_{11}^m+\delta_{11}^m p,\bar{\beta}_{11}^m=\beta_{11}^m+\gamma_{11}^m p,\ \phi_1^0(l_0)=\delta_{11}^0 g'(l_0)+\gamma_{11}^0 g(l_0),\phi_1^1(l_1)=\delta_{11}^1 g'(l_1)+\gamma_{11}^1 g(l_1)$.

We assume $\varphi_l^0(l_0)=0,\varphi_l^l(l_l)=0$. Otherwise, we put $g(x)=\phi(x)+ax+b$ and calculate the coefficients a,b from the algebraic system: (5.7)

$$\begin{cases}\left(\delta_{11}^0+\gamma_{11}^0 l_0\right)a+\gamma_{11}^0 b=\phi_1^0\\ \left(\delta_{11}^1+\gamma_{11}^1 l_1\right)a+\gamma_{11}^1 b=\phi_1^1\end{cases}\ !\tag{5.7}$$

It follows that $\delta_0\equiv\delta_{11}^0\gamma_{11}^1-\delta_{11}^1\gamma_{11}^0-\gamma_{11}^0\gamma_{11}^1(l_1-l_0)\neq 0$ when $a=\left(\phi_1^0\gamma_{11}^1-\phi_1^1\gamma_{11}^0\right)\delta_0^{-1},b=\left[\left(\delta_{11}^0+\gamma_{11}^0 l_0\right)\phi_1^1-\left(\delta_{11}^1+\gamma_{11}^1 l_1\right)\phi_1^0\right]\delta_0^{-1}$. As a result, we obtain a function $\varphi(x)=g(x)+\dfrac{\gamma_{11}^0\phi_1^1-\gamma_{11}^1\varphi_1^0}{\delta_0}x+\dfrac{\left(\delta_{11}^1+\gamma_{11}^1 l_1\right)\phi_1^0-\left(\delta_{11}^0+\gamma_{11}^0 l_0\right)\phi_1^1}{\delta_0}$,

for which we have equations $\left[\delta_{11}^{0}\varphi'(x)+\gamma_{11}^{0}\varphi(x)\right]_{x=l_0}=0,\left[\delta_{11}^{1}\varphi'(x)+\gamma_{11}^{1}\varphi(x)\right]_{x=l_1}=0.$

The functions $chqx$ and $shqx$ form the fundamental system of solutions to the homogeneous equation corresponding to (5.5) [11]. We define the functions:

$$V_{jk}^{m1}(ql_m)\equiv\left(\alpha_{jk}^{m}\frac{d}{dx}+\beta_{jk}^{m}\right)ch\,qx\Big|_{x=l_m}\alpha_{jk}^{m}q\,sh\,\mathrm{ql_m}+\beta_{jk}^{m}\,\mathrm{ch}\,ql_m,,$$

$$V_{jk}^{m2}(ql_m)\equiv\left(\alpha_{jk}^{m}\frac{d}{dx}+\beta_{jk}^{m}\right)\mathrm{sh}\,qx\Big|_{x=l_m}=\alpha_{jk}^{m}q\,\mathrm{ch}\,ql_m+\beta_{jk}^{m}\,\mathrm{sh}\,ql_m,$$

$$\Phi_{jk}^{m}(ql_m,qx)=V_{jk}^{m2}(ql_m)\mathrm{ch}\,q_m x-V_{jk}^{m1}(ql_m)\mathrm{sh}\,q_m x.$$

The general solution to the boundary value problem (5.5) - (5.7) is

$$u^{*}(p,x)=\int_{l_0}^{l}\mathrm{H}^{*}(p,x,\xi)\tilde{g}(\xi)d\xi\ \cdot \tag{5.8}$$

Here $\mathrm{H}^{*}(p,x,\xi)$ - fundamental function Cauchy of the problem (5.5) - (5.7)

$$\mathrm{H}^{*}(p,x,\xi)=\begin{cases}\mathrm{H}^{-*}(p,x,\xi)\equiv A_1\ \mathrm{ch}\ qx+B_1\ \mathrm{sh}\ qx,\ l_0<x<\xi<l_1\\ \mathrm{H}^{+*}(p,x,\xi)\equiv A_2\ \mathrm{ch}\ qx+B_2\ \mathrm{sh}\ qx,\ l_0<\xi<x<l_1\end{cases}, \tag{5.9}$$

that satisfies the conditions [11]:

1) at $x\neq\xi$: $\left(\frac{d^2}{dx^2}-q^2\right)\square^{*}(p,\xi,\xi)\equiv 0$;

2) at $x=\xi$:

$$\text{a)}\ \square^{*}(p,x,\xi)\Big|_{x=\xi+0}-\square^{*}(p,x,\xi)\Big|_{x=\xi-0}=0 \tag{5.10}$$

б) $\frac{d}{dx}\square^{*}(p,x,\xi)\Big|_{x=\xi+0}-\frac{d}{dx}\square^{*}(p,x,\xi)\Big|_{x=\xi-0}=-1$

$$3)\left(\tilde{\alpha}_{11}^{0}\frac{d}{dx}+\tilde{\beta}_{11}^{0}\right)\mathrm{H}^{*}(p,x,\xi)\Big|_{\mathrm{x=l_0}}=0;\ \left(\tilde{\alpha}_{11}^{1}\frac{d}{dx}+\tilde{\beta}_{11}^{1}\right)\mathrm{H}^{*}(p,x,\xi)\Big|_{x=l_1}=0\ \cdot \tag{5.11}$$

Substiting $\mathrm{H}^{*}(p,x,\xi)$ in conditions (5.9), (5.10), we obtain the system for finding unknow coefficients A_j and B_j:

$$\begin{aligned}&(A_2-A_1)\ \mathrm{ch}\ q\xi+(B_2-B_1)\ \mathrm{sh}\ q\xi=0\\ &(A_2-A_1)\ \mathrm{sh}\ q\xi+(B_2-B_1)\ \mathrm{ch}\ q\xi=-q^{-1}\\ &A_1V_{11}^{01}(ql_0)+B_1V_{11}^{02}(ql_0)=0\\ &A_2V_{11}^{11}(ql_1)+B_2V_{11}^{12}(ql_1)=0\end{aligned} \tag{5.12}$$

From the first two equations (5.12) we find:

$$A_2 = A_1 + q^{-1} \text{ sh } q\xi, \quad B_2 = B_1 - q^{-1} \text{ ch } q\xi.$$

Putting A_2, B_2 in he third and fourth equations (5.12), we obtain the system for determinig A_1 and B_1

$$\begin{cases} A_1 V_{11}^{01}(ql_0) + B_1 V_{11}^{02}(ql_0) = 0 \\ A_1 V_{11}^{11}(ql_1) + B_1 V_{11}^{12}(ql_1) = q^{-1}\Phi_{11}^1(ql_1, q\xi) \end{cases}. \tag{5.13}$$

We suppose that contition of unambiguous solvability of boundary value problelm (5.5) - (5.7) is satisfied: the determinant of system (5.13)

$$\Delta^*(p) \equiv V_{11}^{01}(ql_0)V_{11}^{12}(ql_1) - V_{11}^{02}(ql_0)V_{11}^{11}(ql_1) \neq 0 \tag{5.14}$$

for $p = \sigma + i\tau$ з $\text{Re } p = \sigma \geq \sigma_0$, where σ_0 – the abscissa of the convergence of the Laplace integral and $\text{Im } p = \tau \in (-\infty, +\infty)$.

As a result, we uniquely find $A_1 = -\dfrac{V_{11}^{02}(ql_0)}{q\Delta^*(p)}\Phi_{11}^1(ql_1, q\xi)$, $B_1 = \dfrac{V_{11}^{01}(ql_0)}{q\Delta^*(p)}\Phi_{11}^1(ql_1, q\xi)$. This defined the Cauchy function, which has a simmetrical structure relative to the diagonal $x = \xi$:

$$\square^*(p,x,\xi) = -\frac{1}{q\Delta^*(p)} \begin{cases} \Phi_{11}^0(ql_0, qx)\Phi_{11}^1(ql_1, q\xi), & l_0 < x < \xi < l_1 \\ \Phi_{11}^0(ql_0, q\xi)\Phi_{11}^1(ql_1, qx), & l_0 < \xi < x < l_1 \end{cases}. \tag{5.15}$$

Returning to equation (5.8) in the Laplace original, we obtain the solution to the problem (5.1) - (5.3):

$$u(t,x) = \int_{l_0}^{l_1} \square\ (t,x,\xi) g(\xi) \sigma d\xi, \ \sigma = a^{-2} \tag{5.16}$$

Here [19]

$$\text{H}\ (t,x,\xi) = \frac{1}{2\pi i} \int_{\sigma_0 - \infty}^{\sigma_0 + i\infty} \text{H}^*(p,x,\xi) e^{pt} dp \tag{5.17}$$

We calculate the integral (5.17).

Putting $\sqrt{p + \gamma^2} = i\beta$ or $p = -(\beta^2 + \gamma^2)$. As a result, we obtain

$$q = ia^{-1}\beta \equiv i\overline{\beta}, \qquad \text{ch } qx = \cos \overline{\beta} x, \qquad \text{sh } qx = i \sin \overline{\beta} x,$$

$$V_{jk}^{m1}\left(i\overline{\beta}l_m\right)=-\overline{\alpha}_{jk}^{m}\overline{\beta}\,\sin\overline{\beta}l_m+\overline{\beta}_{jk}^{m}\cos\overline{\beta}l_m\equiv\overline{\upsilon}_{jk}^{m1}\left(\beta\right),$$
$$V_{jk}^{m2}\left(i\overline{\beta}l_m\right)=i\left[\overline{\alpha}_{jk}^{m}\overline{\beta}\,\cos\overline{\beta}l_m+\overline{\beta}_{jk}^{m}\sin\overline{\beta}\mathrm{l}_{\mathrm{m}}\equiv i\overline{\upsilon}_{jk}^{m2}\left(\beta\right)\right],$$

$$\Delta^{*}\left(p\right)\Big|_{p=-\left(\beta^2+\gamma^2\right)}\equiv i\overline{\delta}\left(\beta\right)=i\left[\tilde{\upsilon}_{11}^{01}\left(\beta\right)\tilde{\upsilon}_{11}^{12}\left(\beta\right)-\tilde{\upsilon}_{11}^{02}\left(\beta\right)\tilde{\upsilon}_{11}^{11}\left(\beta\right)\right];$$
$$\tilde{\alpha}_{jk}^{m}=\alpha_{jk}^{m}-\delta_{jk}^{m}\left(\beta^2+\gamma^2\right),\ \ \tilde{\beta}_{jk}^{m}=\beta_{jk}^{m}-\gamma_{jk}^{m}\left(\beta^2+\gamma^2\right);m=0,1.$$

We consider the transcendental equation

$$\tilde{\delta}\left(\beta\right)\equiv\tilde{\upsilon}_{11}^{01}\left(\beta\right)\tilde{\upsilon}_{11}^{12}\left(\beta\right)-\tilde{\upsilon}_{11}^{02}\left(\beta\right)\tilde{\upsilon}_{11}^{11}\left(\beta\right)=0. \tag{5.18}$$

Theorem 5.1.1. (*on the discrete spectrum*)*: the roots* β_m *of the transcendental equation (5.18) form a discrete spectrum: the roots are different, real, symmetrical about* $\beta=0$ *the half-axis* $\beta>0$*, form a monotonically increasing numerical sequence with a single boundary point* $\beta=+\infty$.

Proof: the proof of the theorem is carried out on the basis of the method of work [11].

Since for a function $\mathrm{H}^{*}(p,x,\xi)$ the points $p_n=-\left(\beta_n^2+\gamma^2\right)$ are simple poles, then by the generalized development theorem [11] we obtain

.

$$\mathrm{H}^{*}(p,x,\xi)=\sum_{n=1}^{\infty}e^{-\left(\beta_n^2+\gamma^2\right)t}\frac{V_0\left(x,\beta_n\right)V_0\left(\xi,\beta_n\right)}{\left\|V_0\left(x,\beta_n\right)\right\|^2}. \tag{5.19}$$

Here $V_0\left(x,\beta_n\right)$ - spectral function:

$$V_0(x,\beta_n)=\tilde{\upsilon}_{11}^{01}(\beta_n)\sin\frac{x}{a}\beta_n-\tilde{\upsilon}_{11}^{02}(\beta_n)\cos\frac{x}{a}\beta_n\equiv\tilde{\beta}_{11}^{0}\sin\overline{\beta}_n(x-l_0)-\tilde{\alpha}_{11}^{0}\overline{\beta}_n\cos\overline{\beta}_n(x-l_0), \tag{5.20}$$

the square of the norm of which:

$$\left\|V_0\left(x,\beta_n\right)\right\|_1^2=-\tilde{\beta}_n\frac{\tilde{\upsilon}_{11}^{02}\left(\beta_n\right)}{\tilde{\upsilon}_{11}^{12}\left(\beta_n\right)}\left[\left(\frac{1}{i}\frac{d}{dp}\Delta^{*}\left(p\right)\right)\Big|_{p=p_n}\right]\equiv$$
$$\int_{l_0}^{l_1}\left[V_0\left(x,\beta_n\right)\right]^2\sigma dx+\frac{\alpha^{-2}}{\beta_{11}^{0}\delta_{11}^{0}-\alpha_{11}^{0}\gamma_{11}^{0}}\left(\delta_{11}^{0}V_0'\left(l_0,\beta_n\right)+\gamma_{11}^{0}V_0\left(l_0,\beta_n\right)\right)^2+$$
$$+\frac{a^{-2}}{\alpha_{11}^{1}\gamma_{11}^{1}-\beta_{11}^{1}\delta_{11}^{1}}\left(\delta_{11}^{1}V_0'\left(l_1,\beta_n\right)+\gamma_{11}^{1}V_0\left(l_1,\beta_n\right)\right)^2$$

(5.21)

Theorem 5.1.2. (*on the spectral function*) *The function* $V_0(x,\beta_n)$ *defined by formula* (5.21) *is the spectral function of the Sturm-Liouville problem:*

$$(\frac{d^2}{dx^2}+a^{-2}\beta_n^2)u(x,\beta_n)=0 \tag{5.22}$$

$$\left(\tilde{\alpha}_{11}^0\frac{d}{dx}+\tilde{\beta}_{11}^0\right)u\Big|_{x=l_0}=0,\left(\tilde{\alpha}_{11}^1\frac{d}{dx}+\tilde{\beta}_{11}^1\right)u\Big|_{x=l_1}=0. \tag{5.23}$$

Proof: Since $\frac{d^2}{dx^2}\sin\overline{\beta}_n(x-l_0)=-\overline{\beta}_n^2\sin\overline{\beta}_n(x-l_0)$,

$\frac{d^2}{dx^2}\cos\overline{\beta}_n(x-l_0)=-\overline{\beta}_n^2\cos\overline{\beta}_n(x-l_0)$,

then $\frac{d^2}{dx^2}V_0(x,\beta_n)=-\overline{\beta}_n^2\cdot V_0(x,\beta_n)=-a^{-2}\beta_n^2\cdot V_0(x,\beta_n)$, that is, equation (5.22) holds.

We have directly

$$\left(\tilde{\alpha}_{11}^0\frac{d}{dx}+\tilde{\beta}_{11}^0\right)V_0(x,\beta_n)\Big|_{x=l_0}=\tilde{v}_{11}^{01}(\beta_n)\tilde{v}_{11}^{02}(\beta_n)-\tilde{v}_{11}^{02}(\beta_n)\tilde{v}_{11}^{01}(\beta_n)\equiv 0,$$

$$\left(\tilde{\alpha}_{11}^1\frac{d}{dx}+\tilde{\beta}_{11}^1\right)V_0(x,\beta_n)\Big|_{x=l_1}=\tilde{v}_{11}^{01}(\beta_n)\tilde{v}_{11}^{12}(\beta_n)-\tilde{v}_{11}^{02}(\beta_n)\tilde{v}_{11}^{11}(\beta_n)\equiv 0$$

due to identity $\delta(\beta_n)\equiv 0$.

The identy $\tilde{v}_{11}^{01}(\beta_n)\tilde{v}_{11}^{12}(\beta_n)-\tilde{v}_{11}^{02}(\beta_n)\tilde{v}_{11}^{11}(\beta_n)\equiv 0$ allows the spectral function to be rewritten as

$$\begin{aligned}V_0(x,\beta_n)&=\frac{\tilde{v}_{11}^{01}(\beta_n)}{\tilde{v}_{11}^{11}(\beta_n)}\left(\tilde{v}_{11}^{11}(\beta_n)\sin\overline{\beta}_n x-\tilde{v}_{11}^{02}(\beta_n)\frac{\tilde{v}_{11}^{11}(\beta_n)}{\tilde{v}_{11}^{01}(\beta_n)}\sin\overline{\beta}_n x\right)=\\&=\frac{\tilde{v}_{11}^{01}(\beta_n)}{\tilde{v}_{11}^{11}(\beta_n)}\left(\tilde{v}_{11}^{11}(\beta_n)\sin\overline{\beta}_n x-\tilde{v}_{11}^{12}(\beta_n)\sin\overline{\beta}_n x\right)\equiv\\&\equiv\frac{\tilde{v}_{11}^{01}(\beta_n)}{\tilde{v}_{11}^{11}(\beta_n)}\left[\tilde{\beta}_{11}^1\sin\overline{\beta}_n(l_1-x)-\tilde{\alpha}_{11}^1\overline{\beta}_n\cos\overline{\beta}_n(l_1-x)\right]\end{aligned} \tag{5.24}$$

From equations (5.20), (5.24) we have:

$$V_0(l_0,\beta_n)=-\tilde{\alpha}_{11}^0\frac{\tilde{v}_{11}^{01}(\beta_n)}{\tilde{v}_{11}^{11}(\beta_n)};\ V_0(l_1,\beta_n)=-\tilde{\alpha}_{11}^0\overline{\beta}_n\frac{\tilde{v}_{11}^{01}(\beta_n)}{\tilde{v}_{11}^{11}(\beta_n)}\equiv-\tilde{\alpha}_{11}^0a^{-2}\beta_n\frac{\tilde{v}_{11}^{01}(\beta_n)}{\tilde{v}_{11}^{11}(\beta_n)}.$$

Based on the transcendental equation (5.18) and equations (5.20), (5.24) we can obtain the square of the norm of the spectral function $V_0(l_0,\beta_n)$:

$$\left\|V_0(l_0,\beta_n)\right\|^2=\int_{l_0}^{l_1}\left[V_0(l_0,\beta_n)\right]^2\sigma dx=\frac{1}{2a^2}\left[\left(\frac{\tilde{\alpha}_{11}^0}{a}\beta_n\right)^2+\left(\tilde{\beta}_{11}^0\right)^2(l_1-l_0)+\tilde{\alpha}_{11}^0\tilde{\beta}_{11}^0+\tilde{\alpha}_{11}^1\tilde{\beta}_{11}^1\frac{\left(\tilde{v}_{11}^{01}(\beta_n)\right)^2}{\tilde{v}_{11}^{11}(\beta_n)}\right]. \quad (5.25)$$

Due to equality (5.19), the solution to the boundary value problem (5.1) - (5.3) is a function

$$u(t,x)=\sum_{n=1}^{\infty}e^{-\left(\beta_n^2+\gamma^2\right)t}\frac{V_0\left(x,\beta_n\right)}{\left\|V_0\left(x,\beta_n\right)\right\|_1^2}\int_{l_0}^{l_1}g(\xi)V_0\left(\xi,\beta_n\right)\sigma d\xi. \quad (5.26)$$

Hence, due to the initial condition, we obtain at $t = 0$ an integral representation of the function $g(x)$:

$$g(x)=\sum_{n=1}^{\infty}\frac{V_0\left(x,\beta_n\right)}{\left\|V_0\left(x,\beta_n\right)\right\|_1^2}\int_{l_0}^{l_1}g(\xi)V_0\left(\xi,\beta_n\right)\sigma d\xi. \quad (5.27)$$

Since the system of functions $\left\{V_0\left(x,\beta_n\right)\right\}_{n=1}^{\infty}$ is orthogonal in understanding $\|\cdot\|_1$, complete and closed [11], equality (5.29) is a Fourier series for the function g (x).

The consequence of these considerations is the following theorem:

Theorem 5.1.3 (*on Fourier series development*): *If the function* $g(x)\in C^{(3)}(l_0,l_1)$ *and satisfies boundary conditions*

$$B_0[g]\equiv\left\{\left[\alpha_{11}^0+\delta_{11}^0(a^2\frac{d^2}{dx^2}-\gamma^2)\right]\frac{d}{dx}+\gamma_{11}^0(a^2\frac{d^2}{dx^2}-\gamma^2)+\beta_{11}^0\right\}g(x)\Big|_{x=l_0}=0, \quad (5.28)$$

$$B_1[g]\equiv\left\{\left[\alpha_{11}^1+\delta_{11}^1(a^2\frac{d^2}{dx^2}-\gamma^2)\right]\frac{d}{dx}+\gamma_{11}^1(a^2\frac{d^2}{dx^2}-\gamma^2)+\beta_{11}^1\right\}g(x)\Big|_{x=l_1}=0, \quad (5.29)$$

then it is represented by an absolutely and uniformly convergent Fourier series (5.27).

The Fourier series defines direct

$$F_n[g(x)]=\int_{l_0}^{l_1}g(x)V_0(x,\beta_n)\delta dx\equiv g_n \quad (5.30)$$

and inverse

$$F_n^{-1}[g_n]=\sum_{n=1}^{\infty}g_n\frac{V_0(x,\beta_n)}{\left\|V_0(x,\beta_n)\right\|_1^2}\equiv g(x) \quad (5.31)$$

finite integral Fourier transformation with spectral parameter in boundary conditions.

Theorem 5.1.4 (*on basic identity*): *If the function* $\mathrm{g(x)} \in C^{(3)}(l_0, l_1)$ *and satisfies the boundary conditions*

$$B_0[g] = g_0,\ B_1[g] = g_1, \tag{5.32}$$

then the basic identity of the integral transformation of the differential Fourier operator $B = a^2 \dfrac{d^2}{dx^2}$ *is true* :

$$F_n\left[a^2 \frac{d^2}{dx^2} g(x)\right] = -\beta_n^2 g_n + \left(\tilde{\alpha}_{11}^1\right)^{-1} V_0(l_1, \beta_n) g_1 - \left(\tilde{\alpha}_{11}^0\right)^{-1} V_0(l_0, \beta_n) g_0 \equiv -\beta_n^2 g_n - \bar{\beta}_n \frac{\upsilon_{11}^{01}(\beta_n)}{\upsilon_{11}^{11}(\beta_n)} g_1 + \beta_0 g_0 \equiv$$

$$\equiv -\beta_n^2 g_n + (\delta_{11}^0 \beta_{11}^0 - \alpha_{11}^0 \gamma_{11}^0)^{-1} \left[\delta_{11}^0 V_0'(l_0, \beta_n) + \gamma_{11}^0 V_0(l_0, \beta_n)\right] + \tag{5.33}$$

$$+ (\alpha_{11}^1 \gamma_{11}^1 - \delta_{11}^1 \beta_{11}^1)^{-1} \left[\delta_{11}^1 V_0'(l_0, \beta_n) + \gamma_{11}^1 V_0(l_0, \beta_n)\right]$$

Proof: Identity (5.33) is established directly by the method of integration twice by parts under the sign of the integral, followed by the use of the properties of the functions g (*x*) and $V_0(x, \beta_n)$.

5.1.2. Fourier integral transformation for a halflimided homogeneous media

The integral Fourier transformation for a halflimided homogeneous media related to a boundary operator $B = -h_1 \dfrac{\partial}{\partial x} + h_2, \quad h_1 \geq 0, \quad h_2 \geq 0, \quad h_1 + h_2 \neq 0$ is constructed and mathematically substantiated in [11]. We construct it using the Cauchy kernel as a fundamental solution to the Cauchy problem for a parabolic equation under a homogeneous boundary condition.

We consider the problem of limited solution constructing of differential equation of the second-order in the domain $D^+ = \{(t,x) : t \in (0,\infty), x \in (0,\infty)\}$ [19]

$$\frac{\partial u}{\partial t} + \gamma^2 u - a^2 \frac{\partial^2 u}{\partial x^2} = 0, a > 0, \gamma^2 \geq 0 \tag{5.34}$$

under the initial condition:

$$u(t,x)\big|_{t=0} = g(x) \tag{5.35}$$

and boundary conditions:

$$\left[\left(\alpha_{11}^0+\frac{\partial}{\partial t}\right)\frac{\partial}{\partial x}+\beta_{11}^0+\gamma_{11}^0\frac{\partial}{\partial t}\right]u\Big|_{x=0}=0,\frac{\partial u}{\partial x}\Big|_{x=\infty}=0. \tag{5.36}$$

We assume, that $\alpha_{11}^0\le 0,\quad \beta_{11}^0\ge 0,\quad \delta_{11}^0\ge 0,\quad \gamma_{11}^0\ge 0,\quad \left|\alpha_{11}^0\right|+\beta_{11}^0\ne 0,$ $\delta_{11}^0 g'(0)+\gamma_{11}^0 g(0)=0.$

and the function $u(t,x)$ is the original for Laplace with respect to the variable t [29]. In the Laplace image we have the problem of construction of a limited solution to equation in domain D^+:

$$\frac{d^2u*}{dx^2}-q^2u*=-\overline{g}(x);\overline{g}=a^{-2}g,q^2=a^{-2}\left(p+\gamma^2\right),\gamma^2\ge 0 \tag{5.37}$$

under boundary conditions:

$$\left(\overline{\alpha}_{11}^0\frac{d}{dx}+\overline{\beta}_{11}^0\right)u^*(p,x)\big|_{x=0}=0,\ \frac{du}{dx}^*\Big|_{x=\infty}=0. \tag{5.38}$$

Let's fix that a branch of ambiguous function $q=a^{-1}(p+\gamma^2)^{1/2}$, on which $\Re eq>0$. It is directly verified that the solution to the boundary value problem (5.37), (5.38) is the function:

$$u^*(p,x)=\int_{l_0}^{l}\mathrm{E}^*(p,x,\xi)\tilde{g}(\xi)d\xi. \tag{5.39}$$

The formula (5.39) involves the fundamental function of the boundary value problem (5.37), (5.38)

$$\mathrm{E}^*(p,x,\xi)=\frac{e^{-q|x-\xi|}}{2q}+\frac{\overline{\alpha}_{11}^0q+\overline{\beta}_{11}^0}{\overline{\alpha}_{11}^0q-\overline{\beta}_{11}^0}\frac{e^{-q|x+\xi|}}{2q}. \tag{5.40}$$

The special points of the function $\mathrm{E}^*(p,x,\xi)$ are the points of branching $p=-\gamma^2$ and $p=\infty$. As a result of Jordan's lemma and Cauchy's theorem [11], we obtain the formula for calculating the original of the fundamental function:

$$\mathrm{E}\,(t,x,\xi)=L^{-1}\left[\mathrm{E}^{*}\right]\equiv\frac{1}{2\pi i}\int_{\sigma_0-i\infty}^{\sigma_0+i\infty}\mathrm{E}^{*}(p,x,\xi)e^{pt}dp\equiv-\frac{2}{\pi}\int_{0}^{\infty}\mathrm{Im}\left[\mathrm{E}^{*}\left(e^{\pi i}(\gamma^2+\beta^2),x,\xi\right)\right]e^{-\left(\gamma^2+\beta^2\right)t}\beta d\beta$$

. (5.41)

We put $\sqrt{p+\gamma^2}=i\beta,$ or $p=(\beta^2+\gamma^2)\exp\pi i=-(\beta^2+\gamma^2).$ Here $dp=-2\beta d\beta$.

Let us define the spectral function

$$V\left(x,\beta\right)=\tilde{\beta}_{11}^{0}\ \sin\bar{\mathrm{b}}\mathrm{x}-\tilde{\alpha}_{11}^{0}\ \bar{\mathrm{b}}\ \cos\bar{\mathrm{b}}\mathrm{x}$$

and spectral density $\tilde{\beta}_{11}^{0}=\beta_{11}^{0}-\gamma_{11}^{0}\left(\beta^2+\gamma^2\right)$

$$\Omega(\beta)=b^{-1}\beta\left(\left[\tilde{\beta}_{11}^{0}\right]^2+\bar{b}^2\left[\tilde{\alpha}_{11}^{0}\right]^2\right)^{-1},\ \bar{b}=a^{-1}\beta,\ \tilde{\alpha}_{11}^{0}=\alpha_{11}^{0}-\delta_{11}^{0}(\beta^2+\gamma^2),$$

$$\tilde{\beta}_{11}^{0}-\tilde{\gamma}_{11}^{0}(\beta^2+\gamma^2).$$

According to the formula (5.41) we have:

$$\mathrm{E}\ (t,x,\xi)=-\frac{2}{\pi}\int_{0}^{\infty}e^{-\left(\gamma^2+\beta^2\right)t}V\left(x,\beta\right)V\left(\xi,\beta\right)\Omega(\beta)d\beta\sigma a^2. \tag{5.42}$$

The solution to the parabolic boundary value problem of mass transfer (5.34) - (5.36) is the function:

$$u\left(t,x\right)=L^{-1}\left[u^{*}\left(p,x\right)\right]=\int_{0}^{\infty}\mathrm{E}\left(t,x,\xi\right)g\left(\xi\right)\sigma d\xi\ \ \sigma=a^{-2}. \tag{5.43}$$

Due to the initial condition (5.34) we obtain an integral image:

$$g(x)=\frac{2}{\pi}\int_{0}^{\infty}V(x,\beta)\Omega(\beta)d\beta\int_{0}^{\infty}g(\xi)V(\xi,\beta)\sigma d\xi. \tag{5.44}$$

The integral image (5.44) for a halflimited domain $x\geq 0$ generates a direct

$$F_{+}\left[g(x)\right]=\int_{0}^{\infty}g(x)V(x,\beta)\sigma dx\equiv\tilde{g}(\beta). \tag{5.45}$$

and inverse

$$F_{+}^{-1}\left[\tilde{g}(\beta)\right]=\frac{2}{\pi}\int_{0}^{\infty}\tilde{g}(\beta)V(x,\beta)\Omega\left(\beta\right)d\beta\equiv g(x). \tag{5.46}$$

Integral transformation of Fourier with spectral parameter.

Theorem 5.1.5: (*on an integral image*). *If the function* $f(x)$ *is definite, piecewise - continuous, absolutely sum and has limited variation on the set* $(0,\infty)$, *then the integral image comes true*:

$$\frac{1}{2}\left[f(x-0)+f(x+0)\right]=\frac{2}{\pi}\int_0^\infty V(x,\beta)\Omega(\beta)d\beta\int_0^\infty f(\xi)V(\xi,\beta)\sigma d\xi. \quad (5.47)$$

Theorem 5.1.6 (*on the basic identity*): *If a function* $f(x)$ *has three continuous derivatives on the set* $(0,\infty)$, *ie* $f(x)\in C^{(3)}(0,\infty)$, *disappears together with its first-order derivative at* $x\to\infty$ *and at the point* $x=l_0$ *satisfies the boundary condition:*

$$\left(\tilde{\alpha}_{11}^0\frac{d}{dx}+\tilde{\beta}_{11}^0\right)f(x)\Big|_{x=l_0}=f_0\equiv const, \quad (5.48)$$

then the basic identity of the integral transformation of the Fourier differential operator $£=a^2\dfrac{d^2}{dx^2}$ *is true*:

$$F+\left[a^2\frac{d^2f}{dx^2}\right]=-\beta^2\tilde{f}(\beta)+a^{-1}\beta f_0. \quad (5.49)$$

Proof: Proof of identity (5.49) is established directly by the method of double integration of parts under the sign of the integral using the properties of spectral functions $V(x,\beta)$ and conditions (5.49).

5.2 Finite hybrid integral Fourier transforms for bounded heterogeneous n-component media

Consider the Sturm-Liouville problem about the construction on the set $I_n=\left\{z: z\in\bigcup_{j=1}^{n+1}(l_{j-1},l_j);\ l_0\ge 0, l_{n+1}=l<\infty\right\}$ nonzero solution to the system of the second-order differential Fourier equations:

$$L_j\left[V_j\right]\equiv\left(\frac{d^2}{dz^2}+\bar{b}_j^2\right)V_j=0;\ \bar{b}_j^2=\frac{1}{D_j}\left(\beta^2+\gamma_j^2\right)^{1/2}, j=\overline{1,n+1} \quad (5.50)$$

with boundary conditions:

$$\left(\tilde{\alpha}_{11}^{0}\frac{d}{dz}+\tilde{\beta}_{11}^{0}\right)V_1\Big|_{z=l_0}=0,\left(\tilde{\alpha}_{22}^{n+1}\frac{d}{dz}+\tilde{\beta}_{22}^{n+1}\right)V_{n+1}\Big|_{z=l_{n+1}}=0 \tag{5.51}$$

and a system of *n*– interface conditions:

$$\left[\left(\tilde{\alpha}_{j1}^{k}\frac{d}{dz}+\tilde{\beta}_{j1}^{k}\right)V_{k}-\left(\tilde{\alpha}_{j2}^{k}\frac{d}{dz}+\tilde{\beta}_{j2}^{k}\right)V_{k+1}\right]\Big|_{z=l_k}=0,\ j=1,2,k=\overline{1,n}. \tag{5.52}$$

In equalities (5.50) - (5.52) magnitudes are involved:

$$a_j>0,\gamma_j^2\geq 0,\beta\in(o,\infty);\left|\alpha_{11}^{0}\right|+\left|\beta_{11}^{0}\right|\neq 0,\left|\alpha_{22}^{n+1}\right|+\left|\beta_{22}^{n+1}\right|\neq 0;\tilde{\alpha}_{jk}^{m}=\alpha_{jk}^{m}-\delta_{jk}^{m}\left(\beta^2+\gamma^2\right);$$
$$\tilde{\beta}_{jk}^{m}=\beta_{jk}^{m}-\gamma_{k}^{m}\left(\beta^2+\gamma^2\right),m=0,n+1;\gamma^2=\max\{\gamma_1^{2;}\gamma_2^2;....;\gamma_{n+1}^2\}.$$

Let's write numerical matrices

$$A_{j1,k}=\begin{bmatrix}\alpha_{1j}^{k}\beta_{1j}^{k}\\ \alpha_{2j}^{k}\beta_{2j}^{k}\end{bmatrix},\ A_{j2,k}=\begin{bmatrix}\delta_{1j}^{k}\gamma_{1j}^{k}\\ \delta_{2j}^{k}\gamma_{2j}^{k}\end{bmatrix};\ j=1,2;k=\overline{1,n}$$

and numbers:

$$\begin{gathered}c_{j1,k}=-\det A_{j1,k}\equiv\alpha_{2j}^{k}\beta_{1j}^{k}-\alpha_{1j}^{k}\beta_{2j}^{k},\\ c_{j2,k}=-\det A_{j2,k}\equiv\delta_{2j}^{k}\gamma_{1j}^{k}-\delta_{1j}^{k}\gamma_{2j}^{k},;j=1,2;k=\overline{1,n;}\\ c_{11,12}^{12,}=\alpha_{11}^{k}\gamma_{21}^{k}-\alpha_{21}^{k}\gamma_{11}^{k},c_{11,12}^{21,k}=\beta_{11}^{k}\delta_{21}^{k}-\beta_{21}^{k}\delta_{11}^{k},\\ c_{21,22}^{12,k}=\alpha_{12}^{k}\gamma_{22}^{k}-\alpha_{22}^{k}\gamma_{12}^{k},c_{21,22}^{21,k}=\beta_{12}^{k}\delta_{22}^{k}-\beta_{22}^{k}\delta_{12}^{k}.\end{gathered} \tag{5.53}$$

We will also require the fulfillment of relations:

$$\begin{gathered}c_{11,k}c_{21,k}>0;c_{j2,k}=0;c_{11,12}^{12,k}=c_{11,12}^{21,k};\\ c_{21,22}^{12,k}=c_{21,22}^{21,k};j=1,2;k=\overline{1,n.}\end{gathered} \tag{5.54}$$

Fundamental system of solutions to the equation $L_j[V]=0$ form functions $cosq_jz$ та $\sin q_jz$, $q_j\equiv\overline{b}_j$, therefore, the solution to the boundary value problem (5.50) - (5.52) looks as:

$$V_j(z,\beta)=A_j(\beta)\cos q_jz+B_j(\beta)\sin q_jz,\ \text{j}=\overline{1,n+1.}$$

Boundary conditions (5.51) and a system of n - interface conditions (5.52) to determine arbitrary constants A_j and B_j give an algebraic system with $(2n+2)$ equations:

$$\left.\begin{array}{c} \tilde{v}_{11}^{01}(q_1 l_0)A_1 + \tilde{v}_{11}^{02}(q_1 l_0)B_1 = 0 \\ \tilde{v}_{j1}^{k1}(q_k l_k)A_k + \tilde{v}_{j1}^{k2}(q_k l_k)B_k - \tilde{v}_{j2}^{k1}(q_{k+1} l_k)A_{1+k} - \tilde{v}_{j2}^{k2}(q_{k+1} l_k)B_{k+1} = 0,\ j = 1,2; k = \overline{1,n} \\ \tilde{v}_{22}^{n+1,1}(q_{n+1} l)A_{n+1} + \tilde{v}_{22}^{n+1,2}(q_{n+1} l)B_{n+1} = 0 \end{array}\right\} \quad (5.55)$$

In order to have a nonzero solution to an algebraic system (5.55), it is necessary and sufficient that its determinant be equal to zero

$$\delta_n(\beta) \equiv -\omega_{n1}(\beta) \cdot \tilde{v}_{22}^{n+1,2}(q_{n+1} l) + \omega_{n2}(\beta) \cdot \tilde{v}_{22}^{n+1,1}(q_{n+1} l) = 0. \quad (5.56)$$

Here

$$\tilde{v}_{ij}^{k1}(q_s l_m) \equiv (\tilde{\alpha}_{ij}^k \frac{d}{dz} + \tilde{\beta}_{ij}^k)\cos q_s z\Big|_{z=l_m} = -\tilde{\alpha}_{ij}^k q_s \sin q_s l_m + \tilde{\beta}_{ij}^k \cos q_s l_m,$$

$$\tilde{v}_{ij}^{k2}(q_s l_m) \equiv (\tilde{\alpha}_{ij}^k \frac{d}{dz} + \tilde{\beta}_{ij}^k)\sin q_s z\Big|_{z=l_m} = -\tilde{\alpha}_{ij}^k q_s \cos q_s l_m + \tilde{\beta}_{ij}^k \sin q_s l_m;$$

$$\psi_{jm}^k(z,y) = \tilde{v}_{11}^{kj}(z)\tilde{v}_{22}^{km}(y) - \tilde{v}_{21}^{kj}(z)\tilde{v}_{12}^{km}(y);$$

$$\omega_{01}(\beta) = -\tilde{\upsilon}_{11}^{01}(q_1 l_0), \omega_{02}(\beta) = -\tilde{\upsilon}_{11}^{02}(q_1 l_0);$$

$$\omega_{jm}(\beta) = \omega_{j-1,2}(\beta)\psi_{1m}^j(q_j l_j, q_{j+1} l_j) - \omega_{j-1,1}(\beta)\psi_{2m}^j(q_j l_j, q_{j+1} l_j).$$

Theorem 5.2.1 (about the discrete spectrum). *Roots* $\beta_1, \beta_2, ..., \beta_m, ...$ *transcendental equation (5.56) form a discrete spectrum: the roots are real, simple, (except maybe zero), symmetrically located relative to zero and form in the region* $\beta > 0$ *monotonically increasing sequence with a single boundary point* $\beta = +\infty$.

Proof: The proof of the theorem is performed using the method of works [11]. We show that the spectrum of eigenvalues is real numbers. Assuming that the eigenvalue of the boundary value problem (5.50) - (5.52) is a complex number $\beta = \sigma + is$, which corresponds to the eigen-vector function $V(z,\beta)$. At the same time, its own number will be conjugated to it $\beta = \sigma - is$, which corresponds to the eigen-vector function $\tilde{V}(z,\tilde{\beta})$. Since $V(z,\beta)$ and $\tilde{V}(z,\tilde{\beta})$ are eigenvector functions corresponding to different eigenvalues, then the condition of orthogonality is fulfilled (for different are generalized orthogonal):

$$0 = \int_{l_0}^{l} V(z,\beta)\tilde{V}(z,\tilde{\beta})\sigma(z)dz = \int_{l_0}^{l} [V]^2 \sigma(z)dz = \|V\|^2,$$

hence the equality $V(z,\beta) = 0$, which is impossible, and therefore, eigenvalues are not complex, but are real. The symmetry of the roots is obvious here.

It is possible to see by the method of the opposite that the roots $\beta_1, \beta_2, ..., \beta_m, ...$ are different. Because $\delta_n(\beta)$ is the entire analytical function of β, then the transcendental equation (5.56) has a countable set of roots that do not have a finite boundary point [11]. That means that $\lim\limits_{m\to\infty} \beta_m = \infty$. Theorem is proved.

Discrete spectrum of eigenvalues β_n corresponds to a discrete eigenvector function $V(z,\beta_m) = \{V_1(z,\beta_m), V_2(z,\beta_m), ..., V_n(z,\beta_m), V_{n+1}(z,\beta_m)\}$. Structure of functions $V_k(z,\beta_m)$ is obtained as follows:

Substitute into the system (5.55) $\beta = \beta_m$ and discard the last equation due to its linear dependence. Let's put it as $A_1 = -A_0\tilde{\upsilon}_{11}^{02}(q_{1m}l_0) \equiv A_0\omega_{02}(\beta_m)$, $B_1 = A_0\tilde{\upsilon}_{11}^{01}(q_{1m}l_0) \equiv -A_0\omega_{01}(\beta_m)$. For the first component of the eigenvector function, defined on the interval (l_0, l_1) take the function.

$$V_1(z,\beta_m) = A_0(\beta_m)\left[\omega_{02}(\beta_m)\cos q_{1m}z - \omega_{01}(\beta_m)\sin q_{1m}z\right],\ q_{jn} = \frac{1}{\sqrt{D_j}}(\beta_m^2 + \gamma_j^2)^{1/2},\ \gamma_j^2 \geq 0,$$

$$j = \overline{1, n+1}.$$

Coefficient A_0 to be determined. The remaining equations are broken up into n separate systems of two equations each. Due to recurrent dependencies:

$$A_{k+1} = \frac{1}{c_{21,\,k}\,q_{k+1,m}}\left[A_k\psi_{12}^k(q_{km}l_k, q_{k+1,m}l_k) + B_k\psi_{22}^k(q_{km}l_k, q_{k+1,m}l_k)\right],$$

$$B_{k+1} = \frac{1}{c_{21,\,k}\,q_{k+1,m}}\left[A_k\psi_{11}^k(q_{km}l_k, q_{k+1,m}l_k) + B_k\psi_{21}^k(q_{km}l_k, q_{k+1,m}l_k)\right],\ k = \overline{1, n}$$

we get:

$$A_k = \frac{A_0}{\prod\limits_{i=1}^{k} c_{21,\,i}\,q_{i+1,m}}\omega_{k2}(\beta_m);\ B_{k+1} = \frac{A_0}{\prod\limits_{i=1}^{k} c_{21,\,i}\,q_{i+1,m}}\omega_{k1}(\beta_m). \tag{5.57}$$

If we put $A_0 = \prod\limits_{i=1}^{n} c_{21,\,i}\,q_{i+1,m}$;

$G_k(z,\beta_m) = \omega_{k-1,2}(\beta_n)\cos q_{km}z - \omega_{k-1,1}(\beta_m)\sin q_{km}z$,

then components V_k of spectral vector function $V(z,\beta_m)$ will be determined:

$$V_k(z,\beta_m)=\left(\prod_{i=k}^{n}c_{21,\,i}q_{i+1,m}\right)G_k(z,\beta_m),\,k=\overline{1,n};\qquad(5.58)$$

$$V_{n+1}(z,\beta_m)=\omega_{n2}(\beta_m)\cos q_{n+1,m}z-\omega_{n1}(\beta_m)\sin q_{n+1,m}z.$$

If $\theta(x)$ - Heaviside function, the spectral vector function is written as:

$$V(z,\beta_j)=\sum_{k=1}^{n+1}V_k(z,\beta_j)\theta(z-l_{k-1})\theta(l_k-z).\qquad(5.59)$$

Theorem 5.2.2 (about the discrete function). *The system of eigenfunctions* $\left\{V\left(z,\beta_j\right)\right\}_{j=1}^{\infty}$ *Fourier differential operator Fn, defined by equality (1.3.0), is generalized orthogonal, complete and closed on the set In.*

Proof: Let us show that the system of eigenvector functions $\left\{V(z,\beta_j)\right\}_{j=1}^{\infty}$ is generalized orthogonal to the set I_n with weight function

$$\sigma(z)=\sum_{k=1}^{n+1}\sigma_k\theta(z-l_{k-1})\theta(l_k-z),$$

$$\sigma_k=\frac{1}{D_k}\prod_{m=k}^{n}\frac{c_{11,m}}{c_{21,m}},\ k=\overline{1,n},\ \sigma_{n+1}=\frac{1}{D_{n+1}}.$$

Indeed, consider two eigenvector functions $V(z,\beta_j)$ $V(z,\beta_m)$, which correspond to their own values $\beta_j\neq\beta_m$. From identities:

$$\left(\frac{d^2}{dz^2}+q_{sj}^2\right)V_s(z,\beta_j)\equiv 0,\ \left(\frac{d^2}{dz^2}+q_{sm}^2\right)V_s(z,\beta_m)\equiv 0,\ s=\overline{1,n+1}$$

we get the ratio

$$V_s(z,\beta_m)V_s(z,\beta_j)=\frac{a_s^2}{\beta_m^2-\beta_j^2}\frac{d}{dz}\left[V_s(z,\beta_m)\frac{d}{dz}V_s(z,\beta_j)-V_s(z,\beta_j)\frac{d}{dz}V_s(z,\beta_m)\right].\quad(5.60)$$

Multiply the equality (5.60) by $\sigma_z dz$, integrate from l_{s-1} to l_s and add to s from 1 to $n+1$. As a result, we obtain equality

$$\int_{l_0}^{l_{n+1}}V(z,\beta_j)V(z,\beta_m)\sigma(z)dz=\sum_{s=1}^{n+1}\frac{\sigma_s a_s^2}{\beta_m^2-\beta_j^2}\left[V_s(z,\beta_m)\frac{d}{dz}V_s(z,\beta_j)-V_s(z,\beta_j)\frac{d}{dz}V_s(z,\beta_m)\right]\Bigg|_{l_{s-1}}^{l_s}=$$

$$=\frac{1}{\beta_m^2-\beta_j^2}\left\{\sigma_1 a_1^2\left[V_1(l_0,\beta_m)\frac{d}{dz}V_1(l_0,\beta_j)-V_1(l_0,\beta_j)\frac{d}{dz}V_1(l_0,\beta_m)\right]+\left[V_{n+1}(l,\beta_m)\frac{d}{dz}V_{n+1}(l,\beta_j)-\right.\right.$$

$$-V_{n+1}(l,\beta_j)\frac{d}{dz}V_{n+1}(l,\beta_m)\Big]+\sum_{k=1}^{n}\Big[a_k^2\sigma_k(V_k(z,\beta_m)V_{k'}(z,\beta_j)-V_k(z,\beta_j)V_{k'}(z,\beta_m))- \tag{5.61}$$

$$-a_{k+1}^2\sigma_k(V_{k+1}(z,\beta_m)V_{k'+1}(z,\beta_j)-V_{k+1}(z,\beta_j)V_{k'+1}(z,\beta_m)\Big]\Big|_{z=l_k}\Big\}.$$

Consider the matrix $\widetilde{A}_{11,k}=\begin{bmatrix}\widetilde{\alpha}_{11}^k & \widetilde{\beta}_{11}^k\\ \widetilde{\alpha}_{21}^k & \widetilde{\beta}_{21}^k\end{bmatrix}$, $\widetilde{A}_{12,k}=\begin{bmatrix}\widetilde{\alpha}_{12}^k & \widetilde{\beta}_{12}^k\\ \widetilde{\alpha}_{22}^k & \widetilde{\beta}_{22}^k\end{bmatrix}$ and determine the number of

$$\widetilde{c}_{11,12}^{11,k}=\widetilde{\alpha}_{11}^k\widetilde{\alpha}_{22}^k-\widetilde{\alpha}_{21}^k\widetilde{\alpha}_{12}^k,\ c_{11,12}^{12,k}=\widetilde{\alpha}_{11}^k\widetilde{\beta}_{22}^k-\widetilde{\alpha}_{21}^k\widetilde{\beta}_{12}^k,$$

$$\widetilde{c}_{11,12}^{21,k}=\widetilde{\beta}_{11}^k\widetilde{\alpha}_{22}^k-\widetilde{\beta}_{21}^k\widetilde{\alpha}_{12}^k,\ \widetilde{c}_{11,12}^{22,k}=\widetilde{\beta}_{11}^k\widetilde{\beta}_{22}^k-\widetilde{\beta}_{21}^k\widetilde{\beta}_{12}^k.$$

Because of $\widetilde{\alpha}_{11}^k(\beta)\widetilde{\beta}_{21}^k(\beta)-\widetilde{\alpha}_{21}^k(\beta)\widetilde{\beta}_{11}^k(\beta)=-\widetilde{c}_{11,k}+(\widetilde{c}_{11,12}^{12,k}-\widetilde{c}_{11,12}^{21,k})\beta^2-\widetilde{c}_{12,k}\beta^4=-\widetilde{c}_{11,k}\neq 0$, then an algebraic system is

$$\widetilde{\alpha}_{11}^kV_{k'}(l_k,\beta)+\widetilde{\beta}_{11}^kV_k(l_k,\beta)=\widetilde{\alpha}_{12}^kV_{k'+1}(l_k,\beta)+\widetilde{\beta}_{12}^kV_{k+1}(l_k,\beta),$$

$$\widetilde{\alpha}_{21}^kV_{k'}(l_k,\beta)+\widetilde{\beta}_{21}^kV_k(l_k,\beta)=\widetilde{\alpha}_{22}^kV_{k'+1}(l_k,\beta)+\widetilde{\beta}_{22}^kV_{k+1}(l_k,\beta), \tag{5.62}$$

relatively $V_k(l_k,\beta)$ and $V_{k'}(l_k,\beta)$ have a unique solution:

$$V_k(l_k,\beta)=-\frac{1}{c_{11,k}}\Big[\widetilde{c}_{11,12}^{12,k}(\beta)V_{k+1}(l_k,\beta)+\widetilde{c}_{11,12}^{11,k}(\beta)V_{k'+1}(l_k,\beta)\Big],$$

$$V_{k'}(l_k,\beta)=\frac{1}{c_{11,k}}\Big[\widetilde{c}_{11,12}^{22,k}(\beta)V_{k+1}(l_k,\beta)+\widetilde{c}_{11,12}^{21,k}(\beta)V_{k'+1}(l_k,\beta)\Big]. \tag{5.63}$$

Putting for simplicity $\beta_m\equiv\beta,\beta_j\equiv\lambda$, consider the expression

$$V_k(l_k,\beta)V_k'(l_k,\lambda)-V_k(l_k,\lambda)V_k'(l_k,\beta)=\frac{1}{c_{11,k}^2}\{A_{11}(\lambda,\beta)V_{k+1}'(l_k,\lambda)V_{k+1}'(l_k,\beta)+$$

$$+A_{12}(\lambda,\beta)V_{k+1}(l_k,\beta)V_{k+1}'(l_k,\lambda)+A_{21}(\lambda,\beta)V_{k+1}(l_k,\lambda)V_{k+1}'(l_k,\beta)+A_{22}(\lambda,\beta)V_{k+1}(l_k,\lambda)V_{k+1}'(l_k,\beta)\}$$

$$A_{ij}(\lambda,\beta)=\widetilde{c}_{11,12}^{1i,k}(\lambda)\widetilde{c}_{11,12}^{2j,k}(\beta)-\widetilde{c}_{11,12}^{2i,k}(\lambda)\widetilde{c}_{11,12}^{1i,k}(\beta);\ i,j=1,2;\ k=\overline{1,n}. \tag{5.64}$$

We establish equations by direct calculations:

$$\widetilde{\alpha}_{11}^k(\lambda)\widetilde{\beta}_{11}^k(\beta)-\widetilde{\alpha}_{11}^k(\beta)\widetilde{\beta}_{11}^k(\lambda)=-(\beta^2-\lambda^2)\alpha_{11}^k,\ \alpha_{11}^k=\alpha_{11}^k\gamma_{11}^k-\delta_{11}^k\beta_{11}^k\geq 0;$$

$$\widetilde{\alpha}_{21}^k(\lambda)\widetilde{\beta}_{21}^k(\beta)-\widetilde{\alpha}_{21}^k(\beta)\widetilde{\beta}_{21}^k(\lambda)=-(\beta^2-\lambda^2)\alpha_{22}^k,\ \alpha_{22}^k=\alpha_{21}^k\gamma_{21}^k-\delta_{21}^k\beta_{21}^k\geq 0;$$

$$\tilde{\alpha}_{21}^k(\beta)\tilde{\beta}_{11}^k(\lambda)-\tilde{\alpha}_{11}^k(\lambda)\tilde{\beta}_{21}^k(\beta)=c_{11,k}-(\beta^2-\lambda^2)\alpha_{12,1}^k; \tag{5.65}$$

$$\alpha_{12,1}^k = \delta_{11}^k \beta_{21}^k - \alpha_{21}^k \gamma_{11}^k \equiv \alpha_{12,2}^k = \delta_{11}^k \beta_{21}^k - \alpha_{11}^k \gamma_{21}^k .$$

Due to equations (5.65) we have:

$$A_{22}(\lambda,\beta) = -(\beta^2 - \lambda^2)\left[\alpha_{11}^k \tilde{\beta}_{22}^k(\beta)\tilde{\beta}_{22}^k(\lambda) + \alpha_{22}^k \tilde{\beta}_{12}^k(\lambda)\tilde{\beta}_{12}^k(\beta) + \alpha_{12}^k(\tilde{\beta}_{12}^k(\beta)\tilde{\beta}_{22}^k(\lambda) + \tilde{\beta}_{12}^k(\lambda)\tilde{\beta}_{22}^k(\beta)) - c_{11,k}c_{21,22}^{22,k}\right]$$

;

$$A_{11}(\lambda,\beta) = -(\beta^2 - \lambda^2)\left[\alpha_{11}^k \tilde{\alpha}_{22}^k(\beta)\tilde{\alpha}_{22}^k(\lambda) + \alpha_{22}^k \tilde{\alpha}_{12}^k(\lambda)\tilde{\alpha}_{12}^k(\beta) + \alpha_{12}^k(\tilde{\alpha}_{12}^k(\beta)\tilde{\alpha}_{12}^k(\lambda) + \tilde{\alpha}_{12}^k(\lambda)\tilde{\alpha}_{22}^k(\beta)) - c_{11,k}c_{21,22}^{11,k}\right]$$

;

$$A_{12}(\lambda,\beta) = -(\beta^2 - \lambda^2)\left[\alpha_{11}^k \tilde{\alpha}_{22}^k(\beta)\tilde{\beta}_{22}^k(\lambda) + \alpha_{22}^k \tilde{\alpha}_{12}^k(\lambda)\tilde{\beta}_{12}^k(\beta) + \right.$$
$$\left. + \alpha_{12}^k(\tilde{\alpha}_{22}^k(\lambda)\tilde{\beta}_{12}^k(\beta) + \tilde{\alpha}_{12}^k(\lambda)\tilde{\beta}_{22}^k(\beta)) - c_{11,k}c_{21,22}^{12,k}\right] c_{11,k}c_{21,k} .$$

Define the functions $z_{jk}(\beta) = \tilde{\alpha}_{j2}^k(\beta)V'_{k+1}(l_k,\beta) + \tilde{\beta}_{j2}^k(\beta)V'_{k+1}(l_k,\beta)$, $j = 1,2$.

As a result of the substitution of equations (5.66) to (5.64), we obtain:

$$V_k(l_k,\beta)V'_k(l_k,\lambda) - V_k(l_k,\lambda)V'_k(l_k,\beta) = -c_{11,k}^{-1}(\beta^2 - \lambda^2)\left\{a_{11}^k z_{2k}(\lambda)z_{2k}(\beta) + a_{22}^k z_{1k}(\lambda)z_{1k}(\beta) + \right.$$

$$+ a_{12}^k(z_{1k}(\beta)z_{2k}(\lambda) + z_{1k}(\lambda)z_{2k}(\beta)) - c_{11,k}(c_{21,22}^{11,k}V'_{k+1}(l_k,\beta)V'_{k+1}(l_k,\lambda) + c_{21,22}^{11,k}V_{k+1}(l_k,\lambda)V'_{k+1}(l_k,\beta)) +$$
$$\left. + c_{21,22}^{12,k}(V_{k+1}(l_k,\beta)V'_{k+1}(l_k,\lambda) + V_{k+1}(l_k,\lambda)V'_{k+1}(l_k,\beta))\right\} + c_{11,k}c_{21,k} \times$$
$$\times \left[V_{k+1}(l_k,\beta)V'_{k+1}(l_k,\lambda) - V_{k+1}(l_k,\lambda)V'_{k+1}(l_k,\beta)\right]. \qquad (5.67)$$

Because of $(a_{12}^k)^2 - a_{11}^k a_{22}^k \equiv a_{12,1}^k a_{12,2}^k - a_{11}^k a_{22}^k = -c_{11,k}^k c_{12,k}^k = -c_{11,k} \cdot 0 = 0$,

$(c_{21,22}^{12,k})^2 - c_{21,22}^{11,k}c_{21,22}^{22,k} \equiv c_{21,22}^{12,k}c_{21,22}^{21,k} - c_{21,22}^{11,k}c_{21,22}^{22,k} = -c_{21,k}c_{22,k} = 0$, then the sum (5.61) takes the form:

$$-\sum_{k=1}^{n} c_{11,k}^{-2} a_k^2 \sigma_k \left\{\left[\sqrt{a_{11}^k}z_{2k}(\lambda) + \sqrt{a_{22}^k}z_{1k}(\lambda)\right]\left[\sqrt{a_{11}^k}z_{2k}(\beta)\sqrt{a_{22}^k}z_{1k}(\beta)\right] + c_{11,k}\left[\sqrt{-c_{21,22}^{11,k}}V'_{k+1}(l_k,\lambda) + \right.\right.$$

$$\left.\left. + \sqrt{-c_{21,22}^{22,k}}V_{k+1}(l_k,\lambda)\right]\left[\sqrt{-c_{21,22}^{11,k}}V'_{k+1}(l_k,\beta) + \sqrt{-c_{21,22}^{22,k}}V_{k+1}(l_k,\beta)\right]\right\} (\beta^2 - \lambda^2) \equiv -(\beta^2 - \lambda^2)G_n(\beta,\lambda). \qquad (5.68)$$

Assume that $c_{21,22}^{11,k} = \alpha_{12}^k \delta_{22}^k - \alpha_{22}^k \delta_{12}^k \le 0$, $c_{21,22}^{22,k} = \beta_{12}^k \gamma_{22}^k - \beta_{22}^k \gamma_{12}^k \le 0$. At point $z = l_0$ at $\gamma^2 = 0$ (for simplicity) we have identical equations:

$$\alpha_{11}^0 V_1'(l_0,\beta_n) + \beta_{11}^0 V_1'(l_0,\beta_n) - \beta_n^2\left[\delta_{11}^0 V_1'(l_0,\beta_n) + \gamma_{11}^0 V_1(l_0,\beta_n)\right] = 0,$$

$$\alpha_{11}^0 V_1'(l_0,\beta_j) + \beta_{11}^0 V_1(l_0,\beta_j) - \beta_j^2\left[\delta_{11}^0 V_1'(l_0,\beta_j) + \gamma_{11}^0 V_1(l_0,\beta_j)\right] = 0. \qquad (5.69)$$

On the one side

$$\begin{aligned}&\left[\alpha_{11}^0 V_1'(l_0,\beta_m)+\beta_{11}^0 V_1(l_0,\beta_m)\right]\left[\delta_{11}^0 V_1'(l_0,\beta_j)+\gamma_{11}^0 V_1(l_0,\beta_j)\right]-\\&-\left[\alpha_{11}^0 V_1'(l_0,\beta_j)+\beta_{11}^0 V_1(l_0,\beta_j)\right]\times\left[\delta_{11}^0 V_1'(l_0,\beta_m)+\gamma_{11}^0 V_1(l_0,\beta_m)\right]=\\&=(\alpha_{11}^0\gamma_{11}^0-\delta_{11}^0\beta_{11}^0)\left[V_1(l_0,\beta_j)V_1'(l_0,\beta_m)-V_1(l_0,\beta_m)V_1'(l_0,\beta_j)\right]\end{aligned}\tag{5.70}$$

On the other side, due to equations (5.69) we have

$$\begin{aligned}&\left[\alpha_{11}^0 V_1'(l_0,\beta_m)+\beta_{11}^0 V_1(l_0,\beta_m)\right]\left[\delta_{11}^0 V_1'(l_0,\beta_j)+\gamma_{11}^0 V_1(l_0,\beta_j)\right]-\\&-\left[\alpha_{11}^0 V_1'(l_0,\beta_j)+\beta_{11}^0 V_1(l_0,\beta_j)\right]\times\left[\delta_{11}^0 V_1'(l_0,\beta_m)+\gamma_{11}^0 V_1(l_0,\beta_m)\right]=\\&=\beta_m^2\left[\delta_{11}^0 V_1'(l_0,\beta_m)+\gamma_{11}^0 V_1(l_0,\beta_m)\right]\times\left[\delta_{11}^0 V_1'(l_0,\beta_j)+\gamma_{11}^0 V_1(l_0,\beta_j)\right]-\\&-\beta_j^2\left[\delta_{11}^0 V_1'(l_0,\beta_j)+\gamma_{11}^0 V_1(l_0,\beta_j)\right]\left[\delta_{11}^0 V_1'(l_0,\beta_m)+\gamma_{11}^0 V_1(l_0,\beta_m)\right]=\\&=(\beta_m^2-\beta_j^2)\left[\delta_{11}^0 V_1'(l_0,\beta_m)+\gamma_{11}^0 V_1(l_0,\beta_m)\right]\left[\delta_{11}^0 V_1'(l_0,\beta_j)+\gamma_{11}^0 V_1(l_0,\beta_j)\right]\end{aligned}\tag{5.71}$$

From equations (5.70) and (5.71) we find that

$$\begin{aligned}&V_1(l_0,\beta_m)V_1'(l_0,\beta_m)-V_1(l_0,\beta_j)V_1'(l_0,\beta_m)=\\&=\frac{\left(\beta_m^2-\beta_j^2\right)}{\delta_{11}^0\beta_{11}^0-\alpha_{11}^0\gamma_{11}^0}\left[\delta_{11}^0 V_1'(l_0,\beta_m)+\gamma_{11}^0 V_1(l_0,\beta_m)\right]\left[\delta_{11}^0 V_1'(l_0,\beta_j)+\gamma_{11}^0 V_1(l_0,\beta_j)\right].\end{aligned}\tag{5.72}$$

Similarly, we find that

$$\begin{aligned}&V_{n+1}(l_{n+1},\beta_m)V_{n+1}'(l_{n+1},\beta_j)-V_{n+1}(l_{n+1},\beta_j)V_{n+1}'(l_{n+1},\beta_m)=\\&=\frac{\left(\beta_m^2-\beta_j^2\right)}{\delta_{22}^{n+1}\beta_{22}^{n+1}-\alpha_{22}^{n+1}\gamma_{22}^{n+1}}\left[\delta_{22}^{n+1}V_{n+1}'(l_{n+1},\beta_m)+\gamma_{22}^{n+1}V_{n+1}(l_{n+1},\beta_m)\right]\cdot\left[\delta_{22}^{n+1}V_{n+1}'(l_{n+1},\beta_j)+\gamma_{22}^{n+1}V_{n+1}(l_{n+1},\beta_j)\right].\end{aligned}\tag{5.73}$$

Substitution of equations (5.68), (5.72) and (5.73) in (5.61) leads to the relation:

$$\begin{aligned}&\int_{l_0}^{l_{n+1}} V(z,\beta_m)V(z,\beta_j)\sigma(z)\,dz=-\frac{\sigma_1\alpha_1^2}{-\alpha_{11}^0\gamma_{11}^0+\delta_{11}^0\beta_{11}^0}\left[\delta_{11}^0 V_1'(l_0,\beta_m)+\gamma_{11}^0 V_1(l_0,\beta_m)\right]\times\\&\times\left[\delta_{11}^0 V_1'(l_0,\beta_j)+\gamma_{11}^0 V_1(l_0,\beta_j)\right]-\frac{\sigma_{n+1}\alpha_{n+1}^2}{\alpha_{22}^{n+1}\gamma_{22}^{n+1}-\delta_{22}^{n+1}\beta_{22}^{n+1}}\left[\delta_{22}^{n+1}V_{n+1}'(l_{n+1},\beta_m)+\gamma_{22}^{n+1}V_{n+1}(l_{n+1},\beta_m)\right]\times\\&\times\left[\delta_{22}^{n+1}V_{n+1}'(l_{n+1},\beta_j)+\gamma_{22}^{n+1}V_{n+1}(l_{n+1},\beta_j)\right]-G_n(\beta_m,\beta_j)\equiv-G_n^{(1)}(\beta_m,\beta_j)\end{aligned}\tag{5.74}$$

If we determine the generalized scalar product [11]

$$\left(V(z,\beta_m),V(z,\beta_j)\right)_1=\left(V(z,\beta_m)V(z,\beta_j)\right)+G_n^{(1)}(\beta_m,\beta_j)\,,\tag{5.75}$$

where the classical scalar product $\left(V(z,\beta_m)V(z,\beta_j)\right)=\int_{l_0}^{l_{n+1}} V(z,\beta_m)V(z,\beta_j)\sigma(z)\,dz$,

then from equality (5.74) it follows that for all $\beta_m\neq\beta_j$ $\left(V(z,\beta_m),V(z,\beta_j)\right)_1=0$.

The latter equality means that the system of eigenfunctions is generalized orthogonal.

Equation (5.75) generates the square of the norm of eigenfunction $V(z,\beta_j)$:

$$\left\|V(z,\beta_j)\right\|_1^2 = \left\|V(z,\beta_j)\right\|^2 + G_n^{(1)}\left(\beta_j,\beta_j\right). \tag{5.76}$$

The standard method [12] can be shown to be generalized orthogonal to the set I_n system of vector functions $\left\{V(z,\beta_j)\right\}_{j=1}^{\infty}$ is complete and closed.

The following statements are fair.

Theorem 5.2.3 (*type of Steklov's theorem*): *Any three times continuously differentiated on the set I_n vector function f(z), which satisfies the boundary conditions* (1.51) *and a system of interface conditions* (1.52) *is represented on each compact set $I_n^* \subset I_n$ absolutely and uniformly convergent Fourier series according to the system of eigenvector functions $\left\{V(z,\beta_j)\right\}_{j=1}^{\infty}$:*

$$f(z) = \sum_{j=1}^{\infty}\int_{l_0}^{l} f(\xi)V(\xi,\beta_j)\sigma(\xi)d\xi\frac{V(z,\beta_j)}{\left\|V(z,\beta_j)\right\|_1^2} \tag{5.77}$$

Proof: The proof of the theorem is based on the use of the work approach [11]. Taking into account that the vector function $f \in C^2(I_n)$, satisfies the boundary and interface conditions of the boundary value problem and with the help of the influence functions of the problem, taking into account that $L_k\left[f_k(z)\right] = g_k(z)\sqrt{\sigma_k}$, $k=\overline{1,n+1}$, where $g(z)$- defined by f and operator L continuous vector function in I_n, we receive:

$$f_m(z) = \sum_{k=1}^{n+1}\int_{l_{k-1}}^{l_k} \mathrm{H}_{mk}(z,\xi)\sqrt{\sigma_k}\,g_k(\xi) = \sum_{k=1}^{n+1}\int_{l_k}^{l_{k+1}} \mathrm{K}_{mk}(z,\xi)\,g_k(\xi)d\xi \tag{5.78}$$

where core $\mathrm{K}_{mk}(z,\xi) = \mathrm{H}_{mk}(z,\xi)\sqrt{\sigma_m\sigma_k}$ ($m \le k$) are also generalized-symmetric with respect to the diagonal $z=\xi$: $\mathrm{K}_{mk}(z,\xi) = -\prod_{s=i}^{k-1}\frac{c_{1s}}{c_{2s}}\mathrm{K}_{km}(\xi,z)$.

Let's write down the Sturm-Liouville boundary value problem (5.50) - (5.52) in integral form with respect to functions $\varphi_m(z,\beta) \equiv \sqrt{\sigma_m}\,\frac{V_m(z,\beta)}{\left\|V(z,\beta)\right\|}$ through influence functions:

$$\frac{V_m(z,\beta)}{\|V(z,\beta)\|} = \beta^2 \sum_{k=1}^{n+1} \int_{k-1}^{k} \mathrm{H}_{mk}(z,\xi)\sigma_k \frac{V_m(\xi,\beta)}{\|V(z,\beta)\|} d\xi .$$

This statement means that the eigenvalues and eigenvectors are functions for the problem (5.50) - (5.52) are respectively characteristic numbers and characteristic vector-functions of the system of integral equations:

$$\frac{V_m(z,\beta)}{\|V(z,\beta)\|} = \beta^2 \sum_{i=1}^{n+1} \int_{k-1}^{k} \mathrm{K}_{mk}(z,\xi) \sqrt{\frac{\sigma_k}{\sigma_m}} \frac{V_k(\xi,\beta)}{\|V(z,\beta)\|} d\xi \ ; n = \overline{1,n} . \qquad (5.79)$$

Since $V_m(z,\beta_j)$ are generalized orthonormal with weight σ_m vector-functions of the boundary value problem, then we have $\sum_{k=1}^{n+1} \int_{l_k}^{l_{k+1}} \frac{V_k(z,\beta_j)V_k(z,\beta_i)}{\|V(z,\beta_i)\|^2} \sigma(z) dz = \delta_{ji}$.

Cores $\mathrm{K}_{ik}(z,\xi)$ of the systems of integral equations (5.79) are continuous at $\{z,\xi\} \subset I_n$, evenly bounded by z, and therefore are integrated with the square of the variable ξ: $\sum_{k=1}^{n+1} \int_{l_{k-1}}^{l_k} \mathrm{K}^2{}_{mk}(z,\xi) d\xi < \mu = const < \infty$ and then as functions of a variable ξ can be formally developed into a Fourier series by a system of eigenfunctions:

$$\mathrm{K}_{mk}(z,\xi) \sim \sum_{j=1}^{\infty} a_m(z,\beta_j) \sqrt{\sigma_k} \frac{V_k(\xi,\beta_j)}{\|V(z,\beta_j)\|} ;$$

where by definition: $a_m(z,\beta_j) = \sum_{k=1}^{n+1} \int_{l_{k-1}}^{l_k} \mathrm{K}_{mk}(z,\xi) \sqrt{\sigma_k} \frac{V_k(\xi,\beta_j)}{\|V(z,\beta_j)\|} d\xi = \sqrt{\sigma_k} \frac{V_m(\xi,\beta_j)}{\beta_j^2 \|V(z,\beta_j)\|}$,

(according to (5.79)).

So,

$$\mathrm{K}_{mk}(z,\xi) \sim \sum_{j=1}^{\infty} \frac{V_m(z,\beta_j)V_k(\xi,\beta_j)}{\beta_j^2 \|V(z,\beta_j)\|^2} \sqrt{\sigma_m \sigma_k} , \ m,j = \overline{1,n+1} . \qquad (5.80)$$

According to the Bessel inequality, which holds for the series of the right-hand side (5.80), the estimate is fair:

$$\sum_{j=1}^{\infty}\left[\frac{V_m\left(z,\beta_j\right)}{\beta_j^2\left\|V\left(z,\beta_j\right)\right\|^2}\sigma_m\right]^2 \le \sum_{k=1}^{\infty}\int_{l_{k-1}}^{l_k} \mathrm{K}^2{}_{mk}\left(z,\xi\right)d\xi < \infty\cdot \tag{5.81}$$

Vector function g with (5.77), continuous on I_n we develop into a Fourier series according to the system of orthonormal vector functions $\frac{V_k\left(\xi,\beta_j\right)}{\left\|V\left(z,\beta_j\right)\right\|}$:

$$g_m\left(\xi\right) \sim \sum_{j=1}^{\infty} b(\beta_j)\frac{V_m\left(z,\beta_j\right)}{\left\|V\left(z,\beta_j\right)\right\|}\sqrt{\sigma_m}\,; \tag{5.82}$$

$$\text{Тут } b(\beta_j) = \sum_{k=1}^{n+1}\int_{l_{k-1}}^{l_k} g_k\left(\xi\right)\frac{V_k\left(\xi,\beta_j\right)}{\left\|V\left(z,\beta_j\right)\right\|}\sqrt{\sigma_k}\,d\xi\,;$$

$\sum_{j=1}^{\infty} b\left(\beta_j\right)^2 \le \sum_{k=1}^{n+1}\int_{l_{k-1}}^{l_k} g_k^2\left(\xi\right)d\xi < \infty$ (according to the Bessel inequality), coincides with a series with a term $b\left(\beta_j\right)^2$.

Develop the system of vector functions $\frac{V_m\left(z,\beta_j\right)}{\left\|V\left(z,\beta_j\right)\right\|}$ formally in the Fourier series also the left part of the equality (5.78):

$$f_m\left(z\right) \sim \sum_{j=1}^{\infty}\gamma\left(\beta_j\right)\frac{V_m\left(z,\beta_j\right)}{\left\|V\left(z,\beta_j\right)\right\|}, \tag{5.83}$$

where by definition:

$$\begin{aligned}\gamma\left(\beta_j\right) &= \sum_{k=1}^{n+1}\int_{k_{i-1}}^{l_k}\sqrt{\sigma_k}\,f_k\left(z\right)\frac{V_k\left(z,\beta_j\right)}{\left\|V\left(z,\beta_j\right)\right\|}dz = \\ &= \sum_{k=1}^{n+1}\int_{l_{k-1}}^{l_k} g_k\left(\xi\right)d\xi\sum_{k_1=1}^{n+1}\int_{l_{i-1}}^{l_i}\mathrm{K}_{k,k_1}\left(z,\xi\right)\sqrt{\sigma_{k_1}}\,\frac{V_{k_1}\left(z,\beta_j\right)}{\left\|V\left(z,\beta_j\right)\right\|}dz = \\ &= \frac{1}{\beta_j^2}\sum_{k=1}^{n+1}\int_{l_{k-1}}^{l_k} g_k\left(\xi\right)\sqrt{\sigma_k}\,\frac{V_k\left(\xi,\beta_j\right)}{\left\|V\left(z,\beta_j\right)\right\|}d\xi = \sqrt{\sigma_k}\,\frac{b\left(\beta_j\right)}{\beta_j^2\left\|V\left(z,\beta_j\right)\right\|}.\end{aligned} \tag{5.84}$$

Taking into account (5.84) the decomposition (5.83) will look like

$$f_m\left(z\right) \sim \sum_{j=1}^{\infty}\frac{b\left(\beta_j\right)V_m\left(z,\beta_j\right)}{\beta_j^2\left\|V\left(z,\beta_j\right)\right\|}\sqrt{\sigma_m}\,,\ m=\overline{1,n+1}\,. \tag{5.85}$$

We show that a series of (5.85) is completely and evenly convergent and has sum $f_m(z)$. Using the Cauchy criterion of uniform convergence of functional series [11], Cauchy-Bunyakovsky inequality, inequality (5.81) and an estimate of the convergence of the series (5.82), we obtain a segment of a series for evaluation by modulus:

$$\left|\sum_{j_1=j+1}^{j+L}\frac{b_{j_1}V_m\left(z,\beta_{j_1}\right)}{\beta_{j_1}^2\left\|V\left(z,\beta_{j_1}\right)\right\|}\sqrt{\sigma_m}\right|\le\sum_{j_1=j+1}^{j+L}\frac{\left|b\left(\beta_{j_1}\right)\right|\left|V_m\left(z,\beta_{j_1}\right)\right|}{\beta_{j_1}^2\left\|V\left(z,\beta_{j_1}\right)\right\|}\left|\sqrt{\sigma_m}\right|\le$$

$$\le\left(\sum_{j_1=j+1}^{j+L}b\left(\beta_{j_1}\right)^2\right)^{\frac{1}{2}}\left(\sum_{j_1=j+1}^{j+L}\frac{\left[V_m\left(z,\beta_{j_1}\right)\right]^2}{\left(\beta_{j_1}^2\right)^2}\right)^{\frac{1}{2}}\left|\sqrt{\sigma_m}\right|\le\sqrt{M}\left(\sum_{j_1=j+1}^{\infty}b\left(\beta_{j_1}\right)^2\right)^{\frac{1}{2}}\to 0. \tag{5.86}$$

Since the estimates, and hence the marginal ratio (5.86) are absolute and uniform, then according to the Cauchy criterion a number (5.85) coincides regularly and its sum is a continuous function.

Let us show that the sum of this series is $f_m(z)$, estimating the average difference:

$$f_m(z)-\sum_{j_1=1}^{j}\frac{b\left(\beta_{j_1}\right)V_m\left(z,\beta_{j_1}\right)}{\beta_{j_1}^2\left\|V\left(z,\beta_{j_1}\right)\right\|}=\sum_{k_1=1}^{n+1}\int_{l_{k-1}}^{l_k}\mathrm{K}_{mk}(z,\xi)g_k(\xi)d\xi-$$

$$-\sum_{j_1=1}^{\infty}\frac{V_m\left(z,\beta_{j_1}\right)}{\beta_{j_1}^2\left\|V\left(z,\beta_{j_1}\right)\right\|}\left[\sum_{k=1}^{n+1}\int_{l_{k-1}}^{l_k}g_k(\xi)\frac{V_k\left(\xi,\beta_{j_1}\right)}{\left\|V\left(z,\beta_{j_1}\right)\right\|}\sqrt{\sigma_k}d\xi\right]=$$

$$=\sum_{k=1}^{n+1}\int_{k-1}^{k}\left(\mathrm{K}_{mk}(z,\xi)-\sum_{j_1=1}^{j}\frac{V_m\left(\xi,\beta_{j_1}\right)V_k\left(\xi,\beta_{j_1}\right)}{\left\|V\left(z,\beta_{j_1}\right)\right\|^2}\sqrt{\sigma_m\sigma_k}g_k(\xi)\right)d\xi=\sum_{k=1}^{n+1}\int_{l_{k-1}}^{l_k}\mathrm{K}_{mk}^{j}(z,\xi)g_k(\xi)d\xi. \tag{5.87}$$

We show that any characteristic number $\beta_{j+i}^2\left(i>0\right)$ and the corresponding characteristic vector-function $V(z,\beta_{j+i})$ core $\mathrm{K}(z,\xi)$ are respectively characteristic vector core function and $\mathrm{K}^j(z,\xi)$, is also symmetrical. Consider the equation:

$$\alpha_m\left(z,\beta_{j+i}\right)=\frac{V_m\left(z,\beta_{j+i}\right)}{\left\|V\left(z,\beta_j\right)+i\right\|}\sqrt{\sigma_m}-\beta_{j+i}^2\sum_{k=1}^{m}\int_{l_{k-1}}^{l_k}\mathrm{K}_{mk}^{j}\left(z,\xi\right)\frac{V_k\left(\xi,\beta_{j+i}\right)}{\left\|V\left(z,\beta_{j+i}\right)\right\|}\sqrt{\sigma_k}\,d\xi=$$

$$=\varphi_m\left(z,\beta_{j+i}\right)-\beta_{j+i}^2\sum_{k=1}^{n+1}\int_{l_{k-1}}^{l_k}\mathrm{K}_{mk}^{j}\left(x,\xi\right)\frac{V_k\left(\xi,\beta_{j+i}\right)}{\left\|V\left(z,\beta_{j+i}\right)\right\|}\sqrt{\sigma_k}\left(\xi\right)d\xi+$$

$$+\beta_{j+i}^2\sum_{j_1=1}^{j}\frac{V_m\left(z,\beta_{j_1}\right)}{\beta_{j_1}^2\left\|V\left(z,\beta_{j_1}\right)\right\|}\sqrt{\sigma_m}\left(\sum_{k=1}^{n+1}\int_{l_{k-1}}^{l_k}\frac{V_k\left(\xi,\beta_{j+i}\right)V_k\left(\xi,\beta_j\right)}{\left\|V\left(z,\beta_j\right)\right\|^2}\sigma_k d\xi\right).$$

By identity (5.78) and orthogonality of vector functions $V\left(z,\beta_{j_1}\right),V\left(z,\beta_{j+i}\right);\ j_1=\overline{1,j};\ j,i>0$, we get the identity $\alpha_m\left(z,\beta_j\right)=0$ that is needed to be shown.

A fair and converse statement is that any characteristic number μ_j^2 of core $\mathrm{K}^j\left(z,\xi\right)$ will be one of the characteristic numbers β_{j+i}^2 of core $\mathrm{K}\left(z,\xi\right)$, and corresponding to this number nontrivial vector function ψ will be a characteristic function of both cores. For this purpose, it is enough to consider identity (given the symmetry of the nucleus

$$\mathrm{K}^j\left(z,\xi\right)):\ \psi_m\left(z\right)=\mu^2\sum_{k=1}^{n+1}\int_{l_{k-1}}^{l_k}\mathrm{K}_{mk}^{j_1}\left(z,\xi\right)\psi_k\left(\xi,\mu\right)d\xi,\qquad \mu^2=\beta_j^2,\ \ j_1=\overline{1,j},$$

which leads to identity $\psi_m\left(z\right)=\mu^2\sum_{k=1}^{n+1}\int_{l_{k-1}}^{l_k}\mathrm{K}_{mk}\left(z,\xi\right)\psi_{kj}\left(\xi,\mu\right)d\xi$.

Next, using the known quadratic estimate [11] $\left\|\Omega\Theta\right\|\le\frac{1}{\tau}\left\|\Theta\right\|$, for the integrated operator Ω with a symmetrical core, where τ - the minimum characteristic number of the nucleus, with (1.87) we will get an estimate:

$$\left\|f_m\left(z\right)-\sum_{j_1=1}^{j}\frac{b\left(\beta_{j_1}\right)V_m\left(z,\beta_{j_1}\right)}{\beta_{j_1}^2\left\|V\left(z,\beta_{j_1}\right)\right\|}\right\|=\left(\sum_{k=1}^{n+1}\left(\int_{l_{k-1}}^{l_k}f_m\left(z\right)-\sum_{j_1=1}^{j}\frac{b\left(\beta_{j_1}\right)V_m\left(z,\beta_{j_1}\right)}{\beta_{j_1}^2\left\|V\left(z,\beta_{j_1}\right)\right\|}\right)^2dz\right)^{\frac{1}{2}}=$$

$$=\left(\sum_{k=1}^{n+1}\left(\int_{l_{k-1}}^{l_k}\mathrm{K}_{mk}^{j}\left(z,\xi\right)g_k\left(\xi\right)d\xi\right)^2\right)^{\frac{1}{2}}\le\frac{1}{\beta_{j+1}^2}\left(\sum_{k=1}^{n+1}\int_{l_{k-1}}^{l_k}g_k^2\left(\xi\right)d\xi\right)^{\frac{1}{2}}=\frac{1}{\beta_{j+1}^2}\left\|g\left(\xi\right)\right\|,$$

where β_{j+1}^2 is the minimum characteristic number of core $\mathrm{K}^j\left(z,\xi\right)$. According to the theorem on the discrete spectrum $\beta_{j+1}^2\xrightarrow[j\to\infty]{}\infty$, and hence a number (5.85)

coincides on average with the function $f_m(z)$. Since this series coincides uniformly with its sum, which is a continuous function, this sum is a function $f_m(z)$:

$$f_m(z)=\sum_{j=1}^{\infty}\frac{b(\beta_j)V_m(z,\beta_j)}{\beta_j^2\left\|V(z,\beta_j)\right\|}=\sum_{j=1}^{\infty}\alpha_j\frac{V_m(z,\beta_j)}{\left\|V(z,\beta_j)\right\|},$$

where $a_j=\sum_{k=1}^{n+1}\int_{l_{k-1}}^{l_k} f_k(z)\sigma_k V_k(z,\beta_j)dz$.

So, we establish equality

$$f_m(z)=\sum_{j=1}^{\infty}\sum_{k=1}^{n+1}\int_{l_{k-1}}^{l_k} f_k(\xi)V_k(\xi,\beta_j)\sigma_k d\xi\frac{V_k(z,\beta_j)}{\left\|V(z,\beta_j)\right\|_1^2}, \tag{5.88}$$

which confirms the regular convergence of the series to $f_m(z)$. Theorem is proved.

The Fourier series (5.77) generates a direct F_n and inverse F_n^{-1} finite integral Fourier transforms for a finite heterogeneous $n+1$ – component environment in the case when the spectral parameter is included in the boundary conditions and in the system of interface conditions:

$$F_n\left[f(z)\right]=\int_{l_0}^{l} f(z)V(z,\beta_n)\sigma(z)dz\equiv f_n, \tag{5.89}$$

$$F_n^{-1}\left[f_n\right]=\sum_{n=1}^{\infty} f_n\frac{V(z,\beta_n)}{\left\|V(z,\beta_n)\right\|_1^2}\equiv f(z). \tag{5.90}$$

In order to apply the constructed integral transformations to find analytical solutions of the considered mathematical models taking into account the non-stationary modes on the surfaces $z=l_j, j=0,n$ we obtain the basic identity of the integral transformation of the Fourier differential operator

$$L_n=\sum_{i=1}^{n+1}D_i\,\theta(z-l_{i-1})\theta(l_i-z)d^2/dz^2.$$

Theorem 5.2.4 (*about the basic identity*): *If the vector function* $f(z)\in C^{(3)}(I_n)$, *satisfies the system of interface conditions* (5.52) *and boundary conditions*

$$\left(\tilde{\alpha}_{11}^0\frac{d}{dz}+\tilde{\beta}_{11}^0\right)f_1(z)\Big|_{z=l_0}=f_{10},\left(\tilde{\alpha}_{22}^{n+1}\frac{d}{dz}+\tilde{\beta}_{22}^{n+1}\right)f_{n+1}(z)\Big|_{z=l}=f_{n+1,l}, \tag{5.91}$$

then the basic identity of the integral transformation of the differential operator ζ_n *comes true*:

$$F_n\left[\zeta_n\left[f(z)\right]\right]=-\beta_n^2 f_n-\sum_{i=1}^{n+1}\gamma_i^2\int_{l_{i-1}}^{l_i} f_i(z)V_i(z,\beta_n)\sigma_i dz+ \\ +\left(\tilde{\alpha}_{22}^{n+1}\right)^{-1}V_{n+1}(l,\beta_n)f_{n+1,l}-D_1\sigma_1\left(\tilde{\alpha}_{11}^{0}\right)^{-1}\cdot V_1(l,\beta_n)f_{10} \tag{5.92}$$

Substantiation: Based on the system of interface conditions, we establish the basic identity:

$$\left[f_k(z)V_k'(z,\beta_n)-f_k'(z)V_k(z,\beta_n)\right]_{z=l_k}=\frac{c_{21,k}}{c_{11,k}}\left[f_{k+1}(z)V_{k+1}'(z,\beta_n)-f_{k+1}'(z)V_{k+1}(z,\beta_n)\right]_{z=l_k}=\overline{1,n} \tag{5.93}$$

If on the left (5.91) we integrate twice into parts, then the non-integral terms into points z=l_k due the elections σ_k and basic identity (5.93) turn to zero. Additions in points z=l_0 and $z=l\equiv l_{n+1}$ are converted in the standard way. The consequence of all this is equality:

$$F_n\left[\zeta_n\left[f(z)\right]\right]\equiv\sum_{i=1}^{n+1}\int_{l_{i-1}}^{l_i} D_i\frac{d^2 f_i}{dz^2}V_i(z,\beta_n)\sigma_i dz= \\ =\sum_{i=1}^{n+1}\gamma_i^2\sigma_i D_i\left(\frac{df_i}{dz}V_i(z,\beta_n)-f_i(z)\frac{d}{dz}V_i(z,\beta_n)\right)\Bigg|_{z=l_{i-1}}^{z=l_i}+\sum_{i=1}^{n+1}\int_{l_{i-1}}^{l_i} f_i\left(D_i\frac{d^2 f_i}{dz^2}V_i\right)\sigma_i dz= \\ =-\sigma_1 D_1\left[f_1'(z)V_1(z,\beta_n)-f_1(z)V_1'(z,\beta_n)\right]_{z=l_0}+\left[f_{n+1}'(z)V_{n+1}(z,\beta_n)-f_{n+1}(z)V_{n+1}'(z,\beta_n)\right]_{z=l}+ \\ +\sum_{i=1}^{n+1}\int_{l_{i-1}}^{l_i} f_i(z)\left[-D_i\frac{\beta_n^2+\gamma_i^2}{D_i}V_i\right]\sigma_i dz \tag{5.94}$$

Dividing the sum by two terms and converting the non-integral terms in the standard way, we obtain the identity (5.92).

If the system of interface conditions is heterogeneous, namely

$$\left[\left(\tilde{\alpha}_{j1}^k\frac{d}{dz}+\tilde{\beta}_{j1}^k\right)g_k(z)-\left(\tilde{\alpha}_{j2}^k\frac{d}{dz}+\tilde{\beta}_{j2}^k\right)g_{k+1}(z)\right]_{z=l_k}=\psi_{jk}, \tag{5.95}$$

then the basic identity (5.93) takes the form:

$$\left[g_k'(z)V_k(z,\beta_j)-g_k(z)V_k'(z,\beta_j)\right]_{z=l_k}=\frac{c_{21,k}}{c_{11,k}}\left[g_{k+1}'(z)V_{k+1}(z,\beta_j)-g_{k+1}(z)V_{k+1}'(z,\beta_j)\right]_{z=l_k}+ \\ +\frac{1}{c_{11,k}}\left[\left(\tilde{\alpha}_{12}^k\frac{d}{dz}+\tilde{\beta}_{12}^k\right)V_{k+1}(z,\beta_j)\Big|_{z=l_k}\psi_{2k}-\left(\tilde{\alpha}_{22}^k\frac{d}{dz}+\tilde{\beta}_{22}^k\right)V_{k+1}(z,\beta_j)\Big|_{z=l_k}\psi_{1k}\right] \tag{5.96}$$

Due to equalities:

$$\left(\tilde{\alpha}_{11}^{0}\right)^{-1} V_1\left(l_0,\beta_j\right)=\left(\alpha_{11}^{0}\gamma_{11}^{0}-\delta_{11}^{0}\beta_{11}^{0}\right)^{-1}\left[\delta_{11}^{0}V_1'\left(l_0,\beta_j\right)+\gamma_{11}^{0}V_1\left(l_0,\beta_j\right)\right],$$

$$\left(\tilde{\alpha}_{22}^{n+1}\right)^{-1} V_{n+1}\left(l_{n+1},\beta_j\right)=\left(\alpha_{22}^{n+1}\gamma_{22}^{n+1}-\delta_{22}^{n+1}\beta_{22}^{n+1}\right)^{-1}\left[\delta_{22}^{n+1}V_{n+1}'\left(l_{n+1},\beta_j\right)+\gamma_{22}^{n+1}V_{n+1}\left(l_{n+1},\beta_j\right)\right]$$

and basic identity (5.93) the main identity (5.92) has a structure:

$$\begin{aligned}
&F_n\left[L_n\left[g(z)\right]\right]=-\beta_n^2 g_n-\sum_{i=1}^{n+1}\gamma_i^2\int_{l_{i-1}}^{l_i} g_i(z)V_i\left(z,\beta_j\right)\sigma_i dz+\\
&+\frac{\alpha_1^2\sigma_1}{\delta_{11}^{0}\beta_{11}^{0}-\alpha_{11}^{0}\gamma_{11}^{0}}\left(\delta_{11}^{0}V_1'\left(l_0,\beta_j\right)+\gamma_{11}^{0}V_1\left(l_0,\beta_j\right)\right)g_{10}+\\
&+\frac{D_{n+1}\sigma_{n+1}}{\alpha_{22}^{n+1}\gamma_{22}^{n+1}-\delta_{22}^{n+1}\beta_{22}^{n+1}}\times\left[\delta_{22}^{n+1}V_{n+1}'\left(l_{n+1},\beta_j\right)+\gamma_{22}^{n+1}V_{n+1}\left(l_{n+1},\beta_j\right)\right]g_{n+1,l}+\\
&+\sum_{k=1}^{n}\frac{\alpha_k^2\sigma_k}{c_{11,k}}\times\left[\left(\tilde{\alpha}_{12}^{k}\frac{d}{dz}+\tilde{\beta}_{12}^{k}\right)V_{k+1}\left(z,\beta_j\right)\Big|_{z=l_k}\psi_{2k}-\left(\tilde{\alpha}_{22}^{k}\frac{d}{dz}+\tilde{\beta}_{22}^{k}\right)V_{k+1}\left(z,\beta_j\right)\Big|_{z=l_k}\psi_{1k}\right]
\end{aligned}\tag{5.97}$$

The logical scheme of application of the introduced finite integral Fourier transforms F_n and F_n^{-1} will be demonstrated on separate mathematical models for heterogeneous signal propagation media.

Quasi-static hybrid model: Build limited in area $\mathrm{D}_n=\left\{(t,z): t\ge 0; z\in I_n\right\}$ solution to a system of differential equations with partial derivatives of the 2nd order of parabolic type in bounded (*n+1*)- component heterogeneous medium taking into account the rates of change in the gradients of the defining parameters on the surfaces $z=l_j, j=\overline{0,n+1}$

$$\frac{\partial u_m}{\partial t}+\chi_m^2 u_m-D_m\frac{\partial^2 u_m}{\partial z^2}=f_m\left(t,z\right), z\in\left(l_{m-1},l_m\right), m=\overline{1,n+1}\tag{5.98}$$

under the initial conditions:

$$u_m\left(t,z\right)\Big|_{t=0}=g_m\left(z\right), z\in\left(l_{m-1},l_m\right), m=\overline{1,n+1},\tag{5.99}$$

boundary conditions:

$$\begin{aligned}
&\left[\left(\alpha_{11}^{0}+\delta_{11}^{0}\frac{\partial}{\partial t}\right)\frac{\partial}{\partial z}+\beta_{11}^{0}+\gamma_{11}^{0}\frac{\partial}{\partial t}\right]u_1\left(t,z\right)\Big|_{z=l_0}=\omega_0\left(t\right)\\
&\left[\left(\alpha_{22}^{n+1}+\delta_{22}^{n+1}\frac{\partial}{\partial t}\right)\frac{\partial}{\partial z}+\beta_{22}^{n+1}+\gamma_{22}^{n+1}\frac{\partial}{\partial t}\right]u_{n+1}\left(t,z\right)\Big|_{z=l}=\omega_l\left(t\right)
\end{aligned}\tag{5.100}$$

and system *n* - interface conditions:

$$\left\{\left[\left(\alpha_{j1}^{k}+\delta_{j1}^{k}\frac{\partial}{\partial t}\right)\frac{\partial}{\partial z}+\beta_{j1}^{k}+\gamma_{j1}^{k}\frac{\partial}{\partial t}\right]u_{k+1}(t,z)-\left[\left(\alpha_{j2}^{k}+\delta_{j2}^{k}\frac{\partial}{\partial t}\right)\frac{\partial}{\partial z}+\beta_{j2}^{k}+\gamma_{j2}^{k}\frac{\partial}{\partial t}\right]u_{k+1}(t,z)\right\}\Big|_{z=l_k}=\omega_{jk}(t);$$
$$j=\overline{1,2};k=\overline{1,n} \tag{5.101}$$

We write (5.98) and the initial conditions (5.99) in matrix form:

$$\begin{bmatrix}\left(\frac{\partial}{\partial t}+\chi_1^2-D_1\frac{\partial^2}{\partial z^2}\right)u_1\\ \left(\frac{\partial}{\partial t}+\chi_2^2-D_2\frac{\partial^2}{\partial z^2}\right)u_2\\ \ldots\ldots\ldots\ldots\ldots\ldots\ldots\ldots\\ \left(\frac{\partial}{\partial t}+\chi_{n+1}^2-D_{n+1}\frac{\partial^2}{\partial z^2}\right)u_{n+1}\end{bmatrix}=\begin{bmatrix}f_1(t,z)\\ f_2(t,z)\\ \ldots\ldots\ldots\\ f_{n+1}(t,z)\end{bmatrix} \tag{5.102}$$

$$\begin{bmatrix}u_1(t,z)\\ u_2(t,z)\\ \ldots\ldots\ldots\\ u_{n+1}(t,z)\end{bmatrix}\Bigg|_{t=0}=\begin{bmatrix}g_1(t,z)\\ g_2(t,z)\\ \ldots\ldots\ldots\\ g_{n+1}(t,z)\end{bmatrix}.$$

Integral operator F_n we represent in the form of an operator matrix-line:

$$F_n[\ldots]=\left[\int_{l_0}^{l_1}\ldots V_1(z,\beta_m)\sigma_1 dz\int_{l_1}^{l_2}\ldots V_2(z,\beta_m)\sigma_2 dz\ldots\int_{l_{n-1}}^{l_n}\ldots V_n(z,\beta_m)\sigma_n dz\int_{l_n}^{l_{n+1}}\ldots V_{n+1}(z,\beta_m)\sigma_{n+1}dz\right]. \tag{5.103}$$

Assuming that $\max\left\{z_1^2;z_2^2;\ldots;z_n^2;z_{n+1}^2\right\}=z_{n+1}^2$, we will put $\gamma_i^2=\chi_{n+1}^2-\chi_i^2\geq 0, i=\overline{1,n}$.

We apply the operator matrix-string (5.103) to the problem by the rule of multiplication of matrices (5.102). As a result of identity (5.97), we obtain the Cauchy problem:

$$\left[\frac{d}{dt}+\left(\beta_m^2+z_{n+1}^2\right)\right]u_m(t)=\mathrm{F}_m(t);\qquad u_m(t)\big|_{t=0}=g_m \tag{5.104}$$

Here:

$$u_m(t)=\sum_{j=1}^{n+1}u_{jm}(t);u_{jm}(t)=\int_{l_{j-1}}^{l_j}u_j(t,z)V_j(z,\beta_m)\sigma_j dz;$$

$$\mathrm{F}_m(t)=f_m(t)+\frac{\alpha_1^2\sigma_1}{\delta_{11}^0\beta_{11}^0-\alpha_{11}^0\gamma_{11}^0}\left[\delta_{11}^0V_1'(l_0,\beta_m)+\gamma_{11}^0V_1(l_0,\beta_m)\right]\omega_0(t)+$$

$$+\left(\alpha_{22}^{n+1}\gamma_{22}^{n+1}-\delta_{22}^{n+1}\beta_{22}^{n+1}\right)^{-1}\left[\delta_{22}^{n+1}V_{n+1}'(l_{n+1},\beta_m)+\gamma_{22}^{n+1}V_{n+1}(l_{n+1},\beta_m)\right]\omega_l(t)+$$

$$+\sum_{k=1}^{n}\frac{\alpha_k^2\sigma_k}{c_{11,k}}\left[\left(\tilde{\alpha}_{12}^k\frac{d}{dz}+\tilde{\beta}_{12}^k\right)V_{k+1}(z,\beta_m)\Big|_{z=l_k}\bar{\omega}_{2k}-\left(\tilde{\alpha}_{22}^k\frac{d}{dz}+\tilde{\beta}_{22}^k\right)V_{k+1}(z,\beta_m)\Big|_{z=l_k}\bar{\omega}_{1k}(t)\right],$$

$$f_m(t)=\sum_{j=1}^{n+1}f_{jm}(t),\ g_m=\sum_{j=1}^{n+1}g_{jm}(z),$$

The solution to the Cauchy problem (5.104) is a function

$$u_m(t)=e^{-\left(\beta_m^2+\chi_{n+1}^2\right)t}g_m+\int_0^t e^{-\left(\beta_m^2+\chi_{n+1}^2\right)(t-\tau)}\mathrm{F}_m(\tau)d\tau\ . \qquad (5.105)$$

Integral operator F_n^{-1} as inverted to F_n is represented in the form of an operator matrix-column:

$$F_n^{-1}[...]=\begin{bmatrix}\sum_{m=1}^{\infty}...V_1(z,\beta_m)\left(\|V(z,\beta_m)\|_1^2\right)^{-1}\\ \sum_{m=1}^{\infty}...V_2(z,\beta_m)\left(\|V(z,\beta_m)\|_1^2\right)^{-1}\\ .....\\ \sum_{m=1}^{\infty}...V_{n+1}(z,\beta_m)\left(\|V(z,\beta_m)\|_1^2\right)^{-1}\end{bmatrix}\ . \qquad (5.106)$$

If we now apply the operator matrix-column (5.106) to the matrix-element according to the rule of multiplication of matrices $\left[u_m(t)\right]$, where the function $u_m(t)$ is defined by the formula (5.105), then after elementary transformations we receive the following components:

$$u_j(t,z)=\sum_{k=1}^{n+1}\int_0^t\int_{l_{k-1}}^{l_k} Hh_{jk}(t-\tau,z,\xi)\left[f_k(\tau,\xi)-g_k(\xi)\delta_+(\tau)\right]\sigma_k d\xi d\tau+$$

$$+\int_0^t\left[W_{0j}(t-\tau,z)\omega_0(\tau)+W_{lj}(t-\tau,z)\omega_l(\tau)\right]d\tau+ \qquad (5.107)$$

$$+\sum_{k=1}^{n}\int_0^t\left[Rh_{jk}^{(1)}(t-\tau,z)\omega_{1k}(\tau)+Hh_{jk}^{(2)}(t-\tau,z)\omega_{2k}(\tau)\right]d\tau, j=\overline{1,n+1}$$

vector functions $u(t,z)=\left\{u_1(t,z);u_2(t,z);...;u_n(t,z);u_{n+1}(t,z)\right\}$, which completely defines a single solution to boundary problem (5.98) - (5.101).

Here are the main solutions:

- matrix of influence functions generated by the inhomogeneity of the system (5.107):

$$Hh_{jk}(t,z,\xi)=\sum_{m=1}^{\infty}e^{-\left(\beta_m^2+\chi_{n+1}^2\right)t}\frac{V_j(z,\beta_m)V_k(\xi,\beta_m)}{\left\|V(z,\beta_m)\right\|_1^2};\ j,k=1,\overline{n+1},$$

- Green's vector functions generated by boundary conditions at the boundaries $z=l_0$ and $z=l\equiv l_{n+1}$:

$$W_{0j}(t,z)=-D_1\sigma_1\sum_{m=1}^{\infty}e^{-\left(\beta_m^2+\chi_{n+1}^2\right)t}\frac{V_1(l_0,\beta_m)V_j(z,\beta_m)}{\left[\alpha_{11}^0-\sigma_{11}^0\left(\beta_m^2+\chi_{n+1}^2\right)\right]\left\|V(z,\beta_m)\right\|_1^2};$$

$$W_{lj}(t,z)=\sum_{m=1}^{\infty}e^{-\left(\beta_m^2+\chi_{n+1}^2\right)t}\frac{V_j(z,\beta_m)V_{n+1}(l,\beta_m)}{\left[\alpha_{22}^{n+1}-\sigma_{22}^{n+1}\left(\beta_m^2+\chi_{n+1}^2\right)\right]\left\|V(z,\beta_m)\right\|_1^2};\ j=1,\overline{n+1},$$

- matrix of Green's functions generated by the system of interface conditions $z=l_k$.

$$Rh_{jk}^{(1)}(t,z)=-\frac{D_k\sigma_k}{c_{11,k}}\sum_{m=1}^{\infty}e^{-\left(\beta_m^2+\chi_{n+1}^2\right)t}\frac{\tilde{\alpha}_{22}^kV_{k+1}'(l_k,\beta_m)+\tilde{\beta}_{22}^kV_{k+1}(l_k,\beta_m)}{\left\|V(z,\beta_m)\right\|_1^2}V_j(z,\beta_m)$$

$$Rh_{jk}^{(2)}(t,z)=-\frac{D_k\sigma_k}{c_{11,k}}\sum_{m=1}^{\infty}e^{-\left(\beta_m^2+\chi_{n+1}^2\right)t}\frac{\tilde{\alpha}_{12}^kV_{k+1}'(l_k,\beta_m)+\tilde{\beta}_{12}^kV_{k+1}(l_k,\beta_m)}{\left\|V(z,\beta_m)\right\|_1^2}V_j(z,\beta_m).$$

The solution (5.107) to the considered boundary value problem, we obtained provided that

$$\psi_1=\delta_{11}^0g_1'(l_0)+\gamma_{11}^0g_1(l_0)=0,\psi_{n+1}=\delta_{22}^{n+1}g_{n+1}'(l_{n+1})+\gamma_{22}^{n+1}g_{n+1}(l_{n+1})=0,$$

$$\psi_{jk}=\delta_{j1}^kg_k'(l_k)+\gamma_{j1}^kg_k(l_k)-\delta_{j2}^kg_{k+1}'(l_k)+\gamma_{j2}^kg_{k+1}(l_k)=0.$$

Otherwise in the solution (5.107) of functions $\omega_0(\tau), \omega_l(\tau), \omega_{jk}(\tau)$ must be replaced according to the function

$$\left(\omega_0(\tau)+\psi_1\delta+(\tau)\right), \left(\omega_l(\tau)+\psi_{n+1}\delta_+(\tau)\right), \left(\omega_{jk}(\tau)+\psi_{jk}\delta_+(\tau)\right).$$

This means that in formula (5.107) more terms will appear

$$W_{0j}(t,z)\psi_1 + W_{lj}(t,z)\psi_{n+1} + \sum_{k=1}^{n}\left[\mathrm{R}_{jk}^{(1)}(t,z)\psi_{1k} + \mathrm{R}_{jk}^{(2)}(t,z)\psi_{2k}\right].$$

Dynamic hybrid model. Build limited in area D_n solution to a system of differential equations with partial derivatives of the *2*-nd order of hyperbolic type for limited (*n+1*)- component of a heterogeneous environment taking into account the dynamics of changes in the velocities of the gradients of the defining transfer parameters at the edges and interface surfaces $z = l_j, j = 0, n$:

$$\frac{\partial^2 u_j}{\partial t^2} + \chi_j^2 u_j - D_j \frac{\partial^2 u_j}{\partial z^2} = f_j(t,z), z \in \left(l_{j-1}, l_j\right), j = \overline{1, n+1} \tag{5.108}$$

with the initial conditions:

$$u_j(t,z)\big|_{t=0} = g_{1j}(z), \frac{\partial u_j}{\partial t}\bigg|_{t=0} = g_{2j}(z), j = \overline{1, n+1} \tag{5.109}$$

and boundary conditions:

$$\begin{gathered}\left[\left(\alpha_{11}^0 + \delta_{11}^0 \frac{\partial^2}{\partial t^2}\right)\frac{\partial}{\partial z} + \beta_{11}^0 + \gamma_{11}^0 \frac{\partial^2}{\partial t^2}\right] u_1(t,z)\Big|_{z=l_0} = \omega_0(t) \\ \left[\left(\alpha_{22}^{n+1} + \delta_{22}^{n+1} \frac{\partial^2}{\partial t^2}\right)\frac{\partial}{\partial z} + \beta_{22}^{n+1} + \gamma_{22}^{n+1} \frac{\partial^2}{\partial t^2}\right] u_{n+1}(t,z)\Big|_{z=l} = \omega_l(t)\end{gathered} \tag{5.110}$$

and a system of interface conditions:

$$\left\{\left[\left(\alpha_{j1}^k + \delta_{j1}^k \frac{\partial^2}{\partial t^2}\right)\frac{\partial}{\partial z} + \beta_{j1}^k + \gamma_{j1}^k \frac{\partial^2}{\partial t^2}\right] u_{k+1}(t,z) - \left[\left(\alpha_{j2}^k + \delta_{j2}^k \frac{\partial^2}{\partial t^2}\right)\frac{\partial}{\partial z} + \beta_{j2}^k + \gamma_{j2}^k \frac{\partial^2}{\partial t^2}\right] u_{k+1}(t,z)\right\}\Big|_{z=l_k} = \omega_{jk}(t); \tag{5.111}$$

$j = \overline{1,2}; k = \overline{1,n}$

Let's use the system (5.108) and initial conditions (5.111) in matrix form:

$$\begin{bmatrix} \left(\frac{\partial^2}{\partial t^2}+\chi_1^2-D_1\frac{\partial^2}{\partial z^2}\right)u_1(t,z) \\ \left(\frac{\partial^2}{\partial t^2}+\chi_2^2-D_2\frac{\partial^2}{\partial z^2}\right)u_2(t,z) \\ \ldots\ldots\ldots\ldots\ldots\ldots\ldots\ldots\ldots\ldots\ldots\ldots \\ \left(\frac{\partial^2}{\partial t^2}+\chi_{n+1}^2-D_{n+1}\frac{\partial^2}{\partial z^2}\right)u_{n+1}(t,z) \end{bmatrix} = \begin{bmatrix} f_1(t,z) \\ f_2(t,z) \\ \ldots\ldots\ldots\ldots \\ f_{n+1}(t,z) \end{bmatrix} \tag{5.112}$$

$$\left.\begin{bmatrix} u_1(t,z) \\ u_2(t,z) \\ \ldots\ldots\ldots\ldots \\ u_{n+1}(t,z) \end{bmatrix}\right|_{t=0} = \begin{bmatrix} g_{11}(z) \\ g_{12}(z) \\ \ldots\ldots\ldots\ldots \\ g_{1,n+1}(z) \end{bmatrix}; \frac{\partial}{\partial t}\left.\begin{bmatrix} u_1(t,z) \\ u_2(t,z) \\ \ldots\ldots\ldots\ldots \\ u_{n+1}(t,z) \end{bmatrix}\right|_{t=0} = \begin{bmatrix} g_{21}(z) \\ g_{22}(z) \\ \ldots\ldots\ldots\ldots \\ g_{2,n+1}(z) \end{bmatrix}.$$

Assuming that $\max\left\{\chi_1^2;\chi_2^2;\ldots;\chi_n^2;\chi_{n+1}^2\right\}=\chi_{n+1}^2$, apply to the problem (5.112) according to the rule of multiplication of matrices, the operator matrix is a string (5.103). Due to identity (5.97) we obtain the Cauchy problem:

$$\left[\frac{d^2}{dt^2}+\left(\beta_m^2+\chi_{n+1}^2\right)\right]u_m(t)=\mathrm{F}\,\mathrm{h}_m(t);u_m(t)\big|_{t=0}=g_{1m,}\,\frac{d}{dt}u_m(t)\big|_{t=0}=g_{2m}. \tag{5.113}$$

The solution to the Cauchy problem (5.113) is a function

$$u_m(t)=\frac{\sin q_m t}{q_m}g_{2m}+\frac{d}{dt}\frac{\sin q_m t}{q_m}g_{1m}+\int_0^t\frac{\sin q_m(t-\tau)}{q_m}\mathrm{F}\,\mathrm{h}_m(\tau)d\tau, q_m=\left(\beta_m^2+\chi_{n+1}^2\right)^{1/2}. \tag{5.114}$$

Applying to the matrix-element $\left[u_m(t)\right]$, defined by the formula (5.114), by the rule of multiplication of matrices, by the operator matrix-column (5.106), after elementary transformations we obtain a single solution to the hyperbolic problem (5.108) - (5.111):

$$\begin{aligned} u_j(t,z)=&\sum_{k=1}^{n+1}\int_0^t\int_{l_{k-1}}^{l_k}\mathrm{H}\,\mathrm{h}_{jk}(t-\tau,z,\xi)\left[f_k(\tau,\xi)+g_{2k}(\xi)\delta_+(\tau)\right]\sigma_k d\xi d\tau+ \\ &+\sum_{k=1}^{n+1}\frac{\partial}{\partial t}\int_{l_{k-1}}^{l_k}\mathrm{H}\,\mathrm{h}_{jk}(t,z,\xi)g_{1k}(\xi)\sigma_k d\xi+ \\ &+\int_0^t\left[W_{0j}(t-\tau,z)\omega_0(\tau)+W_{lj}(t-\tau,z)\omega_l(\tau)\right]d\tau+ \\ &+\sum_{k=1}^{n}\int_0^t\left[\mathrm{R}_{jk}^{(1)}(t-\tau,z)\omega_{1k}(\tau)+\mathrm{R}_{jk}^{(2)}(t-\tau,z)\omega_{2k}(\tau)\right]d\tau, j=\overline{1,n+1} \end{aligned} \tag{5.115}$$

Here are the main solutions to the hyperbolic problem (5.108) - (5.111):

- matrix of influence functions generated by the inhomogeneity of the system (5.108):

$$\mathrm{H}_{jk}\left(t,z,\xi\right)=\sum_{m=1}^{\infty}\frac{\sin q_m t}{q_m}\frac{V_j\left(z,\beta_m\right)V_k\left(\xi,\beta_m\right)}{\left\|V\left(z,\beta_m\right)\right\|_1^2};\ j,k=\overline{1,n+1}$$

- Green's vector functions generated by boundary conditions at the boundaries $z=l_0$ та $z=l$:

$$W_{0j}\left(t,z\right)=-a_1^2\sigma_1\sum_{m=1}^{\infty}\frac{\sin q_m t}{q_m}\frac{V_1\left(l_0,\beta_m\right)V_j\left(z,\beta_m\right)}{\tilde{\alpha}_{11}^{0}\left\|V\left(z,\beta_m\right)\right\|_1^2};$$

$$W_{lj}\left(t,z\right)=\sum_{m=1}^{\infty}\frac{\sin q_m t}{q_m}\frac{V_j\left(z,\beta_m\right)V_{n+1}\left(l,\beta_m\right)}{\tilde{\alpha}_{22}^{n+1}\left\|V\left(z,\beta_m\right)\right\|_1^2};\ j=\overline{1,n+1}$$

- and matrices of the Green's function generated by the inhomogeneity of the system of interface conditions:

$$\mathrm{R}_{jk}^{(1)}\left(t,z\right)=-\frac{D_k\sigma_k}{c_{11,k}}\sum_{m=1}^{\infty}\frac{\sin q_m t}{q_m}\frac{\tilde{\alpha}_{22}^{k}V_{k+1}'\left(l_k,\beta_m\right)+\tilde{\beta}_{22}^{k}V_{k+1}\left(l_k,\beta_m\right)}{\left\|V\left(z,\beta_m\right)\right\|_1^2}V_j\left(z,\beta_m\right),$$

$$\mathrm{R}_{jk}^{(2)}\left(t,z\right)=\frac{D_k\sigma_k}{c_{11,k}}\sum_{m=1}^{\infty}\frac{\sin q_m t}{q_m}\frac{\tilde{\alpha}_{12}^{k}V_{k+1}'\left(l_k,\beta_m\right)+\tilde{\beta}_{12}^{k}V_{k+1}\left(l_k,\beta_m\right)}{\left\|V\left(z,\beta_m\right)\right\|_1^2}V_j\left(z,\beta_m\right).$$

The solution to this hyperbolic boundary value problem is constructed with the condition:

$$\psi_{1i}\equiv\delta_{11}^{0}g_1'\left(l_0\right)+\gamma_{11}^{0}g_{i1}\left(l_0\right)=0,\ \psi_{n+1,i}\equiv\delta_{22}^{n+1}g_{i,n+1}'\left(l_{n+1}\right)+\gamma_{22}^{n+1}g_{i,n+1}\left(l_{n+1}\right)=0,$$
$$\psi_{jk,i}^{0}=\delta_{j1}^{k}g_{ik}'\left(l_k\right)+\gamma_{j1}^{k}g_{ik}\left(l_k\right)-\delta_{j2}^{k}g_{i,k+1}'\left(l_k\right)+\gamma_{j2}^{k}g_{i,k+1}\left(l_k\right)=0,i=1,2$$

Otherwise, next components will appear in formula (5.115)

$$\frac{\partial^2}{\partial t^2}W_{0j}\left(t,x\right)\psi_{11}+W_{0j}\left(t,x\right)\psi_{12}+\frac{\partial^2}{\partial t^2}W_{lj}\left(t,x\right)\psi_{n+1,1}+W_{lj}\left(t,x\right)\psi_{n+1,1}+$$
$$+\sum_{k=1}^{n}\left\{\left[\frac{\partial^2}{\partial t^2}R_{jk}^{(1)}\left(t,x\right)\psi_{1k,1}+\frac{\partial^2}{\partial t^2}R_{jk}^{(2)}\left(t,x\right)\psi_{2k,1}\right]+\left[R_{jk}^{(1)}\left(t,x\right)\psi_{1k,2}+R_{jk}^{(2)}\left(t,x\right)\psi_{2k,2}\right]\right\}.$$

5.3 Integral Fourier transform for semi-bounded heterogeneous n – component media

Let us introduce an integral transformation generated on the set $I_n^t = \left\{ z:\ \mathrm{z} \in \bigcup_{j=1}^{n+1} \left(l_{j-1}, l_j \right); l_0 \geq 0, l_{n+1} = \infty \right\}$ of the second-order Fourier differential operator:

$$L_n = \left[\sum_{k=1}^{n} D_k \theta\left(z - l_{k-1} \right) \theta\left(l_k - z \right) + D_{n+1} \theta\left(z - l_n \right) \right] \frac{d^2}{dz^2} \tag{5.116}$$

assuming that for any vector function $g(z) = \left\{ g_1(z), g_2(z), \ldots, g_n(z), g_{n+1}(z) \right\}$ from the area of definition of the operator L_n boundary conditions come true:

$$\left(\tilde{\alpha}_{11}^0 \frac{d}{dz} + \tilde{\beta}_{11}^0 \right) g_1(z) \Big|_{x=l_0} = 0, \qquad \lim_{\mathrm{x} \to \infty} \frac{d^m g_{n+1}}{dz^m} = 0, \ \ m = 0,1 \tag{5.117}$$

and interface conditions systems:

$$\left[\left(\tilde{\alpha}_{j1}^k \frac{d}{dz} + \tilde{\beta}_{j1}^k \right) g_k - \left(\tilde{\alpha}_{j2}^k \frac{d}{dz} + \tilde{\beta}_{j2}^k \right) g_{k+1} \right] \ \Big|_{z=l_k} = 0; \ \ j = 1,2; \ \ k = \overline{1,n}. \tag{5.118}$$

Consider the construction problem of a bounded domain $D_n^+ = \{ (t,z) : t \in (0,\infty), z \in \mathrm{I}_n^+ \}$ solution to the system of differential equations in partial derivatives of wave signal propagation [11, 12]

$$\left(\frac{\partial}{\partial t} + \gamma_j^2 - D_j \frac{\partial^2}{\partial x^2} \right) u_j(t,x) = 0, \ \mathrm{z} \in \left(l_{j-1}, l_j \right), j = j = \overline{1,n}, l_{n+1} = \infty \tag{5.119}$$

under the initial conditions:

$$u_j(t,z) \Big|_{t=0} = g_j(z), z \in \left(l_{j-1}, l_j \right), j = \overline{1,n} \tag{5.120}$$

and boundary conditions:

$$\left[\left(\alpha_{11}^0 + \delta_{11}^0 \frac{\partial}{\partial t} \right) \frac{\partial}{\partial z} + \beta_{11}^0 + \gamma_{11}^0 \frac{\partial}{\partial t} \right] u_1 \Big|_{z=l_0} = 0; \frac{\partial u_{n+1}}{\partial z} \Big|_{z=\infty} = 0 \tag{5.121}$$

and a system of interface conditions:

$$\left(L_{j1}^{k}\left[u_k\right]-L_{j2}^{1}\left[u_{k+1}\right]\right)\Big|_{z=l_k}\equiv\left\{\left[\left(\alpha_{j1}^{k}+\delta_{j1}^{k}\frac{\partial}{\partial t}\right)\frac{\partial}{\partial z}+\beta_{j1}^{k}+\gamma_{j1}^{k}\frac{\partial}{\partial t}\right]u_k\left(t,z\right)-\right.$$
$$\left.-\left[\left(\alpha_{j2}^{k}+\delta_{j2}^{k}\frac{\partial}{\partial t}\right)\frac{\partial}{\partial z}+\beta_{j2}^{k}+\gamma_{j2}^{k}\frac{\partial}{\partial t}\right]u_{k+1}\left(t,z\right)\right\}\Big|_{z=l_k}=0;k=\overline{1,n};j=1,2 \quad (5.122)$$

Assume that the vector is a function $u(t,z)=\left\{u_1\left(t,z\right),u_2\left(t,z\right),...,u_{n+1}(t,z)\right\}$ is the original Laplace relative to *t* [29]. Using the transform integral of the Laplace to the problem (5.116) - (5.122), we obtein the problem: to find in domain I_1^+ the solution to differential equation system

$$\left(\frac{d^2}{dz^2}-q_j^2\right)u_j^*\left(p,z\right)=-\overline{g}_j\left(z\right);j=\overline{1,n+1} \quad (5.123)$$

under boundary conditions:

$$\left(\overline{\alpha}_{11}^{0}\frac{d}{dz}+\overline{\beta}_{11}^{0}\right)u_1^*\Big|_{z=l_0}=g_0,\frac{du_{n+1}^*}{dz}\Big|_{z=\infty}=0\ , \quad (5.124)$$

and a system of interface conditions:

$$\left[\left(\alpha_{j1}^{-1}\frac{d}{dx}+\beta_{j1}^{-1}\right)u_1^*\left(p,x\right)-\left(\alpha_{j2}^{-1}\frac{d}{dx}+\beta_{j2}^{-1}\right)u_2^*\left(p,x\right)\right]\Big|_{x=l_1}=\psi_{j1},j=1,2 \quad (5.125)$$

Here:

$$\overline{g}_j=D_j^{-1}g_j\left(z\right);q_j=D_j^{-1/2}\left(p+\gamma_j^2\right)^{\frac{1}{2}},D_j>0,\gamma_j^2\geq 0,Req_j>0;$$
$$\overline{\alpha}_{ji}^{m}=\alpha_{ji}^{m}+\delta_{ji}^{m}p,\overline{\beta}_{ji}^{m}=\beta_{jk}^{m}+\gamma_{jk}^{m}p;m=\overline{0,n};j,k=1,2;$$
$$g_0=\delta_{11}^{0}g_1'\left(l_0\right)+\gamma_{11}^{0}g_1\left(l_0\right);\psi_{jk}=\delta_{j1}^{k}q_k'\left(l_k\right)+\gamma_{j1}^{k}g_k\left(l_k\right)-\left(\delta_{j2}^{k}g_{k+1}'\left(l_k\right)+\gamma_{j1}^{k}q_k\left(l_k\right)\right),j=1,2.$$

Replacing variables in a task (5.123) – (5.125) is easily reduced to a problem with homogeneous boundary conditions ($g_0=0$) and a homogeneous system of interface conditions ($\psi_{j1}=0;j=\overline{1,n}$).

Fundamental system of solutions to the Fourier differential equation $\left(\frac{d^2}{dz^2}-q^2\right)V=0$ form functions $\exp(qz)$ and $\exp(-qz)$ or their linear combinations $V_1=ch(qz)$ and $V_2=sh(qz)$.

Fixing the branch $\operatorname{Re}q_k(p)>0$, solution to a heterogeneous boundary value problem (5.116) – (5.118) is constructed by the method of Cauchy functions [11, 19]:

$$u_k^*(p,z)=A_k\cdot chq_kz+B_k\cdot shq_kz+\int_{l_{k-1}}^{l_k}\mathrm{E}_k^*(p,z,\xi)\mathrm{F}_k^*(p,\xi)d\xi;k=\overline{1,n}; \tag{5.126}$$

$$u_{n+1}^*(p,z)=B_{n+1}e^{-q_{n+1}(z-l_n)}+\int_{l_n}^{\infty}\mathrm{E}_{n+1}^*(p,z,\xi)\mathrm{F}_{n+1}^*(p,\xi)d\xi; \tag{5.127}$$

where $\mathrm{E}_k^*(p,z,\xi),k=\overline{1,n+1}$ - Cauchy functions that satisfy the conditions:

$$\begin{cases}\mathrm{E}_k^*(p,z,\xi)\big|_{z=\xi+0}-\mathrm{E}_k^*(p,z,\xi)\big|_{z=\xi-0}=0\\ \dfrac{d}{dz}\mathrm{E}_k^*(p,z,\xi)\big|_{z=\xi+0}-\dfrac{d}{dz}\mathrm{E}_k^*(p,z,\xi)\big|_{z=\xi-0}=-1.\end{cases} \tag{5.128}$$

Cauchy functions $\mathrm{E}_k^*(p,z,\xi),k=\overline{1,n}$ are as follows:

$$\mathrm{E}_k^*(p,z,\xi)=\begin{cases}\mathrm{E}_k^{-*}=D_{1_k}chq_kz+E_{1_k}shq_kz;l_k<z<\xi<l_{k+1}\\ \mathrm{E}_k^{+*}=D_{2_k}chq_kz+E_{2_k}shq_kz;l_k<\xi<z<l_{k+1}\end{cases}, \tag{5.129}$$

satisfying additional homogeneous conditions:

$$\left(\bar{\alpha}_{12}^k\frac{d}{dz}+\bar{\beta}_{12}^k\right)\mathrm{E}_k^{-*}\Big|_{z=l_{k-1}+0}=0;\left(\bar{\alpha}_{11}^k\frac{d}{dz}+\bar{\beta}_{11}^k\right)\mathrm{E}_k^{+*}\Big|_{z=l_k-0}=0,k=\overline{1,n}. \tag{5.130}$$

Cauchy function $\mathrm{E}_{n+1}^*(p,z,\xi)$ is as follows:

$$\mathrm{E}_{n+1}^*(p,z,\xi)=\begin{cases}\mathrm{E}_{n+1}^{-*}=D_{1_{n+1}}chq_{n+1}z+E_{1_{n+1}}shq_{n+1}z;l_n<z<\xi<\infty\\ \mathrm{E}_{n+1}^{+*}=E_{2_{n+1}}e^{-q_{n+1}(z-l_n)};l_n<\xi<z<\infty\end{cases}, \tag{5.131}$$

satisfying the additional condition:

$$\left(\bar{\alpha}_{12}^{n}\frac{d}{dz}+\bar{\beta}_{12}^{n}\right)\mathrm{E}_{n+1}^{-*}\Big|_{z=l_n+0}=0. \tag{5.132}$$

Find the Cauchy functions $\mathrm{E}_k^*(p,z,\xi);k=\overline{1,n}$. From condition (5.128) we obtain:

$$\left[\square_k^{+*}(p,z,\xi)-\square_k^{-*}(p,z,\xi)\right]\Big|_{z=l_k}=(D_{2_k}-D_{1_k})chq_k\xi+(E_{2_k}-E_{1_k})shq_k\xi=0$$

$$\frac{1}{q_k}\frac{d}{dz}\left[\square_k^{+*}(p,z,\xi)-\square_k^{-*}(p,z,\xi)\right]\Big|_{z=l_k}=(D_{2_k}-D_{1_k})shq_k\xi+(E_{2_k}-E_{1_k})chq_k\xi=-\frac{1}{q_k}$$

So, relatively $(D_{2_k}-D_{1_k})$ and $(E_{2_k}-E_{1_k})$ we obtain an algebraic system:

$$\begin{aligned}&(D_{2_k}-D_{1_k})chq_k\xi+(E_{2_k}-E_{1_k})shq_k\xi=0;\\&(D_{2_k}-D_{1_k})shq_k\xi+(E_{2_k}-E_{1_k})chq_k\xi=-\frac{1}{q_k}.\end{aligned} \tag{5.133}$$

Hence we get value:

$$(D_{2_k}-D_{1_k})=\frac{1}{q_k}shq_k\xi;(E_{2_k}-E_{1_k})=-\frac{1}{q_k}chq_k\xi\ . \tag{5.134}$$

From the interface conditions (5.130) we have equality:

$$\begin{aligned}&\left(\bar{\alpha}_{12}^{k}\frac{d}{dz}+\bar{\beta}_{12}^{k}\right)\mathrm{E}_k^{-*}\Big|_{z=l_{k-1}}=D_{1_k}\cdot V_{12}^{k-1,1}(q_kl_{k-1})+E_{1_k}\cdot V_{12}^{k-1,2}(q_kl_{k-1})=0\\&\left(\bar{\alpha}_{11}^{k}\frac{d}{dz}+\bar{\beta}_{11}^{k}\right)\mathrm{E}_k^{+*}\Big|_{z=l_k}=D_{2_k}\cdot V_{11}^{k1}(q_kl_k)+E_{2_k}\cdot V_{11}^{k2}(q_kl_k)=0\end{aligned} \tag{5.135}$$

Substituting in the first equation of the system (5.135) values D_{2_k}, E_{2_k} from relations (5.134), we obtain a system of equations for determining the unknown coefficients D_{1_k}, E_{1_k}:

$$D_{1_k}\cdot V_{12}^{k-1,1}(q_kl_k)+E_{1_k}\cdot V_{12}^{k-1,2}(q_kl_{k-1})=0$$

$$D_{1_k}\cdot V_{11}^{k1}(q_kl_k)+E_{1_k}\cdot V_{11}^{k2}(q_kl_k)=\frac{1}{q_k}\Phi_{11}^{k}(q_kl_k,q_k\xi).$$

Hence, we find:

$$D_{1_k}=\frac{\begin{vmatrix} 0 & V_{12}^{k-1,2}(q_k l_{k-1}) \\ \frac{1}{q_k}\Phi_{11}^{k}(q_k l_k, q_k\xi) & V_{11}^{k2}(q_k l_k) \end{vmatrix}}{\begin{vmatrix} V_{12}^{k-1,1}(q_k l_{k-1}) & V_{12}^{k-1,2}(q_k l_{k-1}) \\ V_{11}^{k1}(q_k l_k) & V_{11}^{k2}(q_k l_k) \end{vmatrix}}=-\frac{\Phi_{11}^{k}(q_k l_k, q_k\xi)}{q_k\cdot\Delta_{11}(q_k l_{k-1}, q_k l_k)}V_{12}^{k-1,2}(q_k l_{k-1})$$

$$E_{1_k}=\frac{\Phi_{11}^{k}(q_k l_k, q_k\xi)\cdot V_{12}^{k-1,1}(q_k l_{k-1})}{q_k\cdot\Delta_{11}(q_k l_{k-1}, q_k l_k)}.$$

This Cauchy function $\mathrm{E}_k^*(p,z,\xi);k=\overline{1,n}$ determined due to the symmetry relative to the diagonal $z=\xi$ has the following structure:

$$\mathrm{E}_k^*(p,z,\xi)=\frac{1}{q_k\Delta_{11}\left(q_k l_{k-1}, q_k l_k\right)}\begin{cases}\Phi_{12}^{k-1}\left(q_k l_{k-1}, q_k z\right)\cdot\Phi_{11}^{k}\left(q_k l_k, q_k\xi\right), l_{k-1}<z<\xi<l_k \\ \Phi_{12}^{k-1}\left(q_k l_{k-1}, q_k\xi\right)\cdot\Phi_{11}^{n}\left(q_k l_k, q_k z\right), l_{k-1}<\xi<z<l_k\end{cases} \tag{5.136}$$

here

$$\Delta_{11}(q_k l_{k-1}, q_k l_k)=\begin{cases}V_{12}^{k-1,1}(q_k l_{k-1})V_{11}^{k2}(q_k l_k)-V_{11}^{k1}(q_k l_k)V_{12}^{k-1,2}(q_k l_{k-1}); & k=\overline{2,n} \\ \Delta_{11}^{1}(q_1 l_0, q_1 l_1); & k=1\end{cases}$$

$$\Delta_{j1}^{1}(q_1 l_0, q_1 l_1)=V_{11}^{01}(q_1 l_0)\cdot V_{j1}^{12}(q_1 l_1)-V_{j1}^{11}(q_1 l_1)\cdot V_{11}^{0,2}(q_1 l_0)$$

Calculate the expression for the Cauchy function $\mathrm{E}_{n+1}^*(p,z,\xi)$. From condition (5.132) we find an additional equation:

$$\left(\bar{\alpha}_{12}^{n}\frac{d}{dz}+\bar{\beta}_{12}^{n}\right)\mathrm{E}_{n+1}^{-*}(p,z,\xi)\Big|_{z=l_n}=D_{1_{n+1}}V_{12}^{n1}(q_{n+1}l_n)+E_{1_{n+1}}V_{12}^{n2}(q_{n+1}l_n)=0. \tag{5.137}$$

As a result of conditions (5.128), we obtain an algebraic system:

$$\left[\mathrm{E}_{n+1}^{+*}(p,z,\xi)-\mathrm{E}_{n+1}^{-*}(p,z,\xi)\right]_{z=\xi}=E_{2_{n+1}}e^{-q_{n+1}(\xi-l_n)}-\left(D_{1_{n+1}}\cdot chq_{n+1}\xi+E_{1_{n+1}}\cdot shq_{n+1}\xi\right)=0. \tag{5.138}$$

$$\frac{d}{dz}\left[\mathrm{E}_{n+1}^{+*}(p,z,\xi)-\mathrm{E}_{n+1}^{-*}(p,z,\xi)\right]_{z=\xi}=-q_{n+1}E_{2_{n+1}}e^{-q_{n+1}(\xi-l_n)}-q_{n+1}\left(D_{1_{n+1}}shq_{n+1}\xi+E_{1_{n+1}}chq_{n+1}\xi\right)=-1$$

.

From the system (5.130) we obtain:

$$D_{1_{n+1}} = \frac{\begin{vmatrix} E_{2_{n+1}} e^{-q_{n+1}(\xi - l_n)} & shq_{n+1}\xi \\ \dfrac{1}{q_{n+1}} - E_{2_{n+1}} e^{-q_{n+1}(\xi - l_n)} & chq_{n+1}\xi \end{vmatrix}}{ch^2 q_{n+1}\xi - sh^2 q_{n+1}\xi} =$$

$$= -\frac{shq_{n+1}\xi}{q_{n+1}} + E_{2_{n+1}} e^{q_{n+1}l_n}\left[ch^2 q_{n+1}\xi - sh^2 q_{n+1}\xi\right] = -\frac{shq_{n+1}\xi}{q_{n+1}} + E_{2_{n+1}} e^{q_{n+1}l_n};$$

$$E_{1_{n+1}} = \frac{\begin{vmatrix} chq_{n+1}\xi & D_{2_{n+1}} e^{-q_{n+1}(\xi - l_n)} \\ shq_{n+1}\xi & \dfrac{1}{q_{n+1}} - E_{2_{n+1}} e^{-q_{n+1}(\xi - l_n)} \end{vmatrix}}{ch^2 q_{n+1}\xi - sh^2 q_{n+1}\xi} = \frac{chq_{n+1}\xi}{q_{n+1}} - E_{2_{n+1}} e^{q_{n+1}l_n}.$$

Substituting $D_{1_{n+1}}, E_{1_{n+1}}$ in (5.137), we obtain:

$$E_{2_{n+1}} = -\frac{1}{q_{n+1}}\left[V_{12}^{n2}(q_{n+1}l_n)chq_{n+1}\xi - V_{12}^{n1}(q_{n+1}l_n)shq_{n+1}\xi\right] *$$

$$* \frac{e^{-q_{n+1}l_n}}{V_{12}^{n1}(q_{n+1}\xi) - V_{12}^{n2}(q_{n+1}\xi)} = \frac{\Phi_{12}^{n}\left(q_{n+1}l_n, q_{n+1}\xi\right)}{q_{n+1}\cdot\left(\bar{\alpha}_{12}^{n} q_{n+1} - \bar{\beta}_{12}^{n}\right)}.$$

Here

$$V_{12}^{n1}(q_{n+1}\xi) - V_{12}^{n2}(q_{n+1}\xi) = \bar{\alpha}_{12}^{n} q_{n+1} shq_{n+1}l_n + \bar{\beta}_{12}^{n} chq_{n+1}l_n - \bar{\alpha}_{12}^{n} q_{n+1} chq_{n+1}l_n - \bar{\beta}_{12}^{n} shq_{n+1}l_n =$$
$$= \left(\bar{\beta}_{12}^{n} - \bar{\alpha}_{12}^{n} q_{n+1}\right)(chq_{n+1}l_n - shq_{n+1}l_n) = \left(\bar{\beta}_{12}^{n} - \bar{\alpha}_{12}^{n} q_{n+1}\right)e^{-q_{n+1}l_n}.$$

This Cauchy function $\mathrm{E}_{n+1}^{*}(p,z,\xi)$ determined due to the symmetry relative to the diagonal $z=\xi$ has the following structure:

$$\square_{n+1}^{*}(p,z,\xi) = \frac{1}{q_{n+1}\left(\bar{\alpha}_{12}^{n} q_{n+1} - \bar{\beta}_{12}^{n}\right)}\begin{cases} \Phi_{12}^{n}\left(q_{n+1}l_n, q_{n+1}z\right)\cdot e^{-q_{n+1}(\xi - l_n)}, l_n < z < \xi < \infty \\ \Phi_{12}^{n}\left(q_{n+1}l_n, q_{n+1}\xi\right)\cdot e^{-q_{n+1}(z - l_n)}, l_n < \xi < z < \infty \end{cases}. \qquad (5.139)$$

As a result of solving the corresponding systems of algebraic equations to find the unknowns $D_{i_k}, E_{i_k}, E_{i_{n+1}}; k = \overline{1,n}; i = \overline{1,2}$, Cauchy functions will also be defined due to the symmetry with respect to the diagonal $z=\xi$ and will have a structure:

$$\Box_k^*(p,z,\xi) = -\frac{1}{q_k \Delta_{11}\left(q_k l_{k-1}, q_k l_k\right)} \begin{cases} \Phi_{12}^{k-1}\left(q_k l_{k-1}, q_k z\right) \cdot \Phi_{11}^{k}\left(q_k l_k, q_k \xi\right), l_{k-1} < z < \xi < l_k \\ \Phi_{12}^{k-1}\left(q_k l_{k-1}, q_k \xi\right) \cdot \Phi_{11}^{n}\left(q_k l_k, q_k z\right), l_{k-1} < \xi < z < l_k \end{cases},$$

$$k = \overline{1,n}$$

$$\Box_{n+1}^*(p,z,\xi) = \frac{1}{q_{n+1}\left(\bar{\alpha}_{12}^n q_{n+1} - \bar{\beta}_{12}^n\right)} \begin{cases} \Phi_{12}^{n}\left(q_{n+1} l_n, q_{n+1} z\right) \cdot e^{-q_{n+1}(\xi - l_n)}, l_n < z < \xi < \infty \\ \Phi_{12}^{n}\left(q_{n+1} l_n, q_{n+1} \xi\right) \cdot e^{-q_{n+1}(z - l_n)}, l_n < \xi < z < \infty \end{cases}. \qquad (5.140)$$

Here:

$$\Delta_{11}(q_k l_{k-1}, q_k l_k) = \begin{cases} V_{12}^{k-1,1}(q_k l_{k-1}) V_{11}^{k2}(q_k l_k) - V_{11}^{k1}(q_k l_k) V_{12}^{k-1,2}(q_k l_{k-1}); & k = \overline{2,n} \\ \Delta_{11}^1(q_1 l_0, q_1 l_1); & k = 1 \end{cases}$$

$$\Delta_{j1}^1(q_1 l_0, q_1 l_1) = V_{11}^{01}(q_1 l_0) \cdot V_{j1}^{12}(q_1 l_1) - V_{j1}^{11}(q_1 l_1) \cdot V_{11}^{0,2}(q_1 l_0)$$

$$V_{ij}^{k1}(q_S l_k = (\bar{\alpha}_{ij}^k \frac{d}{dz} + \bar{\beta}_{ij}^k) chq_S z\big|_{z=l_k} = \bar{\alpha}_{ij}^k q_S shq_S l_k + \bar{\beta}_{ij}^k chq_S l_k$$

$$V_{ij}^{k2}(q_s l_k) = (\bar{\alpha}_{ij}^k \frac{d}{dz} + \bar{\beta}_{ij}^k) shq_s z\big|_{z=l_k} = \bar{\alpha}_{ij}^k q_s chq_S l_k + \bar{\beta}_{ij}^k shq_S l_k;$$

$$\Phi_{ij}^k(q_S l_k, q_S z) = V_{ij}^{k2}(q_S l_k) chq_S z - V_{ij}^{k1}(q_S l_k) shq_S z.$$

With known Cauchy functions $\mathrm{E}_k^*(p,z,\xi)$ boundary condition at a point $z = l_0$ and interface conditions (5.7) for determining unknown coefficients $A_k, B_k (k = \overline{1,n})$ and B_{n+1}, participating in the structures (5.126) – (5.127) of general solution to the boundary value problem (5.123) – (5.125), give an algebraic system with *(2n+1)* – th equation:

$$\begin{cases} V_{12}^{01}(q_1 l_0)A_1 + V_{12}^{02}(q_1 l_0)B_1 = 0 \\ V_{11}^{11}(q_1 l_1)A_1 + V_{11}^{12}(q_1 l_1)B_1 - V_{12}^{11}(q_2 l_1)A_2 - V_{12}^{12}(q_2 l_1)B_2 = 0 \\ V_{21}^{11}(q_1 l_1)A_1 + V_{21}^{12}(q_1 l_1)B_1 - V_{22}^{11}(q_2 l_1)A_2 - V_{22}^{12}(q_2 l_1)B_2 = G_1^* \\ ---------- \\ V_{11}^{k1}(q_k l_k)A_k + V_{11}^{k2}(q_k l_k)B_k - V_{12}^{k1}(q_{k+1} l_k)A_{k+1} - V_{12}^{k2}(q_{k+1} l_k)B_{k+1} = 0 \\ V_{21}^{k1}(q_k l_k)A_k + V_{21}^{k2}(q_k l_k)B_k - V_{22}^{k1}(q_{k+1} l_k)A_{k+1} - V_{22}^{k2}(q_{k+1} l_k)B_{k+1} = G_k^* \\ ---------- \\ V_{11}^{n,1}(q_n l_n)A_n + V_{11}^{n,2}(q_n l_n)B_n - \left(\overline{\beta}_{12}^n - \overline{\alpha}_{12}^n q_{n+1}\right)B_{n+1} = 0 \\ V_{21}^{n,1}(q_n l_n)A_n + V_{21}^{n,2}(q_n l_n)B_n - \left(\overline{\beta}_{22}^n - \overline{\alpha}_{22}^n q_{n+1}\right)B_{n+1} = G_n^* \end{cases} \quad (5.141)$$

Functions G_k^*, participating in the system (5.134) have the form:

$$G_k^* = c_{2_k} \int_{l_k}^{l_{k+1}} \frac{\Phi_{11}^{k+1}(q_{k+1}l_{k+1}, q_{k+1}\xi)}{\Delta_{11}(q_{k+1}l_k, q_{k+1}l_{k+1})} \mathrm{F}_{k+1}^*(p,\xi)d\xi - c_{1_k} \int_{l_{k-1}}^{l_k} \frac{\Phi_{12}^{k-1}(q_k l_{k-1}, q_k \xi)}{\Delta_{11}(q_k l_{k-1}, q_k l_k)} \mathrm{F}_k^*(p,\xi)d\xi,$$

$$k = \overline{1, n-1}$$

$$G_n^* = c_{2_n} \int_{l_n}^{\infty} \frac{e^{-q_{n+1}(\xi - l_n)}}{\overline{\beta}_{12}^n - \overline{\alpha}_{12}^n q_{n+1}} \mathrm{F}_{n+1}^*(p,\xi)d\xi - c_{1_n} \int_{l_{n-1}}^{l_n} \frac{\Phi_{12}^{n-1}(q_n l_{n-1}, q_n \xi)}{\Delta_{11}(q_n l_{n-1}, q_n l_n)} \mathrm{F}_n^*(p,\xi)d\xi. \quad (5.142)$$

Here $c_{j_k} = \overline{\alpha}_{2j}^k \cdot \overline{\beta}_{1j}^k - \overline{\alpha}_{1j}^k \cdot \overline{\beta}_{2j}^k; k = \overline{1,n}; j = \overline{1,2}$.

Assume that the condition of unambiguous solvability of the boundary value problem is satisfied (5.123) – (5.125): for $p = \sigma + iz$ from $\mathrm{Re}\, p = \sigma \geq \sigma_0$, where σ_0 - the abscissa of the convergence of the Laplace integral and $\mathrm{Im}\, p = \tau \in (-\infty, +\infty)$ the determinant of the algebraic system (5.141) of the nonzero system:

$$\Delta^*(p) = \left(\overline{\alpha}_{22}^n q_{n+1} - \overline{\beta}_{22}^n\right)\Delta_{\overline{1,2n}} - \left(\overline{\alpha}_{22}^n q_{n+1} - \overline{\beta}_{22}^n\right)\Delta_{\overline{1,2n}} \neq 0. \quad (5.143)$$

As a result of the unambiguous solvability of the algebraic system (5.134) and substitution of the received values $A_k, B_k; k = \overline{1,n}$ and B_{n+1} in formulas (5.126), (5.135), we obtain a single solution to the boundary value problem (5.116) – (5.118) as:

$$u_k^*(p,z)=\sum_{j=1}^{n+1}\int_{l_{j-1}}^{l_j} \mathrm{H}_{k,j}^*(p,z,\xi)\cdot\overline{g}_j(\xi)d\xi;k=\overline{1,n+1};l_{n+1}=\infty. \qquad (5.144)$$

Here are the elements of the influence function matrix $\left[\mathrm{H}_{ij}^*(p,z,\xi)\right],\ i,j=\overline{1,n+1}$:

$$\square_{11}^*(p,z,\xi)=\frac{\Phi_{12}^0(q_1l_0,q_1z)}{q_1\Delta^*(p)}\left[\Phi_{21}^1(q_1l_1,q_1\xi)\cdot\mathrm{A}'_{\overline{1,2}}-\Phi_{11}^1(q_1l_1,q_1\xi)\cdot\mathrm{A}_{\overline{1,2}}\right];$$

$$H_{1j}^*(p,z,\xi)=\frac{\prod_{s=1}^{j-1}q_sc_{2_s}}{q_1\Delta^*(p)}\Phi_{12}^0(q_1l_0,q_1z)\left[\Phi_{21}^j(q_jl_j,q_j\xi)\mathrm{A}'_{\overline{1,2j}}-\Phi_{11}^j(q_jl_j,q_j\xi)\mathrm{A}_{\overline{1,2j}}\right];j=\overline{2,n};$$

$$H_{1,n+1}^*(p,z,\xi)=-\frac{\prod_{s=1}^{n}q_sc_{2_s}}{q_1\Delta^*(p)}\Phi_{12}^0(q_1l_0,q_1z)\cdot e^{-q_{n+1}(\xi-l_n)};$$

$$\square_{k1}^*(p,z,\xi)=\frac{\Phi_{12}^0(q_1l_0,q_1\xi)}{q_1\Delta^*(p)}\cdot\prod_{s=1}^{k-1}c_{1_s}q_s\cdot\left[\Phi_{21}^k(q_kl_k,q_kz)\cdot\mathrm{A}'_{\overline{1,2k}}-\Phi_{11}^k(q_kl_k,q_kz)\cdot\mathrm{A}_{\overline{1,2k}}\right];$$

$$\square_{kj}^*(p,z,\zeta)=\frac{\prod_{s=j}^{k-1}q_sc_{1_s}}{q_j\Delta^*(p)}\left[\Phi_{11}^k(q_kl_k,q_kz)\mathrm{A}_{\overline{1,2k}}-\Phi_{21}^k(q_kl_k,q_kz)\mathrm{A}'_{\overline{1,2k}}\right]\cdot$$

$$\cdot\left[\Phi_{22}^{j-1}(q_jl_j,q_j\xi)\cdot\Delta_{\overline{1,2j-2}}-\Phi_{12}^{j-1}(q_jl_{j-1},q_j\xi)\cdot\Delta'_{\overline{1,2j-2}}\right];j=\overline{2,k-1}$$

$$\underset{j=\overline{k+1,n}}{\mathrm{H}_{kj}^*}(p,z,\xi)=\frac{\prod_{s=k}^{s-1}q_sc_{2_s}}{q_k\cdot\Delta^*(p)}\left[\Phi_{12}^{k-1}(q_kl_{k-1},q_kz)\cdot\Delta'_{\overline{1,2k-2}}-\Phi_{22}^{k-1}(q_kl_{k-1},q_kz)\cdot\Delta_{\overline{1,2k-2}}\right]\cdot$$

$$\cdot\left[\Phi_{21}^j(q_jl_j,q_j\xi)\mathrm{A}'_{\overline{1,2j}}-\Phi_{11}^j(q_jl_j,q_j\xi)\mathrm{A}_{\overline{1,2j}}\right];$$

$$\mathrm{H}_{kk}^*(p,z,\xi)=\frac{1}{q_k\cdot\Delta^*(p)}[\Phi_{22}^{k-1}(q_kl_{k-1},q_kz)\cdot\Delta_{\overline{1,2k-2}}-\Phi_{12}^{k-1}(q_kl_{k-1},q_kz)\cdot\Delta'_{\overline{1,2k-2}}]\cdot$$

$$\cdot[\Phi_{11}^k(q_kl_k,q_k\xi)\cdot\mathrm{A}_{\overline{1,2k}}-\Phi_{21}^k(q_kl_k,q_k\xi)\cdot\mathrm{A}'_{\overline{1,2k}}];$$

$$H^*_{k,n+1}(p,z,\xi)=\frac{\prod_{s=k}^{n}q_s c_{2_s}}{q_k\Delta^*(p)}\left[\Phi^{k-1}_{22}(q_k l_{k-1},q_k z)\cdot\Delta_{\overline{1,2k-2}}-\Phi^{k-1}_{12}(q_k l_{k-1},q_k z)\cdot\Delta'_{\overline{1,2k-2}}\right]e^{-q_{n+1}(\xi-l_n)},k=\overline{1,n}$$

$$H^*_{n+1,1}(p,z,\xi)=-\frac{1}{q_1\Delta^*(p)}\prod_{s=1}^{n}c_{1_s}q_s\cdot\Phi^0_{12}(q,l_0,q,\xi)\cdot e^{-q_{n+1}(z-l_n)};$$

$$\square^*_{n+1,j}(p,z,\xi)=\frac{\prod_{s=j}^{n}c_{1_s}q_s}{q_j\cdot\Delta^*(p)}e^{-q_{n+1}(z-l_n)}\left[\Phi^{j-1}_{22}(q_j l_{j-1},q_j\xi)\cdot\Delta_{\overline{1,2j-2}}-\Phi^{j-1}_{12}(q_j l_{j-1},q_j\xi)\cdot\Delta'_{\overline{1,2j-2}}\right],j=\overline{2,n};$$

$$H^*_{n+1,n+1}(p,z,\xi)=-\frac{1}{q_{n+1}\Delta^*(p)}e^{-q_{n+1}(\xi-l_n)}\cdot\left[\Phi^{n}_{22}(q_{n+1}l_n,q_{n+1}z)\Delta_{\overline{1,2n}}-\Phi^{n}_{12}(q_{n+1}l_n,q_{n+1}z)\Delta'_{\overline{1,2n}}\right]$$

.

Here $A_{\overline{1,2k}}$ – determinant formed from the determinant of the system $\Delta^*(p)$ by deleting the first *2k* rows and columns (under the numbers $\overline{1,2k}$, $k=\overline{1,n}$); $A'_{\overline{1,2k}}$ – determinant formed from the determinant of the system $\Delta^*(p)$ by deleting the first *2k+1* lines except *2k*–th (under the numbers $\overline{1,2k-1},2k+1;k=\overline{1,n}$) and the first *2k* columns (under numbers $\overline{1,2k},k=\overline{1,n}$); $\Delta_{\overline{1,2k}}$ – determinant formed from the first *2k* rows and columns (under numbers $\overline{1,2k},k=\overline{1,n}$) determinant of the system $\Delta^*(p)$; $\Delta'_{\overline{1,2k}}$ – determinant formed from the first *2k+1* lines except *2k*–th (under numbers $\overline{1,2k-1},2k+1;k=\overline{1,n}$) and the first *2k* columns (under numbers $\overline{1,2k},k=\overline{1,n}$) of the determinant of the system.

Recurrent algorithms for calculating determinants $A_{\overline{1,2k}}$ $A'_{\overline{1,2k}}$ $\Delta_{\overline{1,2k}}$ $\Delta'_{\overline{1,2k}}$ and matrix elements $\left[H^*_{ij}(p,z,\xi)\right]$, $i,j=\overline{1,n+1}$ were filed in [20].

Special points of functions of influence of a boundary value problem (5.119) - (5.123) $H^*_{k,k_1}(p,z,\xi),k,k_1=\overline{1,n+1}$ there are branching points $p=-\gamma_k^2,k=\overline{1,n+1}$ and $p=\infty$. As a result of Lem Jordan and Cauchy's theorem

[29], we have the following formulas for finding the original functions of influence $\mathrm{H}^{*}_{k,k_1}(p,z,\xi), k,k_1=\overline{1,n+1}$:

$$\square_{k,k_1}(t,z,\xi)=L^{-1}\left[\square^{*}_{k,k_1}(p,z,\xi)\right]=-\frac{2}{\pi}\int_0^{\infty}\square\mathrm{m}\left[\square^{*}_{k,k_1}(-(\beta^2+\gamma^2),z,\xi)\right]\cdot e^{-(\beta^2+\gamma^2)}\beta d\beta. \qquad (5.145)$$

We assumed that $\gamma^2=\max\{\gamma_k^2\}_{k=1}^{n+1}$ and put $q_k=ib_k$, де $b_k=(\beta^2+k^2_k)^{1/2}D^{-1/2}_k$, $k^2_k=\gamma^2-\gamma^2_k\geq 0$, $k=\overline{1,n+1}$. Directly counting, we obtain:

$$\Delta_{m1}\left(ib_kl_{k-1},ib_kl_k\right)=i\cdot\delta_{m1}(b_kl_{k-1},b_kl_k)\equiv i\cdot[v^{k-1,1}_{m2}(b_kl_{k-1})\cdot v^{k2}_{11}(b_kl_k)-v^{k-1,2}_{m2}(b_kl_{k-1})\cdot v^{k1}_{11}(b_kl_k)]$$

$$\Delta_{m2}\left(ib_kl_{k-1},ib_kl_k\right)=i\cdot\delta_{m2}(b_kl_{k-1},b_kl_k)\equiv i\cdot[v^{k-1,1}_{m2}(b_kl_{k-1})\cdot v^{k2}_{21}(b_kl_k)-v^{k-1,2}_{m2}(b_kl_{k-1})\cdot v^{k1}_{21}(b_kl_k)]$$

$$\Delta_{m1}\left(ib_1l_0,ib_1l_1\right)=i\cdot\delta_{m1}(b_1l_0,b_1l_1)\equiv i\cdot[v^{01}_{11}(b_1l_0)\cdot v^{12}_{m1}(b_1l_1)-v^{02}_{11}(b_1l_0)v^{11}_{m1}(b_1l_1)];m=\overline{1,2}$$

$$\Delta_{\overline{1,2}}\left(ib_1\right)=i\cdot\delta_{\overline{1,2}}(\beta)\equiv i\cdot\delta_{11}(b_1l_0,b_1l_1);\Delta'_{\overline{1,2}}\left(ib_1\right)=i\cdot\delta_{\overline{1,2}}(\beta)\equiv i\cdot\delta_{21}(b_1l_0,b_1l_1)$$

$$\Delta_{\overline{1,2k}}\left(i\beta\right)=i^k\cdot[\delta_{11}(b_kl_{k-1},b_kl_k)\cdot\delta'_{\overline{1,2k-2}}(\beta)-\delta_{21}(b_kl_{k-1},b_kl_k)\cdot\delta_{\overline{1,2k-2}}(\beta)]\equiv i^k\cdot\delta_{\overline{1,2k}}(\beta)$$

$$\Delta'_{\overline{1,2k}}\left(i\beta\right)=i^k\cdot[\delta_{12}(b_kl_{k-1},b_kl_k)\cdot\delta'_{\overline{1,2k-2}}(\beta)-\delta_{22}(b_kl_{k-1},b_kl_k)\cdot\delta_{\overline{1,2k-2}}(\beta)]\equiv i^k\cdot\delta_{\overline{1,2k}}(\beta)$$

$$\Delta^{*}\left(-(\beta^2+\gamma^2)\right)=i^n\cdot\left[\left(i\cdot\overline{\alpha}^n_{22}\cdot b_{n+1}-\overline{\beta}^n_{22}\right)\delta_{\overline{1,2n}}(\beta)-\left(i\cdot\overline{\alpha}^n_{12}\cdot b_{n+1}-\overline{\beta}^n_{12}\right)\delta'_{\overline{1,2n}}(\beta)\right]=$$

$$=i^n\cdot\left\{\left[\overline{\beta}^n_{12}\delta'_{\overline{1,2n}}(\beta)-\overline{\beta}^n_{22}\delta_{\overline{1,2n}}(\beta)\right]-i\cdot b_{n+1}\left[\overline{\alpha}^n_{12}\cdot\delta'_{\overline{1,2n}}(\beta)-\overline{\alpha}^n_{22}\cdot\delta'_{\overline{1,2n}}(\beta)\right]\right\}$$

$$V^{k1}_{jm}(i\cdot q_sl_k)=v^{k1}_{jm}(b_sl_k);V^{k2}_{jm}(i\cdot q_sl_k)=i\cdot v^{k2}_{jm}(b_sl_k);\Phi^{k}_{jm}(i\cdot b_sl_k,i\cdot b_kz)=i\cdot\varphi^{k}_{jm}(b_sl_k,b_sz),j,m=\overline{1,2}$$

$$v^{k1}_{jm}(b_sl_k)=-\alpha^k_{jm}b_s\sin b_sl_k+\beta^k_{jm}\cos b_sl_k;v^{k2}_{jm}(b_sl_k)=\alpha^k_{jm}b_s\cos b_sl_k+\beta^k_{jm}\sin b_sl_k$$

;

$$\varphi^k_{jm}(b_sl_k,q_sz)=v^{k2}_{jm}(b_sl_k)\cos b_sz-v^{k1}_{jm}(b_sl_k)\sin b_sz\ ;$$

$$\overline{\alpha}^k_{jm}=\alpha^k_{jm}-\delta^k_{jm}(\beta^2+\gamma^2);\overline{\beta}^k_{jm}=\beta^k_{jm}-\gamma^k_{jm}(\beta^2+\gamma^2).$$

Define numerical matrices $A_{j1,k}=\begin{bmatrix}\alpha^k_{1j} & \beta^k_{1j}\\ \alpha^k_{2j} & \beta^k_{2j}\end{bmatrix}, A_{j2,k}=\begin{bmatrix}\delta^k_{1j} & \gamma^k_{1j}\\ \delta^k_{2j} & \gamma^k_{2j}\end{bmatrix}, j=1,2;k=\overline{1,n};$ and numerical values:

$$c_{j1,k} = -\det A_{j1,k} \equiv \alpha_{2j}^k \beta_{1j}^k - \alpha_{1j}^k \beta_{2j}^k;\ c_{j2,k} = -\det A_{j2,k} \equiv \delta_{2j}^k \lambda_{1j}^k - \delta_{1j}^k \gamma_{2j}^k$$

$$c_{j1,j2}^{12,k} = \alpha_{1j}^k \gamma_{2j}^k - \alpha_{2j}^k \gamma_{2j}^k;\ c_{j1,j2}^{21,k} = \beta_{1j}^k \delta_{2j}^k - \beta_{2j}^k \delta_{1j}^k.$$

Because $\overline{c}_{jk} = c_{1j,k} + (c_{j1,j2}^{21,k} - c_{j1,j2}^{12,k})p + c_{j2,k}p^2$, then we demand the equality $c_{j1,j2}^{12,k} = c_{j1,j2}^{21,k}, c_{j2,k} = 0, j = 1,2; k = \overline{1,n}.$ Regarding numbers $c_{j1,k}$ will require that $c_{11,k}c_{21,k}>0$.

Define the functions:

$$V_1(z,\beta) = c_{21,1}b_2 \cdot \left[\omega_{02}(\beta)\cos b_1 z - \omega_{01}(\beta)\sin b_1 z\right]; \tag{5.146}$$

$$V_k(z,\beta) = \left(\prod_{j=k}^{n} c_{21,j}b_{j+1}\right) \cdot \left[\omega_{k-1,2}(\beta)\cos b_k z - \omega_{k-1,1}(\beta)\sin b_k z\right]; \tag{5.147}$$

$$V_{n+1}(z,\beta) = \omega_{n,2}(\beta)\cos b_{n+1} z - \omega_{n+1,1}(\beta)\sin b_1 z; \tag{5.148}$$

Here

$$\omega_{01}(\beta) = v_{11}^{01}(b_1 l_0); \omega_{02}(\beta) = v_{11}^{02}(b_1 l_0);$$

$$\omega_{km}(\beta) = \omega_{k-1,2}(\beta) \cdot \psi_{1m}^k(b_k l_k, b_{k+1} l_k) - \omega_{k-1,1}(\beta) \cdot \psi_{2m}^k(b_k l_k, b_{k+1} l_k); \tag{5.149}$$

$$\psi_{jm}^k(b_k l_k, b_{k+1} l_k) = v_{11}^{kj}(b_k l_k) \cdot v_{22}^{km}(b_{k+1} l_k) - v_{21}^{kj}(b_k l_k) \cdot v_{12}^{km}(b_{k+1} l_k)$$

We introduce a spectral function

$$V(z,\beta) = \sum_{k=1}^{n} V_k(z,\beta)\theta(z - l_{k-1})\theta(l_k - z) + V_{n+1}(z,\beta)\theta(z - l_n), \tag{5.150}$$

spectral density

$$\Omega_n(\beta) = \frac{\beta}{b_{n+1} \cdot \left[\omega_{n,1}(\beta)^2 + \omega_{n,2}(\beta)^2\right]} \tag{5.151}$$

and weight function

$$\sigma(z) = \sum_{k=1}^{n} \sigma_k(z,\beta)\theta(z - l_{k-1})\theta(l_k - z) + \sigma_{n+1}(z,\beta)\theta(z - l_n) \tag{5.152}$$

$$\sigma_k = \prod_{j=k}^{n} \frac{c_{11,j}}{c_{21,j}} \frac{1}{D_k}, k = \overline{1,n-1}; \sigma_n = \frac{c_{11,n}}{c_{21,n}} \frac{1}{D_n}; \sigma_{n+1} = \frac{1}{D_{n+1}}. \tag{5.153}$$

As a result of the specified in formula (5.145) operations, we have the original elements of the matrix of influence functions:

$$\mathrm{H}_{jk}(t,z,\xi)=\frac{2}{\pi}\int_0^{\infty}e^{-(\beta^2+\gamma^2)t}V_j(z,\beta)V_k(\xi,\beta)\Omega_n(\beta)\sigma_k D_k d\beta;\ j,k=\overline{1,n+1}. \tag{5.154}$$

Returning in formulas (5.144) to the originals, we obtain a single solution to the parabolic boundary value problem (5.119) - (5.123):

$$u_k(t,z)=\frac{2}{\pi}\int_0^{\infty}e^{-(\beta^2+\gamma^2)t}V_k(z,\beta)\sum_{k_1=1}^{n+1}\int_{l_{k_1-1}}^{l_{k_1}}V_{k_1}(\xi,\beta)g_{k_1}(\xi)\sigma_{k_1}d\xi\cdot\Omega_n(\beta)d\beta, \tag{5.155}$$
$$j=\overline{1,n+1},l_{n+1}=\infty$$

From here, due to the initial conditions (5.120), we obtain an integrated image:

$$g_k(z)=\frac{2}{\pi}\int_0^{\infty}V_k(z,\beta)\Omega_n(\beta)\int_{l_{k-1}}^{l_k}V_k(\xi,\beta)g_k(\xi)\sigma_{k_1}d\xi d\beta\,. \tag{5.156}$$

If we put $g(z)=\sum_{k=1}^{n}\theta(z-l_{k-1})\theta(l_k-z)g_k(z)+\Theta(z-l_n)g_{n+1}(z)$ and spectral density functions defined by (5.153), (5.154), the integral image (5.155) can be written in invariant form:

$$g(z)=\frac{2}{\pi}\int_0^{\infty}V(z,\beta)\Omega_n(\beta)\int_{l_0}^{\infty}V(\xi,\beta)g(\xi)\sigma(\xi)d\xi d\beta \tag{5.157}$$

The integral image (5.155) defines a straight line $F_{+,n+1}$ and inverse $F_{+,n+1}^{-1}$ integral Fourier transform with spectral parameter for n -component heterogeneous medium:

$$F_{+,n+1}[g(z)]=\int_{l_0}^{\infty}g(z)V(z,\beta)\sigma(z)dz\equiv\tilde{g}(\beta), \tag{5.158}$$

$$F_{+,n+1}^{-1}[\tilde{g}(\beta)]=\int_0^{\infty}\tilde{g}(\beta)V(z,\beta)\Omega_n(\beta)d\beta\equiv g(z)\,. \tag{5.159}$$

Mathematical substantiation of the introduced formulas (5.150) (5.151) of integral Fourier transform is a statement:

Theorem 5.3.1 (*about the integrated image*): *If the vector-function g(z) continuous, absolutely summed up and she has limited variation on the set then for any* $z \in I_n^+$ *integral image is fair* (5.150).

Proof: Functions $V_j(z,\beta)$ and $V_j(z,\lambda)$ by construction satisfy the differential equations:

$$\left[\frac{d^2}{dz^2} + (\beta^2 + k_j^2)D_j\right]V_j(z,\beta) = 0, \tag{5.160}$$

$$\left[\frac{d^2}{dz^2} + (\lambda^2 + k_j^2)D_j\right]V_j(z,\lambda) = 0. \tag{5.161}$$

Multiply equality (5.133) by the function $V_j(z,\lambda)$, and equality (5.160) by the function $V_j(z,\beta)$ and subtract the second from the first:

$$V_j(z,\beta)V_j(z,\lambda) = \frac{D_j}{\beta^2+\lambda^2}\frac{d}{dz}\left[V_j(z,\beta)\frac{d}{dz}V_j(z,\lambda) - V_j(z,\lambda)\frac{d}{dz}V_j(z,\beta)\right]. \tag{5.162}$$

Let's set a fairly large number $A > l_n$. Due to the properties of the functions $V_j(z,\beta)V_j(z,\lambda)$, structures of constants σ_k and equality (5.152) we receive the following:

$$\int_{l_0}^{A} V(x,\beta)V(x,\lambda)\sigma(x)dx = \frac{1}{\beta^2-\lambda^2}\left[V_{n+1}(A,\beta)\frac{d}{dx}V_{n+1}(A,\lambda) - V_{n+1}(A,\lambda)\frac{d}{dx}V_{n+1}(A,\beta)\right] \tag{5.163}$$

Non-integral term in a point $z = l_0$ equal to zero due to the boundary condition at the point $z=l_0$ function $V_1(z,\ldots)$, non-integral terms in points $z = l_k$ turn to zero due to selection σ_k, and interface conditions (we will remind, that $g_0=0$, $\psi_{jk}=0$, $j=1,2$; $k=\overline{1,n}$). For arbitrary positive numbers c and d ($c < d$) and arbitrary limited to the segment $[c, d]$ of functions $\psi(\beta)$, calculate the double integral:

$$\begin{aligned} J_n &= \frac{2}{\pi}\int_{l_0}^{\infty}\int_{c}^{d}\psi(\beta)V(z,\beta)\Omega_n(\beta)d\beta V(z,\lambda)\sigma(z) = \\ &= \lim_{A\to\infty}\frac{2}{\pi}\int_{l_0}^{A}\int_{c}^{d} g(\beta)V(z,\beta)\Omega_n(\beta)d\beta V(z,\lambda)\sigma(z). \end{aligned} \tag{5.164}$$

Due to equality (5.163) double integral (5.164) takes the form:

$$J_n = \lim_{R\to\infty} \frac{2}{\pi} \int_c^d \frac{\psi(\beta)}{\beta^2 - \lambda^2} \left[V_{n+1}(A,\beta) V'_{n+1}(A,\lambda) - V_{n+1}(A,\lambda) V'_{n+1}(A,\beta) \right] \Omega_n(\beta) d\beta. \quad (5.165)$$

We receive directly:

$$\begin{aligned} 2\left[V_{n+1}(A,\beta) V'_{n+1}(A,\lambda) - V_{n+1}(A,\lambda) V'_{n+1}(A,\beta) \right] &= z^-_{n+1} \left[\omega_{n2}(\beta)\omega_{n2}(\lambda) - \omega_{n1}(\beta)\omega_{n1}(\lambda) \right] \sin z^+_{n+1} A + \\ + z^+_{n+1} \left[\omega_{n1}(\beta)\omega_{n1}(\lambda) + \omega_{n2}(\beta)\omega_{n2}(\lambda) \right] \sin z^-_{n+1} A + z^-_{n+1} \left[\omega_{n1}(\beta)\omega_{n2}(\lambda) + \omega_{n1}(\lambda)\omega_{n2}(\beta) \right] \cos z^+_{n+1} A + \\ + z^+_{n+1} \left[\omega_{n1}(\beta)\omega_{n2}(\lambda) - \omega_{n1}(\lambda)\omega_{n2}(\beta) \right] \cos z^-_{n+1} A; z^\pm_{n+1} = b_{n+1}(\beta) \pm b_{n+1}(\lambda). \end{aligned} \quad (5.166)$$

Assuming that function $\psi(\beta)$ is continuous, fully integrated and has limited variation on the set *[c, d]*, substitution (5.158) into (5.157) followed by the use of Riemann and Dirichlet lemmas [12] leads to equality

$$\frac{2}{\pi} \int_{l_0}^{\infty} \int_c^d \psi(\beta) V(z,\beta) V(z,\lambda) \Omega_n(\beta) d\beta \sigma(z) dz = \begin{cases} \psi(\lambda), & \lambda \in [c,d], \\ 0, & \lambda \Subset [c,d]. \end{cases} \quad (5.167)$$

If the function $\psi(\beta)$ has the above properties on the interval (0,∞), then we get:

$$\frac{2}{\pi} \int_{l_0}^{\infty} \int_0^{\infty} \psi(\beta) V(z,\beta) V(z,\lambda) \Omega_n(\beta) d\beta \sigma(z) dz = \begin{cases} \psi(\lambda), & \lambda \in (0,\infty) \\ 0, & \lambda \Subset (0,\infty) \end{cases}. \quad (5.168)$$

Suppose that a vector is a function $g(z)$ that looks like

$$g(z) = \frac{2}{\pi} \int_0^{\infty} \psi(\beta) V(z,\beta) \Omega_n(\beta) d\beta. \quad (5.169)$$

Multiply (5.168) by $V(z,\lambda)\sigma(z)dz$, where λ - arbitrary positive number and integrated from $z=l_0$ to $z=\infty$. Based on equality (5.168) we obtain:

$$\int_{l_0}^{\infty} g(z) V(z,\lambda) \sigma(z) dz = \psi(\lambda) S_+(\lambda);\ S_+(\lambda) = \begin{cases} 1, & \lambda > 0, \\ 0, & \lambda < 0. \end{cases}$$

If now we substitute the function $g(\beta) = \int_{l_0}^{\infty} f(\xi) V(\xi,\beta) \sigma(\xi) d\xi$ in equation (5.169), then we obtain the formula (5.155) - integral image of a vector function $g(z)=\{g_1(z), g_2(z), \ldots, g_{n+1}(z,\}$. The proof of the theorem is complete.

In order to apply the obtained integral transformation to construct exact analytical solutions to mathematical models we obtain the basic identity of the integral transformation of the differential operator L_n.

Theorem 5.3.2 (*about the basic identity*). *Let the relations hold:*

$$C_{11,k} \cdot C_{21,k} > 0, \quad C_{j2,k} = 0, \quad C^{21,k}_{j1,j2} = C^{12,k}_{j1,j2}; \quad j = 1,2; \; k = \overline{1,n} \tag{5.170}$$

If the vector-function $g(x) \in C^{(3)}(I_n^+)$, *satisfies boundary conditions:*

$$\left(\bar{\alpha}^0_{11}\frac{d}{dz} + \bar{\beta}^0_{11}\right) g_1(z)\Big|_{z=l_0} = g_{10}, \qquad \lim_{z\to\infty}\left[\frac{d^m}{dz^m} g_{n+1}(z)\right] = 0, \; m = 0,1 \tag{5.171}$$

and coupling conditions (5.171), *then the basic identity of the integral transformation of the differential operator comes true* L_n*:*

$$\begin{aligned} F_{+,n}\{L_n[g(z)]\} &= -b^2 \times g(b) - s_1 D_1 (\bar{a}^0_{11})^{-1} V_1(l_0, b) \times g_{10} - \\ &- \sum_{j=1}^{n} k_j^2 \int_{l_{j-1}}^{l_j} g_j(z) V_j(z,b) s_j dx - k_{n+1}^2 \int_{l_n}^{A} g_{n+1}(z) V_{n+1}(z,b) s_{n+1} dz \end{aligned} \tag{5.172}$$

Proof: Because the functions $g_j(z)$ and $V_j(z,b)$ $\left(j = \overline{1,n+1}\right)$ satisfy the system of interface conditions (5.115), then when performing relations (5.163) we obtain the basic identity:

$$\begin{aligned} &\left\{\tilde{g}_j(z) V_j(z,b) - g_j(z) \tilde{V}_j(z,b)\right\}_{z=l_j} = \\ &= \frac{c_{21,j}}{c_{11,j}} \left\{\tilde{g}_{j+1}(z) V_{j+1}(z,b) - g_{j+1}(z) \tilde{V}_{j+1}(z,b)\right\}_{z=l_j}; j = \overline{1,n} \end{aligned} \tag{5.173}$$

Integrate twice in parts in the left part (5.165) under the signs of integrals:

$$\begin{aligned} F_{+,n}\{L_n[g(z)]\} &= \sum_{j=1}^{n} D_j \int_{l_{j-1}}^{l_j} \frac{d^2 g_j(z)}{dz^2} V_j(z,b) s_j dz + D_{n+1} \int_{l_n}^{A} \frac{d^2 g_{n+1}(z)}{dz^2} V_{n+1}(z,b) s_{n+1} dz = \\ &= \sum_{j=1}^{n} D_j s_j \left(\tilde{g}_j(z) V_j(z,b) - g_j(z) \tilde{V}_j(z,b)\right)\Big|_{z=l_{j-1}}^{z=l_j} + \left(\tilde{g}_{j+1}(z) V_{j+1}(z,b) - g_{j+1}(z) \tilde{V}_{j+1}(z,b)\right)\Big|_{z=l_n}^{A} - \\ &- \sum_{j=1}^{n+1} \left(b^2 + k_j^2\right) \int_{l_{j-1}}^{l_j} g_j(x) V_j(x,b) s_j dx, \; l_{n+1} = A \end{aligned} \tag{5.174}$$

Non-integral terms in points $z = l_j (j = \overline{1,n})$ become zero due to the basic identity (5.173) and structure $s_k, \left(k = \overline{1,n+1}\right)$. Non-integral term in a point $x = l_0$ turns into a view $\left(\partial \varphi_{11}^{0}\right)^{-1} V_1(l_0, b) g_{10}$. Due to the condition of behavior $g_{n+1}(z)$ about $z \to A$ we have:

$$\lim_{z \to A} \left(\breve{g}_{n+1}(z) V_{n+1}(z,b) - g_{n+1}(z) \breve{V}_{n+1}(z,b)\right) = 0.$$

Dividing the remaining amount into two, we come to an identity (5.172).

Conclusions

The monograph highlights new approaches to the creation of high-performance supercomputer technologies of multiparameter identification of complex cyberphysical systems (neuro-bio-nanomedical and nanoporous physical systems) with feedback-connections and interactions, including cognitive ones for neuro- biosystems on the basis of parallel computations to determine the parameters of their behavior and the state of individual executive elements of systems. High-performance supercomputer technologies for identification of complex feedback systems (neuro-bio- and nanoporous CPSS) are proposed, in the development of which new science-intensive technologies and computational solutions are used, which have practical application for the development of the European socio-economic systems. The first type of development is related to solving an important social problem - the introduction of effective mobile digital technologies for neurological diagnosis of patients with severe signs of tremor (in the world there are about 100 ml. of such people). The studied nanomedical neuro-bio-system is focused on determining the parameters of abnormal movements of patients with tremor-signs (T-object) caused by the negative effects of a number of neural nodes of cerebral cortex. The second type of information systems being developed is nanoporous cybersystems related to an important global environmental problem - finding ways to reduce the impact of global warming and implementing a European strategy for safe energy by drastically reducing air pollution caused by harmful emissions of carbon products (CO2, CO) and transport, which requires constant research and development of new science-intensive absorption technologies (adsorption and catalysis), the main elements of which are nanoporous catalysts of a new generation. In this context, the main results obtained are as follows.

1. A hybrid model of a neuro feedback system has been developed, which describes the state and behavior of tremors (T) objects based on wave signal propagation.

2. New science-intensive mathematical models of nanoporous CPSoS are built, which take into account a set of limiting physical factors and inverse influences and nano-sources in the competent nanosorption processes occurring in them.

3. High-speed analytical solutions to both classes of feedback models are obtained on the basis of parallelization of calculations and efficient linearization schemes, methods of hybrid integral transformations (Fourier, Bessel) and Heaviside operating method, including adaptive matrices (response) for determining parameters of feedback states, interactions (groups of neuro-objects and nano-sources).

4. The hybrid spectral function of ANM, systems of orthogonal basic functions and spectral values of hybrid transformation of construction of solutions of feedback-models are constructed.

5. Models of multiparameter identification of the specified feedback-systems are developed, including minimization of residual functionalities, and constructing the explicit expressions of gradients of residual functionalities on their basis. High-performance regularization identification algorithms have been constructed, which allow parallelization of calculations taking into account the supercomputer architecture of computer systems.

6. Software is developed for high-performance super-computer identification technologies and modeling tools based on parallel computations of complex feedback systems (neuro-bio- and nanoporous systems), which is an important step in the development and implementation of digital neurodiagnostics and effective strategy for implementation of secure energy based on modern cyberphysical systems, science-intensive technologies and artificial intelligence. The results are new, have a high degree of generalization, and are based on modern neurobiological, nanomedical and nanophysical representations, fundamental laws of transfer, catalysis, cognitive feedback-neuro-bio-interactions and nanoprocesses in media of nanoporous structure particles, on the application of the theory of control of complex systems, gradient methods of parameter identification, software engineering. The results lead to the increase in the quality and accuracy of identifying and recognizing relationships and interactions; make it possible to significantly optimize the amount of calculations by parallelization, reduce the number of computing elements; provide real-time growth in data requirements, develop platform-independent dynamic software architectures of the studied feedback systems.

References

1. Rajaraman V., Jack D., Adamovich S.V., Hening W., Sage J., Poizner H. A novel quantitative method for 3D measurement of Parkinsonian tremor. Clinical neurophysiology, 11(2), 187-369 (2000)
2. Haubenberger D, Kalowitz D, Nahab F B, Toro C, Ippolito D, Luckenbaugh DA, Wittevrongel L, Hallett M. Validation of Digital Spiral Analysis as Outcome Parameter for Clinical Trials in Essential Tremor. Movement Disorders 26 (11), 2073-2080, (2011)
3. Legrand A.P., Rivals I., Richard A., Apartis E., Roze E., Vidailhet M., Meunier S., Hainque E. New insight in spiral drawing analysis methods – Application to action tremor quantification. J Clinical Neurophysiology, 128 (10), 1823–1834. (2017)
4. Wang J.-S., Chuang F.-C. An Accelerometer-Based Digital Pen with a Trajectory Recognition Algorithm for Handwritten Digit and Gesture Recognition. IEEE Transactions on Industrial Electronics, 59(7), 2998-3007 (2012)
5. Louis, E. D., Gillman, A., Böschung, S., Hess, C. W., Yu, Q., & Pullman, S. L. High width variability during spiral drawing: Further evidence of cerebellar dysfunction in essential tremor. Cerebellum, 11, 872-879 (2012).
6. Unger N., Bond T.C., Wang J.S., Koch D.M., Menon S., Shindell D.T., Bauer S. Attribution of climate forcing to economic sectors, Proc. Natl. Acad. Sci., 107(8), 3382-7 (2010).
7. Puertolas B., Navarro M.V., Lopez J.M., Murillo R., Mastral A.M., Garcia T. Modelling the heat and mass transfers of propane onto a ZSM-5 zeolite / Separation and Purification Technology 86, 127–136 (2012)
8. Krisnha R., Van Baten J.M.I nvestigating the Non-idealities in Adsorption of CO 2 -bearing Mixtures in Cation-exchanged Zeolites. Separation and Purification Technology 2018, Volume 206, 208-217.
9. Ruthven D.M. Principles of Adsorption and Adsorption Processes, John Wiley, New York, 1984. 433 p
10. Kärger J., Ruthven D., Theodorou D. Diffusion in Nanoporous Materials. Hoboken, John Wiley & Sons, 2012, 660 p.

11. Leniuk M. P., Petryk M.R. The Methods of integral transformations in the problems of mathematical modeling of masstranser in heterogeneus media. Kyiv: Naukova Dumka. - 2000. - 372 p.
12. Khimich A.N., Petryk M.R., Mykhalyk D.N., Boyko I.V., Popov A.V., Sydoruk. V.A. Methods for mathematical modeling and identification of complex processes and systems based on visoproductive computing (neuro- and nanoporous cyber-physical systems with feedback, models with sparse structure data, parallel computing). Kiev: National Academy of Sciences of Ukraine. Glushkov Institute of Cybernetics. 2019. - 188 p.
13. Mykhalyk D., Mudryk I., Hoi A., Petryk M. Modern hardware and software solution for identification of abnormal neurological movements of patients with essential tremor. IEEE. Proceeding of 2019 9th International Conference on Advanced Computer Information Technologies (ACIT, Budejovice, Czech Republic), 183-186 (2019)
14. Petryk M.R., Mykhalyk D.M., Mudryk I.Ya. Method for digital measurement of parameters of abnormal neurological movements of upper extremities in patients with tremor. Utility model patent №130247, Bul. №22 від 26.11.2018.
15. Lecler S., Petryk M., Canet D., Fraissard J. Competitive Diffusion of Gases in a Zeolite Using Proton NMR and Sclice Selection Procedure. Catalysis Today, Elsevier B.V., 187(1), 104-107 (2012)
16. Petryk M., Leclerc S., D. Canet, Sergienko I.V., Deineka V.S., Fraissard J. The Competitive Diffusion of Gases in a zeolite bed: NMR and Slice Procedure, Modelling and Identification of Parameters. The Journal of Physical Chemistry C. ACS, 119 (47), 26519-26525 (2015).
17. Petryk M.R., Khimich O.M., Boyko I.V, Mykhalyk D.M., Petryk M.M., Kovbashyn V.I. Mathematical modeling of heat transfer and adsorption of hydrocarbons in nanoporous media of exhaust gas neutralization systems. National Academy of Sciences of Ukraine. Kyiv, 2018, 280 p.
18. Petryk M., Khimitch A., Petryk M.M. Simulation of Adsorption and Desorption of Hydrocarbons in Nanoporous Catalysts of Neutralization Systems of Exhaust Gases Using Nonlinear Langmuir Isotherm. Journal of Automation and Information Sciences, Begell House USA, 50 (10), 18-33 (2018)

19. Petryk M., Khimitch A., Petryk M.M., Fraissard J. Experimental and computer simulation studies of dehydration on microporous adsorbent of natural gas used as motor fuel. Fuel. Vol. 239, 1324–1330 (2019)
20. Sergienko I.V., Petryk M.R., Leclerc S., Frassard J. mathematical modeling of masstranser in media of nanoporous structure particles. — Kyiv: National Academy of Ukraine. V.M. Glushkov Institut cybernetics. — 2014. — 210 p.
21. I.V. Sergienko, V.S. Deineka, Optimal Control of Distributed Systems with Conjugation Conditions, New York: Kluwer Academic Publishers 2005.
22. A.N. Tikhonov, V.Y. Arsenin. Solutions of Ill-Posed Problems, Washington D.C.: V.H. Winston; New York: J. Wiley 1977.
23. J.-L. Lions, Perturbations Singulières dans les Problèmes aux Limites et en Contrôle Optimal, New York: Springer. Lecture Notes in Math. Ser. 2008.
24. Sergienko. I.V., Petryk M.R, Leclerc S., Fraissard J. Highly Efficient Methods of the Identification of Competitive Diffusion Parameters in Heterogeneous Media of Nanoporous Particles. Cybernetics and Systems Analysis. Springer, 51(4), 529-546 (2015).
25. Ivanchov M. Inverse Problems for Equations of Parabolic Type. Mathematical Studies. Monograph Series. Vol. 10, Lviv: VNTL Publishers 2003.
26. Petryk M., Ivanchov M., Leclerc S., Canet D., Fraissard J. Competitive Adsorption and Diffusion of Gases in a Microporous Solid.In the book "Zeolites – New Challenges". IntecOpen London, UK. P.1-23. (2019) https://www.intechopen.com/online-first/competitive-adsorption-and-diffusion-of-gases-in-a-microporous-solid
27. Landau L. To the theory of phase transitions. I.ZPhys. Ztshr Sow, 1937, Bd. 7. S. 19.
28. Prudnikov A.P., Brichkov Yu.A. Marychev O.I. Integrals and series. Additional chapters, Nauka, Moscow, 1986, 800 p.
29. Lavrentiev M.A., Shabat B.V. Methods of theory of functions of a complex variable. M.: Nauka, 1973, 736 p.
30. Petryk M., Khimich A., Mykhalylk M., Boyko I., Kovbachun V. High-performance computing technologies of modeling and identification of adsorption in nanoporous systems with feedbacks for gas purification. Vistyk of TNTU. Vol. 3, 139-145 (2019)

31. Petryk M., Khimitch A., Petryk M.M. Simulation of Adsorption and Desorption of Hydrocarbons in Nanoporous Catalysts of Neutralization Systems of Exhaust Gases Using Nonlinear Langmuir Isotherm. Journal of Automation and Information Sciences 2018. Volume 50 (10), 18-33
32. Information website Top500 The List // Access the resource: http://www.top500.org
33. Gorodetsky A.S., Evzerov I.D. Computer models of constructions. Kyiv: Fakt, 2007. 394 p.
34. Khimich A.N., Molchanov I.N., Popov A.V., Chistyakova T.V., Yakovlev M.F. Parallel algorithms for solving computational mathematics problems. Kyiv: Naukova Dumka, 2008.- 248 p.
35. Nesterenko A.N., Khimich A.N., Yakovlev M.F. Some problems of solving systems of nonlinear equations on multiprocessor computing systems with distributed memory. Bulletin of computer and information technologies. Moskow: 2006, Vol. 10, 54 – 56.
36. Nesterenko A.N., Popov A.V., Rudich A.V. Solving systems of nonlinear equations on computers with parallel organization of calculations. Mathematical and computer modeling. Series: Physical and Mathematical Sciences. Coll. of Scient. work. 2019, Vol. 19, 85–91
37. E.A. Velikoivanenko, A.S. Milenin, A.V. Popov, V.A. Sidoruk, A.N. Khimich. Methods of Numerical Forecasting of Serviceability of Welded Structures on Computers of Hybrid Architecture. Cybernetics and Systems Analysis, Vol. 53(1), January, 2019, 117-127
38. Khimich A.N., Popov A.V., Chistyakov A.V. Hybrid algorithms for solving the algebraic problem of eigenvalues with sparse matrices. Cybernetics and systems analysis. 2017, Vol. 53(6), 132 – 146.
39. George A., Liu J. Numerical solution of large sparse systems of equations. Moskow: Mir, 1984, 334p.
40. http://software.intel.com/en-us/intel-mkl. [Electronic resource]
41. http://developer.download.nvidia.com/CUBLAS Library.pdf. . [Electronic resource] CUBLAS Linear Algebra

42. Popov A.V. Parallel algorithms for solving linear systems with sparse symmetric matrices. Problems of programming, 32-3, 2008. Special. output. Proceedings of the Sixth International Scientific and Practical Conference. on programming UkrProg'2008, 111-118.
43. Khimich A.N., Popov A.V., Polyanko V.V. Algorithms of parallel calculations for problems of linear algebra with matrices of irregular structure. Cybernetics and systems analysis. 2011. Vol. 6, 159-174.
44. Khimich A.N., Popov A.V., Polyanko V.V. Problems of parallel and distributed computations in the study of mathematical models with sparse data structures. Proceedings of the International Scientific Conference "Computational Optimization (VO-XL)". Kyiv: V.M. Glushkov Institute of Cybernetics. NAS of Ukraine. 2013, 267-268.
45. Khimich A.N., Baranov A.Yu. Hybrid algorithm for solving linear systems with tape matrices by direct methods. Computer Mathematics 2013, Vol. 2, 80-87.
46. Popov O.V. On parallel algorithms for factorization of sparse matrices. Computer Mathematics. 2013, Vol. 2, 115-124.
47. Velykoivanenko E.A., Milenin A.S., Popov A.V., Sydoruk V.A., Khimich A.N. Methods and Technologies of Parallel Computing for Mathematical Modeling of Stress-Strain State of Constructions Taking into Account Ductile Fracture. Journal of Automation and Information Sciences **2014**. Volume 46 (11), 23-35
48. Baranov A.Yu. Hybrid algorithm for factorization of tape asymmetric matrices. Theory of optimal solutions. 2015, 22-28.
49. Khimich A.N., Sydoruk V.A. Tiled algorithm for factorization of a sparse matrix. Computer Mathematics, 2015. Vol. 2, 109-116.
50. Popov A.V. Rudich O.V. Research of parallel algorithm for solving linear systems with tape asymmetric matrix. Proceedings of the All-Ukrainian scientific-practical conference with international participation "Informatics and systems sciences (CCI-2015)", Poltava, March 19-21, 2015.
51. Baranov A. Yu., Slobodyan Y. E., Popov A.B., Khimich A.N. Mathematical Modeling of Building Constructions Using Hybrid Computing Systems. Journal of Automation and Information Sciences **2017**. Volume 50 (7), 18-32

52. Popov A.V., Rudich A.V. Before solving systems of linear equations on computers of hybrid architecture. Mathematical and computer modeling. Series: Physical and Mathematical Sciences. Coll. of scientific works. 2017, Vol. 15, 158-164.
53. Wilkinson J. H., Reinsch K. Handbook of algorithms in Algol. Linear algebra. - Moscow: Mechanical Engineering. 1976, 389 p.
54. Popov A.V., Khimich A.N. Parallel algorithm for solving a system of linear algebraic equations with a tape symmetric matrix. Computer Mathematics. 2005, Vol.2, 52-59.
55. Khimich A.N., Sydoruk V.A. Fine-tile hybrid algorithm for factorization of a sparse matrix. Proceedings of the VII All-Ukrainian scientific-practical conference with international participation "Informatics and systems sciences (ICH – 2016) ". Poltava, 2016, 326-328.
56. Khimich A.N., Sydoruk V.A. Tile hybrid algorithm for factorization of sparse block-diagonal matrices with a frame. Computer Mathematics – 2016. – Vol. 1, 72-79.
57. Khimich A.N.., Sydoruk V.A. Tile hybrid algorithm for factorization of structurally symmetric matrices. Theory of optimal solutions. 2017, 125-132.
58. Buttari A., Langou J., Kurzak J., Dongarra J. A Class of Parallel Tiled Linear Algebra Algorithms for Multicore Architectures. Parallel Computing. 2009, Vol. 355(1), 8–53.
59. Supercomputer complex SKIT [Electronic resursc], access mode: http://icybcluster.org.ua/
60. Boreskov A.B., Harlamov A.A. – The Basis of work with technology CUDA. Moskov: Press. 2010, 232 p.
61. cuSparse Library. URL: http://docs.nvidia.com/cuda/cuSPARSE/
62. Mykhalyk D., Petryk M., Petryk M., Petryk O., Mudryk I., Mathematical Modeling of Hydrocarbons Adsorption in Nanoporous Catalyst Media using Nonlinear Langmuir's Isotherm using Activation Energy. IEEE. Proceeding of 2019 9th International Conference on Advanced Computer Information Technologies (ACIT, Budejovice, Czech Republic), 72 -75 (2019)